TRANSPORT PROCESSES IN ELECTRODE SYSTEMS

Final Report

Contract Nr. DA36-039 SC-89153
OST 760200201
ARPA Order Nr. 220-61

March 16, 1962 through March 1, 1965

"The work under this contract was made possible by the support of the Advanced Research Projects Agency under Order Nr. 220-61, through the U.S. Army Electronic Laboratories."

U.S. Army Electronic Laboratories
Fort Monmouth, New Jersey

March 1965

Contractor: The Regents of the University of California
Berkeley, California

ERRATA SHEET

Page	Par.	Line	Correction
vii	bottom of page		After "Literature Cited", insert "Figures .....216".
x	6	1	Should read: "....on a 10 x 20 x cm ....".
xi	4	1	Should read: ".... Function of nt' ....".
	11	1	Should read: "Multicomponent Diffusion Coefficients of KCl-H_2O at 25°C."
12	4	last	Insert: "March 18, 1965 - University of California, Berkeley. Same as August 6, 1964 entry."
13	4	2	Should read: Douglas N. Bennion.
27	3	3	Should read: "extension".
37			Title should read: "....Upper curve: Nickel Cathode, lower curve: Silver cathode."
45	2	8	Add: "....with respect to the working electrode: $$\eta = - \Phi - \frac{RT}{4F} \ln \left\{ [O_2]/p \right\} . \qquad (14)$$ Here Φ is the potential of the Hg/HgO reference electrode with respect to the working electrode."
	Footnote		Insert: "....Project V (page 152), ..."
47	1	2	Should read: "....exactly ....".
51	1	4	Should read: "...."diminishing with time."
56	1	3	Ref. numbers should read: 19-31, 34-37.
	Title		Should read: "...Kinetics of.....".
	2	3	Should read: "...reasonable on Ag, Hg, C, and....".
	Eqs. 6&7		Should read: "....= MOH + OH^-" and ... = M + OH^-."
58	5		Should read: "..... Gas Electrodes', Advanced Energy Conversion 4, 109-119 (1964)."
60	Last ref.		Delete Ref. 38.
67	1		Insert heading under title: "Introduction."
109	Last line		Should read: "Levich (2) has proposed that .....".
116	2	1	Should read: "In Table I the effective....."
127			Tables I, II, III should read: Table II, Table III, Table III.
163 164			Reverse order of page numbers.
203	2	4	Eq. 2 should read: "... $\frac{\sqrt{\nu c c_T}}{\kappa \mu}$ = ... ".

BLANK PAGE

TRANSPORT PROCESSES IN ELECTRODE SYSTEMS

Contract Nr. DA36-039 SC-89153
OST 760200201
ARPA Order No. 220-61

Final Report
March 16, 1962 through March 1, 1965

March 1965

Object of Study: To broaden scientific understanding of transport processes as they occur at interfaces between electrolytes-solids and gases, when electrode reactions are in progress.

Report prepared by:

D. N. Bennion
T. W. Chapman
S. L. Gordon
R. G. Hickman
G. L. Horvath
J. S. Newman
J. R. Selman
C. W. Tobias

Department of Chemical Engineering

Charles W. Tobias
Principal Investigator

Disclaimer

The findings in this report are not to be construed as an official Department of the Army position, unless so designated by other authorized documents.

The citation of trade names and names of manufacturers in this report is not to be construed as official Government indorsement or approval of commercial products or services referenced.

TABLE OF CONTENTS

TABLE OF CONTENTS (cont'd.)

TABLE OF CONTENTS (cont'd.)

TABLE OF CONTENTS (cont'd.)

TABLE OF CONTENTS (cont'd.)

TABLE OF CONTENTS (cont'd.)

TABLE OF CONTENTS (cont'd.)

LIST OF FIGURES

A. PURPOSE

The series of investigations reported herein were aimed at gaining physical understanding of certain transport processes of importance in electrochemical systems, and particularly in energy conversion and storage devices. Emphasis was placed on the elucidation of the effect of hydrodynamic conditions on the maximum feasible rates of anodic and cathodic processes, and on the clarification of the role of diffusion and migration of reacting species on the distribution of current along electrode surfaces. Further, the relationships among the various transport properties were investigated, with the purpose of developing techniques for the application of available transport data to electrochemical systems of practical significance.

Several distinct projects were pursued simultaneously, each of them representing a Master of Science or Doctor of Philosophy thesis subject.

Projects completed:

I. Current distribution at a gas-electrolyte-electrode interface.

II. Ionic mass transport in channels by combined free and forced convection.

III. The role of ionic migration in electrolytic mass transport.

IV. Mass tran[illegible] in concentrated binary electrolytes: a method for the prediction of ionic mobilities.

V. The solubility and diffusivity of oxygen in aqueous KOH.

Projects initiated under this contract, and continued after the termination date under new sponsorship:*

VI. Ionic mass transport and current distribution in channels in high velocity flow.

VII. Generalized method for the evaluation of transport properties in concentrated electrolytes.

---

* Under the sponsorship of the Inorganic Materials Research Division of the Lawrence Radiation Laboratory, Berkeley.

B. ABSTRACT

Project I.: Current Distribution at a Gas-Electrode-Electrolyte Interface.

The variation of current density along a cylindrical, partially immersed electrode relative to the position of the apparent or intrinsic meniscus has been measured as a function of total applied current. Measurements of current distribution are reported for the cathodic reduction of O_2 gas in aqueous KOH electrolyte on sectioned Ni and Ag electrodes. A thin film of electrolyte was observed to exist above the intrinsic meniscus. It was found that the charge transfer which takes place at the electrode electrolyte surface occurs almost totally above the bottom of the intrinsic meniscus, and that a large portion of this charge transfer occurs in the thin film as high as 1 to 5 millimeters above the top of the intrinsic meniscus. However, for high total currents the relative portion of current at large distances above the intrinsic meniscus decreases while near the intrinsic meniscus it increases. On nickel the current was more uniformly distributed into the upper areas of the thin film than on silver.

A mathematical model is presented which takes into account diffusion and migration of relevant substances and the solubility of oxygen in the electrolyte. The model accounts for

the concentration dependence of transport properties. A comparison of the theoretical and experimental results indicates that the current density distribution is controlled by a balance between charge transfer overpotential and ohmic resistance drop in the electrolytic film.

Project II.: Ionic Mass Transport by Combined Free and Forced Convection.*

The effects of buoyancy forces on ionic mass transfer at horizontal planar electrodes were studied experimentally with both laminar and turbulent bulk flow. Copper cathodes and an acifidied cupric sulfate electrolyte were used to obtain mass transfer data by the limiting current technique in the ranges of parameters:

$$10^5 < \text{Gr (Grashof Number)} < 10^{12}$$

$$75 < \text{Re (Reynolds Number)} < 7{,}000$$

$$600 < \text{Sc (Schmidt Number)} < 12{,}000$$

$$0.05 < \frac{d}{L} \text{ (duct diam/electrode length)} < 20$$

$$40 < \text{Nu.Sh (Nusselt Sherwood Number)} < 1{,}500$$

With turbulent bulk flow, buoyancy forces were found to have a negligible effect on the mass transfer process in the range of variables covered.

With laminar bulk flow, buoyancy forces can induce free convective secondary flows near the electrode interface. If log (Gr > 2.96 + log (Re), the process is dominated by free convection, and the equation of Fenech and Tobias,

* This project was sponsored by the Lawrence Radiation Laboratory up to March 1961; by NOL-Corona (Contract No. N123 (6738)17178A) to April 1962.

$$Nu' = 0.19\ (Gr.Sc)^{1/3},$$

may be used to predict average mass transfer coefficient. Otherwise, forced convection dominates, and the equation of Norris and Streid,

$$Nu' = 1.85\ (Re.Sc.\frac{d}{I})^{1/3},$$

yields acceptable prediction of the experimental data. The average deviation of all the data from the appropriate correlations was less than ±7%.

The variation of local mass transfer coefficients parallel and normal to the direction of flow may be explained by considering the interaction of the two modes of convection.

Project III.: The Role of Ionic Migration in Electrolytic Mass Transport; Diffusivities of $[Fe(CN)_6]^{3-}$ and $[Fe(CN)_6]^{4-}$ in KOH and NaOH Solutions.

The role of migration in ionic mass transport is discussed, and a rigorous method is presented for the evaluation of the contribution of migration when a constant potential gradient can be assumed to exist in the mass transfer boundary layer.

The influence of supporting electrolytes is shown to depend on the relative mobilities of all ionic species present in the solution.

Theoretical results are applied to the $K_3[Fe(CN)_6]$ - $K_4[Fe(CN)_6]$ - KOH or NaOH systems. Limiting currents were measured by a rotating disk electrode, and the apparent diffusivities calculated from these measurements were corrected

taking into account the influence of the presence of nonreacting ionic species. It is shown that the corrected product, $D\mu$, is constant over a large range of concentrations

for $[Fe(CN)_6]^{3-}$, $\frac{D\mu}{T} = 2.40 \times 10^{-10}$ (cm^2/sec) poise/°K

for $[Fe(CN)_6]^{4-}$, $\frac{D\mu}{T} = 2.02 \times 10^{-10}$ (cm^2/sec) poise/°K.

Project IV.: Mass Transfer in Concentrated Binary Electrolytes.

For a multicomponent system the diffusion law can be expressed in the form

$$c_i \nabla \mu_i = RT \sum_j \frac{c_i c_j}{c_T \mathcal{D}_{ij}} (\underline{v}_j - \underline{v}_i),$$

where μ_i is the electrochemical potential and $\underline{v}_i$ the average velocity of species i and $\mathcal{D}_{ij}$ is a diffusion coefficient accounting for the interaction between species i and j. This diffusion law is self-consistent and can be used to develop equations in a form useful for electrochemical transport problems.

It is suggested that the concentration and temperature dependence for ion-solvent interactions is described by

$$\mu \mathcal{D}_{o+} = kT/A,$$

and for ion-ion interactions is

$$u\mathcal{D}_{+-} = kT \sqrt{\frac{\nu c}{c_T}}/G$$

where μ is the viscosity and A and G are approximately constant.

Project V.: The Solubility and Diffusion Coefficient of Oxygen in KOH.

The solubility of oxygen in aqueous KOH solutions has

been measured by a Van Slyke apparatus and by an absorption technique developed by Hildebrand. In the range of concentration of KOH between 0 and 12 N, at 25°C, the two methods yielded identical results:

$$\log S = .1746\ C + \log 1.26 \times 10^{-3}$$

where .1746 is the solubility coefficient, S = solubility of oxygen, gram-moles per liter, and C = concentration of KOH, gram-moles per liter. The solubility was found to decrease with increasing temperature, in dilute solutions, and to increase with temperature in concentrations of KOH higher than 8.25 normal.

Diffusion coefficients of oxygen in aqueous KOH were evaluated from the limiting current of oxygen on a rotating disk electrode, and also by a stagnant tube technique similar to that used by von Stackelberg. The diffusivity drops sharply with increasing KOH concentration, and increases with temperature. At 25°C and concentrations higher than 2N KOH, the product of the diffusivity and the viscosity is constant:

$$D\mu = 1.30 \times 10^{-7} \text{ gram-cm}$$

where D is the diffusivity, cm^2/sec, and μ is the viscosity in poise. At 60°C the value of this product is

$$D\mu = 1.88 \times 10^{-7} \text{ gram-cm}$$

and is constant for concentrations higher than 1 mole/liter.

Project VI: Ionic Mass Transport and Current Distribution in Channels at High Velocity Flow.

As a tool for extended and refined investigations into the nature of superimposed free and forced convective mass transfer at electrodes, a combination of a high-capacity liquid circulation loop, a controlled current source and an electric measurement system has been designed and constructed.

The central element, the electrode flow cell, consists of a rectangular channel of 15 by 2 cm cross-section containing 40 cm long plane parallel electrodes of 600 cm^2 area, each, separated by a porous diaphragm. Alternatively, a flow cell of 5 by 2 cm cross-section containing two electrodes of 180 cm^2 area, each, can be used. The cathodes are divided into insulated, coplanar sections which allows measurements in axial or lateral directions. The electrolyte circulation system can provide l linear velocities along the electrodes of up to 450 cm/sec, corresponding to Re = 70,000. Special attention has been given to the design of the inlet section of the flow cell.

A regulated d.c. power combined with a linear current ramp generator has been designed and constructed. This source can provide any current maximum up to 100 amp in a preset time range, between 1 and 20 minutes. The section current measuring device has been modified to ensure equipotential conditions at the cathode, within ±1 mV.

The electric measurement system allows simultaneous recording of total current, sectional current densities, local

reference electrode potentials and electrolyte flow rate.

The entire cell system, power supply and measuring circuitry is presently subjected to extensive calibration and evaluation procedures.

Project VII: Transport Properties of Concentrated Electrolytic Solutions.

Available data on transport properties of binary electrolytes have been used to calculate D_{ij} coefficients as defined by Newman, Bennion, and Tobias. The concentration dependence of conductivities of various systems corrected for viscosity indicates that the development of a more generally useful method for the prediction of transport properties in binary and multicomponent systems requires more reliable and more extensive data on diffusion coefficients.

Of the possible methods of measuring diffusivities, the rotating disk electrode and a new type of restricted diffusion cell which uses interferometry for the detection of concentration gradients are shown to be most promising for obtaining precise data because it is possible to interpret the measurements with rigorous mathematical analysis. Therefore an improved rotating disk apparatus (see Project III) and a modified restricted diffusion cell with optical measurements which are applicable to concentration solutions are presently under development.

BLANK PAGE

C. LECTURES, CONFERENCES AND REPORTS

1. Lectures:

Tobias, C. W. "The Solubility and Diffusion Coefficient of Oxygen in KOH"; contribution to the discussion of oxygen electrodes, on the Sixth Advisory Group for Aeronautical Research and Development Combustion and Propulsion Colloquium, Cannes, France, March 15-18, 1964.

Tobias, C. W. "Convective Mass Transport in Electrolytes"; Symposium on Mass Transport in Electrochemical Processes, a keynote address at the 125th National Meeting of The Electrochemical Society, Toronto, Canada, May 3-7, 1964.

Newman, J. S. "The Flow of Charge and Mass Through an Agitated Electrolyte"; Symposium on Mass Transport in Electrochemical Processes at the 125th National Meeting of The Electrochemical Society, Toronto, Canada, May 3-7, 1964.

Bennion, D. N. "Current Distribution at a Gas-Electrode-Electrolyte Interface"; Symposium on Fuel Cells at the 126th Meeting of The Electrochemical Society, Washington, D.C., October 11-14, 1964.

Hickman, R. G. "The Effect of Buoyancy Forces on Forced Convection Ionic Mass Transfer at Horizontal Electrodes"; Symposium on Mechanism of Electro-

deposition at 126th Meeting of The Electrochemical Society, Washington, D. C., October 11-14, 1964.

2. Conferences:

June 23, 1962 - Fort Monmouth, New Jersey.

Organization represented: U.S. Army Electronics Research and Development Laboratories; Department of Chemical Engineering, University of California, Berkeley. The meeting was held to review the status and future plans for this research program.

April 17, 1963 - Fort Monmouth, New Jersey.

Organizations represented: U.S. Army Electronics Research and Development Laboratories; Department of Chemical Engineering (Charles W. Tobias), University of California, Berkeley. The meeting was held to review the status and future plans for this research program.

August 20-21, 1963 - University of California, Berkeley.

Organizations participating: U.S. Army Electronics Research and Development Laboratories (Mr. John Murphy); Department of Chemical Engineering, University of California, Berkeley.

August 6, 1964 - University of California, Berkeley.

Organizations participating: U.S. Army Electronics Research and Development Laboratories (Mr. John Murphy); Department of Chemical Engineering, University of California, Berkeley.

3. Reports:

Quarterly letter reports:

Report No. 1 - 30 June 1962

Report No. 2 - 30 September 1962

Report No. 3 - 31 December 1962

Report No. 4 - 31 March 1963

Report No. 5 - 30 June 1963

Report No. 6 - 30 September 1963

Report No. 7 - 31 December 1963

Report No. 8 - 31 March 1964

Report No. 9 - 30 June 1964

Report No. 10 - 30 September 1964

Report No. 11 - 31 December 1964

Report No. 12 - 31 March 1965.

Technical Reports:

Report No. 1. "Investigation of Ionic Diffusion and Migration by a Rotating Disk Electrode", by Stanley L. Gordon (M.S. Thesis), issued May 15, 1963.

Report No. 2. "The Effect of Buoyancy Forces on Forced Convection Ionic Mass Transfer at Horizontal Planar Electrodes", by Robert G. Hickman (Ph.D. Thesis), issued December 1, 1963.

Report No. 3. "Phenomena at a Gas-Electrode-Electrolyte Interface", by douglas N. Bennion (Ph.D. Thesis) issued June 1, 1964.

Publications:

The results of investigations under this contract have not as yet been published in the open scientific literature. Papers with contents closely similar to the descriptions of projects, will be submitted to journals following the issuance of this report.

SECTION D.

FACTUAL DATA, INTERPRETATIONS AND CONCLUSIONS.

PROJECT I.

Current Distribution at a Gas - Electrode-Electrolyte Interface

a) Experimental Treatment

Introduction

Many of the possible fuels and oxidants proposed for use in fuel cells are gases. To gain an understanding of electrodes involving gaseous reactants, analysis of transport phenomena at gas-electrode-electrolyte interfaces is necessary. Various studies of porous media involving only electrode-electrolyte interfaces have been presented recently[1,2,3,4]. The presence of a gas phase provides additional problems which are to be considered here.

Porous electrodes are used to increase the reaction area per unit volume and, in the case of gaseous reactants, to provide separation between gas and electrolyte. In such electrodes, many simultaneous and consecutive processes occur, and the nature and extent of the actual reaction area within the pores is not well defined or understood. A plane electrode partially immersed in an electrolytic solution offers a simpler system for studying the behavior of gas-electrode-electrolyte interfaces.

In 1957 Wagner[5] suggested that a thin film of electrolyte might exist above the visible meniscus on the surface of a partially immersed electrode. From his calculations it

appeared as if the electrode surface contacting this thin film might contribute appreciably to the charge transfer reaction.

Weber, Meissner, and Sama[6] performed experiments using an oxygen cathode to study the reaction rate distribution. They did not consider the possibility of a thin film above the intrinsic or readily visible meniscus, and copper oxide formation may have influenced their experimental results.

Will[7,8] has performed experiments with a hydrogen, sulfuric acid, and platinum system. For a give applied overpotential, he observed the variation in current with the length of platinum extending above the liquid level of the electrolytic solution. Will concluded that a thin film did exist above the intrinsic meniscus and that most of the current was transferred into the film in a narrow region adjacent to the upper edge of the meniscus. He also showed that surface migration of hydrogen along the platinum was not a significant mode of mass transfer. Diffusion of hydrogen through the film was determined to be the rate controlling step. This was the first really definitive experiment to show the role of thin electrolyte films. However, as the platinum electrode was extended further and further out of the electrolyte, new area on which an electrolyte film could exist was produced. Thus, the film geometry and resulting current distribution changed during the course of an experiment.

Our work has been undertaken to obtain a more quantitative description of the reaction rate distribution and to

investigate the role of the thin film during oxygen reduction. For the experimental work, oxygen gas, aqueous 3.5 molar KOH, and either nickel or silver electrodes were chosen.

Experimental Equipment and Procedures

The objective was to measure the variation of current density along a partially immersed electrode relative to the bulk electrolyte surface. In order to accomplish this, sectioned electrodes[9] were employed. The sections must be insulated electrically from one another, and the insulating separators should not significantly disturb the geometry of the thin liquid film on the surface of the electrode. Also, the sections of the metal electrode must be at the same potential.

In order to satisfy these requirements as closely as possible, only two sections and a single separation were used (see Figure 1). With this approach, the variation in the current from each section could be measured as a function of the distance, ΔL, of the bulk electrolyte level below the separation (see Figure 1). The sum of the two currents equals the total; therefore, only one of the currents is independent. In order to compare the results of different total currents more easily, the percent current out of the top section, defined as %C.O.T. = (Current out top section)(100)/Total Current), was used as the independent variable.

The experimental procedure involved determination of the %C.O.T. as a function of ΔL at various total currents on nickel and silver electrodes. To determine the actual

current density variation one plots the %C.O.T. vs. ΔL and takes the slope of this curve. The slope at a given value of ΔL, in cm^{-1}, times the applied current, I in $\mu A/cm$, gives the transfer current density at a height ΔL above the electrolyte level. The readings were consistent to within 3% for a single run except at the lowest current levels when variations up to 10% of the measured current were inherent in the circuit design.

To avoid edge effects a cylindrical electrode was used. The working length of the electrode was approximately 12 cm; this was found to be long enough to avoid appreciable end effects at the top and bottom. The electrode was constructed using a cylindrical plexiglass spindle over which two cylinders of nickel* (or silver**) were slipped (see Figure 2). These were separated by a thin "gasket" made from a sheet of oriented polystyrene 25 microns thick. This thickness was necessary to insure that no metallic electrical connection occurred between the two sections.

In order to avoid the possibility of systematic errors and to confirm the reproducibility of the data, 2 different silver cells and 5 separate nickel cells were built. The procedures in constructing the separations in the working electrodes (such as rounding the corners of the electrode where it contacts the insulating jacket) were modified

---

* The nickel was 99.5% pure. The principal impurities were Mn and Fe.

** The silver was 99.95% pure.

slightly to see if the results were affected. No effects on the results were noted from these changes. For one of the silver electrodes, runs were also made with the 25 micron thick polystyrene gasket replaced by a separator made from filter paper approximately 70 microns thick. This was done to check the results for any dependence on the nature of the material used as the separator.

The cell consisted of two cylindrical compartments as shown in Figure 2. The cylindrical electrode spindle described above was screwed into the left-hand compartment. In the right-hand compartment, nickel screens served as the counter electrode. The reaction at the working electrode was

$$O_2 + 2H_2O + 4e^- = 4OH^-.$$

The reaction at the counter electrode was just the reverse of the above reaction. The reactions were driven externally by a constant current power supply.*

The two compartments mentioned above were connected to a storage reservoir, not shown in Figure 2. By carefully adjusting the height of the storage reservoir, the liquid level in the cell compartments could be accurately adjusted. The value of ΔL was determined by measuring the height of the bulk liquid and the height of the separation, to ± 0.05 mm, using a cathometer.

The electrolyte entered the working electrode compartment through radial holes drilled in the lower part of the

* Electronics Measurements, Inc., Constant Current Power Supply, Model C612.

plexiglass spindle. This provided for an axially symmetric electric field. To align the electric field more nearly parallel to the electrode and to reduce convection effects, a precision-bore glass tube was placed over the electrode as shown in Figure 2. The bulk electrolyte was confined in an annular space about 1 mm wide. The bottom of the meniscus was used as the reference level for measuring ΔL. The distance from the bottom of the meniscus to the top of the apparent or "intrinsic" meniscus was in the range of 0.6 - 1.1 mm. The electrolyte in the cell outside the jacket did not participate in the reaction and need not be considered.

Convection currents in the electrolyte below the meniscus would tend to give abnormally high currents from the bottom section. The glass jacket which confined the electrolyte next to the electrode in an annular region reduced this effect. Smaller spacing would have reduced the probability of convection further[10], but this would have caused variations in the annular space. The value chosen was considered to be a suitable compromise.

The readings were sensitive to the surface conditions of the electrodes. If any oxide formed on either the nickel or silver electrodes, the results were not reproducible. Care was always taken that, following polishing*, the electrode was immediately placed in the cell and cathodically

---

* Of the various polishing compounds, "Flow-five" aluminum oxide proved to be the most satisfactory.

Although the roughness of surfaces was different depending on the polishing compounds used, no significant differences in the pattern of current distribution resulted.

polarized to prevent oxide formation. The current was increased to approximately 200 ma yielding vigorous hydrogen evolution. During the 24-48 hour cleaning period, the electrolyte was changed each 2-5 hours. The cleanliness of the surface was considered satisfactory when, upon lowering the electrode level, the surface remained uniformly wetted.

Electrolytic contact was made to a Hg, HgO reference electrode through a hole drilled lengthwise down the spindle and out through a small hole at the bottom of the metal electrode[11]. Electrical connection to the bottom section of the electrode was made with a nickel rod down a hole in the spindle. A stainless stell screw went through the electrode and was threaded into the nickel rod. The electrical connection to the top section was made by a nickel plate in the bottom of the cap. When the cap was screwed down, the nickel plate pressed down on the upper electrode section and completed the contact. The resistances due to these connections were less than 0.1 ohm.

Figure 3 shows a schematic drawing of the electrical circuit. Before the measurements were started, the variable resistors* were set at zero; the two electrode sections were then shorted togather and thus were at the same potential. When measurements were to be made, the resistances were increased until a measurable voltage drop** was obtained. When properly adjusted, the potential drop across each resistor

---

* General Radio type 1432-U or 1432-K decade resistance boxes were used.

** This voltage drop was measured using a Keithly Model 149 milli-microvoltmeter.

was equal. As small a voltage drop as practical was used so that errors in balancing would be negligible. These potential differences varied between 10 and 1000 microvolts for the lowest and highest total applied currents. From the voltage drop and the known resistance, the current from each section could be calculated. The potential of the working electrode with respect to the Hg, HgO reference cell was measured with an electrometer*.

The start-up procedure was to refill the cell with 3.5 molar KOH, begin bleeding in O_2 saturated with water with respect to 3.5 molar KOH, and to set the total current at a fixed level. The liquid level was then lowered to below the lowest value of ΔL desired. The cell was left for about 15 hours to allow the liquid film to drain and reach an equilibrium thickness. The level was next raised a small distance and a set of readings taken. After each set of readings, the level was raised again and in this manner a series of readings for different values of ΔL were obtained. Observations were made at thirty-minute intervals which was sufficient to allow steady state conditions to prevail during readings. At each electrolyte level the value of %C.O.T. could easily be calculated.

Experimental Results

Exploratory experiments showed[12] that shortly after the electrolyte level was lowered, a thin electrolyte film was left

* Keithly Model 610R electrometer was used here. Its internal resistance is rated at 10^{14} ohms or greater.

behind on the exposed electrode, the fraction of current from the upper section was very high but that it dropped off with time. This decrease with time continued for up to 90 hours, after which a steady state value remained as long as the run was continued, for several more days in some cases. This behavior was attributed to the draining of the electrolytic film which was initially thick but became thinner as draining progressed. Thicker films have a small resistance and thus tend to allow penetration of the current higher into the film.

Simple optical observations were made in an attempt to observe the film and determine its thickness by light interference techniques. The existence of the film was confirmed by the observation of weak interference colors when white incident light was used and by the observation of a "wake" when a small corner of tissue paper was drawn over the surface. Quantitative measurements of the film thickness were beyond the scope of this work. Müller[13] has made a detailed investigation of the optical properties of thin electrolytic films on nickel electrodes and found that in the range of 2 to 5 mm above the meniscus the film thickness is in the order of 1 micron for 3.5 molar KOH.

Plots showing %C.O.T. as a function of ΔL are shown in Figures 4, 5, and 6 for 4.84, 15.4, and 48.4 $\mu A/cm$ applied current, respectively. Figure 7 shows the observed dependence of the electrode potential on the applied current.

A feature to be noted is that at higher currents the reaction tends to be concentrated nearer the top of the

intrinsic meniscus. A comparison of the results for equal applied currents shows that the reaction on nickel spreads more into the film than on silver.

One of the requirements of the sectioned electrode was that the separation should not disrupt the film. This becomes especially important when it is realized that the film is about 1 micron thick and the separation is 25 microns wide. Such a wide gasket obviously causes some distrotion. The distortion can be broken down into three categories as follows:

1) Assume that the insulating gasket is perfectly flush with the metal surface and that the film thickness does not vary. The only error from such an ideal situation results from no electrode reaction occurring along the insulating section. This inactive length of the film will act as an "unnatural" resistance. If this occurs near the bottom of the film where the current might reach 100 μA/cm as a maximum and if the film is one micron thick, the "unnatural" resistance will cause a potential drop of 4.2 millivolts. This compares to a total potential drop in the film of about 140 millivolts.

2) Referring to case 1), the net effect of the separation might be such that the film appears to be thicker as it passes the separation. For this situation, the "unnatural" resistance will be lowered, and the error will be less than for case 1).

3) The situation might also be an effective thinning of the film as it passes the separation. At worst, this thinning

will occur along the full length of the separation. A thinning of this type, for example, to one-fourth of the normal thickness, will increase the "unnatural" resistance so that, using the example of case 1), the added potential drop would be 19 millivolts. Such an added potential drop would cause a shift in the results, such that less current would pass to the upper section than on an uninterrupted surface.

The reproducibility of the data was confirmed by using different cells of slightly modified design. Similarly, no change in the results was detected by replacing the 25 micron-thick polystyrene separator with a 70 micron thick separator made from filter paper (see Figures 5 and 6).

From these observations it is concluded that the film on the separator was not significantly thinner than on the adjacent metal surfaces, and therefore, the maximum error in the current out the tope, due to the presence of the separator, is estimated to be 3%.

Discussion

These experiments have confirmed that a stable, thin film of electrolyte adheres to the electrode surface above the top of the intrinsic meniscus. A large part of the reaction takes place on the surface of the electrode exposed to this film. The reaction rate drops off very rapidly within the visible meniscus and is very small along the electrode area exposed to the bulk electrolyte. The obvious reason for the decrease in reaction rate in the bulk electrolyte is mass transport limitation of the molecular oxygen. However,

the controlling feature in the film region can arise from two sources.

Will[7,8] concluded that the rate limiting step was the mass transfer of the gaseous reactant, hydrogen in this case, through the film to the electrode surface. He also found that the reaction rate dropped off very rapidly above the "top of the intrinsic meniscus." The observations with the oxygen - KOH system show that the reaction rate remains appreciable for several millimeters above the "top of the intrinsic meniscus." In addition, it is observed that the reaction extends further up the film for nickel than for silver.

It is also possible that the limiting step can be charge transfer at the electrode surface. It is known that silver is a better catalyst for the reduction of oxygen than is nickel[14]. Thus one would expect that if the dependence of charge transfer "overpotential" on current density were higher for nickel than for silver, the reaction would tend to "spread out" or be distributed over a wider area, thus further up into the film.

Both the charge transfer and mass transfer overpotential tend to cause the reaction to spread out farther. It is the resistance drop in the film which limits the extention of the reaction up into the film. From either standpoint, if the film were thicker, the reaction would tend to extend further into the film. Observations made during the initial stages when the film was draining confirm this argument.*

* Measurements of film thickness on silver were not available at the conclusion of this work.

Conclusions*

1) The existence of a thin film of electrolyte above the intrinsic meniscus on clean nickel and silver has been confirmed. The thickness of this film is established as being in the order of magnitude of the wave length of visible light.

2) For the cathodic oxygen electrode, current density distribution measurements on cylindrical nickel and silver electrodes established that a large portion of the current arises in the thin electrolytic film above the intrinsic meniscus. The fraction of current transferred as much as 10-20 mm above the bottom of the intrinsic meniscus is not negligible.

3) The thicker the film and the smaller the applied current, the further the current spreads over the electrode surface covered by the film. At a given value of applied current, the reaction is concentrated nearer the intrinsic meniscus on silver than on nickel surfaces.

---

* After the completion of this manuscript, an account of the work of Yu A. Mazitov et al[15] has come to the author's attention. Current distribution along a silver wire in the reduction of oxygen in 10.6 N KOH was measured by the method originally used by Will[7,8]. Although their experimental observations are in qualitative agreement with the results presented above, the reader's attention is called to the use of an uninterrupted cathode and the much shorter draining times (3-4 minutes) reported by Mazitov et al.

LITERATURE CITED

1. John S. Newman and Charles W. Tobias, "Theoretical Analysis of Current Distribution in Porous Electrodes", J. Electrochem. Soc., 109, 1183-91 (1962).

2. Edward A. Grens II and Charles W. Tobias, "Analysis of the Dynamic Behavior of Flooded Porous Electrodes", Berichte der Bunsen Gesellschaft für Physikalishe Chemie, 3, 236-249 (1964).

3. John L. Bomben, "Current Distribution in a Porous Electrode," Master's Thesis, University of California, Department of Chemical Engineering, September 1963.

4. J. Euler and W. Nonnenmacher, "Stromverteilung in Porösen Elektroden," Electrochimica Acta, 2, 268-86 (1960).

5. Carl Wagner, "Polarization Characteristics of Gas Electrodes in Stagnant Electrolytes," unpublished work, dated June 13, 1957.

6. H. C. Weber, H. P. Meissner and D. A. Sama, "Oxygen Transport and Reaction Rates at an Air-Depolarized Copper Cathode," J. Electrochem. Soc., 109, 884-9 (1962).

7. Fritz G. Will, "Electrochemical Oxidation of Hydrogen on Partially Immersed Platinum Electrodes, I. Experiments and Interpretation," J. Electrochem. Soc., 110, 145 (1963).

8. Fritz G. Will, "Electrochemical Oxidation of Hydrogen on Partially Immersed Platinum Electrodes, II. Theoretical Treatment," J. Electrochem. Soc., 110, 152 (1963)

9. E. Mantzell, "Zur Kenntnis der Kathodischen Stromverteilung in Galvanischen Elektrolyten. 1. Untersuchugen an Zinkbädern," Z. Elektrochem., 42, 303-315 (1936).

10. U. Böhm, N. Ibl and A. M. Frei, "Study of Mass Transport by Natural Convection in Narrow Spaces." Presented at the 13th C.I.T.C.E. meeting in Rome, 24-29 September, 1962, in press in Electrochimica Acta.

11. M. Eisenberg, C. W. Tobias, and C. R. Wilke, "Application of Backside Luggin Capillaries in the Measurement of Non-uniform Polarization", J. Electrochem. Soc., 102, 415-419 (1955).

12. Douglas Noel Bennion. Phenomena at a Gas-Electrode-Electrolyte Interface. Dissertation, University of California, Berkeley, June, 1964. Technical Report No.3, this contract.

13. Rolf H. Muller, "Optical Studies of Electrolytic Films on Metal Surfaces," paper presented before the Electrochemical Society, Toronto, May, 1964.

14. Heiner M. Dittman, Edward W. Justi and August W. Winsel, "DSK Electrodes for the Cathodic Reduction of Oxygen," Fuel Cells, Vol. II, G. J. Young, Editor, Reinhold Publishing Corp., New York, 1963.

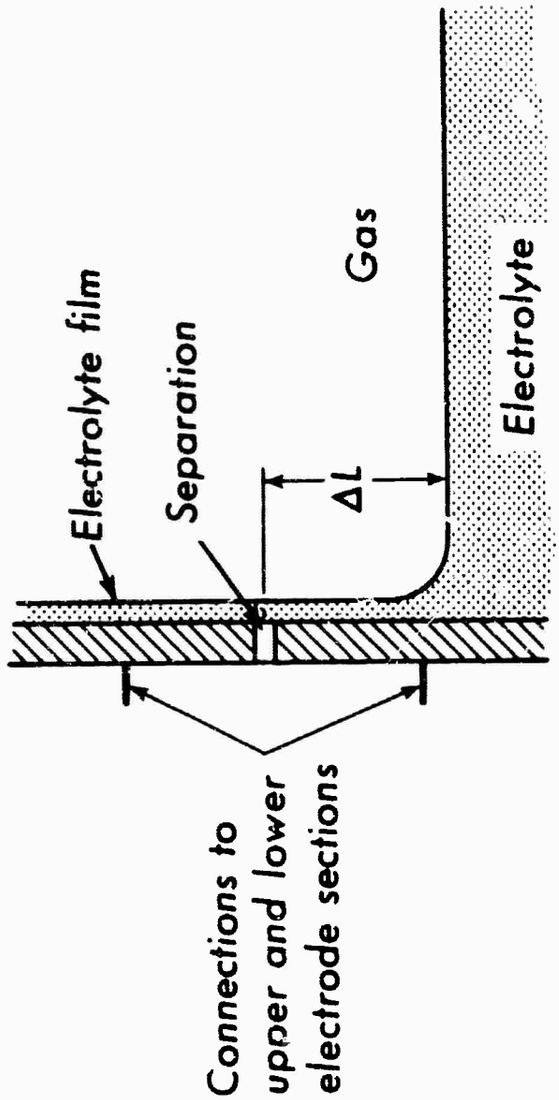

Figure 1. Schematic representation of gas-electrolyte interface showing the insulating separator. L could be changed by raising or lowering the electrolyte level.

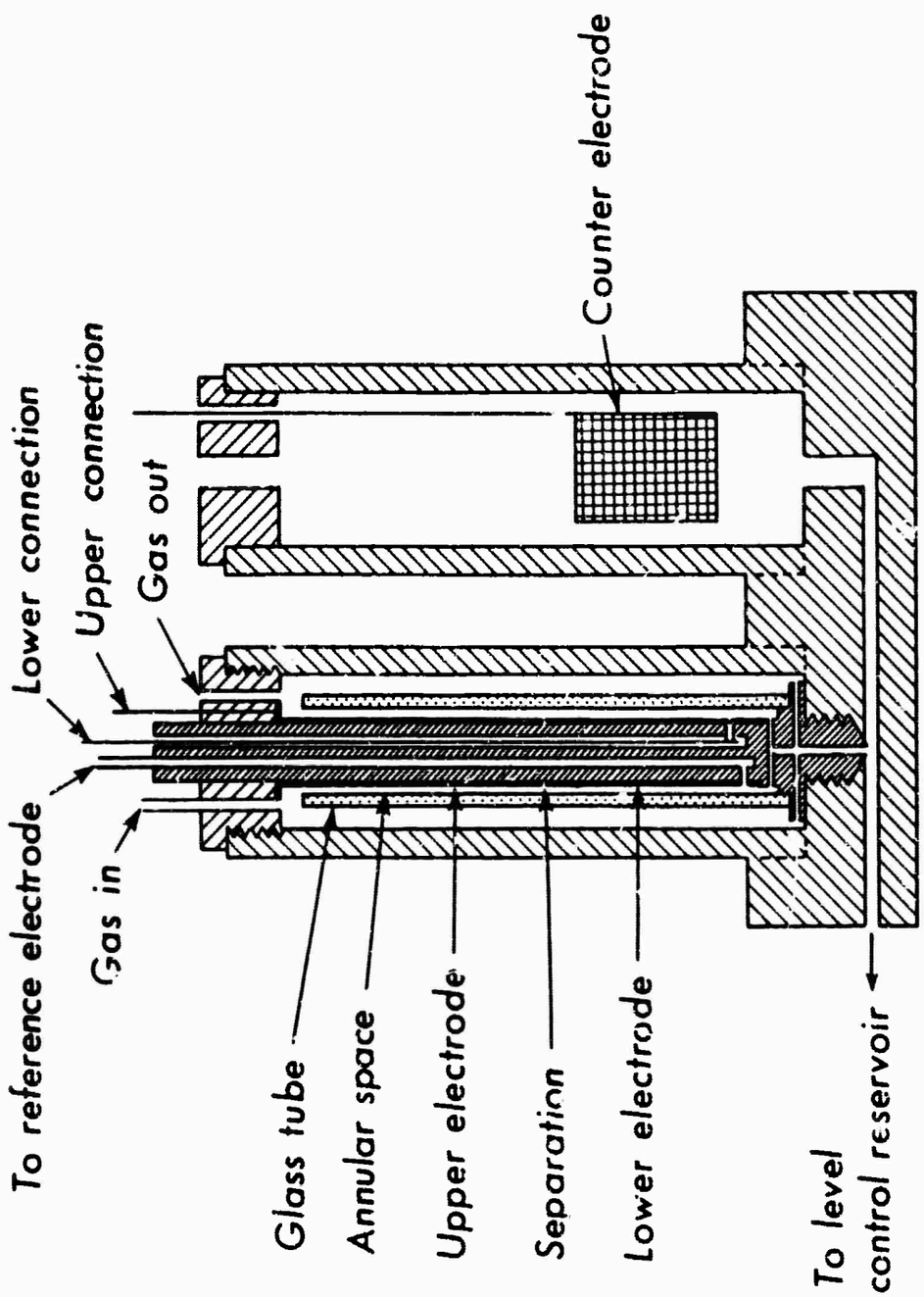

Figure 2. Cross-sectional view of cell used for measurement of distribution of current relative to position of meniscus.

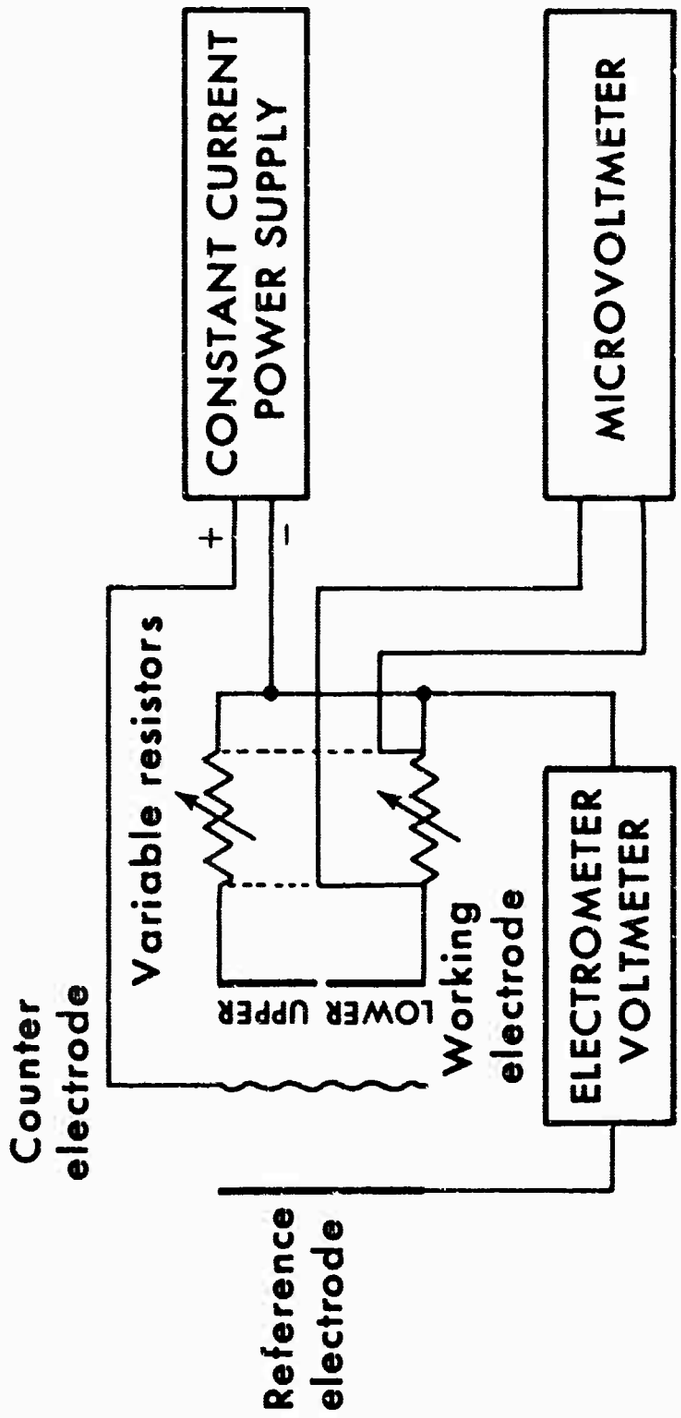

Figure 3. Power - and measurement circuit for sectioned electrode cell.

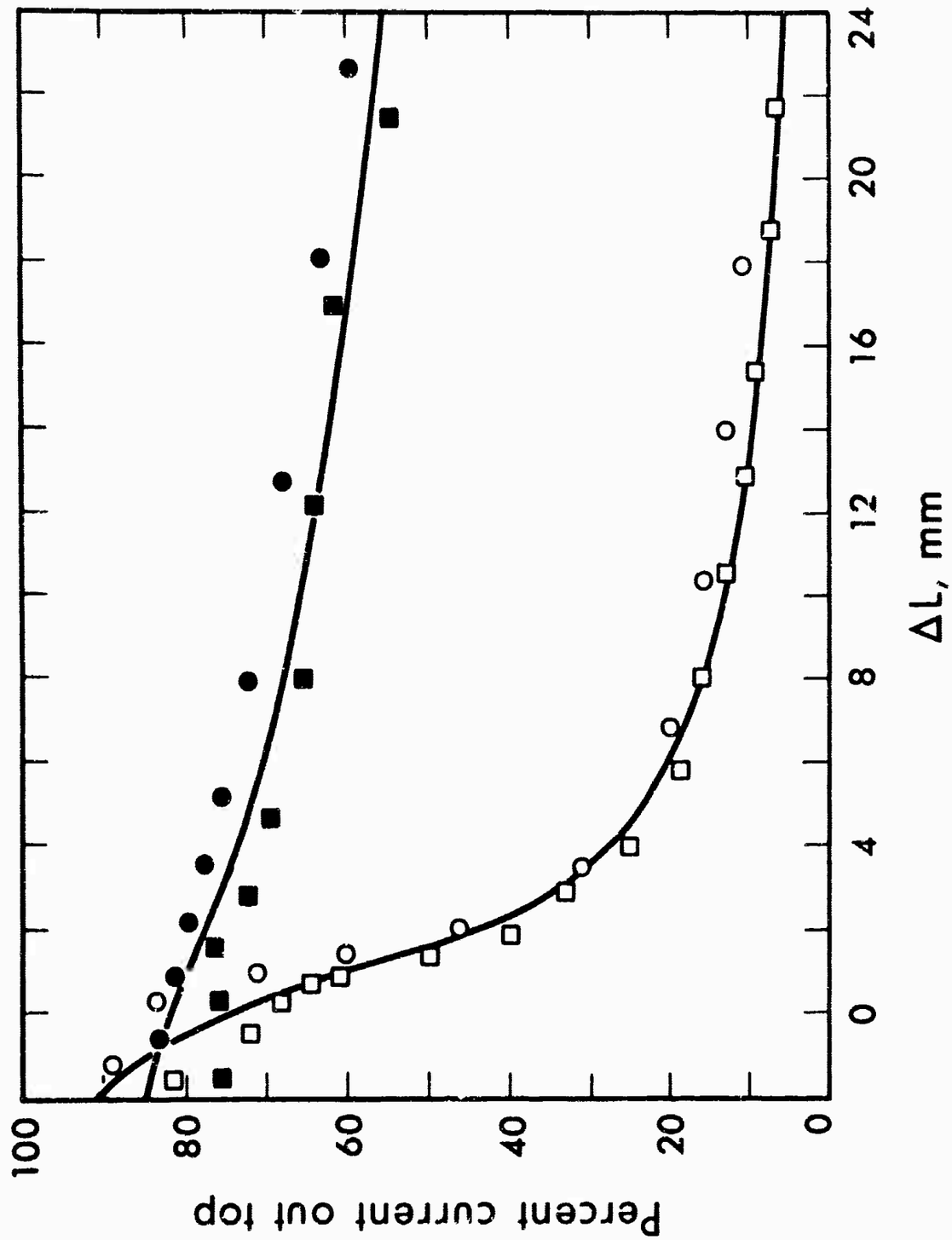

Figure 4. Penetration of current in the electrolyte film. I = 4.84 μA/cm.
Upper curve: Nickel cathode, cells no. 2 and 3, runs 6 and 6'.
Lower curve: Silver cathode, cell no. 4, runs no. 6 and 15.

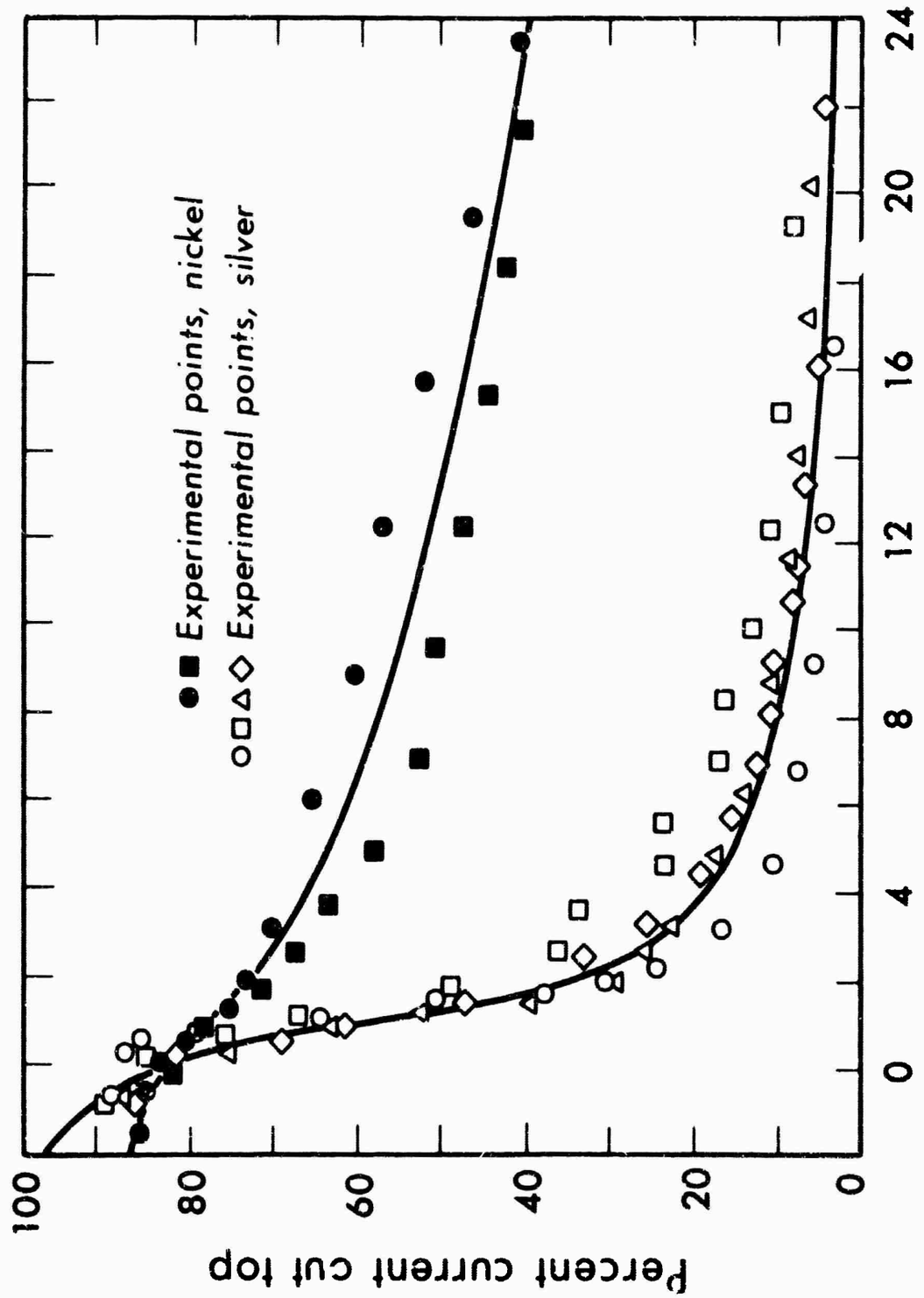

Figure 5. Penetration of current in the electrolyte film. I = 15.4 μA/cm.
Upper curve: Nickel cathode, cells no. 2 and 3, runs 5 and 5'.
Lower curve: Silver cathode, cell no. 4, runs no. 5, 11 and 14.

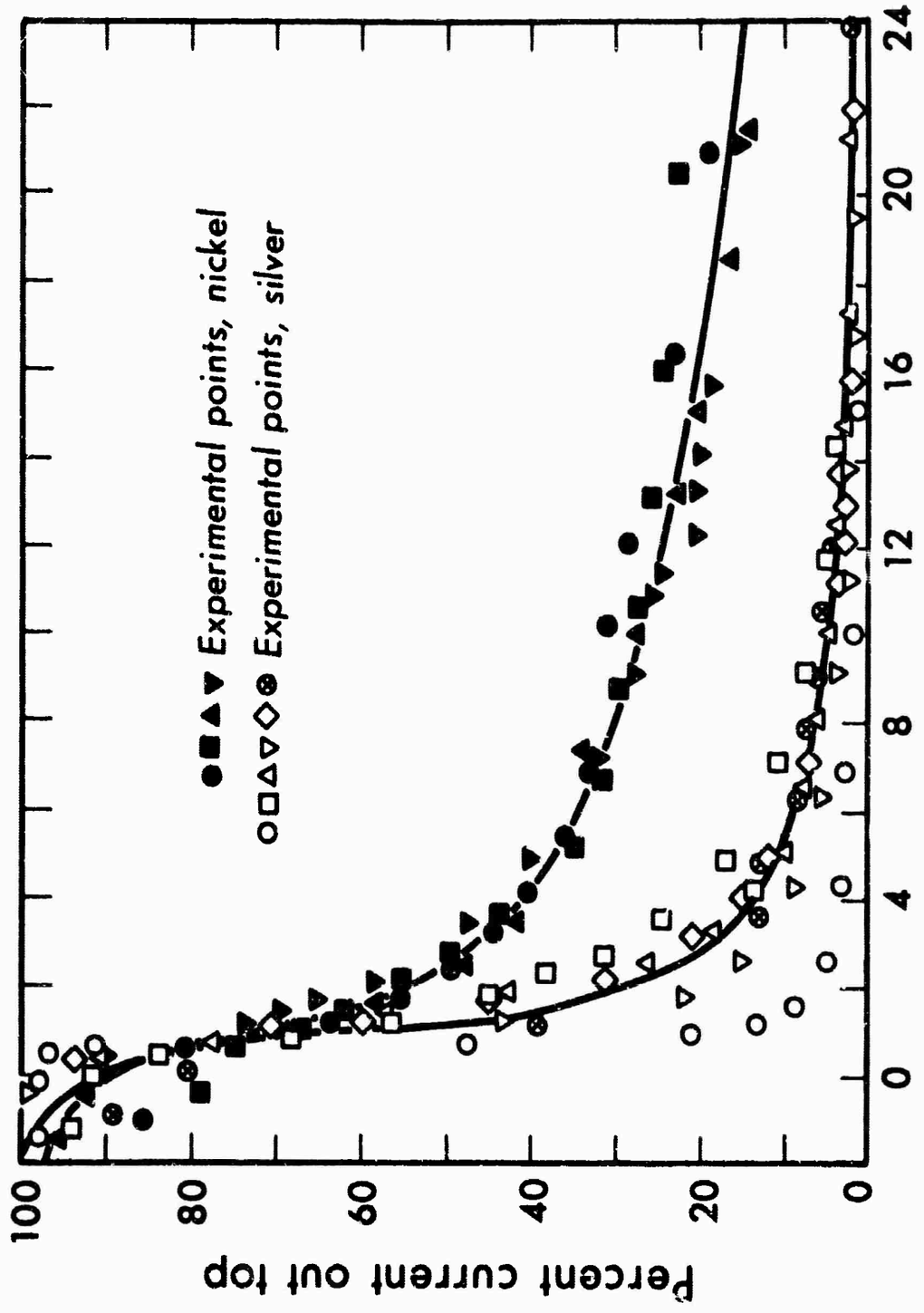

Figure 6. Penetration of current in the electrolyte film. I = 48.4 μA/cm.
Upper curve: Nickel cathode, cells 2, 3, and 7; runs 4, 4', 19, 20.
Lower curve: Silver cathode, cells 4 and 6, runs 4, 10, 13, 19, 20.

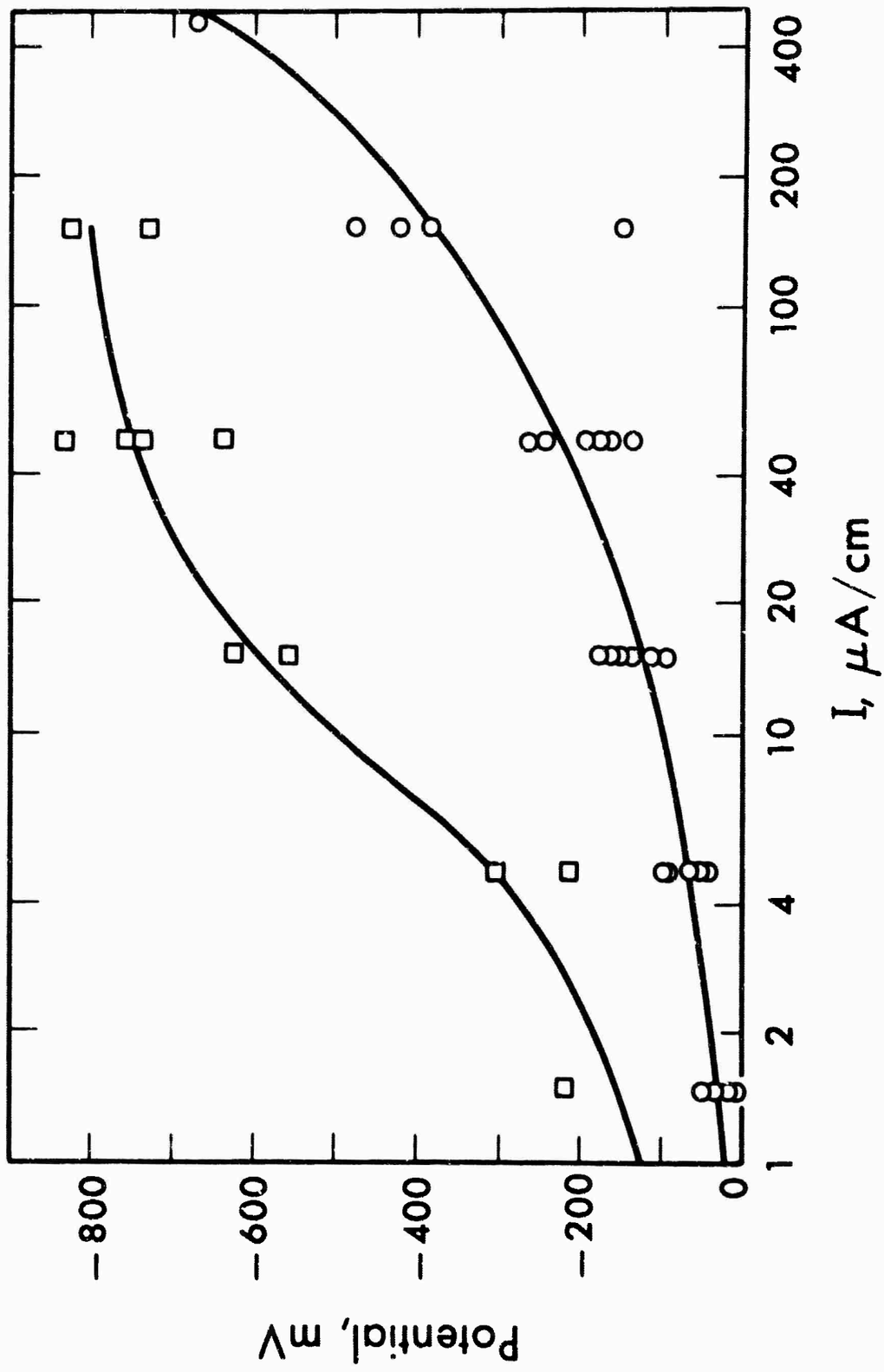

Figure 7. Potential of the oxygen cathode (not corrected for ohmic drop) relative to the Hg/HgO reference electrode. Upper curve: Silver cathode, lower curve: Oxygen cathode.

Current Distribution at a Gas - Electrode-Electrolyte Interface

b) Theoretical Treatment

Introduction

An experimental study[1] in this laboratory has shown that on partially immersed gas electrodes a thin film of electrolyte may exist on the electrode above the bulk electrolyte, and when this film exists the electrochemical reaction takes place primarily on the surface of the electrode which contacts the thin film.

By considering several possible physical models Wagner[2], in 1957, demonstrated the likelihood of the importance of thin electrolyte films in actual gas electrodes. Since then, various models have been proposed which attempt to duplicate more closely actual physical conditions. Will[3,4] was able to explain his experimental results obtained on partially immersed, plane electrodes in terms of a theoretical model. His model did not include consideration of charge transfer overpotential, and the only transport property of the electrolyte employed was the conductivity which he assumed to be invariant. Grens et al[5] in a model geometrically similar to the one by Will included an Erdey-Gruz-Volmer type charge transfer overpotential expression. Transport of ions by both diffusion and migration is accounted for, and the movement of water is assumed to occur only in the electrolyte phase. Grens et al were able to show how systems can become charge

transfer or mass transfer limited depending on the magnitude of the physical parameters involved. Although variations of transport properties were not considered, their model predicts large concentration gradients in the thin film. It should be noted that, of these models, only that of Will has been compared directly to experiments, and that his model incorporated features characteristic of the hydrogen, sulfuric acid, platinum system.

The above theories provide primarily a guide to understanding the detailed behavior of the electrode reaction within and near a thin electrolyte film which may exist on plane, metal electrodes. Other models have been proposed which attempt to explain the behavior of porous electrodes in terms of certain assumed microstructures of the porous matrix. Some recent models by Gurevich[6], Rockett[7], Iczkowski[8], and Burshtein *et al*[9], have incorporated the possibility of thin film existing on the walls of the gas filled pores or cavaties within the electrode. Of these, the one by Burshtein *et al* is of particular interest, since it includes a transformation of a rather sophisticated model into one where equations developed for two phase porous electrodes can be applied[10,11,12]. In Burshtein *et al's* model, a detailed description of what is taking place within the thin film is not undertaken, and a simple, linear relation between the local overpotential and the current being transferred is assumed.

The theoretical model to be presented here is one in

which the details of the film behavior are described. Our model is to be for the oxygen, KOH, silver system and is to include a realistic charge transfer overpotential relation. It also allows for variation of electrolyte composition and consequent changes in the solubility of oxygen and in the transport properties of oxygen and KOH. Consideration is given to whether water transport occurs in the gas phase or the liquid phase. Direct comparison of the theoretical model and experimental results is designed to further our understanding of the system and its controlling features.

The mathematical model

Geometric considerations: The model describes an oxygen half cell operating cathodically in aqueous KOH electrolyte. From the analysis of experimental results, it has been concluded that a large portion of the reaction takes place in a thin film which extends above the bulk electrolyte on the surface of the electrode. Measurements of the film thickness by Müller[13] show that the thickness of this film decreases with height about the bulk liquid. However, the percent change in thickness is small compared to the observed percent changes in the reaction rate over comparable distances[15]. In our model, to avoid unnecessary mathematical difficulties, the thin film is assumed to have a constant thickness, δ.

Since the current density was observed to spread out over a comparatively large area, the current transferred in the vicinity of the curved meniscus is small compared to the total current. This suggests that the precise geometry

of the meniscus is not important[1,3,4]. Consequently, in our model the thin film is assumed to change its thickness abruptly, yielding a hypothetical film (see Figure 1).

Mass transport considerations: Mathematically, the model is one dimensional. No variations in concentration, c, or current density, i, across the width of the film is considered. Oxygen is assumed to reach the electrode by diffusion in the negative x direction through the upper film (see Figure 1). In the lower (bulk) electrolyte region oxygen is assumed to move only in the negative y direction. The consumption of oxygen through reaction at the electrode is treated as a homogeneous sink term (see equation (10)).

The system is assumed to be at steady state. The overall electrode reaction is

$$O_2 + 2H_2O + 4e^- = 4OH^-.$$

The rate of reaction at the electrode is proportional to the transfer current density, J. J is taken as positive when the reaction proceeds from left to right as written. In the thin film, O_2 migrates toward the electrode in the negative x direction, OH^- ions move down the film, and the K^+ ions remain stationary at steady state. The water can reach a reaction site by two mechanisms or combinations thereof. It can diffuse up into the film countercurrently to the OH^- ions or condense from the gas phase onto the film surface and diffuse co-currently with the oxygen. Convection is assumed to be negligible.

Equations for electrolytic transport: Algebraically, the ionic fluxes and water flux can be written as

$$N_+ = 0,$$

$$N_- = -1/F,$$

$$N_o = -\frac{1}{2} Q N_-,$$

$$v^* = \frac{1}{c_T}(N_+ + N_- + N_o) = \frac{-i}{c_T F}\left(1 - \frac{Q}{2}\right). \qquad (1)$$

By electroneutrality

$$c_+ = c_- = c. \qquad (2)$$

Q is equal to unity if the water is supplied wholly by diffusion up the film, and it is equal to zero if supplied totally by condensation from the gas phase. It seems reasonable that one mechanism or the other will be controlling so that Q will be assumed to equal either one or zero. The model is not suitable for fractional values of Q.

The equations representing the flow of current and movement of the K^+ and OH^- ions have been discussed elsewhere[14]. Incorporating the concentration dependence of the transport properties, we obtain

$$\underline{i} = -K\nabla\Phi - \frac{K}{F} RT \nabla \ln a \left[\frac{2B}{A+B} + \frac{c}{c_o}\right], \qquad (3)$$

$$\underline{N}_+ = \frac{D}{RT}\frac{\nu_+}{\nu} c\nabla\mu_e + \frac{t_+^* \underline{i}}{F z_+} + c_+ v^* \qquad (4)$$

$$\underline{N}_- = \frac{-D}{RT}\frac{\nu_-}{\nu} c\nabla\mu_e + \frac{t_-^* i}{F z_-} + c_- \underline{v}^* \qquad (5)$$

$$\frac{-z_+ z_- \epsilon F \sqrt{\nu c c_T}}{K\mu} = G + \frac{AB}{\nu_+ A + \nu_- B} \frac{\sqrt{\nu c_o}}{\sqrt{c\, c_T}} \tag{6}$$

$$\mathfrak{D} = \frac{\nu kT/\mu}{\nu_+ A + \nu_- B} \tag{7}$$

$$t_+^\star = 1 - t_-^\star = \frac{c_-}{c_T} + \frac{c_o}{c_T} \frac{B}{A+B} \tag{8}$$

Values of A, B, and G for KOH are[14]:

$A = 28.89 \times 10^{-8}$ cm, $B = 8.63 \times 10^{-8}$ cm, $G = 9.63 \times 10^{-8}$ cm.

Equations for oxygen transport: In the thin film, oxygen diffusion can be represented by

$$J = \frac{FD_1(pc_1^o - c_1)}{\delta}, \quad (y \geq 0). \tag{9}$$

The transfer current density, J, is equal to the oxygen flux times 4F. It is assumed that Henry's law holds and that p is the partial pressure of oxygen in atmospheres. D_1 is the diffusion coefficient of oxygen at the concentration of KOH existing at the point under consideration in the film. The numerical calculations were easily adapted to allow for the variation of D_1 as a function of the KOH concentration at different positions in the film.*

In the lower or bulk electrolyte region the following equation applies to steady state oxygen transport.

$$D_1 \frac{d^2 c_1}{d\, y^2} = \frac{J}{4F\Delta}, \quad (y \leq 0). \tag{10}$$

---

* For the diffusion coefficient of oxygen in KOH solutions, see report on Project V, pages 173-174.

Equations relating current and overpotential*: A relationship between local overpotential and local transfer current density, J, is still needed. A review of the literature on the kinetics of the oxygen electrode[15,16] indicates that a generally accepted kinetic description for the oxygen electrode is not yet available[17,18,19]. Based on work by Krasilshchikov, Nefodova, Belina, and Andreeva[20,21,22,23,24,25] and work by Bogotskii and Yablokova[26], a sequence of elementary steps emerges which seems to be satisfactory for use with Ag, Au, and Hg electrodes. From this reaction sequence, summarized by Vetter[16], the following kinetic expression can be developed[15]

$$J = k[O_2]^{\alpha}[OH^-]^{\lambda}[H_2O]^{\gamma}\left\{e^{\frac{4(\alpha-1)F\eta}{RT}} - e^{\frac{4\alpha F\eta}{RT}}\right\}, \qquad (11)$$

where k is a constant, square brackets indicate the activity of the enclosed species, and η is the overpotential defined as the potential of the working electrode compared to a reversible oxygen electrode located just outside the double layer. For a silver electrode in alkaline solution

$$\alpha = 0.625, \quad \lambda = 0.5, \quad \gamma = 0.5. \qquad (12)$$

Work on carbon electrodes[27,28,29,30] also seems to support the above mentioned reaction sequence. However, information regarding the kinetics of oxygen reduction on nickel is quite contradictory. The surface oxides of nickel form at about the same potential at which oxygen reduction takes place and a generally applicable reaction sequence or kinetic rate expression does not appear available[17,18,31,32].

* A more detailed discussion and references are given in an Appendix (page 56).

Because of the lack of availability of a suitable kinetic expression for the reduction of oxygen on nickel, no attempt is made to apply the present mathematical model to the nickel electrode.

Two relations are needed in addition to the equations already mentioned. Since charge must be conserved, the transfer current density, J, and the current density in the solution, i, which is assumed to vary only in the y direction, are related by

$$J = -\delta \frac{di}{dy}, \ (y \geq 0); \ J = -\Delta \frac{di}{dy}, \ (y \leq 0). \qquad (13)$$

It is convenient to replace the potential of the reversible oxygen electrode by that of a Hg/HgO reference electrode with respect to the working electrode.

Activities used in kinetic equation: The activities of the reacting species are assumed to be represented by the following:

$[O_2]$ is assumed to be the concentration of oxygen with unit activity being the concentration of oxygen in equilibrium with gaseous oxygen at a partial pressure of one atmosphere. In the numerical work it was possible to allow the solubility of the oxygen to depend on the concentration of KOH.*

---

* As reported under Project V (page), the solubility of oxygen at 25°C in aqueous KOH as determined in this laboratory may be represented by

$$c_1 = (1.18 \times 10^{-3} \text{mol/liter}) \exp(-0.405\ c),$$

where c = concentration of KOH, moles/liter.

$[OH^-]$ is assumed to be the same as the mean ionic activity, a, of the KOH. The activity coefficients were taken from Robinson and Stokes[29]. The activity at a KOH concentration of 3.866 molar is taken to be unity.

$[c_o]$ is assumed to be the concentration of free water. This is determined by subtracting from the total water concentration the concentration of water that is associated with the KOH ions[15]. Unit activity is assumed to be the activity of water in 3.866 molar KOH solution.

Numerical Solution

There are 5 dependent variables, c, c_1, J, η, and i. These are related by equations (3), (4), (9) or (10), (11), and (13). Equation (9) is used in the upper film and equation (10) in the lower region. Equation (14) allows one to convert from η to Φ when desirable. Since the equations are slightly different for the upper and lower sections, the two sections are solved for separately and their boundary conditions matched, i.e., the potential and current are continuous in the electrolyte.

The boundary conditions at the top of the upper film are:

$$y \longrightarrow +\infty,\ \eta \longrightarrow 0 \text{ and } i \longrightarrow 0.$$

The boundary conditions at the bottom of electrode are:

$$\text{at } y = \text{bottom of electrode, } \eta = \eta_o \text{ or } i = i_o.$$

The equations are nonlinear, 1st and 2nd order differential equations. They were transformed into finite difference form and solved numerically using an IBM 7090

digital computer. In a numerical sense, it was possible to solve the equations for the thin film region exactly. That is, no iterations were necessary. This was accomplished through an appropriate change of variables. In the lower section, it was necessary to linearize the equations, put them in matrix form, and solve the matrix[15]. The nonlinearities were mild and only three or four iterations were necessary. The method appeared to be stable and to converge rapidly to the correct answer.

Theoretical Results and Comparison with Experimental Observations.

Explanation of figures: The experimental results are summarized in Figures 2 through 6. A comparison between the calculated variation of current above a fixed point on the electrode, ΔL, and the experimental observations corresponding to similar conditions is given in Figure 2. Experimental observations at 48.4, 15.4, and 1.48 $\mu A/cm$ were presented in Part a, Fig.4-6. The agreement of the theoretical results with the experimental results for the silver electrode is equally as good as the best curves drawn in by hand to represent the data. No experimental data are available for the voltage variation in the film.

Figure 3 shows the theoretical variation of potential and the percent current above a fixed point on the electrode as a function of applied current. Figures 4 and 5 present the current density variation along the electrode. The curves in Figure 3 are the integrals of the curves in

Figures 4 and 5 for corresponding total applied currents. Figure 6 shows examples of concentration variation in the film as a function of electrode height. A comparison is made between the concentration variations for both modes of water transport to the reaction sites.

Current distribution and the square meniscus assumption:

ΔL is the independent variable used in the experimental work which indicates position on the electrode relative to the bottom of the intrinsic or visible meniscus. The variable y is used in the theoretical work to indicate position along the electrode relative to the sudden, right angle widening of the thin film. In order to make direct comparison between the two approaches, y and ΔL must be properly related.

The distance from the top of the intrinsic meniscus over which the current density remains appreciable is to be noted. Even at the lowest currents observed (1.45 μA/cm), the area lying under the level of the bottom of the intrinsic meniscus contributes less than a third to the total current. At the highest currents observed (154 μA/cm) this fraction falls to below a hundreth. The discontinuity of the current density distribution curves at ΔL of 1 mm (see Figures 4 and 5) results from the square shaped meniscus used in the model. In reality, the transition from the charge transfer and conductance controlled region in the film to the oxygen mass transport controlled area below the top of the intrinsic meniscus and then drops off rapidly as the film begins to thicken from approximately 1 micron to a thickness in the order of 1 mm at

the bottom of the intrinsic meniscus. The region of high current density at the bottom of the thin film contributes a large portion of the total current. However, the reaction remains appreciable for several millimeters above the intrinsic meniscus. Due to the large area available in the upper film, the contribution to the total current from that region is appreciable.

In matching the theoretical and experimental current distribution curves, it was found that y = 0 corresponded to a ΔL of 1 mm. This implies that at one millimeter above the bottom of the intrinsic meniscus the film thickness is sufficient to cause oxygen transport to become controlling.

A theoretical treatment using a curved meniscus and a tapered film is possible. However, it appears this would greatly increase the numerical complexity due to a second geometric dimension. Such a modification is not expected to yield significant further information or insight. It is established by experimental evidence[1] and a reasonably realistic, theoretical model that an overwhelming proportion of the current originates well abcve the bottom of the intrinsic meniscus. The changes in the pattern of the current density distribution that can be expected if one substitutes a smoothly curving meniscus for the square meniscus are not expected to be appreciable.

Effect of exchange current density, i_o: Of the parameters which appear in the numerical calculations, many can be calculated from independent experimental data. Where values are not available, reasonable estimates have to be made.

The parameter known with the least certainty is k in equation (11). When multiplied by the concentration term raised to the appropriate power in equation (11), k can be identified with an exchange current density, i_o. A value for i_o of 1.76×10^{-9} A/cm^2 was found to "fit" the data the best. However, this could be varied by plus or minus three orders of magnitude with little effect on the position or shape of the theoretical curve. Although literature reports on measurements of i_o for the oxygen electrode vary widely, a comparison to the Tafel lines shown by Belina and Krasilshchikov[25] indicate that the value used is not unreasonable.

Effect of the film thickness parameter, δ: The theoretical results were very sensitive to changes in the film thickness parameter, δ. It should be remembered that in reality the film tapers while the model assumed δ to be constant. Since the current extends further up the film at low currents, it is to be expected that the effective average film thickness will decrease with decreasing total current.* The following values of δ were used for the indicated total applied currents.

I	1.48 μA/cm	4.84 μA/cm	15.4μA/cm	48.4 μA/cm	154 μA/cm
δ	0.33 micron	0.43 micron	0.75 micron	1.50 micron	2.25 micron

The values of δ used in the numerical solutions are in reasonable agreement with the average film thicknesses obtained from Müller's[13,15] data.

* It should be remembered that at low total current the relative current distribution is more spread out. Thus, the averaging of the film thickness includes more of the thinner, upper parts of film.

As confirmed by our models, experimental observations have shown that the current density distribution varies a great deal while the film is draining, i.e., while the film thickness is dimishing with time. In thinning films, the overall overpotential increases and the reaction spreads less and less into the film.

Influence of variable transport parameters and water transport: In the present work, current distributions were calculated both with constant and variable transport properties. Although the assumption of constant (average) properties did not yield significantly different distributions, this finding should be regarded as valid only under the specific experimental conditions employed. By providing water to the reaction sites through the film from the vapor phase, the steady state concentration gradient in the film is quite mild compared to the case when water transport occurs by diffusion from the bulk electrolyte in the liquid phase (see Figure 6).

The high concentration gradients which are predicted when water is assumed to be transported only within the film cause the KOH concentration to exceed the saturation limit. It is suggested that in actual porous gas electrodes water is supplied to the reaction site, at least in part, by condensation from the vapor phase.

Charge transfer kinetics: The shape and position of the theoretical current distribution curves also depends on the reaction orders, α, λ, and γ. These appear as the exponents of the OH^-, H_2O and O_2 activities, respectively, in equation

(11).* The values of α, λ, γ given in equation (12) were based on the reaction sequence, rate controlling step, ($HO_2 + e^- = HO_2^-$), and value of the transfer coefficient recommended by Krasilshchikov[18]. There are, of course, a very large number of reaction sequences and rate controlling steps which might be chosen. Calculations involving another rate controlling step ($O_2 + e^- = O_2^-$) yielded a good fit of the experimental data only when unrealistic values of b were employed.

Oxygen transport: Except for the region below the meniscus, oxygen transport should not be a limiting factor. The numerical results show that throughout and across the entire length of the film, the activity of oxygen is very close to unity**, i.e., nearly identical to the activity at the electrolyte-gas interface. However, once one moves below the meniscus where the diffusion path for the oxygen becomes large, the oxygen activity drops quickly resulting in the rapid decrease in current density below the top of the intrinsic meniscus.

Rate controlling process: Since our model shows that the oxygen activity does not vary noticeably in the thin film, it follows that the penetration of the reaction into the film depends on a balance between the charge transfer overpotential and resistance drop in the electrolyte. As stated in Part a, the qualitative differences between behavior of the nickel and silver electrodes also suggest this to be the case.

---

* Note that the parameter α is related to (but not the same as) the transfer coefficient.

** It should be remembered that although the activity remains constant, the concentration of oxygen varies along the length of the film due to the decreasing solubility with increasing KOH concentration.

Will[3] in his work with the hydrogen electrode on platinum found that the transport of hydrogen gas to the electrode surface through the thin film was controlling, along with ohmic resistance drop. except at very low currents. This is not necessarily in contradiction with the results found for the oxygen electrode.

The hydrogen electrode on platinum is much more reversible than is oxygen on silver. Consequently, the concentration of current in the immediate vicinity of the intrinsic meniscus is rendered less possible in the case of oxygen, and charge transfer overpotential along with the ohmic drop in the film can be expected to control the current distribution.

Conclusions

1. Oxygen transport is not limiting in the thin upper film. The current density distribution in this region arises from a balance between charge transfer overpotential and resistance drop in the film.

2. Below the intrinsic meniscus, the bulk electrolyte region, the oxygen activity decreases rapidly due to the mass transport limitations of dissolved oxygen. Thus, the current density is small in this region.

3. The high concentration gradients which result when water is not supplied from the gas phase point to the desirability of supplying water as vapor in the oxygen gas.

Nomenclature

A, B, G - subsidiary transport properties defined so as to reduce the concentration dependence (Å).

a - mean molar activity of KOH = $f_{\pm}c$.

c - $c_+/\nu_+ = c_-/\nu_-$ - concentration of KOH (mole/cm^3).

c_1 - concentration of oxygen (mole/cm^3).

c_1^o - saturation concentration of oxygen under a partial pressure of 1 atm. (mole/cm^3-atm).

c_+ - concentration of K^+ (mole/cm^3).

c_- - concentration of OH^- (mole/cm^3).

c_o - concentration of water (mole/cm^3).

$c_T = c_+ + c_- + c_o$ - total concentration (including solvent).

D_1 - diffusion coefficient of oxygen in aqueous KOH (cm^2/sec).

$\mathfrak{D}$ - molecular diffusion coefficient of KOH based on activity gradients (cm^2/sec).

e - electronic charge (coulombs).

e^- - symbol for an electron.

$f_{\pm}$ - mean molar activity coefficient. (Values from reference 33 were used.)

F - Faraday's constant (coulombs/equivalent).

$\underline{i}$ - current density in the solution (amp/cm^2).

i_o - exchange current density (amp/cm^2).

J - transfer current density (amp/cm^2).

k - kinetic parameter related to exchange current density.

N_+ - flux of k^+ (mole/cm^2-sec).

N_- - flux of OH^- (mole/cm^2-sec).

N_o - flux of H_2O (mole/cm^2-sec).

p - partial pressure of oxygen (atm).

Q - one when H_2O is transferred in liquid phase, zero when H_2O transferred in the gas phase

R - universal gas constant (joule/mole-°K).

$t^\star$ - transference number of species i with respect to molar average velocity.

T - absolute temperature (°K).

$v^\star$ - molar average velocity (cm/sec).

x - coordinate perpendicular to the plane of the electrode (cm).

y - coordinate parallel to the electrode in the vertical direction, the independent variable (cm).

z_i - valence or charge number of species i (negative for anions).

α - kinetic parameter related to reaction order of oxygen and to the transfer coefficient.

γ - kinetic parameter indicating reaction order of H_2O.

δ - film thickness crons).

Δ - width of annular electrolyte region below meniscus (cm).

η - overpotential referred to a reversible oxygen electrode (volts).

κ - conductivity (mho/cm).

λ - kinetic parameter indicating reaction order of OH^-.

μ_e - chemical potential of KOH (joule/mole). (RT $ln\ f_\pm\ c$).

μ - viscosity (poise).

ν_+ - number of cations per molecule of electrolyte.

ν_- - number of anions per molecule of electrolyte.

$\nu = \nu_+ + \nu_-$.

Φ - overpotential referred to a reversible Hg/HgO electrode (volts).

APPENDIX

Notes on the Kinetic of the Oxyger Electrode

There has been accumulated a body of information which suggests that hydrogen peroxide is an intermediate in oxygen reduction[19-31, 34-38]. Although the evidence is fairly conclusive for such electrodes as Ag, Hg, C, and Au, it appears that there may be competing sequences of steps on such electrodes as Pt and Ni[17,31,34,37]. At this point only the former category of electrodes appears amenable to a simple kinetic analysis.

A review of the above mentioned references indicates that the assumption of the following sequence of elementary kinetic steps is reasonable on Ag, Hg, c, and Au electrodes.

(1) $O_2 + M = MO_2$
(2) $MO_2 + e^- = MO_2^-$
(3) $MO_2^- + H_2O = MHO_2 + OH^-$
(4) $MHO_2 + e^- = MHO_2^-$
(5) $MHO_2^- + H_2O = MH_2O_2 + OH^-$
(6) $MH_2O_2 + e^- = MOH\ OH^-$
(7) $MOH + e^- = M \quad OH^-$

The M represents an adsorption site, and when associated with a molecular symbol implies that the molecule is adsorbed. It is possible for any adsorbed molecule on the right side of an equation to desorb before reacting in the next step. The O_2^- and HO_2 are so reactive that this is unlikely. The desorption of HO_2^- or H_2O_2 (depending on the pH) could occur. However, there is evidence[20, 25] which indicates that on silver

and in alkaline solution the rate of desorption is small compared to reaction by steps (6) and (7). It should be noted that because the O_2^- and HO_2 radicals are very reactive, they have not been positive identified.

It appears that the adsorption step is not rate controlling and that either step (2) or (4) is rate determining. The choice appears to depend on pH and on the electrode material. For silver in alkaline solution step (4) appears to be rate controlling. With these assumptions, the kinetic expression can be written as

$$J = k[O_2]^{\frac{\alpha_4+2}{4}} [H_2O]^{\alpha_4}[OH^-]^{(1-\alpha_4)} \left\{ e^{\frac{(\alpha_4-2)F\eta}{RT}} - e^{\frac{(\alpha_4+2)F\eta}{RT}} \right\}$$

where J is the local transfer current density, α_4 is the transfer coefficient for step (4), η is the local overpotential, and k is a kinetic rate constant. Brackets signify the activity of the enclosed species.

LITERATURE CITED

1. Douglas N. Bennion and Charles W. Tobias, "Current Distribution at a Gas-Electrode-Electrolyte Interface. Part a) Experimental Treatment", page 16, this report.

2. Carl Wagner, "Polarization Characteristics of Gas-Electrodes in Stagnant Electrolytes," private communication dated June 13, 1957.

3. Fritz G. Will, "Electrochemical Oxidation of Hydrogen on Partially Immersed Platinum Electrodes, I: Experiments and Interpretation," J. Electrochem. Soc., 110, 145 (1963).

4. Fritz G. Will, "Electrochemical Oxidation of Hydrogen on Partially Immersed Platinum Electrodes, II: Theoretical Treatment," J. Electrochem. Soc., 110, 152 (1963).

5. E. A. Grens II, R. M. Turner and T. Katan, "A Model for Analysis of Porous Gas Electrodes," a paper presented before the Division of Fuel Chemistry, American Chemical Society, New York, New York, September 1963.

6. I. G. Gurevich, "The Operation Mechanism of a Diffusion Electrode (Applicable to Hydrogen-Oxygen Fuel Elements)," Inzhener. Fiz. Zhur., Akad. Nauk Belorus, SSR, 2, 78-86 (1959).

7. John A. Rockett, "The Performance of Porous Fuel Cell Electrodes," (Pratt and Whitney Aircraft, East Hartford, Connecticut), Extended Abstracts of Battery Division, Vol.8, Fall meeting Electrochem. Soc., 1963.

8. Raymond P. Iczkowski, "Polarization Characteristics of the Hydrogen Gas Diffusion Electrode," J. Electrochem. Soc., 111. 605-609 (1964).

9. R. Chs. Burshtein, V. S. Markin, A. G. Pshenichnikov, V. A. Chismadgev, and Y. G. Chirkov, "The Relationship between Structure and Electrochemical Properties of Porous Gas Electrodes," Electrochimica Acta, 9, 773-787 (1964).

10. John S. Newman and Charles W. Tobias, "Theoretical Analysis of Current Distribution in Porous Electrodes," J. Electrochem. Soc., 109, 1183-1191 (1962).

11. Edward A. Grens II and Charles W. Tobias, "Analysis of the Dynamic Behavior of Flooded Porous Electrodes," Ber. Bunsen Gesell., phys. chem., 68, 236-249 (1964).

12. J. Euler and W. Nonnenmacher, "Stromverteilung in Porösen Elektroden," Electrochimica Acta, 2, 268-286 (1960).

13. Rolf H. Müller, "Optical Studies of Electrolytic Films on Metal Surfaces," paper presented before the Electrochemical Society, Toronto, May 1964.

14. John S. Newman, Douglas N. Bennion, Charles W. Tobias, "Mass Transfer in Concentrated Binary Electrolytes," Project IV, this contract, page .

15. Douglas Noel Bennion. Phenomena at a Gas-Electrode-Electrolyte Interface. Dissertation, University of California, Berkeley, June 1964, Tech. Rpt. 3, this contract.

16. Klaus J. Vetter, Electrochemische Kinetik, Springer-Verlag, Berline, 1961.

17. Donald T. Sawyer and Leonard V. Interrante, "Electrochemistry of Dissolved Gases. II. Reduction of Oxygen at Platinum, Palladium, Nickel and other Metal Electrodes" Journal of Electroanalytical Chemistry 2, 310-327 (1961).

18. A. I. Krasilshchikov, "Electrochemical Reactions of Oxygen," Soviet Electrochemistry, Trudy 4-go Soveshchaniya Po Elektrokhimi, II, (1956). (English trans. Soviet Electrochemistry, Vol II, Consultants Bureau New York 1961).

19. J. O'M. Bockris and A. K. M. Huq, "The Mechanism of the Electrolytic Evolution of Oxygen on Platinum," Proceedings of the Royal Society of London, A237, 277-296 (1956).

20. A. I. Krasilshchikov, "Kinetics of the Cathodic Reduction of Oxygen," Zhurnal Fizicheskoi Khimii, 26, 216-223 (1952).

21. A. I. Krasilshchikov, "Air Depolarization of a Nickel Cathode," Zhurnal Fizicheskoir Khimii, 21, 849-854 (1947).

22. I. D. Nefedova and A. I. Krasilshchikov, "Study of a Silver Cathode in the Presence of Dissolved Oxygen," Zhurnal Fizicheskoi Khimii, 21, 855-862 (1947).

23. A. I. Krasilshchikov, "Processes of Depolarization of Oxygen," Zhurnal Fizicheskoi Chimii, 23, 332-338 (1949).

24. A. I. Krasilshchikov and V. A. Andreeva, "Kinetics of Ionization of Oxygen," Zhurnal Fizicheskoi Khimii, 27, 389-393 (1953).

25. T. N. Belina and A. I. Krasilshchikov, "Kinetics of the Electrochemical Reduction of Oxygen," Zhurnal Fizicheskoi Khimii, 28, 1286-1291 (1954).

26. V. S. Bagotskii and I. E. Yablokova, "Mechanism of Electrochemical Reduction of Oxygen and Hydrogen Peroxide on a Mercury Electrode," Zhurnal Fizicheskoi Khimii, 27, 1663-1675 (1953).

27. W. G. Berl, "A Reversible Oxygen Electrode", Transactions of the Electrochemical Society, 93, 128 (1948).

28. R. S. Weizz and S. S. Jaffe, "The Mechanism of the Reduction of Oxygen at the Air Electrode," Transactions of the Electrochemical Society, 93, 128 (1948).

29. Myron O. Davies, M. Clark, E. Yeager, and F. Hovorka, "The Oxygen Electrode," J. Electrochem. Soc., 106, 56-61 (1959).

30. Ernest Yeager and Akiya Kozawa, "Kinetic Factors in Fuel Cell Systems: The Oxygen Electrode," paper presented before the Sixth AGARD Combustion and Propulsion Collogquium on "Energy Sources and Energy Conversion," Sponsored by NATO, Cannes, France, 16-20 March 1964.

31. James J. Lingane, "Chronopotentiometric Study of Oxygen Reduction at a Platinum Wire Cathode," Journal of Electroanalytical Chemistry, 2, 296-309 (1961).

32. L. N. Nekrasov and L. Muller, "The Use of a Rotating Disk Electrode with a Ring in Studying the Cathodic Reduction of Oxygen on Platinum in Alkaline Solutions," Akademiia Nauk SSSR, 149, 5 (Physical Chemistry Section) 1107-1110 (1963).

33. R. A. Robinson and R. H. Stokes, "Tables of Osmotic and Activity Coefficients of Electrolytes and their Mixtures," Ind. and Eng. Chem., 4, 461-6 (1935).

34. W. G. Berl, "A Reversible Oxygen Electrode", Trans. Electrochem. Soc., 83, 253 (1943).

35. R. S. Weizz and S. S. Jaffe, "The Mechanism of the Reduction of Oxygen at the Air Electrode," Trans. Electrochem. Soc. 93, 128 (1948).

36. A. Frumkin, L. Nekrasov, B. Levich and Ju. Ivanov, "Die Anwendung der Rotierenduen Scheibenelektrode Mit Einem zur Untershucung von Zwischenprodukten Elektrochemischer Reaktionen", Journal of Electroanalytical Chemistry, 1, 84-90 (1959).

37. A. I. Krasilshchikov, "Electrochemical Reactions of Oxygen", Soviet Electrochemistry, Trudy 4-go Soveshchaniya Po Elektrochimi, II, (1956). (English Transl., Consultants Bureau, N.Y., 1961).

38. Klaus, J. Vetter, "Electrochemische Kinetik," Springer-Verlag, Berline, 1961.

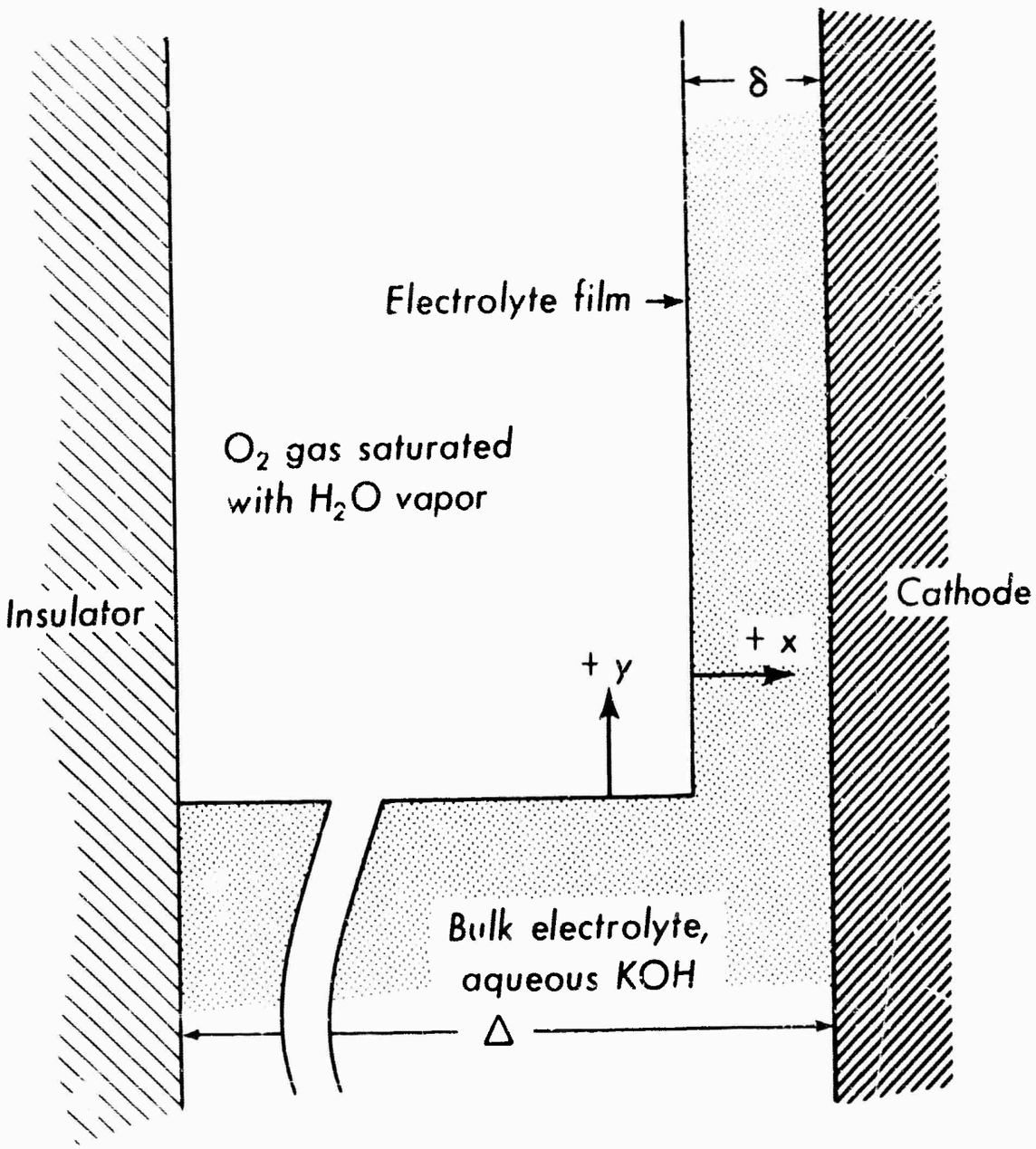

Figure 1. Mathematical model of the gas electrolyte-electrode interface.

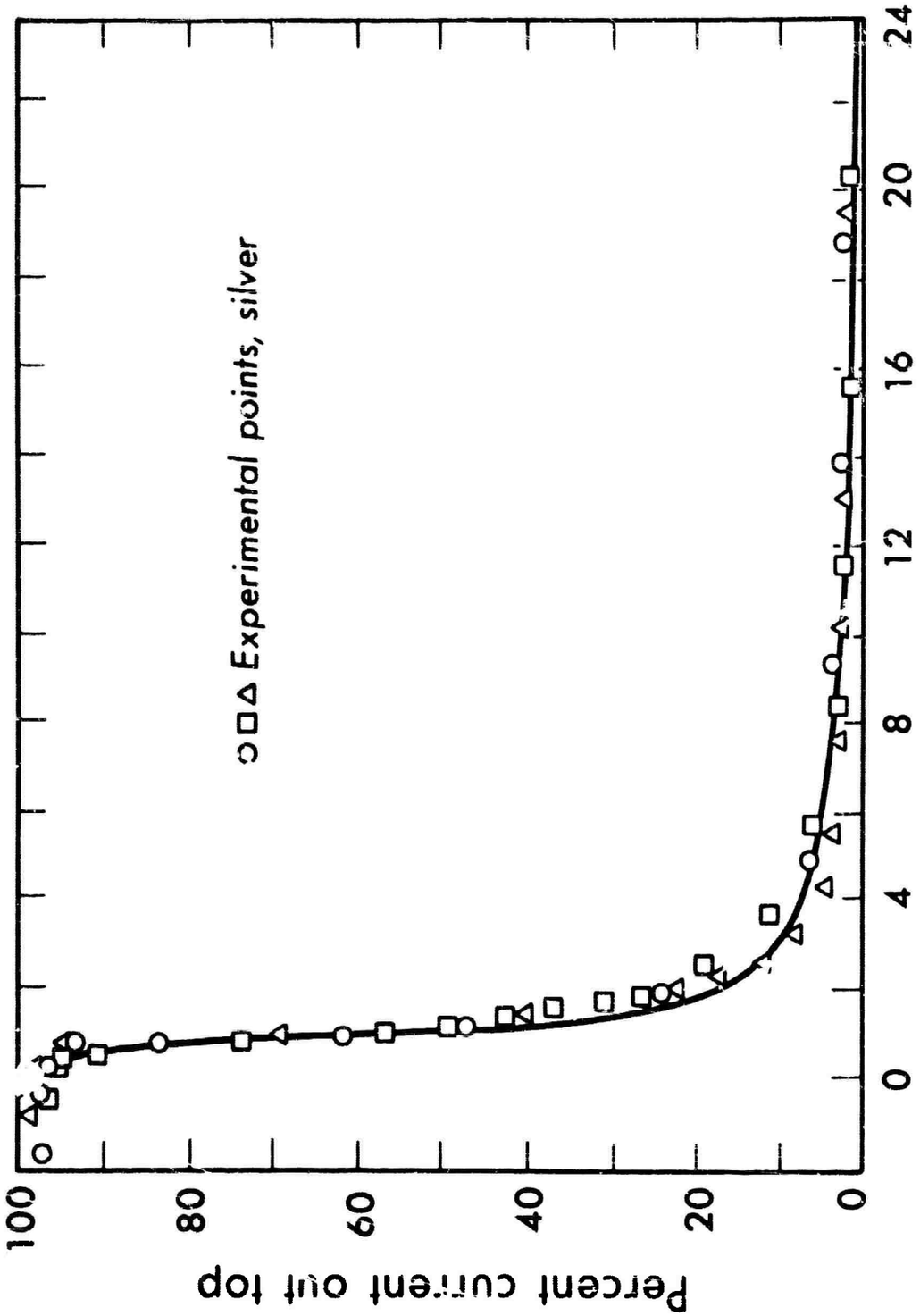

Figure 2. Comparison of experimentally observed current distribution with the distribution calculated using the theoretical model. Nickel cathode, I = 154 μA/cm. Cell no. 4, runs 7, 9 and 12. Numerical solution with δ = 2.25 μ, i_o = 1.[illegible] x 10^{-9} A/cm^2.

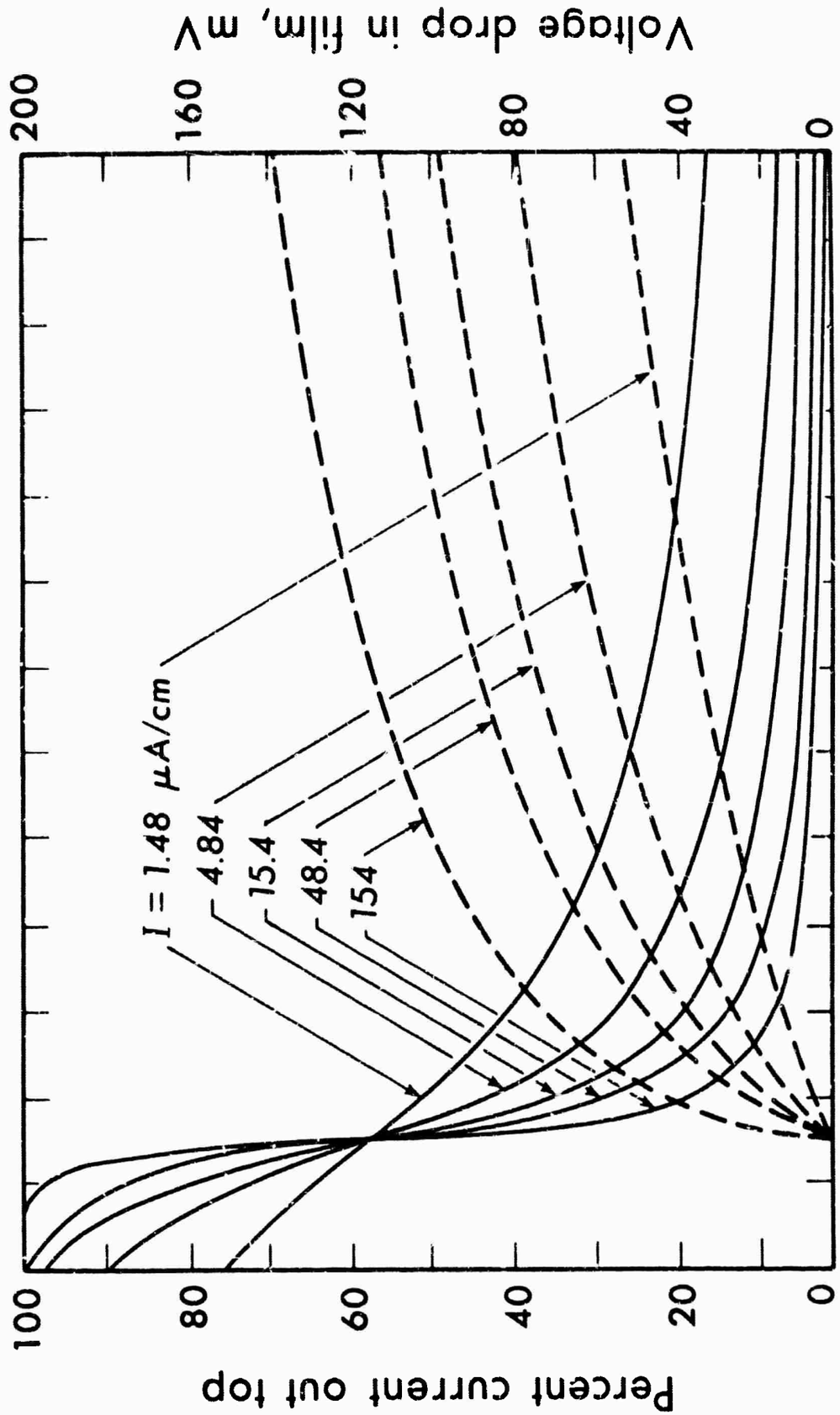

Figure 3. Theoretical variation of potential, and percent current above a fixed level on the electrode as a function of applied current.

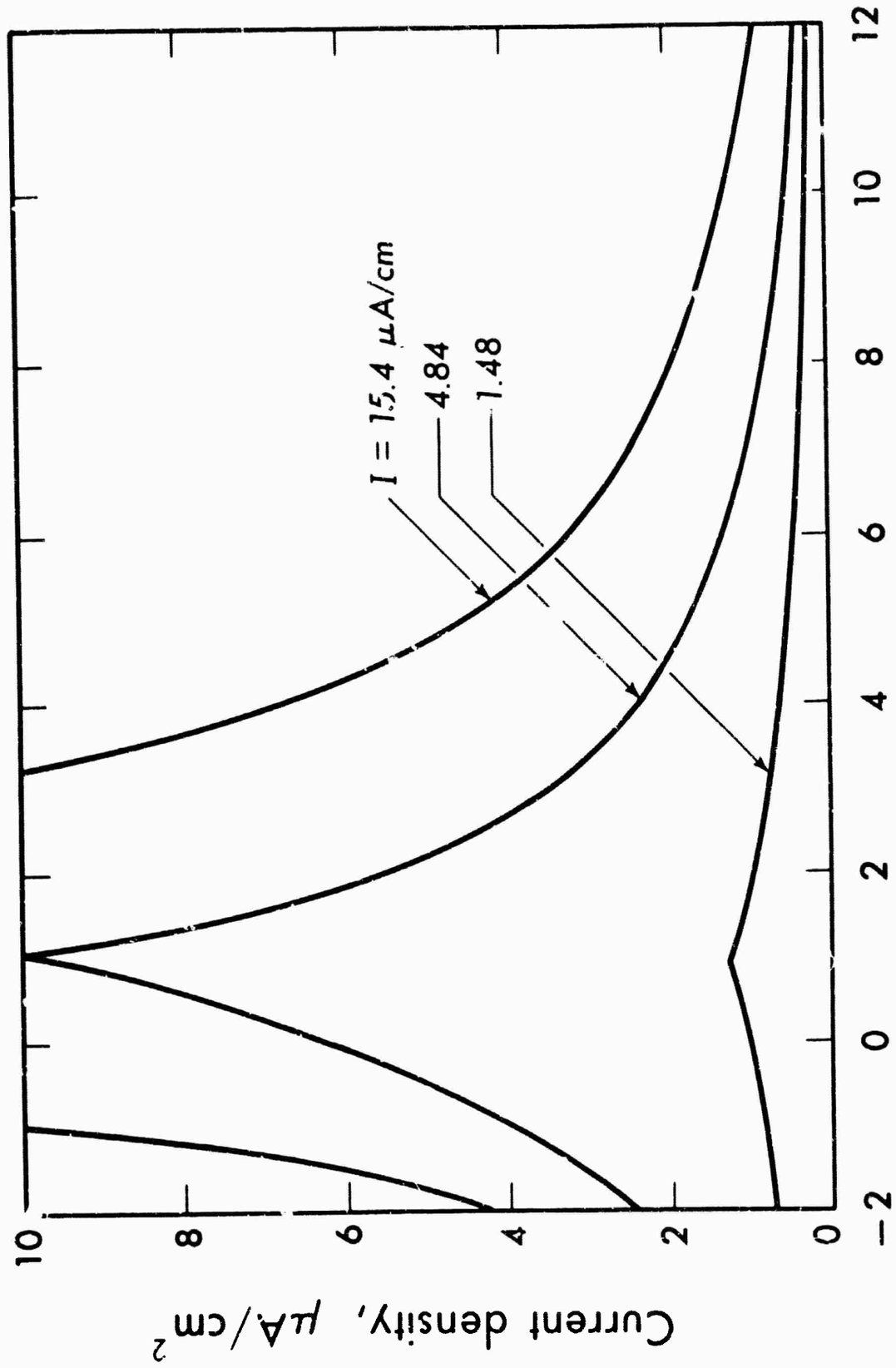

Figure 4. Theoretical current density distribution relative to the position of the meniscus. Low current range.

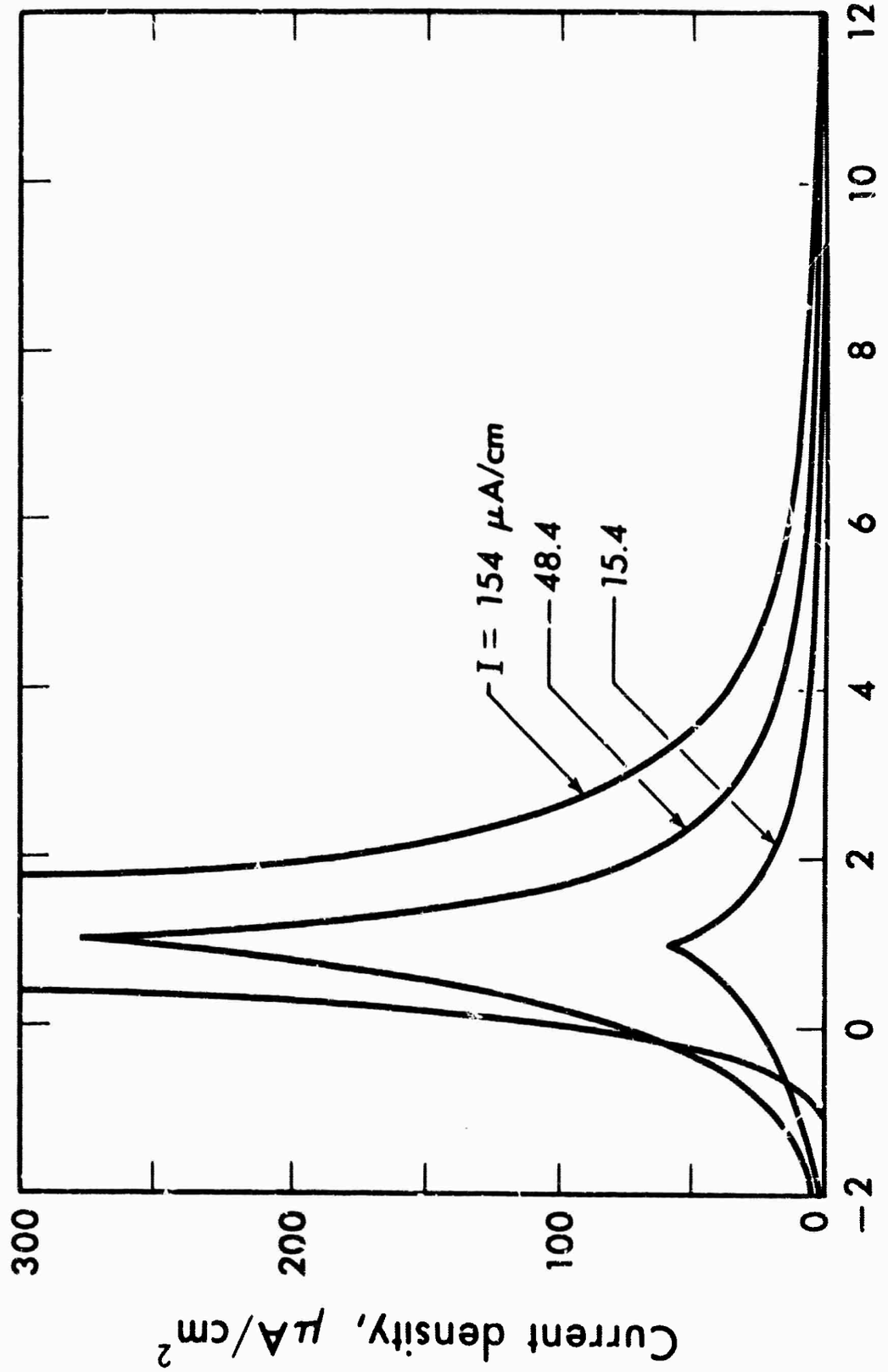

Figure 5. Theoretical current density distribution relative to the position of the meniscus. High current range.

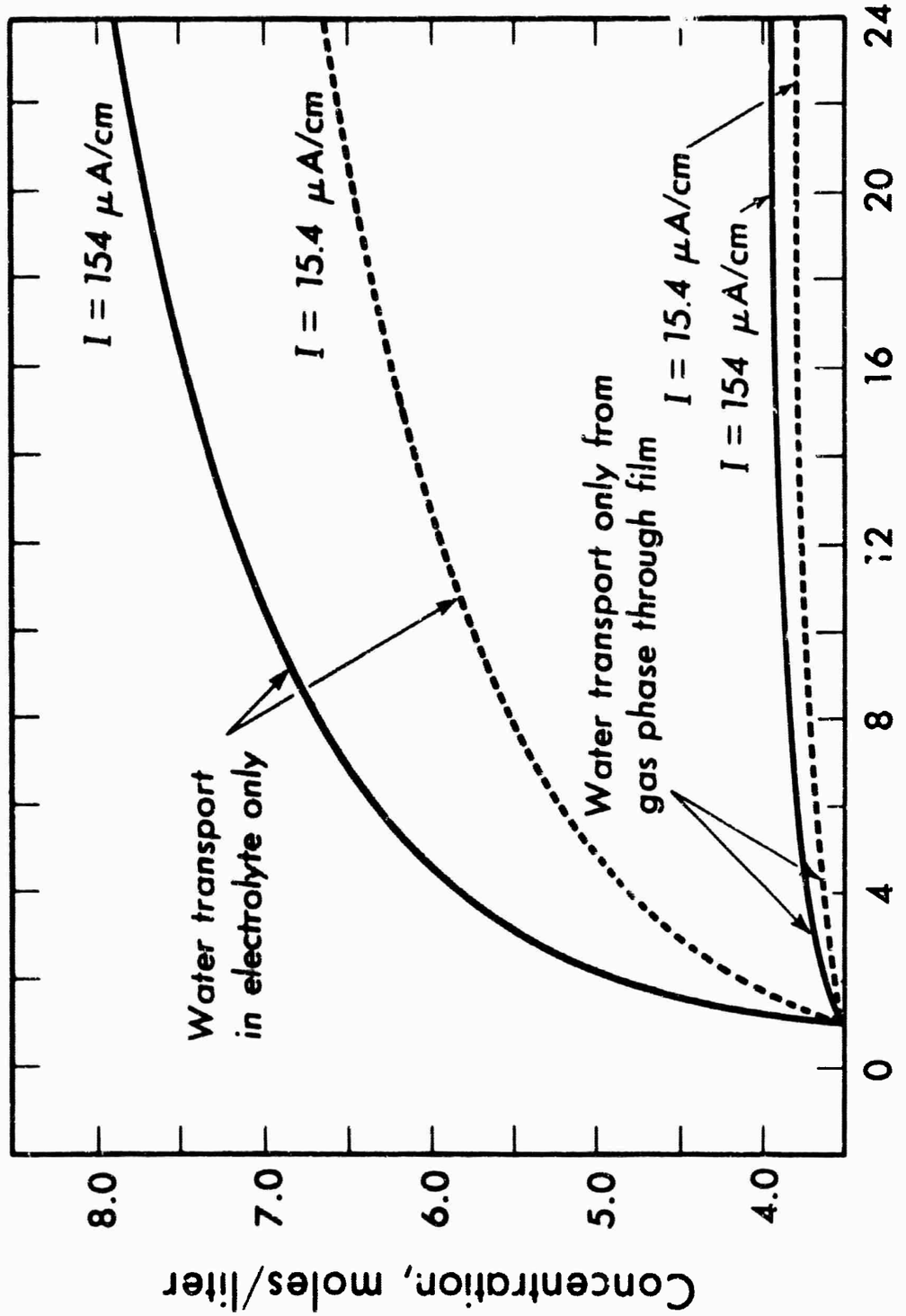

Figure 6. Calculated variation of KOH concentration in the electrolyte film.

PROJECT II.

Ionic Mass Transport by Combined Free and Forced Convection

The problem of hydrodynamic flow caused by density gradients existing in the vicinity of working electrodes has been the subject of numerous experimental and theoretical studies (10,17,18,31,32). The complex nature of the role of solution properties, geometric factors and current densities in the case of laminar or turbulent free convection at vertical electrodes is reasonably well understood, and satisfactory quantitative relations describing the functional relationships between pertinent process variables are available. Mass transport by free convection at horizontal electrodes has also been treated, and although the convectional mode is not well understood in this case, correlation of variables in dimensionless form proposed by Fenech and Tobias (10) quite satisfactorily predicts experimental behavior. Free convection, because of the high velocity gradients generated in the boundary layer adjacent to the electrode, provides a very effective mode of mass transport. In so-called unstirred solution "equivalent" mass transfer film thicknesses (29) in the order of a few tenths of millimeters are commonly encountered.

Examination of typical laboratory and industrial electrolysis conditions reveals that stirring (or bulk flow)

rates are often not adequate to overshadow the effects of free convection.

The scientific literature appears to be void of studies aimed at the clarification of the effects of combined free and forced convection on mass transfer rates. A general theoretical description of the convectional modes in the presence of free and forced convection represents a formidable task (2,12,24,30). Rudimentary experimentation on the analogous heat transfer case in the 1930's (3,14,26) did not lead to quantitative description of the phenomena observed. Attempts at correlating experimental results have been unsuccessful (1,20).

For the case of pure laminar forced convection experimental and theoretical investigations have provided a reasonable basis for prediction of ionic mass transport rates. Lin et al (22) found that in the cell of annular geometry, limiting currents on the outer electrode are well represented by

$$Nu'_d = 1{\cdot}62(Re.Sc.d/L)^{1/3} \qquad (1)$$

This equation is based on the Leveque approximation and is applicable when the velocity profile is fully developed in the electrolyte approaching the leading edge of the electrode. It should be noted that the equation applies only when the concentration profile is still not fully developed at the trailing edge of the electrode. Except for extremely low flow rates, this condition would be met in typical situations

involving electrode reactions. On the basis of Norris and Streid's work on heat transfer in rectangular flat ducts (25), one would expect the numerical constant to change from 1·62 to 1·85 for the case of ionic mass transport in laminar flow to planar electrodes in rectangular channels:

$$Nu'_d = 1{\cdot}85(Re.Sc.d/L)^{1/3} \qquad (2)$$

The present investigation was undertaken to gain some insight into the nature of mass transport under combined free and forced convection conditions. As an experimental model, a horizontal channel type electrolytic cell was chosen. In such a cell, when the electrodes at which ions are consumed (e.g., a cathode at which a metal is deposited) faces upward, in the absence of bulk flow the electrolyte layer adjacent to the electrode becomes unstable, and except for the case of extremely dilute solutions, turbulent eddies are formed. The distribution of eddies over the electrode surface is statistically uniform, and as a consequence the effective mass transfer boundary layer thickness over extended horizontal electrode surfaces does not vary with position (11). In a typical case, the turbulent eddy motion extends only a few millimeters from the surface; above this distance any opposing limiting surface has no noticeable effect on the transport rates (11).

Limiting currents in pure free convection extended over horizontal electrode surfaces were successfully correlated

by Fenech and Tobias (10), who found that

$$Nu'_L = 0{\cdot}19(Gr_{L^3}Sc)^{1/3} \qquad (3)$$

represents the experimental values in the range of $10^8 < Gr.\ Sc < 1{\cdot}4 \times 10^{12}$ with a correlation coefficient of 0·994.

If one introduces a steady state bulk flow into a horizontal electrolyzer, the viscous shear near the walls interferes with the development of the turbulent free convection motion in the boundary layer. At the leading electrode edge the mass transfer boundary layer thickness is zero, and only at some distance downstream will appreciable boundary layer thickness develop. Eventually this thickness exceeds the stability limit, and motion due to the gravitational field will begin. Proceeding further downstream, the boundary layer reflecting the contributions of both forced and free convection reaches a steady state conditions. This qualitative image of the transport process indicates that, unlike in the case of pure free convection, current densities will change in the direction of flow - probably from a high initial value at the leading edge to some steady state value downstream.

EXPERIMENTS

Limiting currents were measured in a cell that was designed to yield values of average and local mass transfer rates over a broad range of the pertinent variables. The cell had separate parallel flow channels for the anolyte and catholyte as shown in isometric section in Figure 1. The channels were separated by a lucite plate, except between the

anode and cathode, where a porous ceramic separator was used. This separator permitted free passage of ions but insured that there would be no disturbance at the cathode by the hydrodynamic effects from the dissolution process occurring at the anode. A saw-toothed profile was cut into the anode to minimize the possibility of reaching the saturation conditions at the anode during experiments with high concentrations of copper. This possibility was further decreased by the dual set of channels which made possible a higher flow-rate past the anode than past the cathode. The 60 cm entrance length necessary to always insure a fully developed velocity profile was calculated by the methods proposed by Han (15). The flow channel dimensions could be altered by placing lucite inserts into the channel.

The cathode fit into a holder that was clamped to the side of the cathode flow channel, so that the electrode surface was coplanar with the rest of the duct wall. This holder could accommodate two types of electrodes: continuous electrodes of various lengths for use in experiments designed to yield average mass transfer coefficients and a sectioned electrode (11,23) for use in obtaining local mass transfer rates.

In the latter case, the general technique of cutting the electrode into segments, insulating the segments from one another, and then measuring the current flowing to each segment. Within the cathode holder were the electrode contacts,

the low resistance shunts for measuring segments currents, and a switching circuit for calibrating the shunt resistances. Starting from the leading edge the segment lengths were 0·5, 0·5, 1, 2, 3, 3, 5, 5, 8, and 8 cm for a total electrode length of 36 cm. The segments were insulated from one another by 0·004 inc. polyethylene sheeting and electrically contacted from the rear by twist screws. The entire assembly was fitted with large wheels and mounted on rollers so that the cell could be oriented with the cathode facing either upward or downward. This feature was found to be very useful, as will be shown later.

For the segmented electrode to truly represent the corresponding continuous electrode, it was important that the segments all be coplanar and equipotential. The first condition was met by polishing the segments to a coplanar surface in a special jig that held the segments in the same position as they assumed in the cathode holder. The second requirement could not be exactly met. During the electrodiposition of copper from the acid solution, the overpotential plateau at limiting current reaches approximately half a volt before hydrogen evolution begins. Limiting current measurements are made on the upper end of the plateau, so the electrode overpotential is usually in the order of 400 to 500 mv. It was arbitrarily decided that a satisfactory approximation to an equipotential electrode would be one in which the potential of any two segments did not differ by more than two

millivolts. With this approximation, measurements of the individual section currents was straightforward. Very low resistance shunts were introduced between a busbar and the electrode segments. The potential drops across them were selected sequentially amplified with a low noise D.C. amplifier and then read out on a multipoint printing recorder. This circuit is shown schematically in Figure 2. Contact resistances between the busbar and the electrode segments were kept to a minimum by silverplating all the mating parts. Limiting current curves were plotted continuously on an x - y recorder while current was passed through the cell by a programmed current source which provided a preset linear increase of current with time. This device is described in detail elsewhere (16). Electrolyte was continuously pumped through both flow channels and its flowrate was measured with calibrated rotameters.

PROCEDURE

The following consecutive steps were made during the performace of each experiment:

1. The cathode was polished with number 600-A silicon carbide paper until all trace of the previous deposit disappeared. Surface was dusted with lint-free paper and degreased with acetone.

2. Cathode was mounted in the cathode holder and the holder clamped to the body of the cell. Electrodes were connected to the current source and measuring circuitry.

3. The pump was turned on and the flow channels were filled with electrolyte, carefully expelling all air bubbles. Then the desired flowrate was set, current rate selected, and the measuring circuits put into operation.

4. The current was turned on. When limiting current was reached, the following data were recorded: limiting current, flowrate, electrode length, channel cross section, electrolyte used, measuring circuits used, and electrolyte temperature.

5. Following each run, the cell was disassembled and preparations were made for the next experiment.

6. The bulk concentrations of species in the electrolyte were determined by standard techniques of analysis (8).

7. The scheme developed by Fenech and Tobias (10) was used throughout to calculate the physical properties and the dimensionless groups.

Table 1. Range of variables covered.

The ranges of variables covered in this investigation were as follows:

Electrode length(cm)	0·2, 0·5, 1, 2, 5, 10, 20, 30, 36
Channel cross section (cm)	2 x 10, 1 x 10, 1 x 8, 1 x 5
Viscosity (cps)	1-12
Density (g/cm^3)	1·1-1·3
Velocity (cm/sec)	0-35
Concentration of Cu(M)	0·01-0·45
Schmidt number	600-12,000
Reynolds number	75-7000
Grashof number	10^5-10^{12}
Electrode Length/Duct Diam.	0·05-20

QUALITATIVE OBSERVATIONS

From the appearance of the electrode deposits obtained on continuous cathodes, it was evident that there was a considerable variation in current density in both the direction of bulk flow and in the transverse direction. Variation of current density in the direction of flow was, of course, predictable from forced convection theory, but it appeared that the magnitude and distribution of the nonuniformity was quite different from that expected. A typical deposit is shown in Figure 3. To explain the appearance of the streaked deposit it is suggested that a secondary convection effect was present which took the form of "roll cells" with a velocity profile similar to that shown in Figure 4 The secondary convection results from an instability which is caused by the density gradient across the mass transfer boundary layer. Such an explanation finds support in the fluid dynamics and heat transfer literature (3,4,13,30). It should be noted that the scale of periodicity of the electrode deposit was in the order of half a millimeter after the roll cells have grown to a fully developed array across the electrode surface.

On the basis of this observation, the significant length in the Rayleigh number (equal to the product of the Grashof and Schmidt numbers) which determines the stability of the system should be the distance across which the density difference is manifest. In the system under consideration

here, this distance is the mass transfer boundary layer thickness, δ. For flow between flat plates with a fully developed velocity profile at the leading edge of the transfer section, this is given by (21)

$$\delta = A(d^2.x/Re.Sc)^{1/3} \qquad (4)$$

Experiments were performed on a 30 cm electrode to see how the onset of this secondary convection pattern was influenced by the bulk velocity of the electrolyte. From eqn. (4) it can be seen that if the physical and geometric parameters of a system are held constant, δ varies as $(x\ V$ $(x/V)^{1/3}$. Therefore one might expect that the onset of instability will occur at positions on the electrode which correspond to the same value of the Rayleigh number. Since the Rayleigh number varies as the cube of δ, at some constant value of δ the position at which the vortices begin should be linear in the bulk velocity. That this is actually the case is shown in Figure 5.

As might be expected, the presence of roll cells has a pronounced effect on the local mass transfer process. In the direction normal to the bulk flow, variations in deposit thickness were measured by two optical methods. The first were made on a microscope equipped with a movable stage that could be located in two directions with an accuracy of one micron. The barrel could be positioned with the same accuracy. Using 250 x magnification, the depth of focus was reduced to about one micron, and a two dimensional relief of

the surface normal to the direction of flow was made before and after deposition. The thickness of the copper deposit was then obtained with an accuracy of ±2 microns by taking the difference of the two profiles. Representative deposition profiles are shown in Figure 6. Within the accuracy of the optical technique employed, the measured average thickness of the deposits agreed with that calculated from Faraday's law. The profiles indicate that the character of the deposits caused by the presence of roll cells is essentially independent of flowrate and deposition rate.

The physical nature of the grooves in the deposit was also asserted by photomicrography. After prolonged (up to one hour) electrolysis at limiting current, electrodes were metallographically sectioned, transverse to the direction of flow and photographed at low-power magnification. The photomicrographs gave similar profiles to the one illustrated in Figure 6.

Local mass transfer rates in the direction of flow were measured with sectioned cathodes. Typical smoothed data obtained with this technique are given in Figures 7 through 11. On each figure, a series of experiments with the same electrolyte is shown, the independent variables then being limited to the velocity and electrode orientation. With the cathode facing upward, both convective processes are operative, whereas the inverted position causes stratification of the electrolyte during deposition and only pure forced convection occurs. The natural convective

contribution to the local mass flux can therefore be obtained as the difference between the curves for the two cell orientations.

The following observations and comments can be made regarding these curves:

1. At the leading edge and for some distance downstream, the current density distribution is independent of the electrode orientations.

2. At some position downstream from the leading edge a considerable increase of current density above that for pure forced convection occurs for the orientation resulting in superimposed free convection. The position of current rise was always found to correspond to the appearance of the streaks in the deposit.

3. Regardless of the velocity of flow, for a given electrolyte with the cathode facing upward it appears that the value of current density far down the electrode reaches or approaches the same steady state value. On many of the experiments the electrode was not sufficiently long to allow this value to be reached.

4. For systems with relatively large Rayleigh numbers (i.e., systems with low velocity [see eqn. (4)], high density differences [high copper concentrations], and low viscosities), the increase in current density above that for the pure forced convection case occurs closer to the leading edge.

5. Even at high laminar Reynolds numbers, natural convection can play a very important role. If the electrode is sufficiently long, it can be expected to dominate the mass transfer process.

6. In many of the experiments dominated by free convection, the initial rise in current density is not maintained, but gradually declines to some lower value farther long the electrode. This behavior is particularly marked in systems with a high Rayleigh number, where the character of electrode deposits after the onset of roll cells gradually changes from well-defined streaks to no streaks at all. This suggests a transition to a turbulent mode of free convection near the interface as the mass transfer boundary layer increases (higher Rayleigh number). In experiments where the streaks retained their identity for the full length of the electrode, a drop in current density is still present, suggesting that the initial vortex motion is in unsteady state, and some time is required before the fully developed convectional mode is established.

From these observations, a fair understanding of the combined flow processes begins to emerge. As the electrolyte flows past the electrode at limiting current, an increasing mass transfer boundary layer thickness raises the Rayleigh number leading to an instability. Due to the inertia of the electrolyte some time passes before the instability causes a significan roll cell motion. During

this incubation period the pure forced convection mode of mass transfer continues making the system increasingly unstable. Finally, at some position on the electrode downstream from the point of initial instability, roll cell motion begins, but on a short electrode, the unstable fluid may be swept off the electrode before the buoyancy forces can influence the fluid dynamic conditions. Prior to the onset of the natural convective motion the mass transfer process appears to be the same as for pure forced convection, even though buoyancy forces are present.

Onset of roll cells was found to be a function of the size and number of the imperfections on the electrode surface, just as in the case of initiating turbulence (5,9). It was observed that a small dent in the surface or a small bubble sticking to the surface could initiate a roll cell 2 or 3 cm before the others.

CORRELATION OF DATA

Several hundred experiments were performed with continuous cathodes and laminar bulk flow to develop a general correlation which could be used to predict average mass transfer coefficients.

It was hoped that it would be possible to define the limits of the flow regime in which the superimposed convective processes both play important roles in the mass transport, so that all experimental systems outside this regime could be dealt with by using the existing correlations for

either pure free or pure forced convection. Such a scheme is appealing because from physical reasoning it is to be expected that at high flowrates and very small density differences, forced convection should dominate the mass transfer process. Conversely, if the bulk flowrate is very slow and the density difference between the bulk and interface is very large, natural convection should dominate.

Previous work on heat transfer from vertically orientated plates into laminar fluid streams (6) indicated that three flow regimes could be defined as shown in Figure 12. As a first attempt for the correlation of the present data, therefore, the position of these two lines was sought. First, for each value of d/L the slope and position of line A was established in such a manner as to result in the least standard deviation of all data points lying above it from eqn. (3) for pure free convection control. Similarly, the position of line B was established, yielding the best agreement of the data points below it with eqn. (2) for pure laminar forced convection. In comparing the data points with the above correlations, the significant lengths may be chosen as the electrode length, or the hydraulic diameter. It was found that if the electrode length was used in the Grashof number, and the hydraulic diameter in the Reynolds number, lines A and B coincide with a slope of unity.[1]

---

[1] It should be noted that the length dimension in eqn. (3) cancels out. Thus, the choice of the electrode length as the significant dimension serves only to determine which convectional mode is dominant. For a given electrolyte composition and flow velocity, the longer the electrode, the more influence free convection effects will have.

When the mass transfer coefficient expressed from eqns. (2) and (3) are equated along the separating line, we obtain

$$\frac{D}{d}\,1{\cdot}85\left(\mathrm{Re.Sc.}\,\frac{d}{L}\right)^{1/3} = \frac{D}{L}\,0{\cdot}19(\mathrm{Gr}_{L^3}\mathrm{Sc})^{1/3} \qquad (5)$$

Cubing both sides and then taking logarithms, we have

$$\log\frac{L^2}{d^2} + 2{\cdot}964 + \log\,(\mathrm{Re.Sc}) = \log\,(\mathrm{Gr}_{L^3}\mathrm{Sc}) \qquad (6)$$

In agreement with the empirically obtained separating lines, $\log\,(\mathrm{Gr}_{L^3}\mathrm{Sc})$ is linear in $\log\,(\mathrm{Re.Sc})$ with a slope of unity, and the intercept is given by

$$\text{Intercept} = 2{\cdot}964 + \log\frac{L^2}{d^2} \qquad (7)$$

It is no longer necessary, therefore, to include the Schmidt number as a parameter, as it appears on both sides to the same power. If, in addition, the term $\log\frac{L^2}{d^2}$ of eqn. (6) is grouped with the Grashof number, a new Grashof number may be defined,

$$\mathrm{Gr}_{d^2L} = \frac{g\rho^2\Delta\rho_{d^2L}}{\mu^2\rho_i}$$

The resulting equation of the separating line is

$$2{\cdot}964 + \log\mathrm{Re} = \log\mathrm{Gr}_{d^2L}\,. \qquad (8)$$

This makes a separate plot for each value of d/L unnecessary and all the experimental data can be shown on one figure (Fig. 13). The points judged by this scheme

to be dominated by free convection are shown in Figure 14, as compared with eqn. (3), while in Figure 15 the points below the dividing line (forced convection control) are shown together with eqn. (2). The average deviation of all the points shown is seven percent. If it is assumed that the points in the two flow regions should be exactly predicted by the correlating equations appropriate to the respective modes of control, and if it is also assumed that all errors in the data are random, then confidence limits for the fit of the data to the equations may be calculated. This has been done, and the resulting confidence limits at the 95 per cent level are shown on both Figures 14 and 15.

The validity of using a Grashof number with $(d^2L)^{1/3}$ as the characteristic length can be partially rationalized from the following considerations: In the Rayleigh number which determines the stability of the system, the significant length should be δ, as given by eqn. (4). Since this distance appears to the third power in the Rayleigh number, at the end of the transfer section the Rayleigh (or Grashof) number is proportional to d^2L. While the actual value of δ is not used, the proper geometric parameters do appear and probably to the correct relative powers. Systems judged to be under forced convection control are those in which roll cell formation does not occur. Those under free convection control have both types of flow, but the average mass transfer coefficient for the entire electrode is nearly the same as for pure free convection.

EXPERIMENTS WITH TURBULENT BULK FLOW

In the case of turbulent bulk flow, one would not expect as marked an influence of the buoyancy forces as with laminar flow. The mass transfer boundary layer is thinner than for laminar flow, thus lowering the Rayleigh number of the system. In addition, the turbulent eddies continually penetrating the mass transfer boundary layer might be expected to dominate the mass transfer process, even if instability due to forces existed.

No theory or empirical correlation is available for describing the turbulent mass transfer entry region in a flat duct, making it impossible to predict either the average or local mass transfer rates. Again two of the sectioned cathodes were used. Experiments were performed under conditions which maximized the buoyancy forces, i.e., low flowrates and high copper concentration. Although the averaged data shown in Figure 16 indicate that at Re = 4000 and with the highest Cu^{++} concentrations employed there is some contribution due to free convection, already at Re = 5000 such differences could not be detected.

CONCLUSIONS

1. In the presence of buoyancy forces, average rates of ionic mass transport to horizontal electrodes in channel type cells may be predicted with satisfactory accuracy by:

a) The equation proposed by Fenech and Tobias

$$Nu'_L = 0{\cdot}19(Gr_{L^3}Sc)^{1/3}$$

when the process is controlled by free convection, or

b) The equation proposed by Norris and Streid

$$Nu_d = 1{\cdot}85(Re.Sc.d/L)^{1/3}$$

when superimposed laminar flow is the controlling convectional mode.

2. Laminar flow causes a nonuniform distribution of local transport rates; while the mass transfer coefficient decreases from the leading edge in pure laminar flow, onset of secondary convection (probably roll cells) causes an increase in local coefficients at a predictable distance downstream. At great distances from the entry region, the transport process is dominated by free convection.

3. Evidence of secondary convection, probably roll cell motion, is given by stratified deposits obtained in locations where free convection contribution to the transport process is significant.

4. When the bulk flow is turbulent (Re > 4000), the effect of free convection on mass transport rates appears to be negligible within the ranges of Rayleigh and Schmidt numbers, and d/L ratios considered in this study.

NOMENCLATURE

A	a constant
a	activity moles/l
b	subscript denotes taken in the bulk
C	concentration moles/l
d	equivalent duct diameter cm
D	diffusion coefficient cm^2/sec
ΔE	cathodic overpotential volts
F	Faraday's constant coul/eq
g	acceleration of gravity cm^2/sec
I_L	limiting current density A/cm^2
k_L	mass transfer coefficient cm/sec
L	electrode length cm
n	number of electrons per ion participating in the electrode reaction
R	universal gas constant cal/mole °C
t	transference number of cupric ion
T	temperature °C
X	location on electrode from the leading edge cm
δ	mass transfer boundary layer thickness cm
μ	viscosity gm/cm sec
ρ	density gm/cm^3
$\Delta\rho$	density difference between the bulk and interface gm/cm^3
Gr_{d^2L}	modified mass transfer Grashof number $\rho^2 d^2 L g \Delta\rho/\mu^2\rho_1$
Gr_{L^3}	modified mass transfer Grashof number $\rho^2 L^3 g \Delta\rho/\mu^2\rho_1$

Nu'_d mass transfer Nusselt number $k_L d/D$

Nu'_L mass transfer Nusselt number $k_L L/D$

Re Reynolds number $dV\rho/\mu$

Sc Schmidt number $\mu/\rho D$

LITERATURE CITED

1. Altman, M., and F. W. Staub: CEP Symposium Series 55 (1959) 111.

2. Casal, E. D., and W. N. Gill: J. AIChE 8 (1962) 570.

3. Chandra, K.: Roc. Roy. Soc., London A 164 (1938) 231.

4. Chandrasekhar, S.: "Hydrodynamic and Hydromagnetic Stability". Oxford Univ. Press, London 1961.

5. Charters, A. C.: NACA TN 891 March (1943).

6. Eckert, R. G., and A. J. Diaguila: Trans ASME 76 (1954) 496.

7. Eisenberg, M., C. W. Tobias and C. R. Wilke: J. Electrochem. Soc. 102 (1955) 415.

8. Eisenberg, M., C. W. Tobias and C. R. Wilke: J. Electrochem. Soc. 103 (1956) 434.

9. Emmons, H. W.: J. Aero. Sci. 18 (1951) 490.

10. Fenech, E. J., and C. W. Tobias: Electrochimica Acta 2 (1960) 311.

11. Fenech, E. J.: Ph.D. Thesis, Univ. of Calif., Berk., Dept. of Che (1960).

12. Gill, W. N., and E. D. Casal: J. AIChE 8 (1962) 513.

13. Görtler, H.: Ingenieur Archiv. 18 (1959) 463.

14. Graham, A.: Philos. Trans. A 232 (1933) 291.

15. Han, L. S.: J. App. Mech. 82 (1960) 403.

16. Hickman, R. G.: The Effect of Buoyancy Forces on Forced Convection Ionic Mass Transfer at Horizontal Planar Electrodes. Ph.D. Thesis, Univ. of Calif., Berk. 1963, Technical Report No. 2, this contract.

17. Ibl, N., and R. H. Müller: Z. Electrochem. 59 (1955) 671.

18. Ibl, N., and R. H. Müller: J. Electrochem. Soc. 105 (1958) 346.

19. Ibl, N.: Advances in Electrochemistry and Electrochemical Engineering, Vol. 2, Interscience Publishers, New York 1962.

20. Jackson, T. W., J. M. Spurlock and K. R. Purdy: J. AIChE 7 (1961) 38.

21. Levich, V. C.: Physicochemical Hydrodynamics, 2nd Ed. Prentice-Hall, Englewood Cliffs, N.J. 1962.

22. Lin, C. S., et al: Ind. Eng. Chem. 43 (1951) 2136.

23. Mantzell, E.: Z. Elektrochem. 42 (1936) 303.

24. Mori, Y.: Trans. ASME J. Heat Transfer 83 (1961) 479.

25. Norris, R. H., and D. D. Streid: Trans. ASME 62 (1940) 525.

26. Phillips, C. T.: J. R. Met. Soc. 58 (1932) 23.

27. Shaw, P. V., L. P. Reiss and T. J. Hanratty: J. AIChE 9 (1963) 362.

28. Sieder, E. N., and G. E. Tate: Ind. Eng. Chem. 28 (1936) 1429.

29. Tobias, C. W., M. Eisenberg and C. R. Wilke: J. Electrochem. Soc. 99 (1952) 359C.

30. Velte, W.: Z. angew. Math. und Physik 13 (1962) 591.

31. Wagner, C.: J. Electrochem. Soc. 95 (1949) 161.

32. Wilke, C. R., M. Eisenberg and C. W. Tobias: J. Electrochem. Soc. 100 (1953) 513.

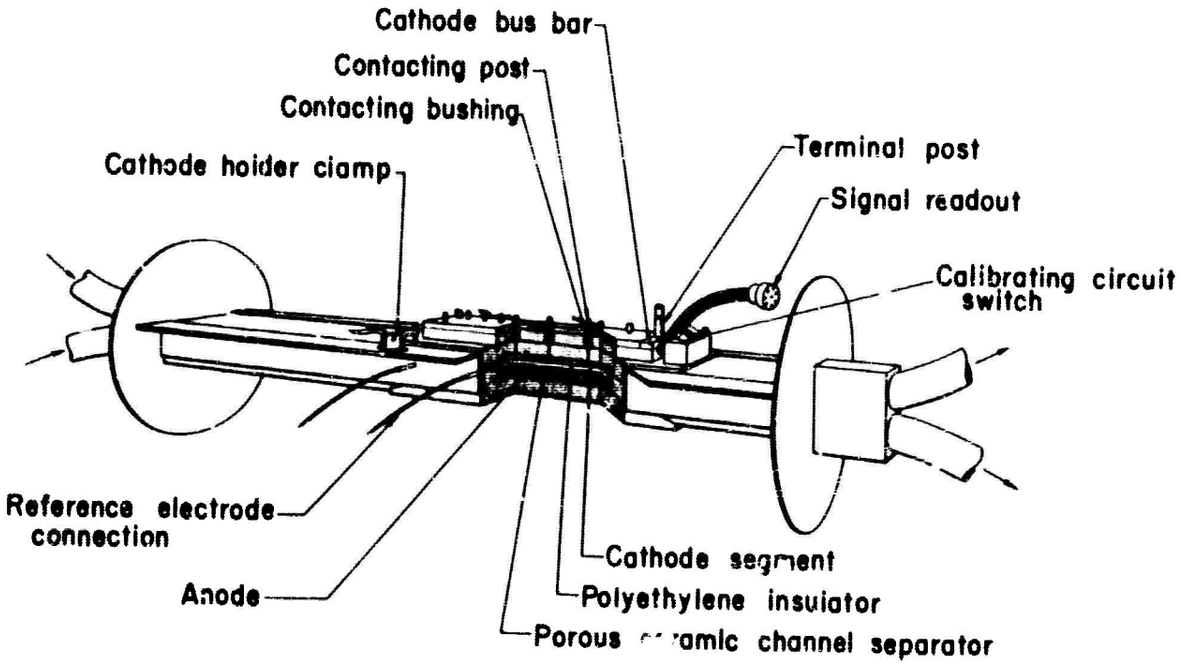

Figure 1. View of the experimental cell with a sectioned electrode in place.

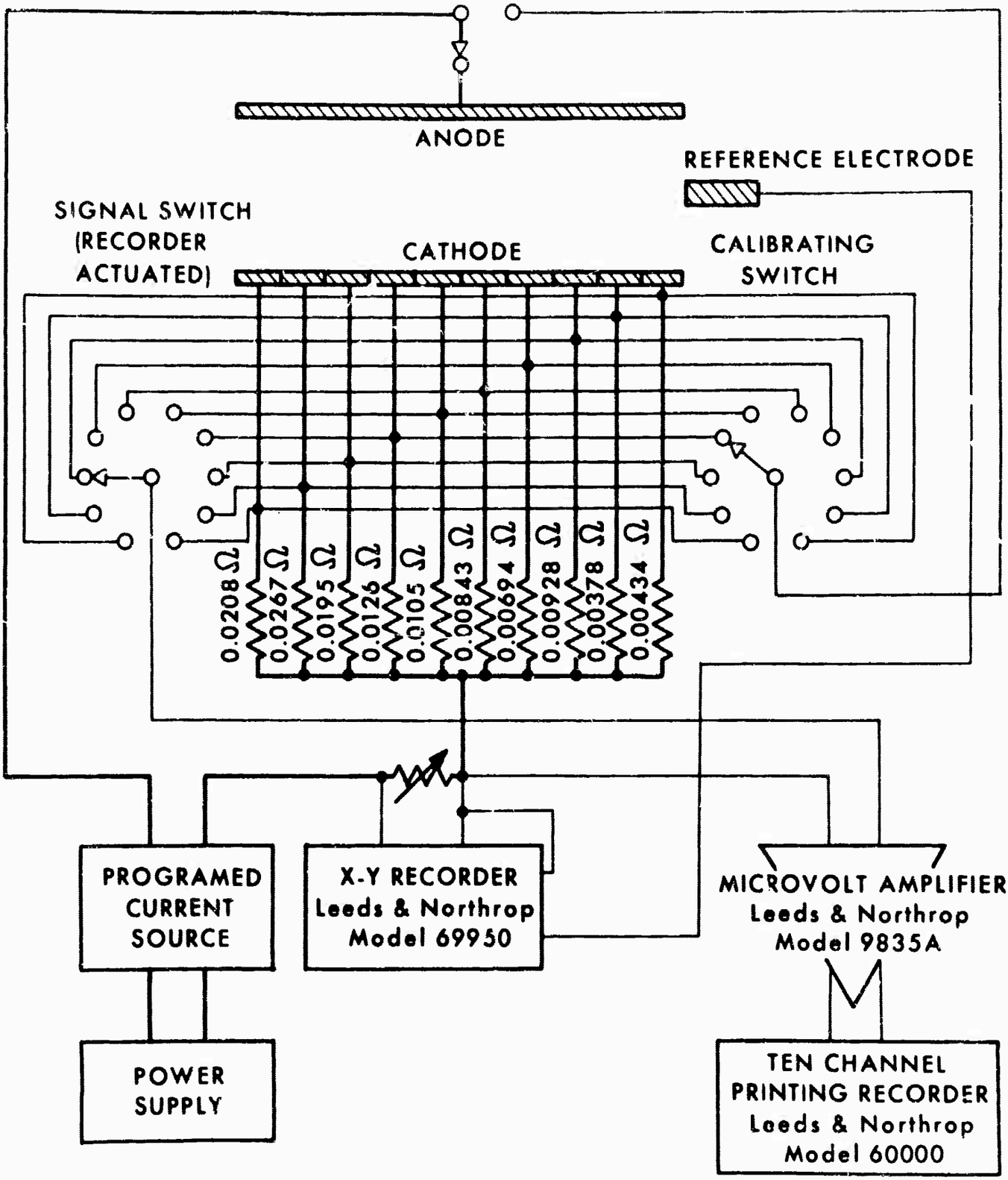

Figure 2. Schematic diagram of the experimental cell and measuring circuit

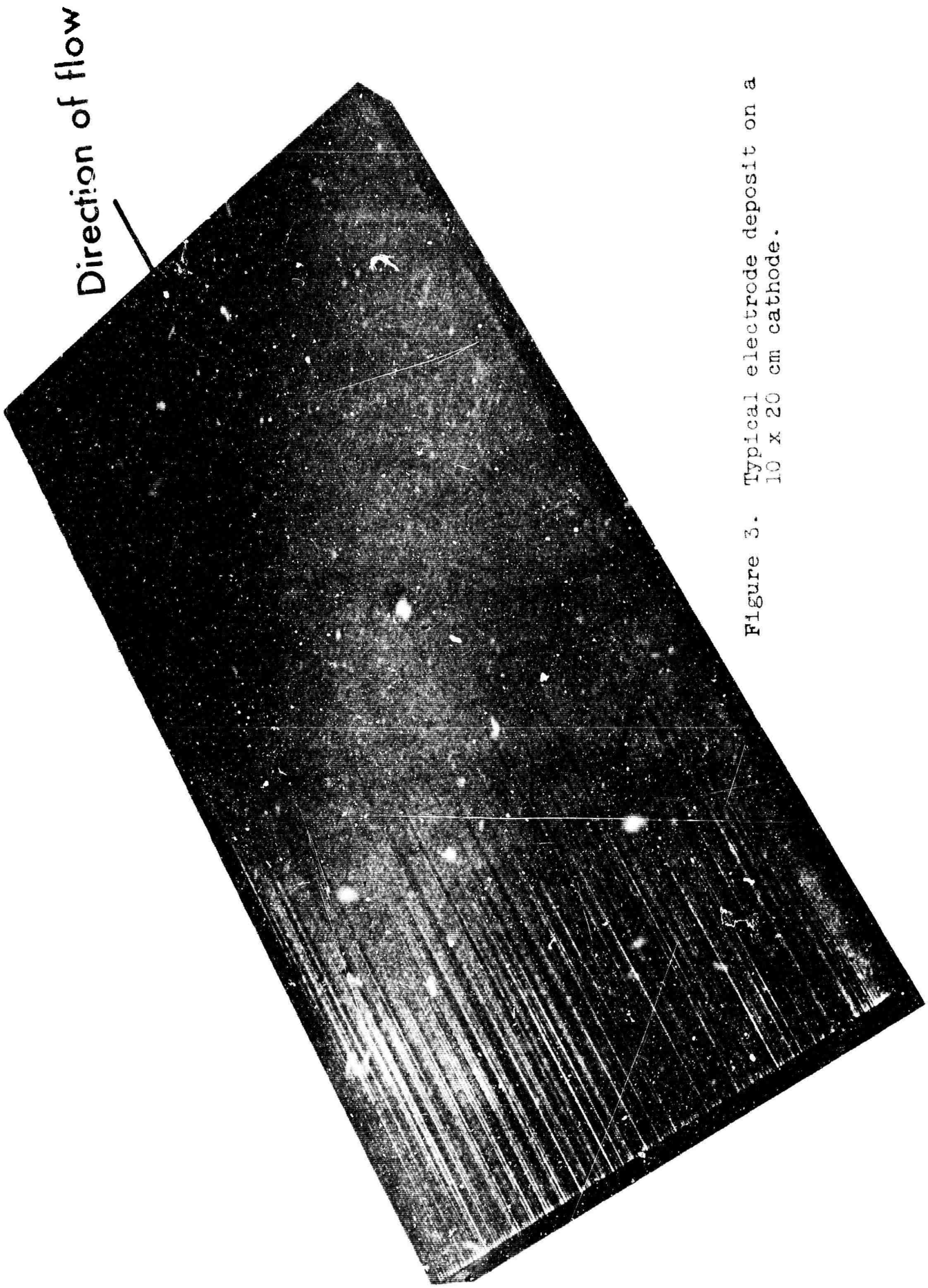

Figure 3. Typical electrode deposit on a 10 x 20 cm cathode.

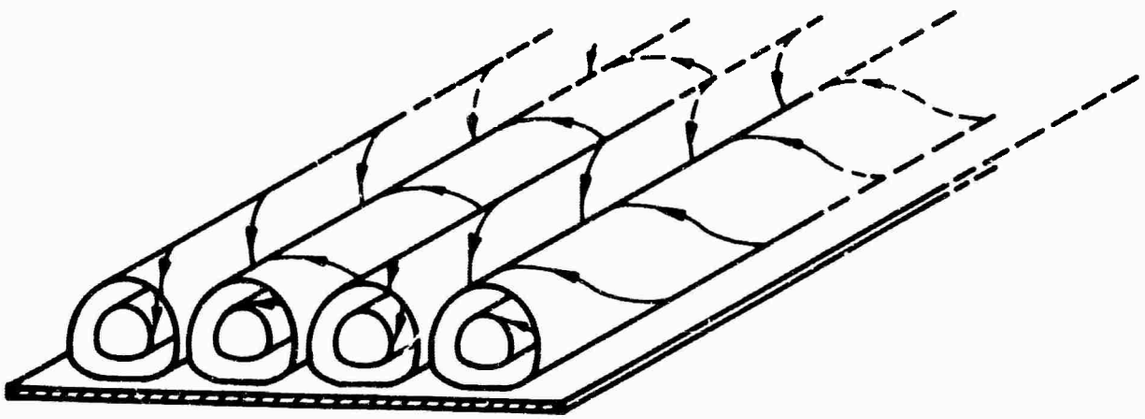

Figure 4. Expected roll cell velocity profile.

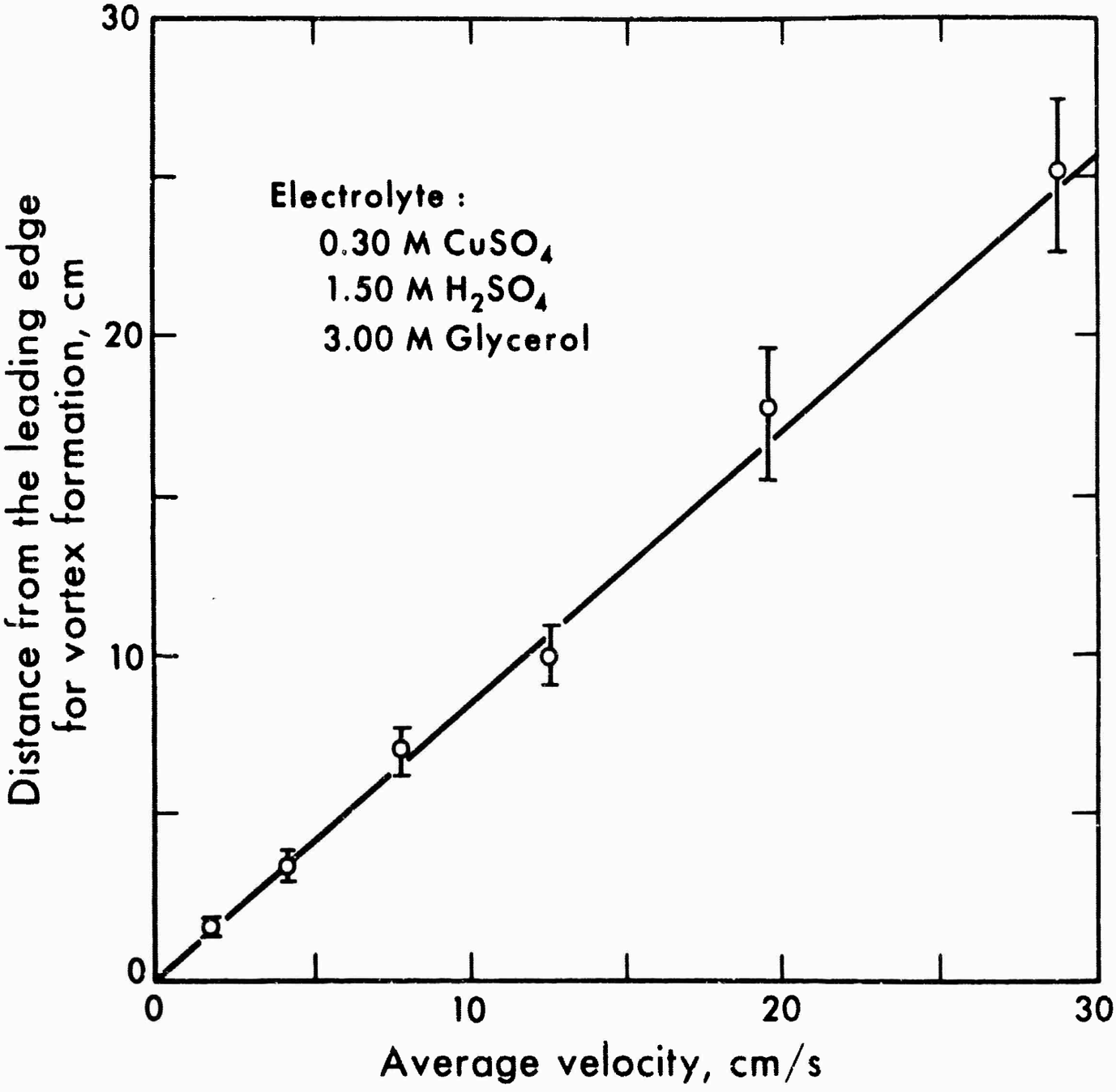

Figure 5. The influence of bulk velocity on the onset of roll cells

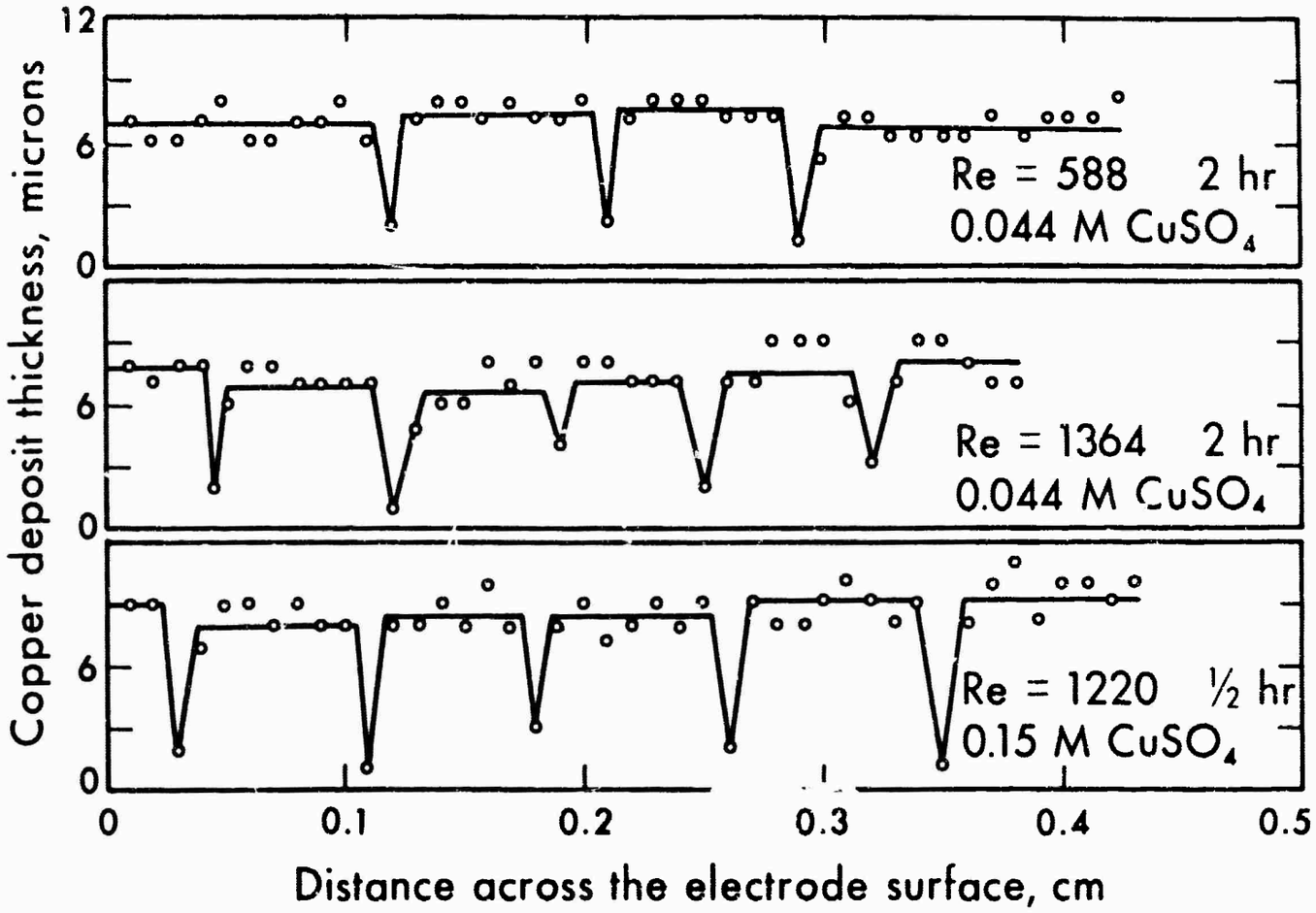

Figure 6. Transverse deposition profiles for three systems as measured by microscope focusing.

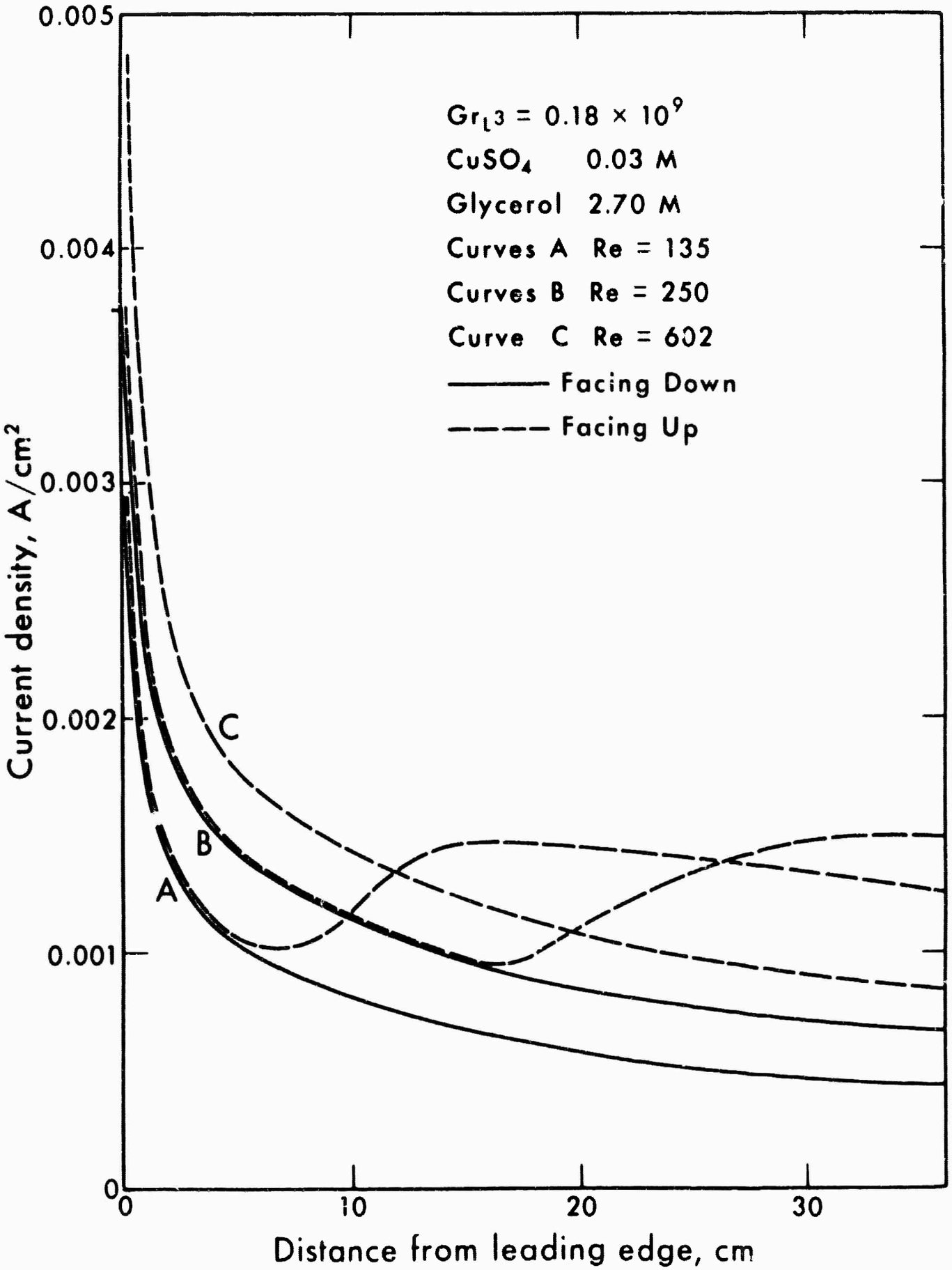

Figure 7. Smoothed data from the sectioned electrode cell for 0.03 M $CuSO_4$ and 2.7 M Glycerol.

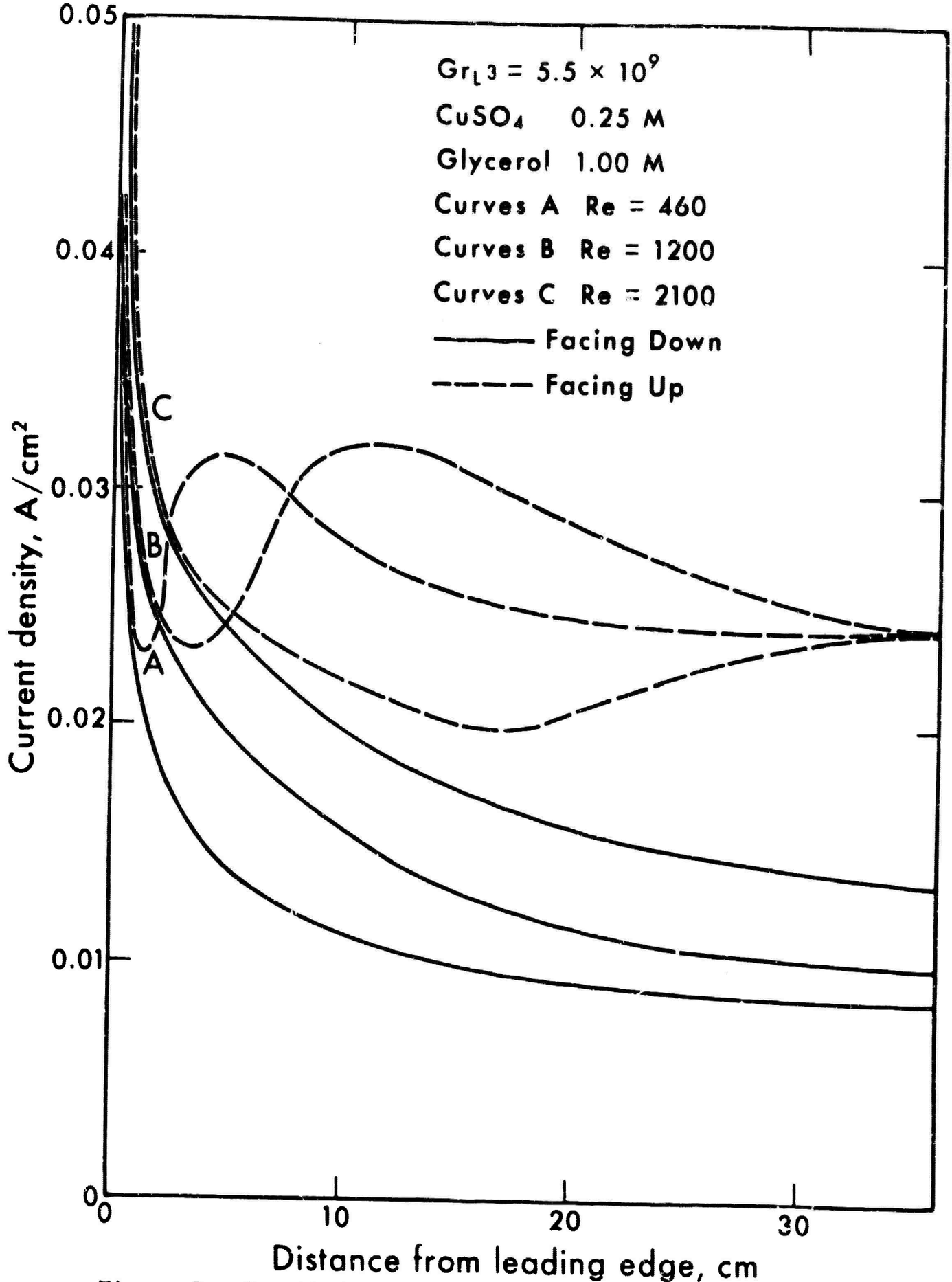

Figure 8. Smoothed data from the sectioned electrode cell for 0.25 M $CuSO_4$ and 1.0 M Glycerol.

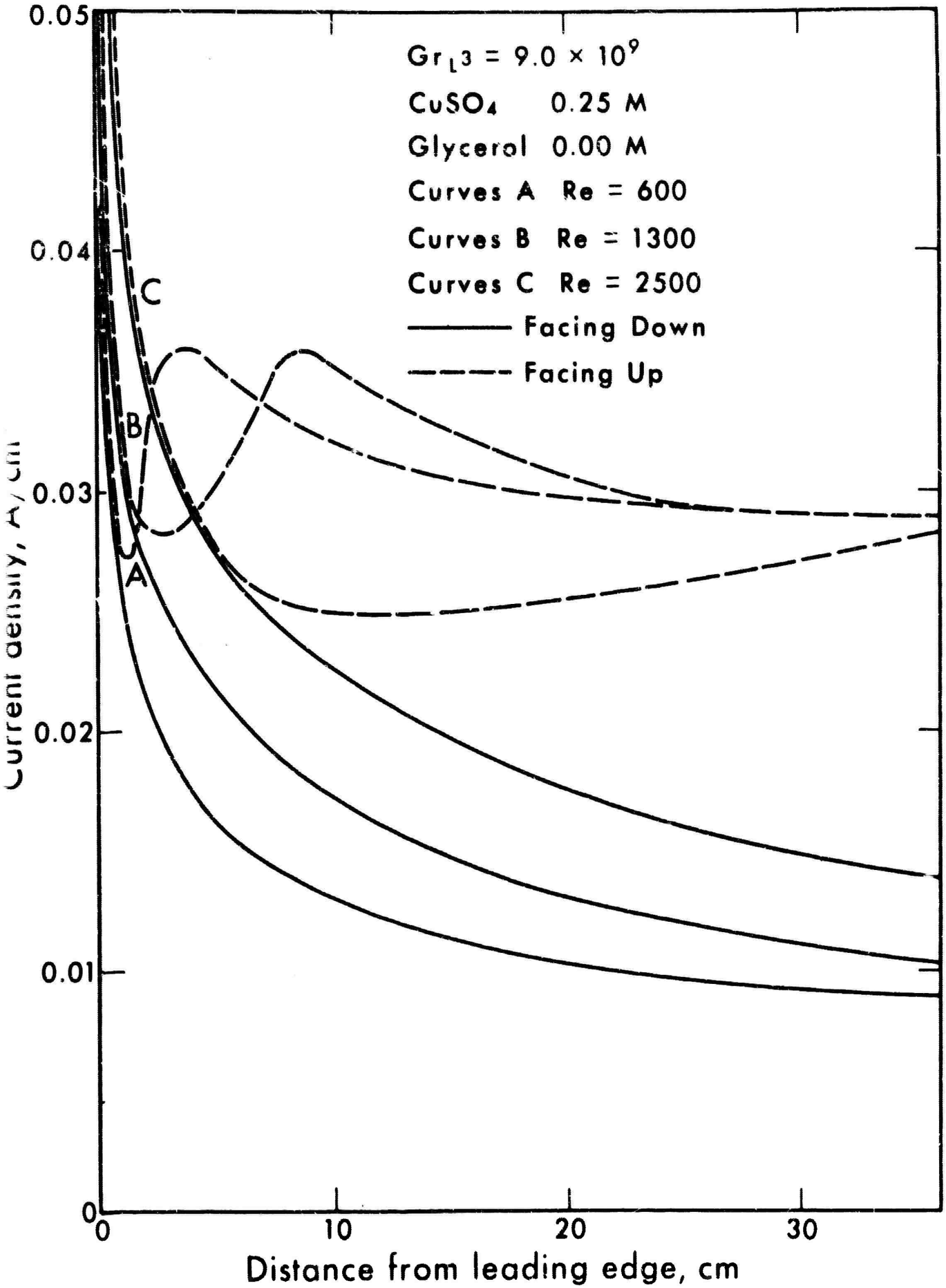

Figure 9. Smoothed data from the sectioned electrode cell for 0.25 M $CuSO_4$ and 0.0 M Glycerol.

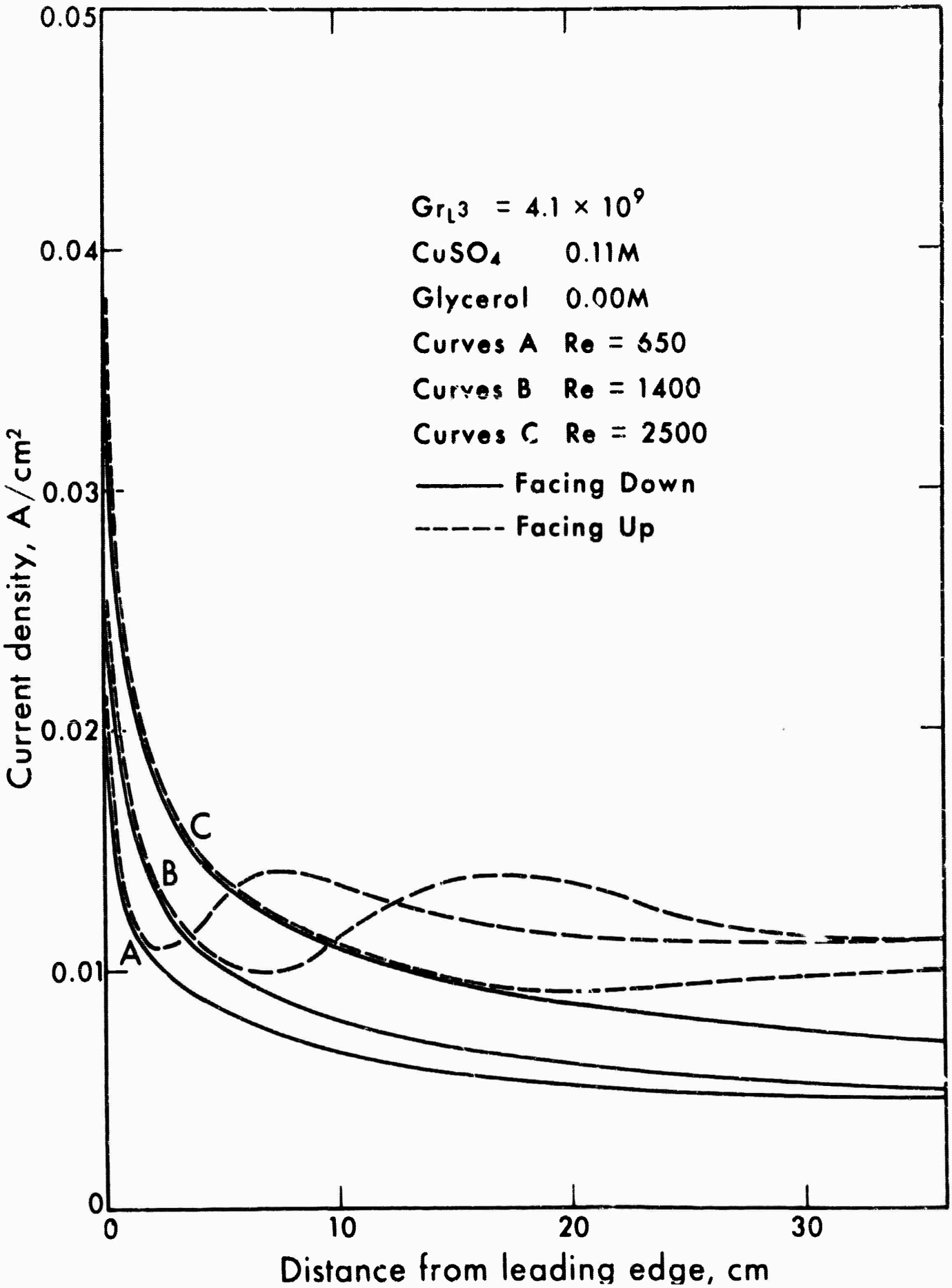

Figure 10. Smoothed data from the sectioned electrode cell for 0.11 M $CuSO_4$ and 0.0 M Glycerol.

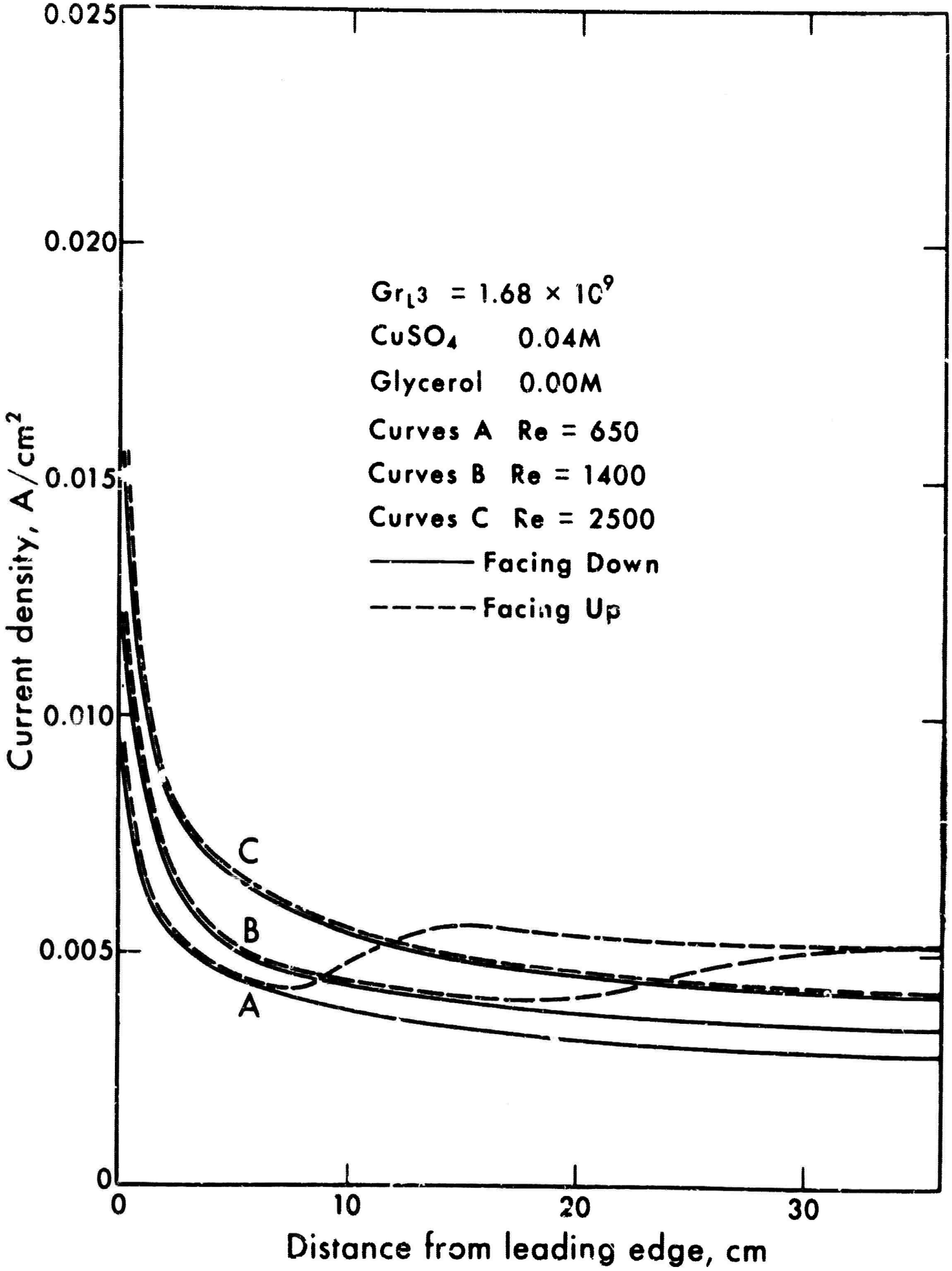

Figure 11. Smoothed data from the sectioned electrode cell for 0.04 M $CuSO_4$ and 0.0 M Glycerol.

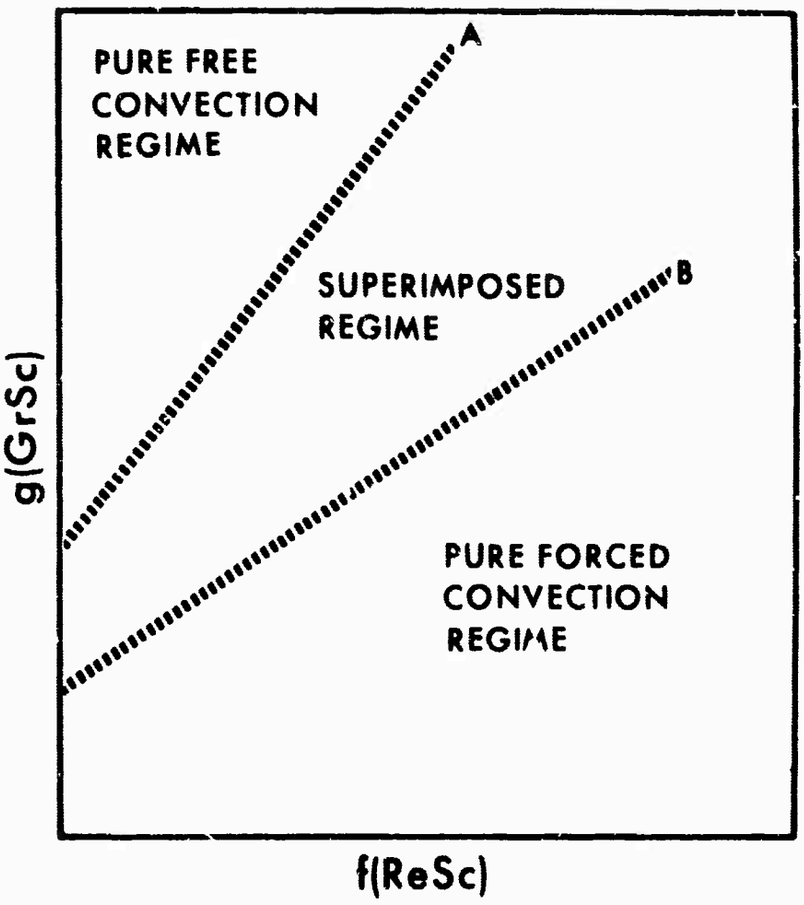

Figure 12. Flow regimes expected in combined free and forced convection.

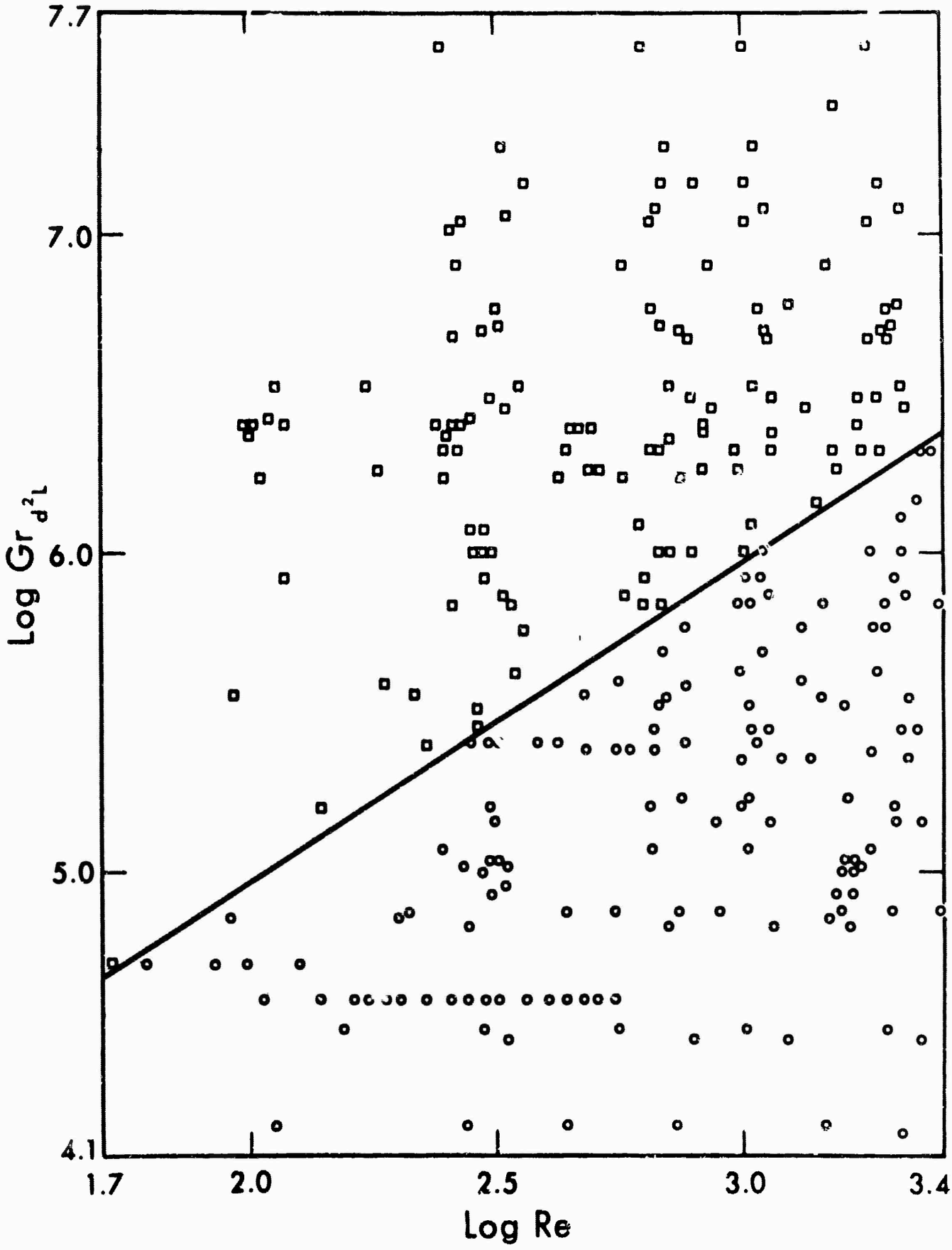

Figure 13. Definition of flow regimes by use of the modified Grashof number.

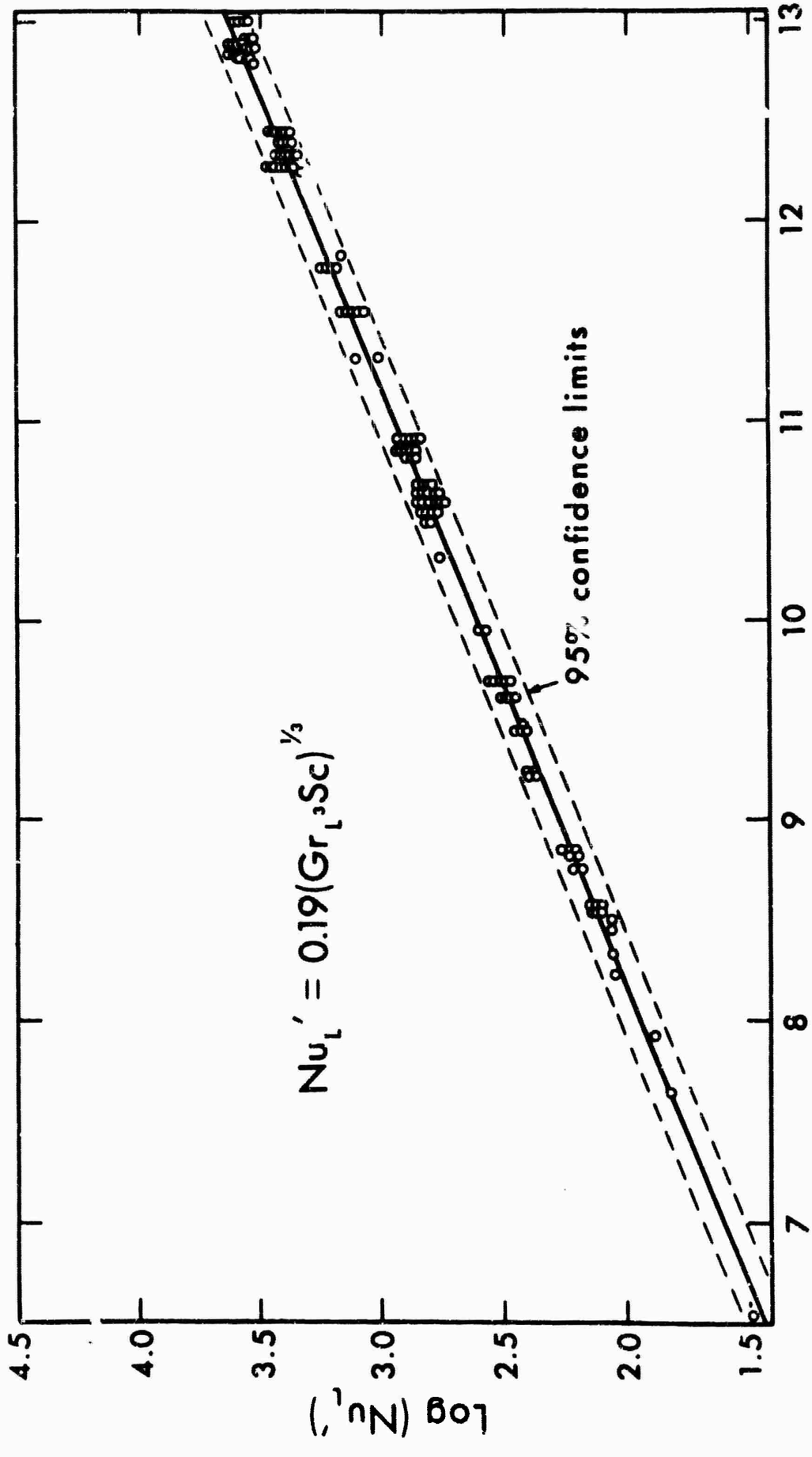

Figure 14. Comparison of experimental data on free convection con rolled systems with the equation of Fenech and Tobias.

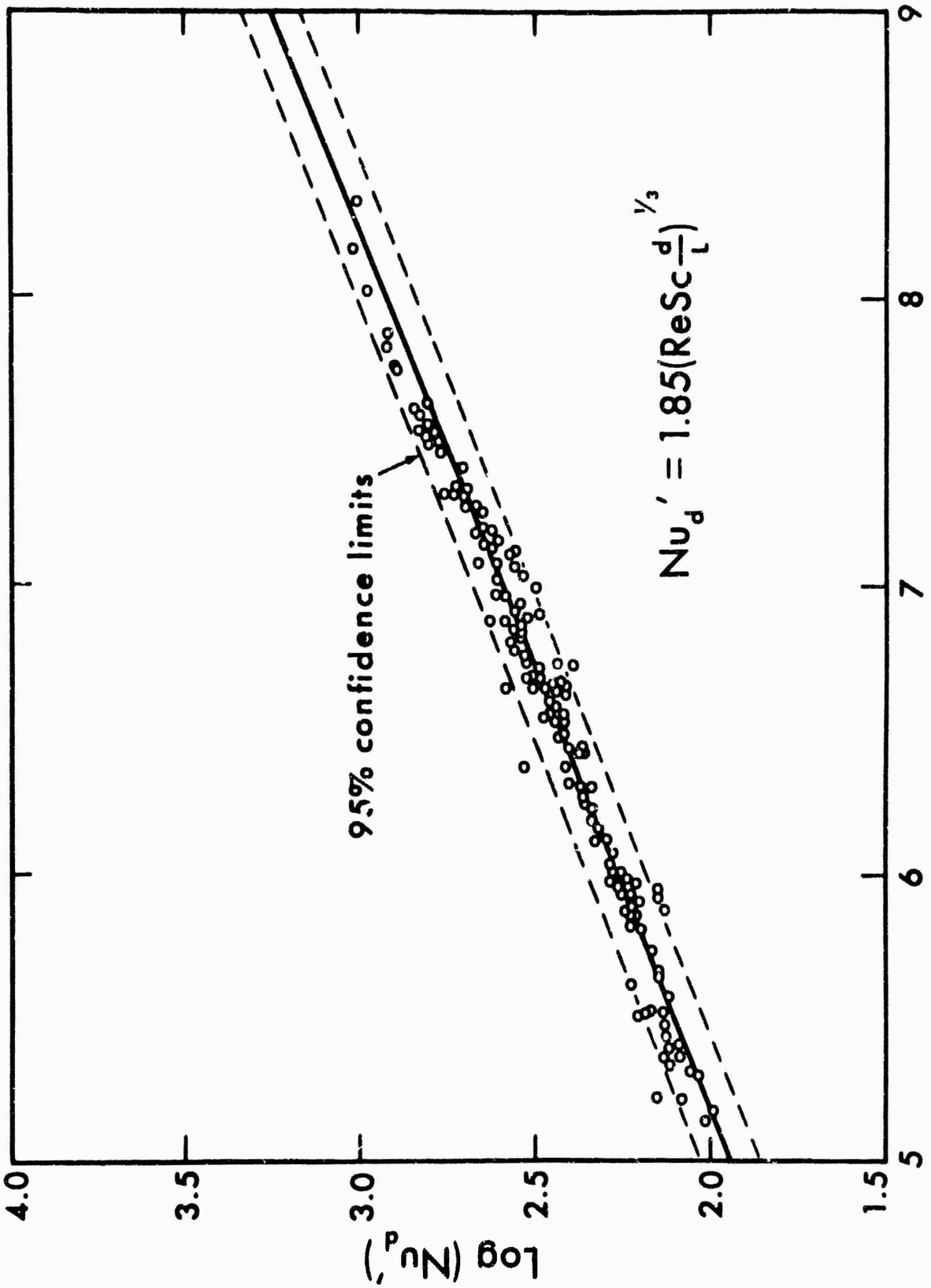

Figure 15. Comparison of experimental data on laminar forced convection controlled systems with the equation of Norris and Streid.

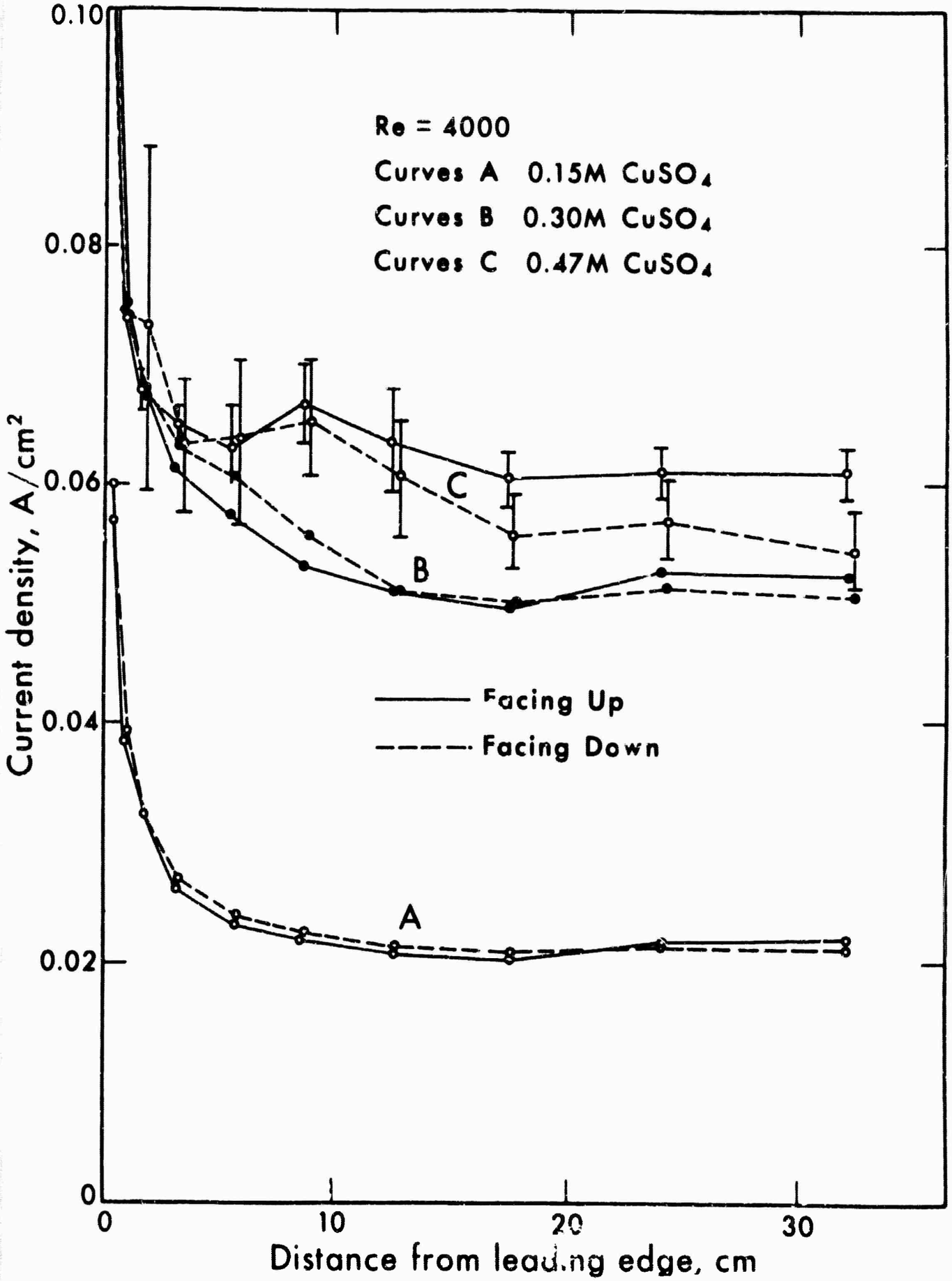

Figure 16. Turbulent flow data from the sectioned electrode cell for Re = 4000.

PROJECT III.

The Role of Ionic Migration in Electrolytic Mass Transport; Diffusivities of $[Fe(CN)_6]^{3-}$ and $[Fe(CN)_6]^{4-}$ in KOH and NaOH Solutions

a) Theoretical Considerations

Mass transfer in an electrolyte can be described by four relationships: a flux equation, continuity equation, and a charge conservation equation, which are analogous to non-electrolytic mass transfer systems; and the statement of electroneutrality which is unique to ionic mass transfer.[1]

The principal equations used are

$$N_i = - D_i \nabla c_i - U_i e z_i c_i \nabla \phi + v c_i \qquad (1)$$

$$\nabla \cdot N_i = - \partial c_i / \partial t \qquad (2)$$

$$I = F \sum_{i=1}^{\ell} z_i N_i \qquad (3)$$

$$\sum_{i=1}^{\ell} c_i z_i = 0. \qquad (4)$$

where c_i is the concentration of species i, D_i is the ionic diffusivity, e is the electronic charge, F is the Faraday constant, I is the current density, N_i is the ionic flux, t is the time, U_i is the ionic mobility, v is the velocity of the fluid, z_i is the number of charges on an ion and ϕ is the potential.

Within the mass transfer boundary layer the concentrations of all ions change due to migration, diffusion and convective fluxes (equation 1). Ions that migrate towards the electrode must diffuse away if they are not involved in the electrode reaction. The concentration of each ionic species departs from the bulk value, but the solution, to a good approximation, remains electrically neutral at all points (equation 4).

The potential gradient, the migration driving force, at any point in the solution is obtained by combining equations (1,2,3) and solving for $\nabla\phi$.

$$\nabla\phi = -\frac{I}{K} - \frac{F\sum_{i=1}^{m} z_i D_i \nabla c_i}{K} \qquad (5)$$

where

$$K = F\sum_{i=1}^{m} U_i e z_i^2 c_i^2 \qquad (6)$$

which is commonly known as the solution conductivity.

The potential gradient is composed of an ohmic drop and a term which includes the concentration gradients and the conductivity. The second term, which appears in all electrolyte systems where a concentration gradient and diffusivity differences exist, is the diffusion potential.

To understand more fully the effect of migration, consider the cathodic discharge of a metal ion. Assume that a large amount of supporting electrolyte relative to the reacting ion is present, and therefore the migration flux

is negligible. In the bulk of a well-stirred solution, the concentration remains practically constant because the swiftly moving fluid rapidly replenishes the loss due to diffusion. As the electrode is approached the fluid velocity decreases and the concentration gradients increase because the total flux is constant at steady state (equation 2). Concentration gradients attain maxima at the electrode surface where the fluid velocity is zero.

The contribution of migration can be increased by decreasing the amount of supporting electrolyte. As in the supporting electrolyte case, the fluid velocity decreases in the vicinity of the electrode. However, a migration velocity (towards the electrode for the metal deposition case being considered) affects the entire concentration profile. The reacting ion in the faster moving lamina migrates to the slower lamina nearer the electrode, therefore shifting the concentration profile towards the electrode surface as shown in Figure 1.

The change in the concentration profile of the reacting ion is of interest because the limiting current I_L is directly related to the concentration gradient at the interface. Combining equation (1) and (3), one obtains

$$I_L = nF\, D_i \nabla c_i^o \qquad (7)$$

Quantitative Calculation of the Limiting Current for a Special Case

Until this point a consideration of the physical model has not been necessary, but a quantitative analysis can be performed only on a specific flow system. The rotating disk is one of the few physical models where the velocity distribution is known within the vicinity of the surface.[2]

The limiting current, including the migration contributions, to a rotating disk electrode can be calculated for a constant potential gradient in the mass transfer boundary layer. A constant potential gradient is possible if all ionic diffusivities are equal and the solution contains enough supporting electrolyte so that the conductivity remains essentially constant through the boundary layer. Then the potential gradient from equation (5) will be (at limiting current)

$$\nabla\phi = - I_L/K^b \qquad (8)$$

Applying a constant potential and eliminating the flux between equation (2) and equation (1), one obtains at steady state

$$D_i\nabla^2 c_i = (v - U_i e z_i \nabla\phi)\nabla c_i \qquad (9)$$

where the velocity gradient was eliminated by the continuity condition and the fluid properties were assumed to be constant.

For the rotating disk electrode, equation (9) can be simplified further. Levich ( ) has proposed that

the concentration is a function of only one dimension, y, which is the perpendicular distance from the plane of the disk

$$D_1 \frac{d^2 c_1}{dy^2} = (v - U_1 ez_1 \frac{d\phi}{dy}) \frac{dc_1}{dy} \qquad (10)$$

In equation (10) v and $d\phi/dy$ are known as functions of y. These functions do not involve c_1 or its derivatives. Therefore, we have a linear second-order differential equation which can be readily solved for c_1 and related to the limiting current, I_L. The solution to equation (8) which satisfied the boundary conditions:

$$\begin{cases} y = 0, & c_1 = 0 \text{ for } I = I_L, \ \frac{dc_1}{dy} = \left(\frac{dc_1}{dy}\right)^o \\ y = \infty, & c_1 = c_1^b \end{cases}$$

is

$$c_1^b = \left(\frac{dc_1}{dy}\right)^o \int_{y=0}^{y=\infty} e^{\int_o^{\xi'} \frac{v - U_1 ez_1 \nabla\phi}{D_1} d\xi} d\xi' \qquad (11)$$

The fluid velocity component, v, in equation (9) is[4]

$$v = (\nu\omega)^{1/2}(-0.510(\tfrac{\omega}{\nu})\xi^2 + 0.333(\tfrac{\omega}{\nu})^{3/2}\xi^3 - 0.103(\tfrac{\omega}{\nu})^2\xi^4 + \ldots. \qquad (12)$$

where ω is the angular frequency of the disk and ν is the kinematic viscosity of the solution.

The development is simplified by letting

$$x = \xi'/\delta_1 .$$

According to Levich: $\delta_1 = \delta_H (Sc)^{-1/3}$ (diffusion boundary layer), and $\delta_H = 1.805 (\frac{\nu}{\omega})^{1/2}$ (hydrodynamic boundary layer), where $Sc = \frac{\nu}{D_1}$ (Schmidt number).

Performing the variable transformation to equations (11) and (12) we have

$$c_1^o = \left(\frac{dc_1}{dy}\right)^o \delta_1 \int_o^\infty e^{-x^3+.885(Sc)^{-1/3}x^4-.103} \; e^{-\frac{U_1 e z_1 \nabla\phi \delta_1}{D_1}} x \; dx \quad (13)$$

The value of the limiting current, from equation (6) and equation (13), is:

$$I_L = -\frac{nF\, D_1 c_1^o}{\delta_1 M_1} \quad (14)$$

where

$$M_1 = \int_o^\infty \exp\left(-x^3+.885(Sc)^{-1/3}x^4-.103(Sc)^{-2/3}x^4\ldots\right)$$

$$\exp\left(-\frac{U_1 e z_1 \nabla\phi \delta_1}{D_1}\right) dx \quad (13)$$

The migration integral, M_1, is a function of the parameter $\left(-\frac{U_1 e z_1 \delta_1 \nabla\phi}{D_1}\right)$ which can be related to solution properties by the application of equations (7), (11)

$$\frac{U_1 e z_1 \nabla\phi}{D_1 \delta_1} = -\frac{U_1 e z_1 I_L \delta_1}{K^b D_1} = \frac{n\, t_1}{z_1 M_1}$$

where t_1 is the transference number of the reacting ion in the bulk.

$$t_1 \equiv \frac{U_1 e z_1^2 c_1^b}{\sum U\, e z_1^2 c_1^b}$$

Equation (15) can be expanded into an infinite series of gamma functions. When evaluated, neglecting cross products and higher terms, one obtains:*

* Note: Setting $t_1=0$ in equation (16) gives the relationship $M_1=.8934+.2747\ Sc^{-1/3}$, which compares with the empirical and commonly used Gregory and Riddiford correction.[2]

$$M_1 = .893 + .2747\ Sc^{-1/3} - .4913\ \frac{n\ t_1}{z_1 M_1} + .1667\left(\frac{nt_1}{z_1 M}\right)^2 \quad (16)$$

Figure 2 gives the values of M_1, for large Schmidt numbers, as a function of nt_1/z_1.

Comparison of Migration Correction Methods

A comparison can be made between the commonly used migration correction and the present results. By equating the migration flux to the product, $\frac{t_1 I_L}{z_1 F}$, we have

$$I_L\left(1 - \frac{nt_1}{z_1}\right) = -\ nF\ D_1 \nabla c_1^o \quad (17)$$

for an arbitrary mass transport system. Applying the effective film thickness, δ_1', for the rotating disk electrode[3] equation (17) becomes

$$I_L = -\ \frac{nF\ D_1 c_1^b}{.8934\left(1 - \frac{nt_1}{z_1}\right)} \quad (18)$$

(since $\nabla c_1^o = c_1^b/\delta_1' = c_1^b/.8934\ \delta_1$) whereas from equation (14) and equation (16), at small t_1 and large Sc_1 we have

$$I_L = -\ \frac{nF\ D_1 c_1^b}{.8934\left(1 - .502\ \frac{nt_1}{z_1}\right)} \quad (19)$$

The transference number appears in a rigorous solutions as, approximately, the arithmetic average over the boundary layer (t_1=0 at the electrode surface). In equation (18) the t_1 was considered to be constant.

To clarify further the role of ionic migration the

effect of a changing potential gradient within the boundary layer should be estimated.

Changing Potential Gradient Effect on Mass Transfer

The interfacial potential gradient can be estimated for an arbitrary number of ions by allowing the interfacial concentrations to be represented by

$$c_i^o = c_i^b - \nabla c_i^o \delta_i' \qquad (20)$$

where δ_i' is the equivalent diffusion in film thickness. To satisfy electroneutrality all δ_i' must be equal when a linear representation such as equation (20) is used for c_i^o. At $I = I_L$, $c_1^o = 0$, hence

$$c_i^o = (\gamma_i - \beta_i)\, c_1^b \qquad (21)$$

where

$$\gamma_i = c_i^b / c_1^b$$

and

$$\beta_i = \nabla c_i^o / \nabla c_1^o$$

By eliminating the potential gradient between the flux equations for the non-discharging ions, applying the Nernst-Einstein relationship ($D_i = kTU_i$), eliminating the interfacial concentrations by equation (21) and solving for β_i, we obtain for:

Case 1. Ion discharge (deposition) reaction

$$\beta_i = \frac{z_i \gamma_i \beta_2}{z_2 \gamma_2 + \beta_2 (z_i - z_2)}$$

and since $\sum_{i=1}^{m} z_i \beta_i = 0$ and $\sum_{i=1}^{m} z_i \gamma_i = 0$

by electroneutrality β_2 is given by

$$z_1 + \beta_2 \sum_{i=2}^{m} \frac{z_i\gamma_i(z_i - z_m)}{z_2\gamma_2 + \beta_2(z_1 - z_2)} = 0$$

and analogously for

Case 2. Oxidation-Reduction ($Ox^{+z_1} + (z_1-z_2)e^- = Red.^{+z_2}$)

$$z_1 + z_2 \frac{-D_1/D_2[z_3\gamma_3+\beta_3(z_m-z_3)] + \gamma_2\beta_3(z_2-z_m)}{z_3 + \beta_3(z_2-z_3)} + \beta_3 \sum_{i=3}^{m-1} \frac{z_i\gamma_i(z_i-z_m)}{z_3\gamma_3 + \beta_3(z_i-z_3)} = 0 ,$$

$$\beta_2 = \frac{-D_1/D_2\ z_2(\gamma_3-\beta_3) + z_2\gamma_2\beta_3}{z_3\gamma_3 + \beta_3(z_2-z_3)} ,$$

and

$$\beta_i = \frac{z_i\gamma_i\beta_3}{z_3\gamma_3 + \beta_3(z_i-z_3)} .$$

The interfacial potential gradient can be written as

$$\nabla\phi^o = \frac{-I_L}{K^b} \frac{[1+I^*]}{[1+\alpha]}$$

where

$$\alpha = \frac{K^o-K^b}{K^b} = \frac{-\sum U_i e z_i^2 \beta_i}{\sum U_i e z_i^2 \gamma_i}$$

from equation (6) and equation (21)

and

$$I^* = -\sum_{i=1}^{m} \left(\frac{z_i D_i}{nD_i}\right) \beta_i .$$

A rigorous calculation of a proper average potential gradient across the mass transfer boundary layer could be a complex, and perhaps, an impossible task by analytical

techniques. For purposes of illustration an arithmetic average gradient has been selected. Physically an arithmetic average would not provide a proper weighting of the more influential interfacial potential gradient where the fluid velocity approaches zero and migration and diffusion prevail. However, this analysis is only intended to provide additional insight into the effect of a change in potential gradient within the boundary layer. This average gradient is

$$\nabla\phi_{ave} = \frac{-I_L}{K^b}\left[1 + \frac{1+I^*}{1+\alpha}\right](1/2) \qquad (22)$$

The results for M_1 remain equivalent for a constant average potential gradient if an effective transference number is defined. Applying the potential gradient of equation (20), we arrive at the following equation for the effective transference number

$$t_1' = \frac{t_1}{2}\left[1 + \frac{1+I^*}{1+\alpha}\right] \qquad (23)$$

which embodies corrections for a diffusion potential and conductivity changes in the boundary layer that appear in real systems.

Numerical Illustrations for an Average Potential Gradient

Calculations were performed for several typical electrolytes. The parameters β_1, I^*, α and t_1' were calculated from limiting ionic conductances at 25.0°C.[5] Since only values of ionic properties are involved, the use of

limiting conductances is not too unrealistic and suitable for illustrative purposes. The results of these calculations are shown in Table I.

In each of these tables the effective transference number t_1' and the transference number in the bulk, t_1, have been compared. If the supporting electrolyte is a better conductor than the reacting ion, the diffusion potential is positive, thereby increasing the effective transference number. At the other extreme, as shown in Table I, the diffusion potential is negative, hence $t_1' < t_1$.

Conclusions

1. The changing concentrations in the mass transfer boundary layer are important in determining the contribution of ionic migration to the limiting current. For the special case of a constant potential gradient, the limiting current, including migration effects, can be calculated rigorously.

2. The diffusion potential contributes to the electric field which promotes migration. Although an approximate calculation was used to illustrate the effect of the diffusion potential, additional insight about the capacity of various supporting electrolytes for suppressing ionic migration was obtained by evaluating effective transference numbers for some typical binary and quaternary electrolyte systems. Highly conducting supporting electrolytes

significantly increase the effective transference number of the reacting ionic species decreasing the effectiveness of these salts for suppressing ionic migrations.

b. Densities and Viscosities of Aqueous Solutions of $K_3|Fe(CN)_6|$ - $K_4|Fe(CN)_6|$ - KOH (or NaOH), and the Diffusion Coefficients of the Ferrous- and Ferricyanide Ions.

Density, viscosity, and diffusivity data were obtained in equimolar ferrous- ferricyanide solutions (0.01 - 0.20 molal) in the presence of NaOH or KOH (0.0 - 3.5 molal).

Solution Preparation and Analysis

Solutions were prepared with distilled water and reagent grade chemicals. Ferricyanide ion was titrated with thiosulfate[6] and ferrocyanide was determined by a ceric titration[7]. Hydroxyl ion was titrated with standard HCl to a bromthymol blue endpoint.

Densities and Viscosities

A. Experiment.

Densities and viscosities were determined by standard techniques (pycnometer and U-tube viscometer[8], respectively). All solutions were thermostated to 25.00±.05°C before measurements were taken.

B. Results.

A second degree polynomial involving C_{redox} (average of ferri- and ferrocyanide concentrations) and C_{KOH} or C_{NaOH} was fitted to the data by a least squares

technique. A total of 26 points for KOH supported solutions and 28 points for NaOH solutions were used in the curve plotting.

The equations and their associated standard errors of estimate are:

a. Potassium hydroxide as a supporting electrolyte.

$$\mu[cp] = .8937 + .6178\ C_{redox} + .1064\ C_{KOH} + .00656\ C^2_{KOH} + .0205\ C_{KOH}\ C_{Redox} \quad (1)$$

Standard Error of Estimate = 1.0%.

$$\rho[g/cp] = .9971 + .3989\ C_{Redox} + .0502\ C_{KOH} - .000140\ C^2_{KOH} - .0032\ C_{KOH}\ C_{Redox} \quad (2)$$

Standard Error of Estimate = 0.5%.

b. Sodium hydroxide as a supporting electrolyte.

$$\mu[cp] = .8937 + .6969\ C_{Redox} + .1539\ C_{NaOH} + .0235\ C^2_{Redox} + .0450\ C^2_{NaOH} + .2527\ C_{NaOH}C_{Redox} \quad (3)$$

Standard Error of Estimate = 1.0%.

$$\rho[g/cp] = .9971 + .3996\ C_{Redox} + .0427\ C_{NaOH} - .00113\ C^2_{NaOH} - .00657\ C_{NaCH}C_{Redox} \quad (4)$$

Standard Error of Estimate = 0.1%.

Ranges of validity: C_{Redox} (.01 - .20 M) and C_{KOH}, C_{NaOH} (.0 - 3.5 M).

The data compared with literature values, through equations (1) - (4), as shown in Tables II-IV.

Diffusivities

Experiment

A rotating disk electrode was applied for the measurement of the ionic diffusion coefficients of the ferrous and ferricyanides[9,10,11,12]. This tool, first analyzed by Levich (8) for a binary electrolyte, then treated by Hogge and Kraichman[13] for a completely flooded electrolyte, has been extended to partially flooded systems where migration effects can not be neglected.

The theory developed in part a was used to determine the diffusivity of the reacting ion from limiting current measurements by a rotating disk electrode. The equation used is:

$$D_1 = \left[\frac{-1.805\ I_L \nu^{1/6} M_1}{nF\ c_1^b \omega^{1/2}}\right]^{3/2} \qquad (5)$$

Migration effects are included in the parameter M_1 which contains the effective transference number (see part a) of the reacting ion. M_1 has a value of $.893 + .2661\ Sc_1^{-1/3}$ when the transference number of the reacting ion is zero.

The electrode was a 1 cm Pt. disk embedded in epoxy resin and attached to an aluminum spindle rotated at precisely controlled speeds between 600 - 3600 rpm. Figure 1 is a schematic drawing of the apparatus.

Results

From the limiting current measurements the diffusivities of ferri- and ferrocyanide ions were determined by equation (5). The data were correlated in the form of

the Stokes-Einstein relation, $D\mu/T$, as a function of the ionic strength Γ.

$$\Gamma = 1/2 \sum_{i=1}^{m} c_i z_i^2 \qquad (6)$$

Preliminary calculations performed on the data of Newson and Riddiford indicated that $D\mu/T$ was independent of μ and T at Γ = const.

Although temperature was not a variable in the present study, the parameter $D\mu/T$ should be independent of temperature, since the benavior of the ferrous- or ferric cyanide ion should be similar in this respect to that of the large tri-iodide ion.

A least squares fit of the data (values obtained with KOH or NaOH agreed within range of experimental error, ±4%) gives the following empirical relationships and standard errors of estimate:

$$\frac{D\mu}{T}(\text{ferri}) = (.234 + .0014\ \Gamma) \times 10^{-9}\ \frac{cm^2}{sec}\ \frac{poise}{^\circ K} \qquad (7)$$

$$\pm\ .005$$

$$\frac{D\mu}{T}(\text{ferro}) = (.187 + .0036\ \Gamma) \times 10^{-9}\ \frac{cm^2}{sec}\ \frac{poise}{^\circ K} \qquad (8)$$

$$\pm\ .007$$

As a comparison, the data of Eisenberg, et al[15] gives

$$\frac{D\mu}{T}(\text{ferri}) = .250 \times 10^{-9}\ \frac{cm^2}{sec}\ \frac{poise}{^\circ K}$$

and

$$\frac{D\mu}{T}(\text{ferro}) = .215 \times 10^{-9}\ \frac{cm^2}{sec}\ \frac{poise}{^\circ K}$$

whereas equations (7) and (8) give

$$\frac{D\mu}{T}(\text{ferri}) = .240 \times 10^{-9} \frac{cm^2}{sec} \frac{poise}{^\circ K}$$

and

$$\frac{D\mu}{T}(\text{ferro}) = .202 \times 10^{-9} \frac{cm^2}{sec} \frac{poise}{^\circ K}$$

Although no conclusion can be reached about the discrepancies between the data presented, the inherent errors in the effusion capillary technique used by Eisenberg et al could be responsible for the differences. These empirical relationships are considered adequate representations of the data for use in mass transfer studies, and are reliable within the error estimates presented.

NOMENCLATURE

Lower Case Letters

c concentration - moles/cm^3

e electronic charge - coulombs

g parameter - dimensionless

j index of series - dimensionless

k Boltzman constant - erg/deg

m total number of species - dimensionless

n number of electrons reacting

t time - sec

t transference number - dimensionless

v fluid velocity - cm/sec

v migration velocity - cm/sec

x transformed variable - dimensionless

y coordinate axis - cm

z charge on an ion - dimensionless

Upper Case Letters

A constant of integration - moles/cm^3-cm

B constant of integration - moles/cm^3

C concentration - moles/liter

D diffusion coefficient - cm^2/sec

F Faraday constant - coulombs/equiv

I current density - amp/cm^2

I* "diffusion current" - dimensionless

K solution conductivity - $ohm^{-1}cm^{-1}$

M molarity - moles/liter

M migration integral - dimensionless

N ionic flux - moles/cm^2-sec

R gas constant - ergs/deg-mole

T absolute temperature - deg. absolute

U mobility - cm-sec^{-1}/dynes

Greek Letters

α fractional conductivity change - dimensionless

β relative concentration gradient - dimensionless

γ relative concentration - dimensionless

δ_H hydrodynamic boundary layer - cm

δ diffusion boundary layer - cm

δ' equivalent diffusion thickness - cm

ϵ dielectric constant - dimensionless

λ ionic conductance - $ohm^{-1}cm^2$/equiv

μ bulk viscosity - poise

ν kinematic viscosity - cm^2/sec

ξ variable of integration - cm

ξ' variable of integration - cm

ρ density - gm/cm^3

ϕ electric potential - volt

ω angular frequency - radians/sec

Γ ionic strength - moles/liter

Subscripts and Superscripts

b bulk

i index of species

o interfacial property

L limiting current

LITERATURE CITED

1. Stanley L. Gordon, "Investigation of Ionic Diffusion and Migration by a Rotating Disk Electrode", Master's thesis, University of California, Berkeley, May 1963; Technical Report No. 1, this contract.

2. V. G. Levich, Acta Physicochimica U.R.S.S. 17, 257 (1942).

3. L. L. Bircumshaw and A. C. Riddiford, Quart. Rev. 6, 157 (1952).

4. T. von Karman, Z. angew. Math. Mech. 1, 244 (1921).

5. B. E. Conway, Electrochemical Data, p. 145, Elsevier (1952).

6. I. M. Kolthoff and E. B. Sandell, Textbook of Quantitative Inorganic Analysis, 34d, p. 595, MacMillan Co., N.Y. (1952).

7. Ibid., p. 583.

8. E. A. Willihnganx, W. B. McCluer, M. R. Fenske, and R. V. McGrew, Ind. Eng. Chem., Anal. Ed., 6, 231 (1934).

9. Z. Gaius and R. Adams, Anl. Chem. 34, 164B (1962).

10. D. John and W. Vielstich, J. Electrochem. Soc. 109, 849 (1962).

11. A. Frumkin, L. Nekrasov, V. Levich and J. Ivanov, J. Electroanal. Chem. 1, 84 (1959-1960).

12. Y. Koutetsky and V. Levich, Acad. Nauk SSSR, Ph. Chem. 112-113, 697 (1957).

13. E. Hogge and M. B. Kraichman, J. Amer. Chem. Soc. 76, 1431 (1954).

14. J. D. Newson and A. C. Riddiford, J. Electrochem. Soc. 108, 699 (1961).

15. M. Eisenberg, C. W. Tobias and C. R. Wilke, J. Electrochem. Soc. 103, 414 (1956).

16. N. A. Lange (Ed.), Handbook of Chemistry, 8th ed. (1952).

17. L. B. Hitchcock and J. S. McIlhenny, Ind. Eng. Chem. 27, 461 (1935).

Table 1. Effect of Supporting Ionic Species on the Effective Transference Numbers of Reacting Ions for Various Concentration Levels.

System			γ_3	β_2	β_3	I^*	α	t_i	t_i'	I_L/I_D
OH^-	$z_{OH^-} = -1$	$\lambda^o_{OH^-} = -197.6$	100	1/2	-1/2	-.7035	-.0158	.0165	.0121	1.006
Na^+	$z_{Na^+} = +1$	$\lambda^o_{Na^+} = 50.11$	50	1/2	-1/2	-.7035	-.0310	.0324	.0239	1.012
ClO_4	$z_{ClO_4^-} = -1$	$\lambda^o_{ClO_4^-} = -6$?	20	1/2	-1/2	-.7035	-.0730	.0763	.0580	1.038
			10	1/2	-1/2	-.7035	-.1332	.1392	.1105	1.057
			5	1/2	-1/2	-.7035	-.2268	.2371	.2029	1.105
Reaction: $4OH^- \longrightarrow O_2 + 2H_2O + 4e$										
H^+	$z_{H^+} = +1$	$\lambda^o_{H^+} = +349.8$	100	+1/2	-1/2	-.7811	-.0229	.0228	.0157	1.008
Cl^-	$z_{Cl^-} = -1$	$\lambda^o_{Cl^-} = -76.3$	50	1/2	-1/2	-.7811	-.0446	.0444	.0309	1.016
K^+	$z_{K^+} = +1$	$\lambda^o_{K^+} = +73.5$	20	1/2	-1/2	-.7811	-.1031	.1028	.0738	1.038
			10	1/2	-1/2	-.7811	-.1832	.1827	.1381	1.071
			5	1/2	-1/2	-.7811	-.2998	.3000	.2463	1.128
Reaction: $2H^+ + 2e^- \longrightarrow H_2$										
Cu^{++}	$z_{Cu^{++}} = +2$	$\lambda^o_{Cu^{++}} = +54.0$	100	+2/3	-2/3	4.303	.0004	.0025	.0089	1.004
$SO_4^=$	$z_{SO_4^=} = -2$	$\lambda^o_{SO_4^=} = -80.0$	50	+2/3	-2/3	4.303	.0009	.0050	.0178	1.009
H^+	$z_{H^+} = +1$	$\lambda^o_{H^+} = +349.8$	20	+2/3	-2/3	4.303	.0021	.0122	.0439	1.022
			10	+2/3	-2/3	4.303	.0041	.0237	.0869	1.044
			5	+2/3	-2/3	4.303	.0078	.0447	.1705	1.088
Reaction: $Cu^{++} + 2e^- \longrightarrow Cu$										
Cu^{++}	$z_{Cu^{++}} = +2$	$\lambda^o_{Cu^{++}} = +54.0$	100	2/3	-2/3	.8928	-.0106	.0069	.0114	1.006
$SO_4^=$	$z_{SO_4^=} = -2$	$\lambda^o_{SO_4^=} = -80.0$	50	2/3	-2/3	.8928	-.0209	.0014	.0226	1.011
K^+	$z_{K^+} = +1$	$\lambda^o_{K^+} = +73.52$	20	2/3	-2/3	.8928	-.0496	.0329	.0558	1.028
			10	2/3	-2/3	.8928	-.0918	.0600	.1093	1.056
			5	2/3	-2/3	.8928	-.1600	.1044	.2110	1.110
Reaction: $Cu^{++} + 2e^- \longrightarrow Cu$										

Table 1. (cont.) Effect of Supporting Ionic Species on the Effective Transference Numbers of Reacting Ions for Various Concentration Levels

System			γ_3	β_2	β_3	β_4	I*	α	t_i	t_i'	I_L/I_D
$[Fe(CN)_6]^{-3}$	z = -3	λ^o = -101.0	100	-1.152	-.837	.770	5.578	.0041	.0107	.0447	.992
$[Fe(CN)_6]^{-4}$	z = -4	λ^o = -111.0	50	-1.107	-.796	.657	4.911	.0076	.0204	.0775	.987
K^+	z = -1	λ^o = + 73.5	20	-1.028	-.651	.460	3.754	.0162	.0453	.1406	.976
OH^-	z = -1	λ^o = -197.6	10	- .967	-.561	.309	2.868	.0263	.0762	.1968	.967
			5	- .191	-.488	.188	2.154	.0389	.1158	.2506	.958

Reaction $[Fe(CN)_6]^{-3} + e^- = Fe(CN)_6^{-4}$ Note: Solutions are equimolar in respect to both cyanides

System			γ_4	β_2	β_3	β_4	β_5	I*	α	t_i	t_i'	I_L/I_D
$[Fe(CN)_6]^{-3}$	z = -3	λ^o = -101.0	100	-1.199	-.016	.443	-.447	.854	.0074	.0109	.0173	.997
$[Fe(CN)_6]^{-4}$	z = -4	λ^o = -111.0	50	-1.182	-.030	.421	-.428	.858	.0137	.0208	.0328	.994
K^+	z = +1	λ^o = + 73.5	20	-1.139	-.066	.366	-.380	.870	.0285	.0461	.0718	.988
Mg^{++}	z = +2	λ^o = + 53.1	10	-1.089	-.111	.301	-.321	.882	.0440	.0774	.1192	.980
SO_4	z = -2	λ^o = - 80.0	5	-1.028	-.169	.224	-.247	.915	.0600	.1171	.1784	.970

Reaction: $[Fe(CN)_6]^{-3} + e^- = [Fe(CN)_6]^{-4}$

Note: Solutions are equimolar in respect to both cyanides

Table I.

Comparison of Viscosity and Density Data with Those of Eisenberg et al[15]

Conditions: 1. τ = 25.0°C.

$K_3Fe(CN)_6$ (molar)	$K_4Fe(CN)_6$ (molar)	NaOH (molar)	μ (lit.)	μ (calc.)	Dev. (%)	ρ (lit.)	ρ (calc)	Dev. (%)
.00998	.01011	1.958	1.368	.1379	+0.8	1.0807	1.0807	+0.0
.01224	.01228	2.011	1.382	1.400	+1.3	1.0833	1.0834	+0.0
.04996	.05052	1.923	1.394	1.415	+1.5	1.0949	1.0952	+0.0
.0994	.1008	2.007	1.494	1.505	+0.7	1.1174	1.1169	-0.0
.1994	.2030	2.004	1.642	1.626	-1.0	1.1535	1.1560	+0.2

Table II.

Comparison of Viscosity Data with Those of Lange[16]

Conditions: 1. Pure sodium or potassium hydroxide
2. τ = 25.0°C.

KOH (molar)	μ (lit.)	μ (calc.)	Dev. (%)	NaOH (molar)	μ (lit.)	μ (calc.)	Dev. (%)
1.00	1.009	1.007	-0.2	1.00	1.104	1.093	-1.0
0.50	0.951	0.949	-0.2	0.50	0.991	0.982	-0.9
0.25	0.922	0.921	-0.1	0.25	0.944	0.935	-0.8
0.125	0.905	0.907	+0.2	0.125	0.921	0.913	-0.7

Table III.

Comparison of Density Data with Those of Hitchcock et al[17]

Conditions: 1. Pure sodium and potassium hydroxide
2. τ = 25.0°C.

KOH (molar)	ρ (lit.)	ρ (calc.)	Dev. (%)	NaOH (molar)	ρ (lit.)	ρ (calc.)	Dev. (%)
4.00	1.1726	1.1754	+0.2	4.00	1.1491	1.1500	+0.1
3.00	1.1314	1.1351	+0.3	3.00	1.1145	1.1154	+0.1
2.00	1.0886	1.0919	+0.3	2.00	1.0776	1.0803	+0.3

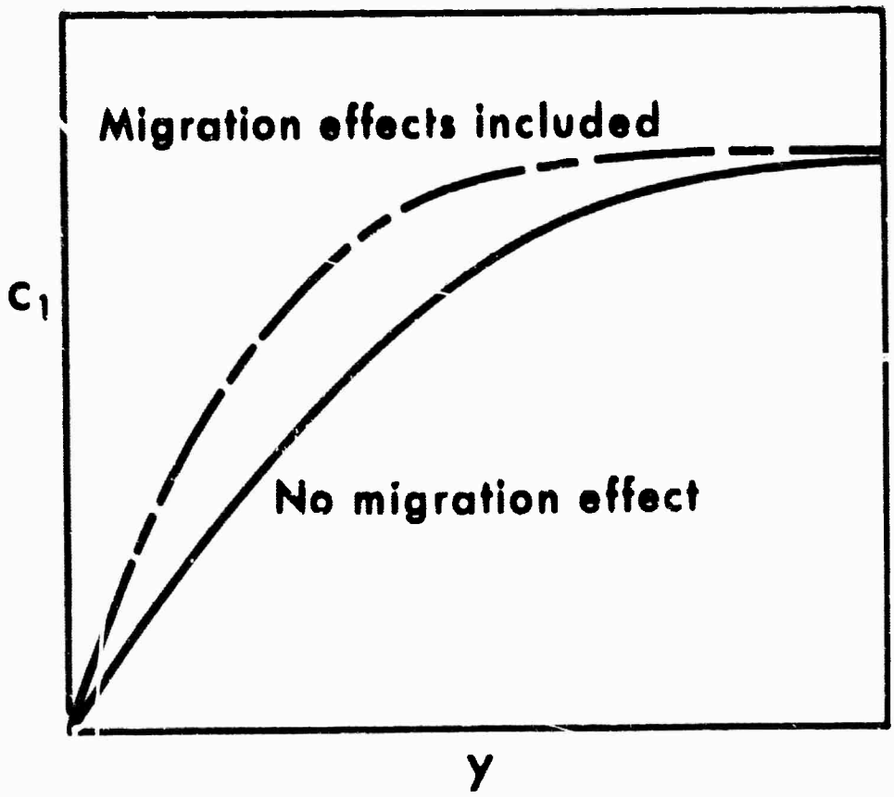

Fig. 1 Alteration of Concentration Profiles by Ionic Migration

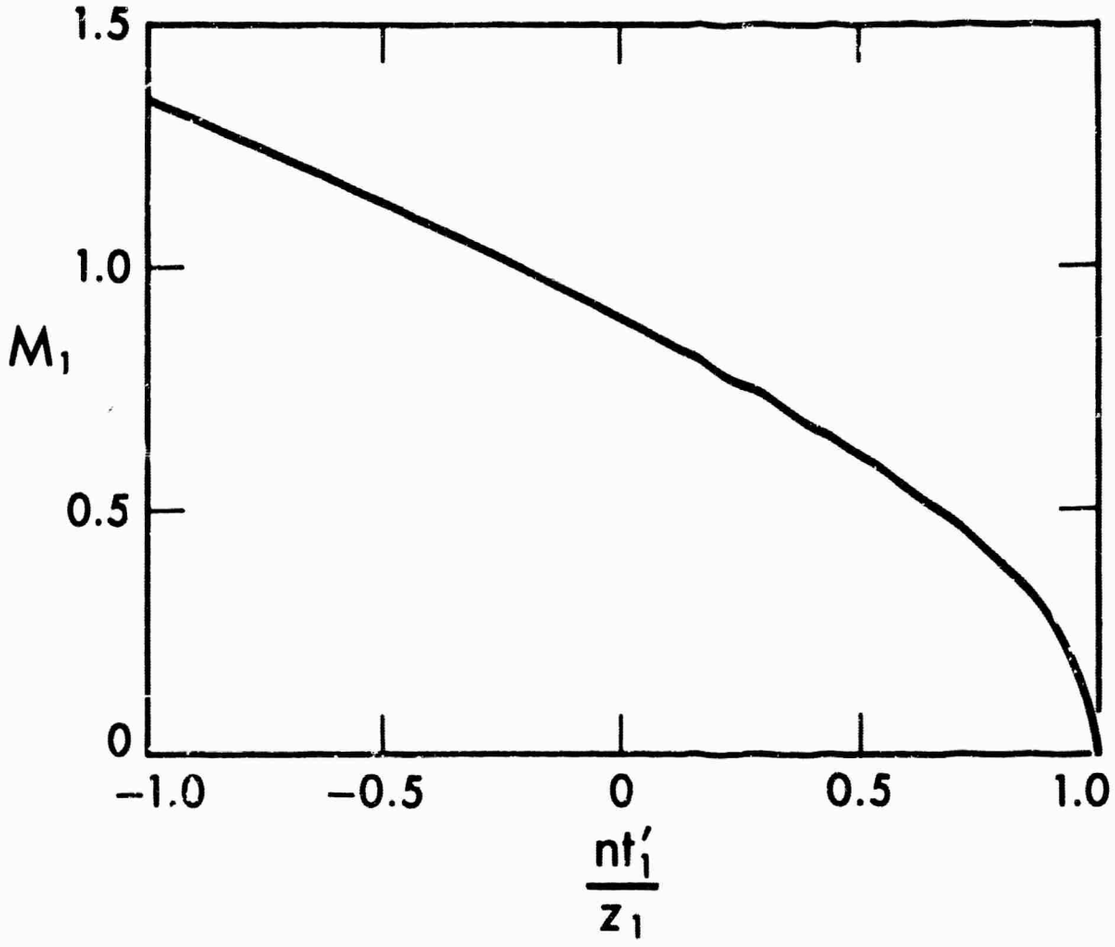

Fig. 2 The Migration Integral as a Function of nt_1'/z_1

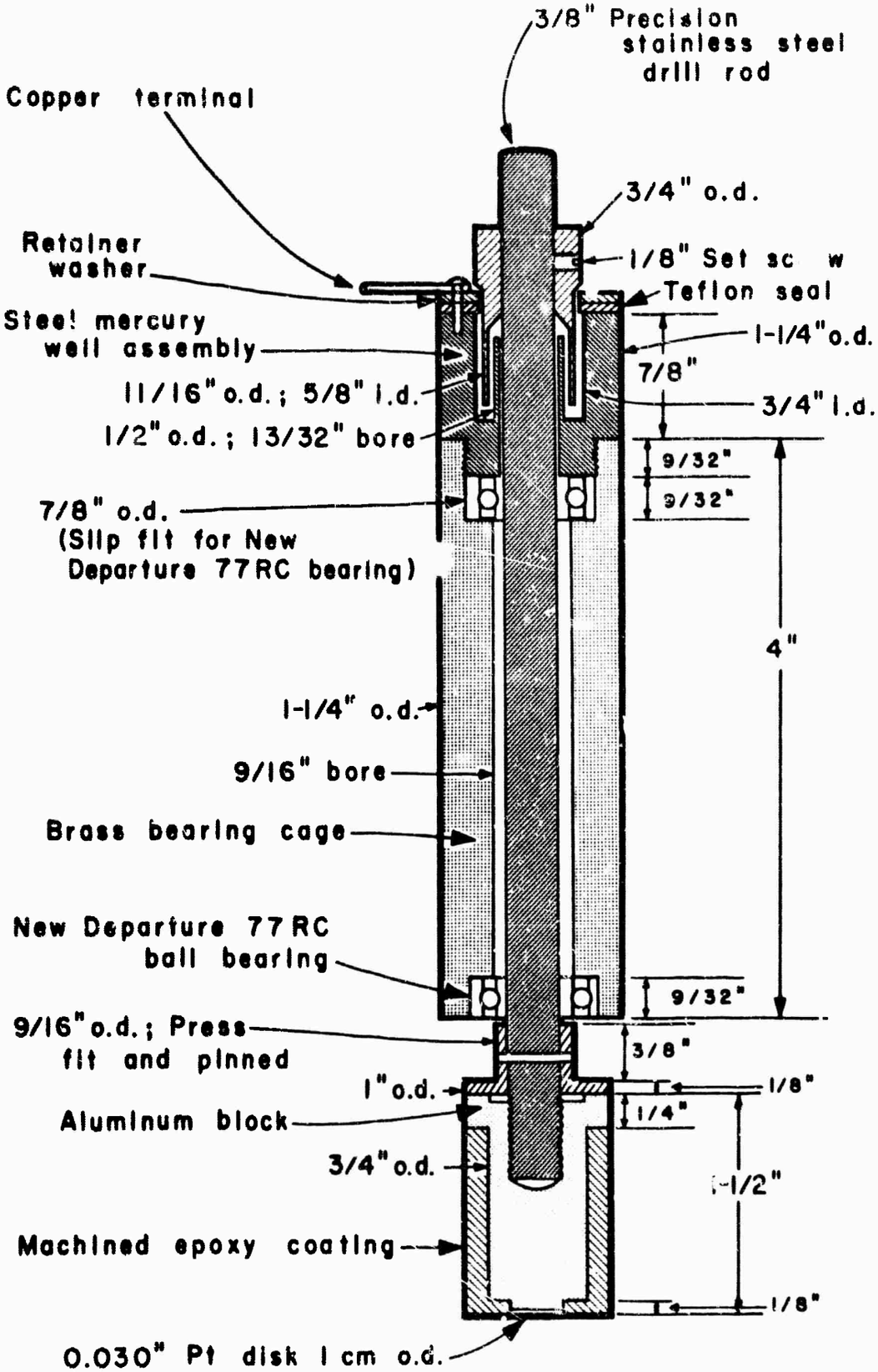

Figure 3. Cross-sectional view of the rotating spindle.

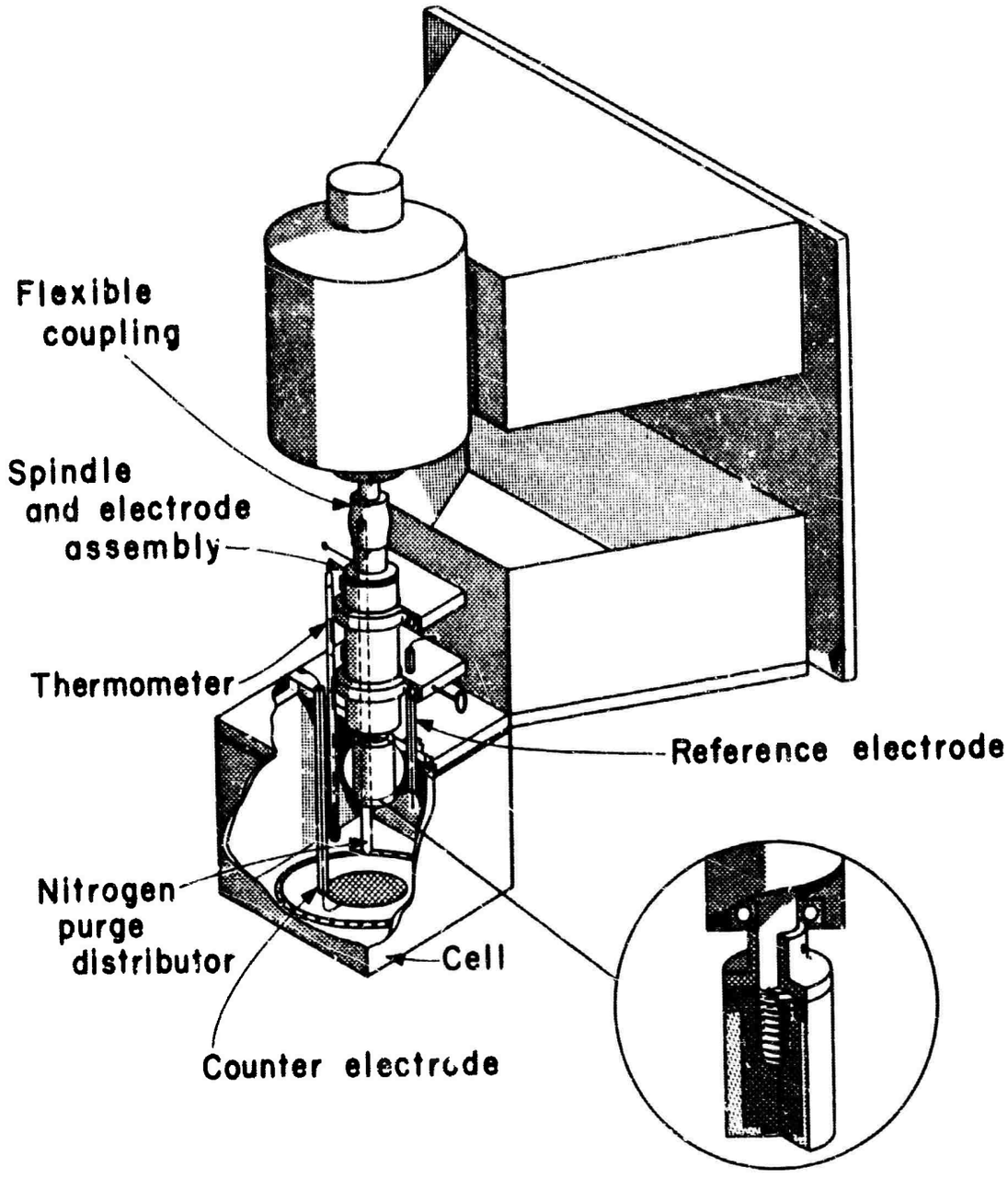

Figure 4. Schematic diagram of the rotating cell apparatus.

PROJECT IV.

Mass Transfer in Concentrated Binary Electrolytes

Introduction

The flux of minor components in a dilute electrolytic solution may be expressed as[1]

$$\underline{N}_i = - z_i u_i F c_i \nabla \Phi - D_i \nabla c_i + c_i \underline{v} . \qquad (1)$$

This equation clearly accounts for three mechanisms of mass transfer: the motion of a charged species in an electric field (so-called migration), molecular diffusion due to a concentration gradient, and convection due to the bulk motion of the medium. Although this equation has been applied fruitfully to many electrochemical problems, its validity is restricted to dilute solutions.

The problem is most conveniently considered in two parts. First one seeks transport equations, such as equation (1), which correctly relate driving forces and fluxes and thereby introduce certain transport properties, such as D_i and u_i. The transport properties should be measurable state properties which should be <u>independent</u> of the driving forces such as $\nabla\Phi$ and ∇c_i.

The second part of the problem is to characterize the variation of the transport properties with temperature, pressure, and composition. This usually takes either the form of a theoretical linkage to more fundamental concepts of the structure of matter or the form of an empirical correlation of available measurements.

Transport Equations

Equation (1) is inadequate even in ternary solutions of non-electrolytes, since in these there are two

independent concentration gradients and the diffusion flux of each species can be affected by both concentration gradients.

As pointed out by Guggenheim[2,3,4,5], the electrostatic potential in equation (1) does not have a clearly defined physical significance. The mobility u_i and the diffusion coefficient D_i are no longer related by the Nernst-Einstein equation at high concentrations. Few independent measurements of single ionic mobilities and diffusion coefficients are available.

In order to avoid these difficulties, equation (1) can be replaced by

$$c_i \nabla \mu_i = RT \sum_j \frac{c_i c_j}{c_T \mathcal{D}_{ij}} (\underline{v}_j - \underline{v}_i). \qquad (2)$$

This equation is similar to the Stefan-Maxwell equation[6] and is equivalent to one* developed by Onsager[7]. The Stefan-Maxwell equations apply to diffusion in dilute gas mixtures and express the driving force as a mole fraction gradient or a gradient of partial pressure instead of the gradient of the electrochemical potential. The reciprocal of the $\mathcal{D}_{ij}$'s can be regarded as friction coefficients similar to those used by Laity[8,9] and Klemm[10,11] to describe transport in ionic solutions and melts. Burgers[12] has also used this concept to treat the conductivity of ionized gases, and Lightfoot, et al[13], have applied equation (2) to liquid solutions. See also Lamm[14] and Truesdell[15].

---

* Equation (14), page 245, in reference 7.

The term $-c_i \nabla \mu_i$ in equation (2) can be regarded as a driving force per unit volume acting on species i and causing it to move with respect to the surrounding fluid. The force per unit volume exerted by species j on species i as a result of their relative motion is expressed as

$$RT \frac{c_i c_j}{c_T \mathcal{D}_{ij}} (\underline{v}_j - \underline{v}_i) ,$$

that is, proportional to the difference in velocity of the two species. By Newton's third law of motion $\mathcal{D}_{ij} = \mathcal{D}_{ji}$. Equation (2) thus expresses the balance between the driving force and the total drag force exerted by the other species.

The number of independent equations of the form (2) is one less than the number of species. When equation (2) is summed over i, the left side is zero by the Gibbs-Duhem relation, and the right side is zero by Newton's third law of motion.

In contrast to equation (1), equation (2) is not a direct expression for the fluxes. However, the material balance for a species reads

$$\frac{\partial c_i}{\partial t} = - \nabla \cdot \underline{N}_i \qquad (3)$$

and requires an expression for the flux. In particular cases we invert equation (2) to obtain these expressions. For example, for a binary electrolyte composed of anions, cations, and solvent, equation (2) yields two independent equations which may be rearranged[16] to read

$$\left.\begin{aligned} \underline{N}_+ &= c_+\underline{v}_+ = -\frac{\nu_+\mathscr{D}}{\nu RT}\, c\, \nabla \mu_e + \frac{\underline{i}\, t_+^*}{F\, z_+} + c_+\underline{v}^*. \\ \underline{N}_- &= c_-\underline{v}_- = -\frac{\nu_-\mathscr{D}}{\nu RT}\, c\, \nabla \mu_e + \frac{\underline{i}\, t_-^*}{F\, z_-} + c_-\underline{v}^*. \\ \underline{N}_o &= c_o\underline{v}_o = -\frac{\mathscr{D}}{RT}\, c_o\, \nabla \mu_o + \frac{\underline{i}}{F}\left(\frac{t_+^*}{z_+} + \frac{t_-^*}{z_-}\right) + c_o\underline{v}^*. \end{aligned}\right\} \quad (4)$$

The molar average velocity

$$\underline{v}^* = \frac{1}{c_T}\sum_i c_i\underline{v}_i$$

has been chosen as the reference velocity, and the current density is

$$\underline{i} = F\,(z_+c_+\underline{v}_+ + z_-c_-\underline{v}_-).$$

The parameters $\mathscr{D}$, t_+^*, and t_-^* in equations (4) are transport properties related to the $\mathscr{D}_{ij}$ of equation (2). The transference numbers (with respect to the molar average velocity) are

$$t_+^* = 1 - t_-^* = \frac{c_-}{c_T} + \frac{c_o}{c_T}\,\frac{z_+\mathscr{D}_{o+}}{z_+\mathscr{D}_{o+} - z_-\mathscr{D}_{o-}}. \quad (5)$$

The diffusion coefficient of the salt, based on a thermodynamic driving force, is

$$\mathscr{D} = \frac{\mathscr{D}_{o+}\mathscr{D}_{o-}(z_+ - z_-)}{z_+\mathscr{D}_{o+} - z_-\mathscr{D}_{o-}}. \quad (6)$$

The diffusion driving force used in equations (4) is the gradient of the chemical potential μ_e of the electrolyte in the solution. This chemical potential is readily measurable, and no reference to single ionic activity coefficients is necessary.

Now we want to define a "potential in the solution" for use as a driving force for the current. For this purpose the potential of a suitable reference electrode, at the point in question, with respect to a fixed reference electrode is used. Application of thermodynamic principles to such a reference electrode yields in this case

$$s_- \nabla \mu_- + s_+ \nabla \mu_+ + s_o \nabla \mu_o = - nF \nabla \Phi, \qquad (7)$$

where the electrode reaction is given by

$$s_- M_-^{z_-} + s_+ M_+^{z_+} + s_o M_o \longrightarrow ne^- .$$

Equation (7) can be rearranged[16] to give

$$\underline{i} = - \kappa \nabla \Phi - \frac{\kappa}{F z_+ \nu_+} \nabla \mu_e \left[\frac{z_+ s_+}{n} + \frac{z_+ \vartheta_{o+}}{z_+ \vartheta_{o+} - z_- \vartheta_{o-}} - \frac{s_o z_+ c_+}{n c_o} \right], \qquad (8)$$

where the conductivity κ is another transport property and is related to the ϑ_{ij}'s of equation (2) by

$$\kappa = - \frac{z_+ z_- F^2 c_T}{RT} \frac{(c_- \vartheta_{o+} + c_+ \vartheta_{o-}) \vartheta_{+-}}{c_- \vartheta_{o+} + c_+ \vartheta_{o-} + c_o \vartheta_{+-}} . \qquad (9)$$

Note that the potential defined here as the potential of a reference electrode is considerably different from the electrostatic potential used in equation (1). This definition avoids the questionable concepts regarding potentials in the solution brought up by Guggenheim.

The transport parameters usually considered in a binary electrolyte are the conductivity, the diffusion coefficient, and the transference number, and these are related to ϑ_{o+}, ϑ_{o-}, and ϑ_{+-} by equations (5), (6), and (9). Actually, the transference number with respect

to the solvent velocity is usually measured and reported. This is

$$t_+^o = 1 - t_-^o = \frac{z_+ \mathscr{D}_{c+}}{z_+ \mathscr{D}_{o+} - z_- \mathscr{D}_{o-}} . \qquad (10)$$

The diffusion coefficient of the salt which is usually measured and reported is related to the thermodynamic diffusion coefficient by

$$D = \mathscr{D} \frac{c_T}{c_o} \left(1 + \frac{d \ln \gamma}{d \ln m}\right) . \qquad (11)$$

The difference between D and $\mathscr{D}$ is due to the choice of the driving force and to the choice of the reference velocity.

Concentration Dependence of Transport Properties

The theory up to this point is macroscopic in nature. In order to gain further insight into the nature of the $\mathscr{D}_{ij}$'s, it is necessary to resort to microscopic theories or empirical interpretation based on experimental observations. From the latter it is known that over moderate ranges of concentration the product of the diffusion coefficient and the viscosity μ is reasonably constant[6]. On this basis, $\mu \mathscr{D}_{o+}$ and $\mu \mathscr{D}_{o-}$ may be assumed constant for ion-solvent interactions, where electrostatic forces are small. Such an assumption will not account for the interactions between ions. The Debye-Hückel-Onsager theory of conductance and the experimental confirmation of this theory show that $\mathscr{D}_{+-}$ is proportional to $\sqrt{c}$ in dilute

solutions. As a first approximation we shall assume that this dependence persists at higher concentrations. Thus we write

$$\left.\begin{aligned} \mu\vartheta_{o+} &= kT/A \ , \\ \mu\vartheta_{o-} &= kT/B \ , \\ \mu\vartheta_{+-} &= kT\sqrt{\frac{\nu c}{c_T}}/G \ , \end{aligned}\right\} \qquad (12)$$

where A, B, and G are assumed to be constants, independent of concentration.

Substitution into equation (9) yields

$$- z_+z_-eF\frac{\sqrt{\nu cc_T}}{\kappa\mu} = G + \frac{AB}{\nu_+A + \nu_-B}\frac{\sqrt{\nu}\,c_o}{\sqrt{cc_T}} \ . \qquad (13)$$

For A, B, and G to be constant thus requires that a plot of $\sqrt{\nu cc_T}/\kappa\mu$ against $\sqrt{\nu}\,c_o/\sqrt{cc_T}$ should be a straight line. Such plots are shown in figures 1 and 2 for aqueous KOH solutions and in figures 3 and 4 for aqueous KCl solutions, both at 25°C.* The value of G can be determined from the intercept, and the slope gives the value of $AB/(\nu_+A+\nu_-B)$.

Substitution of equations (12) into equation (10) gives

$$t_+^o = 1 - t_-^o = \frac{\nu_-B}{\nu_+A + \nu_-B} \ , \qquad (14)$$

which suggests that the transference numbers with respect to the solvent velocity should be constant. For KOH, $t_+^o = 0.23$ is approximately constant between 1 and 17 molal[29] concentration. The transference number for KCl is near

* The values of viscosity were taken from references 17, 18, and 19 for KCl and from references 20, 21, and 22 for KOH. The values of conductivity were taken from references 23, 24, 25, and 26 for KCl and from references 20, 21, 27, and 28 for KOH.

t_+^o = 0.489, although a value as low as 0.4857 at 3 molar has been measured by the Hittorf method[30,31].

The assumption that A, B, and G are constant, together with the slopes and intercepts from figures 1-4 and the above values of the transference numbers, enables us to calculate the following values of A, B, and G:

	$A \times 10^8$	$B \times 10^8$	$G \times 10^8$
	cm	cm	cm
KCl	24.06	23.02	39.71
KOH	28.89	8.63	9.63

This determination of A, B, and G requires values for the viscosity, conductivity, transference number, and density. Then it is possible to predict the diffusion coefficient. Equation (6) becomes

$$\mathcal{D} = \frac{\nu kT/\mu}{\nu_+ A + \nu_- B} \quad . \tag{15}$$

Reliable data on the diffusion coefficients of KOH are not available. However, for KCl precise diffusion coefficient data are available[32,33]. Thus values of $\mathcal{D}_{o+}$, $\mathcal{D}_{o-}$, and $\mathcal{D}_{+-}$ can be calculated directly from experimental data without the assumption that A, B, and G are independent of concentration. The results are plotted in figure 5. The corresponding values of A, B, and G as functions of concentration are shown in table I.

Table I.

Transport Parameters for KCl

c $\frac{\text{mole}}{\text{liter}}$	A x 10^8 cm	B x 10^8 cm	G x 10^8 cm
0.0001	23.53	22.65	58.84
0.0005	23.53	22.63	72.72
0.001	23.53	22.63	76.54
0.005	23.48	22.59	79.17
0.01	23.45	22.56	78.60
0.05	23.25	22.34	80.08
0.1	23.11	22.18	70.69
0.5	23.03	22.01	53.87
1.0	23.53	22.48	46.29
2.0	24.41	23.28	38.83
3.9	25.21	23.99	34.47

An inspection of table I shows that A and B do not vary from the predicted values by more than 5%. This is satisfactory for most calculations. G shows variations of up to 100%. This could no doubt be improved upon by a more sophisticated relation than the last of equations (12). However, Δ_{+-} varies by more than three orders of magnitude, and thus the proposed relation offers considerable improvement. It should be noted that over a large part of the range of figures 1-4

$$G << \frac{A\ B}{\nu_+ A + \nu_- B} \frac{\sqrt{\nu}\ c_o}{\sqrt{c\ c_T}},$$

so that these plots are fairly insensitive to variations in G.

Conclusions

It is felt that the equations presented for the macroscopic description of ionic mass transport offer a

rational framework for the correlation of the transport properties of electrolytic solutions. The relations proposed for the description of the concentration dependence of the δ_{ij}'s are rather simple and can no doubt be improved upon through a more sophisticated consideration of the structure of liquids and molecular interactions. They do allow the diffusion coefficient to be predicted with sufficient accuracy for solutions where measurements are not available.

NOMENCLATURE

$\left.\begin{matrix} A \\ B \\ C \end{matrix}\right\}$ subsidiary transport properties defined so as to reduce the concentration dependence.

c - concentration of binary electrolyte = $c_+/\nu_+ = c_-/\nu_-$.

c_i - concentration of species i (mole/cm^3).

$c_T = \sum_i c_i$, the total concentration (including the solvent).

D - molecular diffusion coefficient of binary electrolyte.

D_i - diffusion coefficient of species i (cm^2/sec).

$\mathscr{D}$ - molecular diffusion coefficient of binary electrolyte based on activity gradients (cm^2/sec).

$\mathscr{D}_{ij}$ - "diffusion coefficient" describing the interaction of species i and j.

e - magnitude of the electronic charge (coulomb).

e^- - symbol for an electron.

$f_\pm$ - mean molar activity coefficient.

F - Faradav's constant (coulomb/equivalent).

i - current density (amp/cm^2).

k - Boltzmann's constant (erg/°K).

m - molality (moles per 1000 grams of solvent).

M_i - a symbol for the chemical formula of species i.

n - number of electrons transferred.

N_i - flux of species i (mole/cm^2-sec).

R - universal gas constant (joule/mole-°K).

s_i - stoichiometric coefficient of species i.

t_i^* - transference number of species i with respect to molar average velocity.

t_i^o - transference number of species i with respect to the solvent velocity.

T - absolute temperature (°K).

u_i - mobility of species i (cm^2-mole/joule-sec).

$\underline{v}$ - fluid velocity (cm/sec).

$\underline{v}_i$ - velocity of species i (an average velocity for the species, not the velocity of individual molecules).

$\underline{v}^*$ - molar average velocity (cm/sec).

z_i - valence or charge number of species i (negative for anions).

γ - mean molal activity coefficient.

κ - conductivity (mho/cm).

μ - viscosity (poise).

μ_e - chemical potential of binary electrolyte (joule/mole).

μ_i - the electrochemical[5] potential of species i (joule/mole).

ν_+ - number of cations per molecule of electrolyte.

ν_- - number of anions per molecule of electrolyte.

$\nu = \nu_+ + \nu_-$.

Φ - electrostatic potential (volts).

LITERATURE CITED

1. Veniamin G. Levich. Physicochemical Hydrodynamics. Englewood Cliffs, N. J.: Prentice-Hall, Inc., 1962.

2. E. A. Guggenheim. Thermodynamics. Amsterdam: North-Holland Publishing Company, 1959.

3. E. A. Guggenheim. "The Conceptions of Electrical Potential Difference Between Two Phases and the Individual Activities of Ions." J. Phys. Chem., 33, 842-849 (1929).

4. E. A. Guggenheim. "On the Conception of Electrical Potential Difference Between Two Phases. II." J. Phys. Chem., 34, 1540-1543 (1930).

5. E. A. Guggenheim. "On the Meaning of Diffusion Potential." Phil. Mag., ser. 7, 22, 983-987 (1936).

6. R. Byron Bird, Warren E. Stewart, and Edwin N. Lightfoot. Transport Phenomena. New York: John Wiley & Sons, Inc., 1960. Page 570.

7. Lars Onsager. "Theories and Problems of Liquid Diffusion." Ann. N. Y. Acad. Sci., 46, 241-265 (1945).

8. Richard W. Laity. "General Approach to the Study of Electrical Conductance and its Relation to Mass Transport Phenomena." J. Chem. Phys., 30, 682-691 (1959).

9. Richard W. Laity. "An Application of Irreversible Thermodynamics to the Study of Diffusion." J. Phys. Chem., 63, 80-83 (1959).

10. Alfred Klemm. "Thermodynamik der Transportvorgänge in Ionengemischen und ihr Anwendung auf istopenhaltige Salze und Metalle." Z. Naturforsch., 8a, 397-400 (1953).

11. A. Klemm. "Zur Phänomenologie der isothermen Diffusion in Elektrolyten." Z. Naturforsch., 17a, 805-807 (1962).

12. J. M. Burgers. "Some Problems of Magneto-Gasdynamics," in Sydney Goldstein, Lectures on Fluid Mechanics. London: Interscience Publishers, Ltd., 1960. pp. 271-299.

13. E. N. Lightfoot, E. L. Cussler, Jr., and R. L. Rettig. "Applicability of the Stefan-Maxwell Equations to Multicomponent Diffusion in Liquids." A.I.Ch.E. J., 8, 708-710 (1962).

14. Ole Lamm. "Studies in the Kinematics of Isothermal Diffusion. A Macro-Dynamical Theory of Multicomponent Fluid Diffusion." I. Prigogine, ed. Advan. Chem. Phy. Vol. 6, pp. 291-313. New York: Interscience Publishers, 1964.

15. C. Truesdell. "Mechanical Basis of Diffusion." J. Chem. Phys., 37, 2336-2344 (1962).

16. Douglas Noel Bennion. Phenomena at a Gas-Electrode-Electrolyte Interface. Dissertation, University of California, Berkeley, June, 1964.

17. Grinnell Jones and Samuel K. Talley. "The Viscosity of Aqueous Solutions as a Function of the Concentration. II. Potassium Bromide and Potassium Chloride." J. Am. Chem. Soc., 55, 4124-4125 (1933).

18. Grinnell Jones and Samuel K. Talley. "The Viscosity of Aqueous Solutions as a Function of the Concentration." J. Am. Chem. Soc., 55, 624-642 (1933).

19. Taizo Kume and Mitsuru Tanaka. "Studies on the Concentrated Solution of Electrolyte: Viscosity." Nippon Kagaku Zasshi, 81, 534-539 (1960). (In Japanese.)

20. M. A. Klochko and M. M. Godneva. "Electrical Conductivity and Viscosity of Aqueous Solutions of NaOH and KOH." Zh. Neorgan. Khim., 4, 2127-2135 (1959).

21. M. I. Usanovich and T. I. Sushkenvich. "Conductance and Viscosity in the KOH-K_2CO_3-H_2O System." Zh. Prikl. Khim., 24, 590-592 (1951)

22. L. B. Hitchcock and J. S. McIlhenny. "Viscosity and Density of Pure Alkaline Solutions and Their Mixtures." Ind. Eng. Chem., 4, 461-466 (1935).

23. H. E. Gunning and A. R. Gordon. "The Conducance and Ionic Mobilities for Aqueous Solutions of Potassium and Sodium Chloride at Temperatures from 15° to 45°C." J. Chem. Phys., 10, 126-131 (1942).

24. Benton Brooks Owen and Henry Zeldes. "The Conductance of Potassium Chloride, Potassium Bromide and Potassium Iodide in Aqueous Solutions from 5 to 55°." J. Chem. Phys., 18, 1083-1085 (1950).

25. Harry M. Daggett, Jr., Edward J. Bair, and Charles A. Kraus. "Properties of Electrolytic Solutions. XLVII. Conductance of Some Quaternary Ammonium and Other Salts in Water at Low Concentration." J. Am. Chem. Soc., 73, 799-803 (1951).

26. L. Nickels and A. J. Allmand. "The Electrical Conductivities and Viscosities at 25°C of Solutions of Potassium, Sodium, and Lithium Chlorides, in Water and in One-Tenth Molar Hydrochloric Acid." J. Phys. Chem., 41, 861-872 (1937).

27. Lawrence S. Darken and Harry F. Meier. "Conductances of Aqueous Solutions of the Hydroxides of Lithium, Sodium, and Potassium at 25°C." J. Am. Chem. Soc., 64, 621-624 (1942).

28. S. M. Mehta, M. B. Kabadi, and V. T. Sheth. "The Electrical Conductivity of Concentrated Solutions of Sodium and Potassium Hydroxides." Current Sci., 15, 129 (1946).

29. S. Lengyel, J. Giber, Gy. Beke, and A. Vértes. "Determination of the Transference Number in Concentrated Aqueous Solutions of Sodium and Potassium Hydroxide." Acta Chim. Acad. Sci. Hung., 39, 357-363 (1963).

30. D. A. MacInnes and L. G. Longsworth. "Transference Numbers by the Method of Moving Boundaries. Theory, Practice, and Results." Chem. Rev., 11, 171-230 (1932).

31. Duncan A. MacInnes and Malcolm Dole. "The Transference Numbers of Potassium Chloride. New Determinations by the Hittorf Method and a Comparison with Results Obtained by the Moving Boundary Method." J. Am. Chem. Soc., 53, 1357-1364 (1931).

32. Herbert S. Harned and Ralph L. Nuttall "The Diffusion Coefficient of Potassium Chloride in Aqueous Solution at 25°C." Ann. N. Y. Acad. Sci., 51, 781-788 (1949).

33. Louis J. Gosting. "A Study of the Diffusion of Potassium Chloride in Water at 25°C. with the Gouy Interference Method." J. Am. Chem. Soc., 72, 4418-4422 (1950).

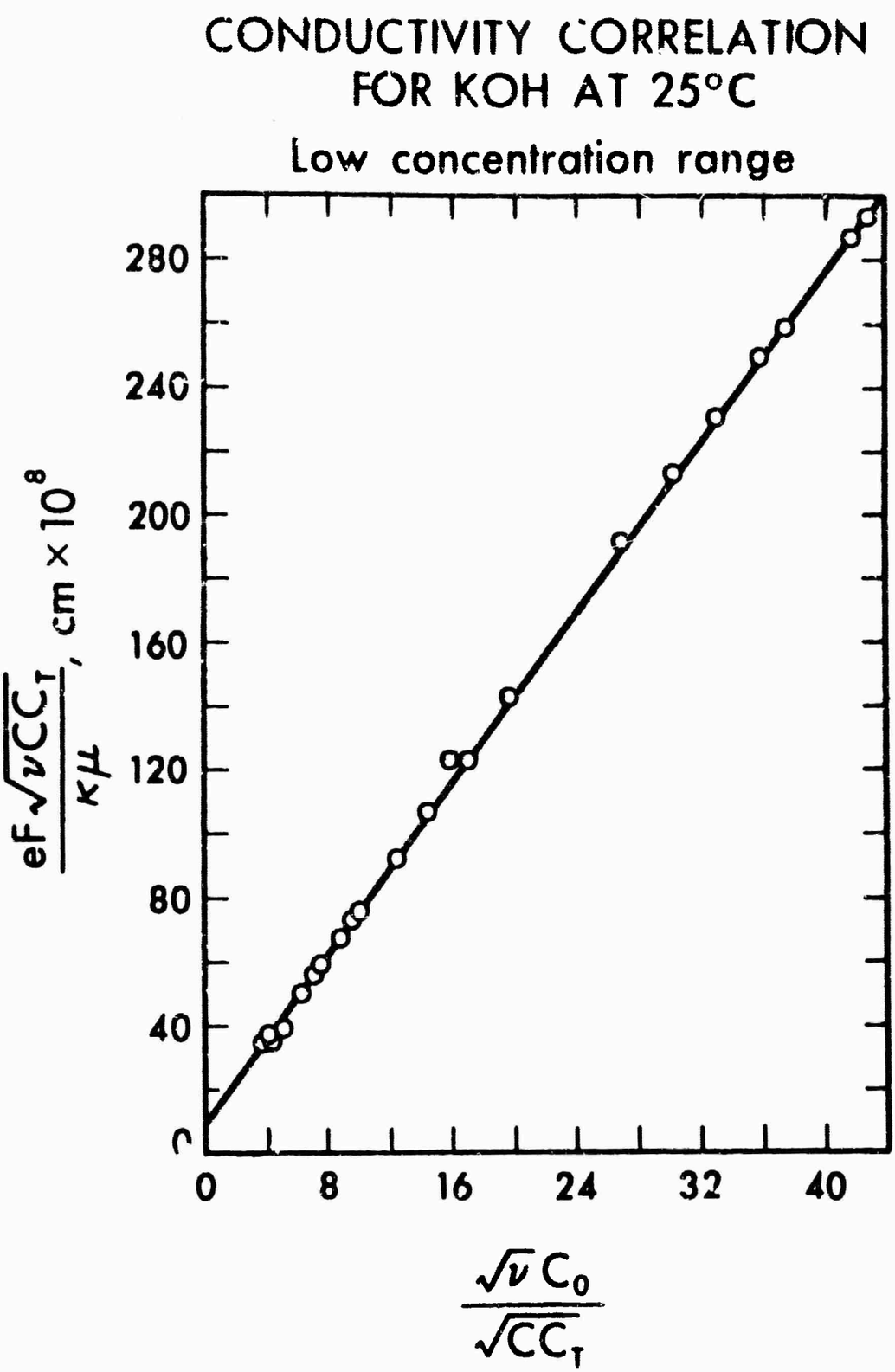

Experimental points based on conductivity and interpolated values of viscosity and density. The curve is the best least squares straight line through the data. Slope = 6.646 x 10^{-8}cm. Intercept = 9.627 x 10^{-8}cm.

FIGURE 1

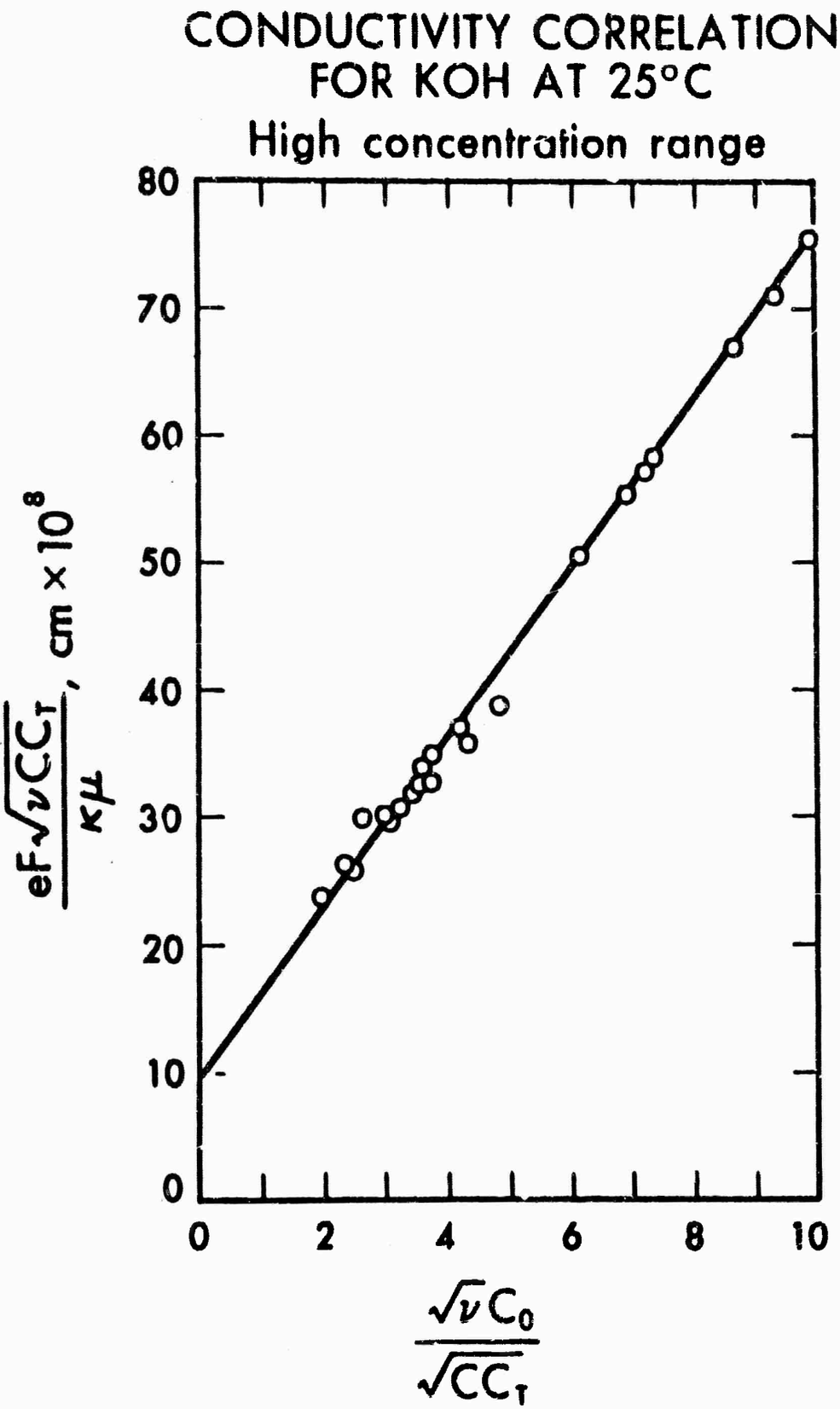

Experimental points based on conductivity and interpolated values of viscosity and density. The curve is the best least squares straight line through the data. Slope = 6.646×10^{-8} cm. Intercept = 9.627×10^{-8} cm.

FIGURE 2

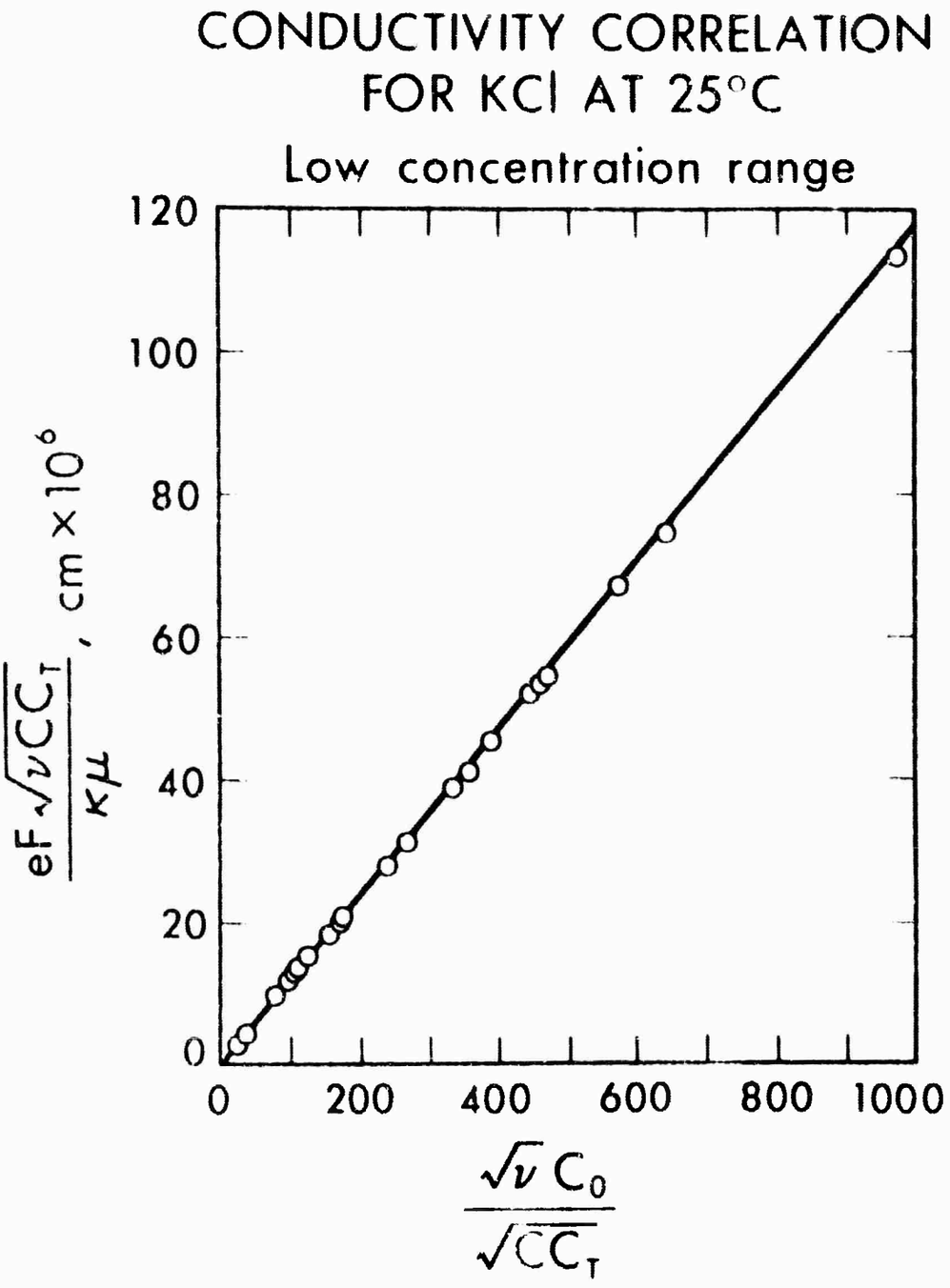

Experimental points based on conductivity and interpolated values of viscosity and density. The curve is the best least squares straight line through the data. Slope = 11.766 x 10^{-8}cm. Intercept = 39.710 x 10^{-8} cm.

FIGURE 3

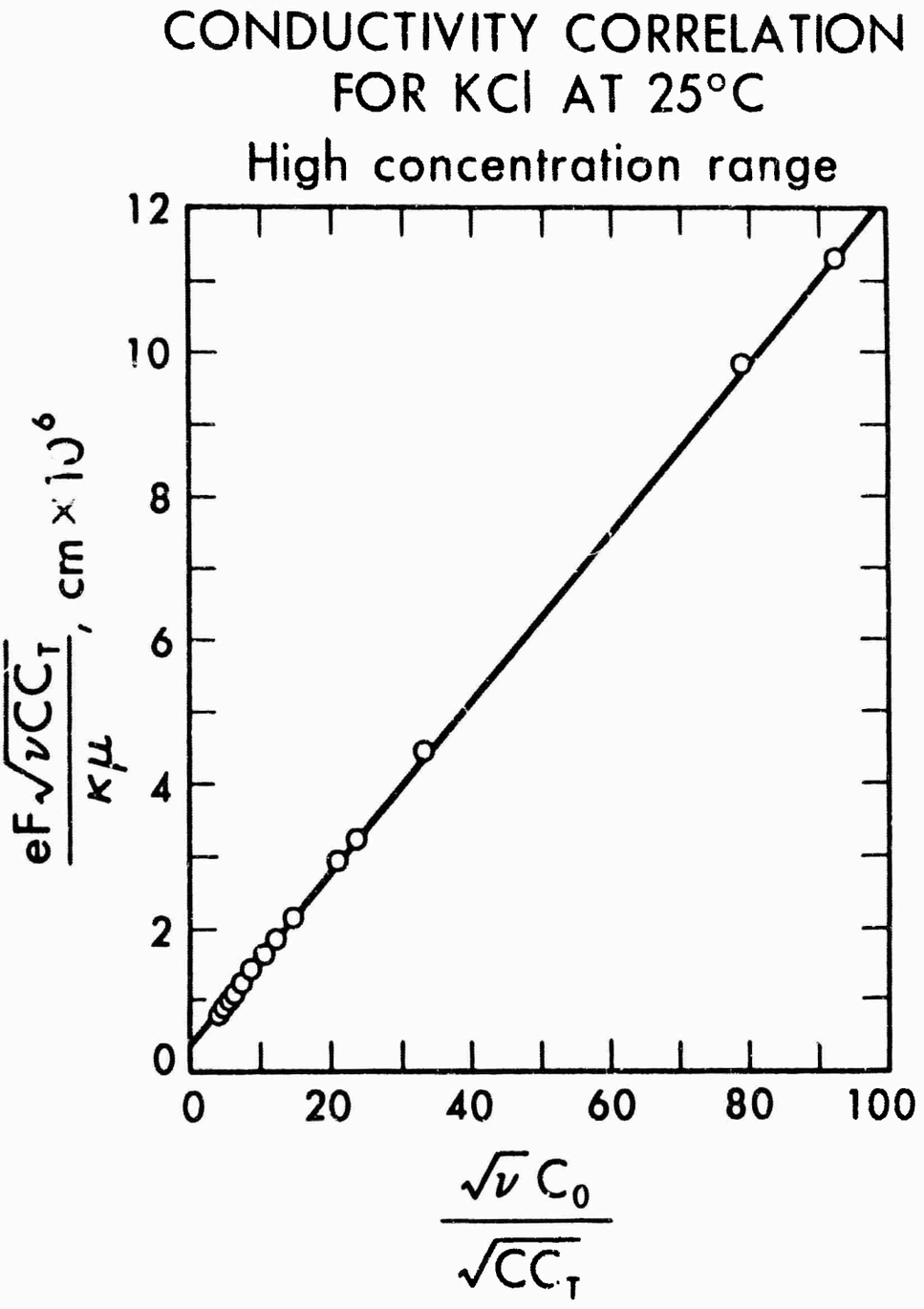

Experimental points based on conductivity and interpolated values of viscosity and density. The curve is the best least squares straight line through the data. Slope = 11.766 x 10^{-8}cm. Intercept = 39.710 x 10^{-8}cm.

FIGURE 4

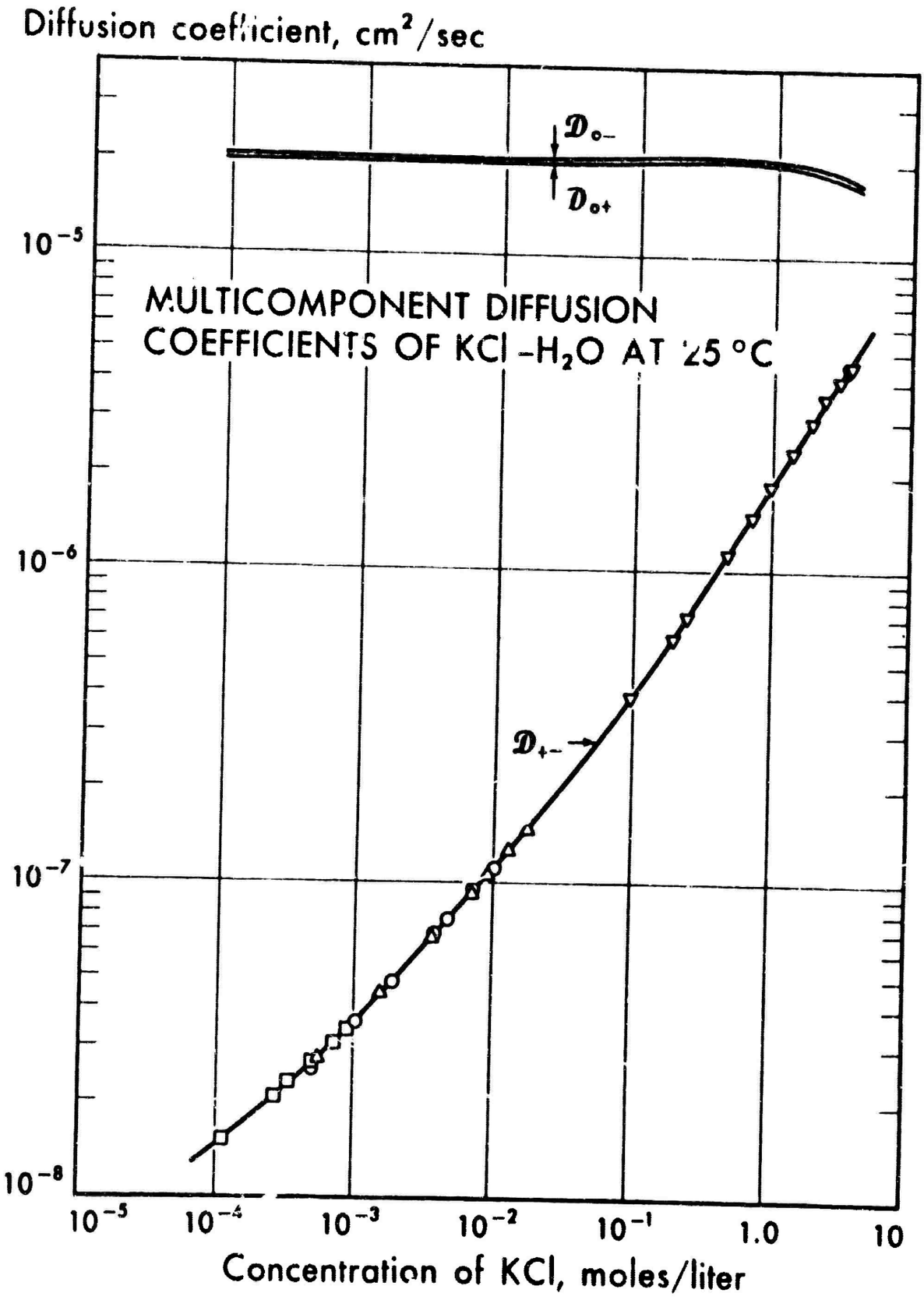
Diffusion coefficient, cm²/sec
$\mathcal{D}_{o-}$
$\mathcal{D}_{o+}$
MULTICOMPONENT DIFFUSION COEFFICIENTS OF KCl -H_2O AT 25 °C
$\mathcal{D}_{+-}$
10^{-5}
10^{-6}
10^{-7}
10^{-8}
10^{-5}
10^{-4}
10^{-3}
10^{-2}
10^{-1}
1.0
10
Concentration of KCl, moles/liter

FIGURE 5

PROJECT V.

Diffusion Coefficient and Solubility of O_2 in Aqueous KOH Solutions

Introduction

The dynamic behavior of gas electrodes is strongly dependent on the solubility and diffusion coefficient of the reacting gas. These properties which greatly influence the transport process should be known with a reasonable degree of accuracy over a wide range of temperature and electrolyte concentrations. Of particular interest is the case of oxygen in aqueous potassium hydroxide solutions. A search of the literature produced few data concerning the solubility of oxygen in basic media[1-4]. No comprehensive data on the diffusion coefficient of oxygen in aqueous KOH solutions was found.

The solubility of oxygen in distilled water has been investigated by many workers[5] at 25°C, and it is now generally agreed that the value is 1.26×10^{-3} ±1% mole per liter. Values of 1.8 to 2.6 x 10^{-5} cm^2/sec have been reported[6-9] for the diffusion coefficient in distilled water. Other workers have recently investigated the solubility of oxygen in potassium hydroxide solutions[10,11]. However, one finds significant inconsistencies when comparing the results of the various experimenters, especially in regard to concentrated caustic solutions.

In this laboratory two methods were utilized in making the solubility measurements. In the first a Van Slyke manometer

apparatus was used in which dissolved gas was boiled off from a presaturated solution and the pressure of the gas measured at a known volume. The second method involved bringing a known amount of gas into contact with degassed solution and measuring the amount absorbed.

The experimental methods chosen for determining the diffusion coefficient involved the measurement of transport rates to an electrode at which oxygen was consumed. Since it was felt that the equation describing transport to the electrode should be unambiguous and free of empirical constants, a rotating disk electrode and a stagnant diffusion cell were employed, rather than the dropping mercury electrode.

O_2 solubility measurements

Experimental: The Van Slyke manometer was used for the major portion of the solubility values reported. The apparatus is shown in Figure 1. The experimental procedure consisted of admitting a known amount of liquid through stopcick A into chamber B which was initially filled with mercury. After all of the liquid was in the chamber, stopcock A was closed and the mercury level dropped to the 50 ml level. The sample, now under vacuum, was agitated by a magnetic stirrer in order to facilitate the boiling off of the dissolved gases. After a suitable period of agitation, the liquid level was raised to the 2 ml mark which confined the gas to a precalibrated volume. The pressure of the evolved gas was determined by the height of the mercury in the manometer column C. The gas was ejected and the liquid returned to the 50 ml mark. After reboiling, a second

pressure reading was taken. The difference between the two pressures represented the pressure of the dissolved gas at the calibrated volume.

The absorption apparatus and experimental procedure are described in detail by Kabatake and Hildebrand[12] and will not be discussed here.

The solutions for the Van Slyke experiments were prepared by bubbling 99.6% pure oxygen through the sample for 15 minutes. The sample was in a constant temperature bath controlled to ±0.2°C during this period. The gas was presaturated with water vapor by first bubbling the oxygen through a solution of the same temperature and composition as the sample. After a 2-5 minute period during which the bubbling was stopped and an oxygen blanket was maintained, the sample was withdrawn and analyzed for oxygen content.

For the absorption experiments two methods were tried in preparing the degassed solution. In the first, KOH solutions were boiled for 24 hours under vacuum while boiling and freezing the liquid sample. A single stage vacuum distillation was used in the other procedure. Distilled water was frozen over pellets under vacuum and the resulting solution boiled and cooled to 0°C under vacuum to insure a gas-free sample.

The principal factors affecting the solubility results utilizing the Van Slyke apparatus were: a) measurement of the sample volume; b) measurement of the pressure and volume of the gas boiled off; and c) the degree of saturation of the sample introduced into the manometer. Sample volumes were measured

with a maximum probable error of ±1.0%, the measurement of the gas volume and pressure introduced a maximum probable error of 0.5% with a maximum precision of 3×10^{-6} mole gas per liter.

Supersaturation was believed to be a source of error since the samples were prepared by bubbling gas through the liquid. Experiments were conducted in which samples were taken from saturated liquid and the solubility determined as a function of time after the bubbling was stopped. After two to three minutes, the solution had developed its equilibrium state and no change in the solubility could be detected within the limits of sensitivity of the Van Slyk apparatus. It was also suggested that the hydrostatic head could cause a supersaturation condition; however, Livingston, Morgan, and Richardson[13] showed that with a ten centimeter high flask the height of the column would have little effect on the solubility. This is especially true when agitation occurs in the liquid which was the case in these experiments.

Livingston et al also showed that Henry's law is obeyed for oxygen dissolved in water. In order to compare our results with those by other experimenters, who present their data at a partial pressure of O_2 of 760 mm Hg, we assumed that Henry's law applies to solutions of KOH.

Kabataka and Hildebrand stated that the largest source of error in their experiments was the degassing process. Substantial improvement was made by our addition of the vacuum distillation to the degassing process.

The error in absorption determinations was estimated to be less than 1%; however, as with the Van Slyke, this error increases as one increases the KOH concentration. The solubility drops by a factor of 100 as the KOH concentration increases from 0 to 10 molar, thus approaching the limits of the apparatus.

Results and discussion

The results of the Van Slyke experiments are presented in Figure 2. This plot shows the variation of oxygen solubility as a function of potassium hydroxide concentration at a total pressure of one atmosphere. At 25°C and a partial pressure of 760 mm Hg oxygen this variation is represented by the equation

$$\text{Log } S = -0.1746\ C + \text{Log } 1.26 \times 10^{-3}$$

where S = the solubility of oxygen in gram-moles per liter and C = the concentration of KOH in gram-moles per liter.

The linear variation of the logarithm of oxygen concentration with KOH concentration is typical of the "salting out" of a non-electrolyte in an electrolyte solution. The vapor pressure of the solvent changes by 15 mm Hg at 25°C over the range of KOH concentration investigated; therefore the partial pressure of the non-electrolyte is very nearly constant. At 0°C the difference in partial is negligible and at 60°C the change is in the order of 100 mm Hg.

The theoretical explanation of the "salting out" (or in some cases "salting in") of a non-electrolyte by an electrolyte has been attempted by several workers[14,15,16,17]. In all cases assumptions must be made which cannot be expected to be valid over a wide range of salt concentrations. With the

exception of the theory of McDevit and Long, the assumption is made that the non-electrolyte affects the dielectric constant of the solution. This variation is considered to be the principal effect of the non-electrolyte. By assuming the dielectric constant is a linear function of the non-electrolyte concentration, a logarithmic "salting out" behavior is predicted. The theory of McDevit and Long is based on the concept of an "internal pressure" of the solution.

In none of the available theories are the parameters sufficiently well-known to allow verification. The temperature variation of the parameters is even less precisely known. However, for most cases, experimental measurements show that the slope of the log concentration non-electrolyte versus salt concentration plot decreases with increasing temperature.

After the experiments with the Van Slyke were completed it was noted that there were large differences between the results of this work and those presented by Pospisil and Luzny[4]. Although their value agreed with ours for distilled water, the discrepancy was in the order of 200% in 4 molar KOH solution. Results obtained with the Hildebrand apparatus are plotted on Figure 3 for 25°C. Included in the figure are points from other investigators as well as results from the Van Slyke experiment corrected to a partial pressure of O_2 of 760 mm Hg.

Walker et al[10] used a gas chromatographic method for their measurements in which the precision is said to be of the order of ±1%; however, because of the very low oxygen solubility in

concentrated KOH solutions, they say these results are probably only accurate to ±15-20% for KOH concentration higher than 7 molar.

Knaster and Apel'baum[11] have recently investigated the solubility of oxygen in KOH solutions at 21°C, 45°C, and 75°C. An apparatus similar to the Van Slyke was used for their experiments. As in the present work, the method of saturation was bubbling oxygen through KOH solutions. Solubility values for 4, 7, and 10 molar at 25°C were interpolated from their data and shown in Figure 3.

Pospisil and Luzny[4] estimate their experimental error to be less than 0.9%; however, their results do not follow the trend seen by other investigators.

Diffusion coefficient measurements:

Theory of experimental methods: The rotating disk electrode has been considered by Levich[18] in detail. Gregory and Riddiford[19] have pointed out an error introduced by an approximation in the Levich solution. Newman[20] has provided a correction to the Levich statement which is more exact than that given by Gregory and Riddiford. The Levich expression for the limiting current density in Amp per cm^2 is

$$\frac{i_{lim}}{nF\, C_{bulk}\, w^{1/2}\, \nu^{1/2}} = 0.6205\, Sc^{-2/3}$$

where n is the number of electrons transferred per molecule, F is the Faraday, C_{bulk} is the bulk concentration in moles per cm^3, w is the angular velocity in radians per second, ν is

the kinematic viscosity - $\frac{cm^2}{sec}$ and Sc is the Schmidt number $(\frac{\nu}{D})$. The Newman correction which is valid for the range $400 < Sc < 1400$ is

$$\frac{i_{lim}}{nF\ C_{bulk}\ w^{1/2}\nu^{1/2}} = \frac{0.6205\ Sc^{-2/3}}{1 + 0.298\ Sc^{-1/3} + 0.14514\ Sc^{-2/3}}\ .$$

The case of diffusion through a stagnant liquid to an electrode has been the subject of investigations by Stackelberg[21], Laitinen and Kolthoff[22], and Lingane[23]. The absence of natural convection is essential to this method. Even though this condition may be difficult to realize, the low current densities used in stagnant diffusion cells make them attractive in the cases where activation polarization prevents determination of limiting current densities in the forced convection regime. Diffusion in a pore to a flat electrode appears to provide the best opportunity to eliminate natural convection.

Although chronopotentiometry has been demonstrated to be a powerful analytical tool, it was felt that for work with the oxygen electrode constant potential operation offered special advantages. In chronopotentiometric determinations any current which is not due to diffusion of the species under investigation will increase the transition time and thus the apparent diffusion coefficient will be incorrect. In the case of constant potential operation such effects are not as important as long as the concentration of the diffusing species eventually become zero at the electrode.

The equation

$$\frac{\partial c}{\partial t} = D\ \frac{\partial^2 c}{\partial x2} \qquad (1)$$

solved for the boundary conditions

$$\text{I.} \quad C = C_{bulk} \quad \text{at all } x \quad \text{for } t = 0$$

$$\text{II.} \quad C = 0 \quad \text{at } x = 0 \quad \text{for } t > 0$$

$$\text{III.} \quad C = C_{bulk} \quad \text{at } x = \infty \quad \text{for } t > 0$$

yields the solution

$$i = nF\ D \left.\frac{\partial C}{\partial x}\right|_{x=0} = \frac{nF\ C_{bulk}}{\sqrt{\pi}} \sqrt{\frac{D}{t}} \qquad (2)$$

Thus if diffusion in the pore is unidirectional and the electrode is operating at limiting current, the current should drop as $t^{-1/2}$. The correction for the finite length of the pore is found to be negligible for time periods of several hours.

If a first order rate equation is assumed such that

$$i = K\ C_{electrode}\ e^{\eta}$$

where η is the overpotential and the cell is to be run at constant overpotential, boundary condition II becomes

$$\text{II'} \quad C = \frac{i}{K\ e^{\eta}} = \frac{NF\ D}{K\ e^{\eta}} \left.\frac{\partial C}{\partial x}\right|_{x=0} \quad \text{at } x=0 \quad \text{for } t>0.$$

A typical solution of equation (1) with boundary condition II is plotted in Figure 4. It can be seen that the current converges to that predicted equation (2). Therefore even if the electrode is not at limiting current when the potential is first applied, it does converge on equation (2) regardless of the rate constant or overpotential applied.

Experimental

Disk electrodes were constructed as indicated in Figure 5. The disks were rotated on a double ball bearing shaft by

a 1/4 horsepower D.C. motor. The speed was varied from 900 rpm to 3600 rpm and measured with a stroboscopic tachometer. Current was provided by a Lambda Electronic Model 28 constant current supply and measured by means of the voltage drop across a calibrated precision resistor. Electrode potentials were measured relative to a saturated mercury/mercury oxide reference electrode and recorded by a Bausch and Lomb V.O.M-5 recorder.

Platinum, silver, nickel, amalgamated silver and gold plated copper were used as working electrodes. The counter electrode was a platinum screen. The diameter of the rotating disk was measured by a comparator to an accuracy of ±0.5%.

The cell used in the stagnant diffusion experiments is shown in Figure 6. The working electrode and counter electrode were silver. The diameter of the diffusion pore was measured with micrometered wire to an accuracy of ±1.5%. Current and potential measurements were made in the same manner as the disk experiments with an accuracy of ±0.5%.

All solutions were prepared from distilled water and reagent grade potassium hydroxide. 99.6% pure oxygen was used saturating the solution. Viscosity of the solutions at 25°C was taken from the data of McIlhenny[24] and from the data of the Solvay Technical Service[25] for 60°C.

The electrodes in all cases were pretreated by cathodic evolution of hydrogen. Experiments were carried out in a constant temperature bath controlled to 0.2°C. Saturation was achieved by sparging oxygen into the solution through a fritted

glass tube for 15 minutes prior to making a determination. In some cases the bulk concentration of oxygen was determined by a Van Slyke analysis to insure that saturation was being developed.

In the rotating disk experiments, the limiting current was determined at 3 to 4 rotational speeds with both silver and plainum electrodes. These limiting currents were plotted versus the square root of the rotational speed and the best straight line fitted. From these plots and the reproducibility of duplicate runs, the error in the determination of limiting current was estimated to be of the order of 3%. The diffusion coefficients were calculated on the basis of the Newman correction to the Levich solution for the transport equation.

The current versus time behavior of the stagnant diffusion cell was recorded for periods of 15 to 30 minutes. A constant potential between 1.0 and 1.2 volts was applied to the cell during each experiment. Before applying the potential, the liquid in the pore was withdrawn into a syringe through a hypodermic needle, thus drawing fresh solution from the bulk into pore. Five to ten minutes was allowed for the solution to become quiescent.

In general the experimental curves did not have the same shape as those calculated assuming a first order rate equation, but did converge to a straight line of slope -1/2. The diffusion coefficient was calculated using equation (2). From the scatter of the points on the current versus time plot the probable error in the diffusion coefficients was estimated to be ±8% in the high concentration range.

solutions, the activation overpotential was low and the limiting current plateau was well defined. As the KOH concentration was increased the activation overpotential increased and the limiting current plateau became less distinct.

When platinum was the metal used at a constant current and rotational speed, the overpotential was found to vary with time. As was noted by Palous and Buret[27], the potential depended not only on time but also on the previous current setting. If the current had been decreased the overpotential was considerably lower than if it had been increased. As the concentration of KOH was increased, the variation of potential with time increased until in 2.0 molar KOH it was nearly impossible to determine a reproducible current versus a potential curve. Therefore, at higher than 2 molar KOH concentration, investigations were made using the stagnant diffusion cell.

Walker et al[10] have recently measured the diffusion coefficient for O_2 in KOH solutions at 25°C by the polarographic technique. The calculated diffusivity values are 10-20% higher than those obtained in this laboratory. The modified form of the Ilkovic equation[27] which employs an empirical constant was used to evaluate the diffusion coefficient from the polarographic data. Because of the uncertainty in the constant, as reported by Walker et al, no critical evaluation can be made of their results.

Results and Discussion

The diffusion coefficient for 25°C and 60°C is plotted as a function of potassium hydroxide concentration in Figures 7, 8. Because of the rapid increase of the oxygen diffusion coefficient with decreasing KOH concentration in dilute solutions, it is difficult to make an accurate extrapolation to determine the value in water. From Figure 7 it may be estimated to be between 1.9 and 2.0 x 10^{-5} cm^2/sec at 25°C, and from Figure 8 to be between 4.6 and 4.8 x 10^{-5} cm^2/sec at 60°C. The diffusivity at 25°C compares well with values between 1.9 x 10^{-5} and 2.0 x 10^{-5} cm^2/sec reported by Himmelblau[26] and 2.12 x 10^{-5} cm^2/sec reported by Jordan et al[8].

These estimates correspond to a temperature coefficient of 2.4% per degree for the diffusion coefficient in water. The data summarized by Millington[7] indicates a temperature coefficient between 2 and 3.5% per degree in the temperature range 16°C to 25°C.

The product of the diffusion coefficient and the viscosity is plotted in Figure 9. As is noted in this figure, the decrease in viscosity with increasing temperature does not account for the temperature coefficient of the diffusion coefficient.

The rapid increase of the product $D\mu$ in dilute solutions was also reported by Jordan, Ackerman and Berger[8]. It may be explained by assuming a cage-like structure for water. As the solution becomes more concentrated the cages become filled and diffusion becomes more hindered.

With silver rotating disk electrodes in dilute KOH

LITERATURE CITED

1. Geffcken, Z. Physik Chem. 49, 257 (1904).
2. "International Critical Tables", Vol. III.
3. Comey, "Dictionary of Chemical Solubilities", MacMillan, New York, 1921, pp. 637.
4. Pospisil and Luzny, Coll. Czeck. Chem. Commun. 25, 589 (1960).
5. Douglas, J. of Phys. Chem. 68, 169 (1964).
6. Semerana, Riccoboni and Faffani, Gazz Chem. Ital. 79, 395 (1949).
7. Millington, Science 122, 1090 (1955).
8. Jordan, Ackerman and Berger, J. Am. Chem. Soc. 78, 2979 (1956).
9. "International Critical Tables", Vol. III.
10. Walker, "Diamond Laboratories Quarterly Progress Report, Fuel Cells, UFCG-13, July-September (1964).
11. Knaster and Apel'baum, Russ. J. of Phys. Chem. 38, 120 (1964).
12. Kabatake and Hildebrand, J. Phys. Chem. 65, 331 (1961).
13. Livingston, Morgan, and Richardson. J. Phys. Chem. 34, 2356 (1930).
14. Debye and Mc Auley, Physik Z. 26, 22 (1925).
15. Debye, Z. Physik Chem. 130, 56 (1927).
16. Kirkwood, Chem. Revs. 24, 233 (1939).
17. McDevit and Long, Chem. Revs. 51, 131 (1952).
18. Levich, Acta Physiochem. USSR 17, 257 (1942).
19. Gregory and Riddiford, J. Chem. Soc. 3756 (1956).
20. Newman, J., Dept. of Chem. Eng., Univ. of Calif., Berkeley, Private communication.
21. Stackelberg, Z. Electrochimie 57, 342 (1953).

22. Laitinen and Kolthoff, J. Am. Chem. Soc. 61, 3344 (1939).

23. Lingane, "Electroanalytical Chemistry", Interscience, New York, 1958, Chapter 22.

24. Hitchcock and McIlhenny, Ind. Eng. Chem. 27, 466 (1935).

25. "Caustic Potash", Solvay Technical Service, Bulletin 15 (1960).

26. Himmelblau, "Diffusion of Gases in Aqueous Solutions", University of Texas, March (1963).

27. Palous and Buret, Bull. Chem. Soc. France/606 (1962).

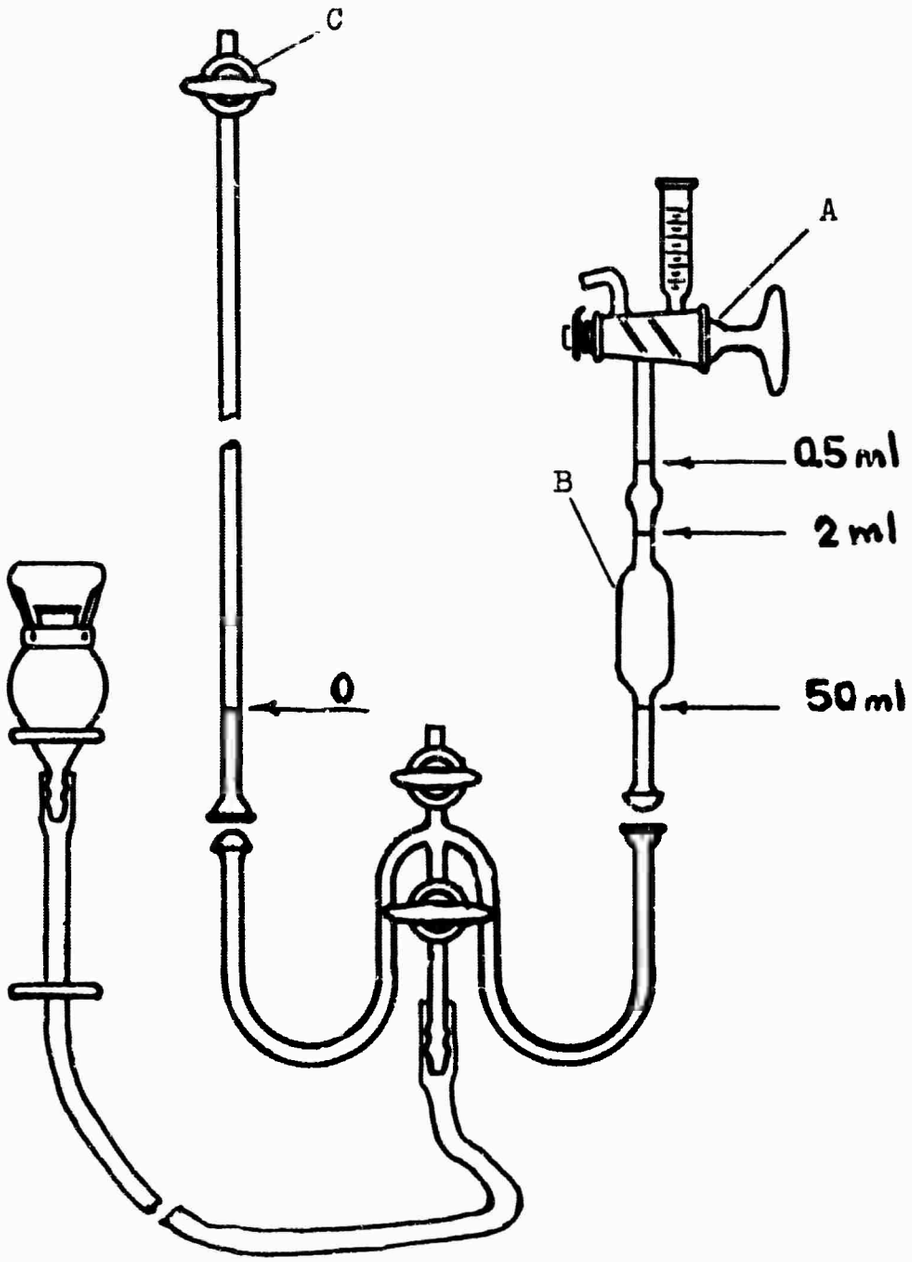

Figure 1.

Van Slyke Apparatus.

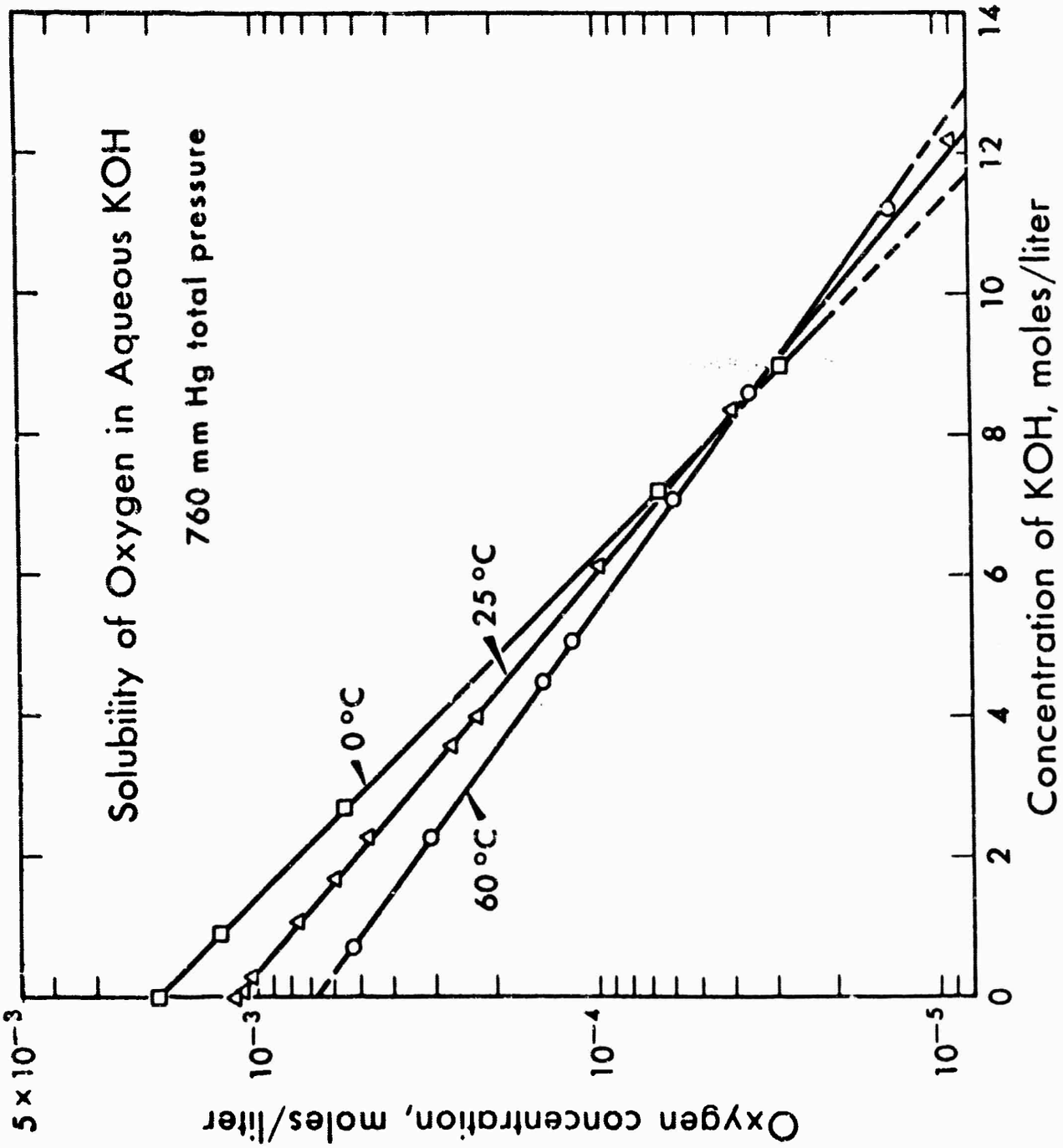
Solubility of Oxygen in Aqueous KOH
760 mm Hg total pressure
0 °C
25 °C
60 °C
Oxygen concentration, moles/liter
Concentration of KOH, moles/liter
5 × 10⁻³
10⁻³
10⁻⁴
10⁻⁵
0
2
4
6
8
10
12
14

Figure 2.

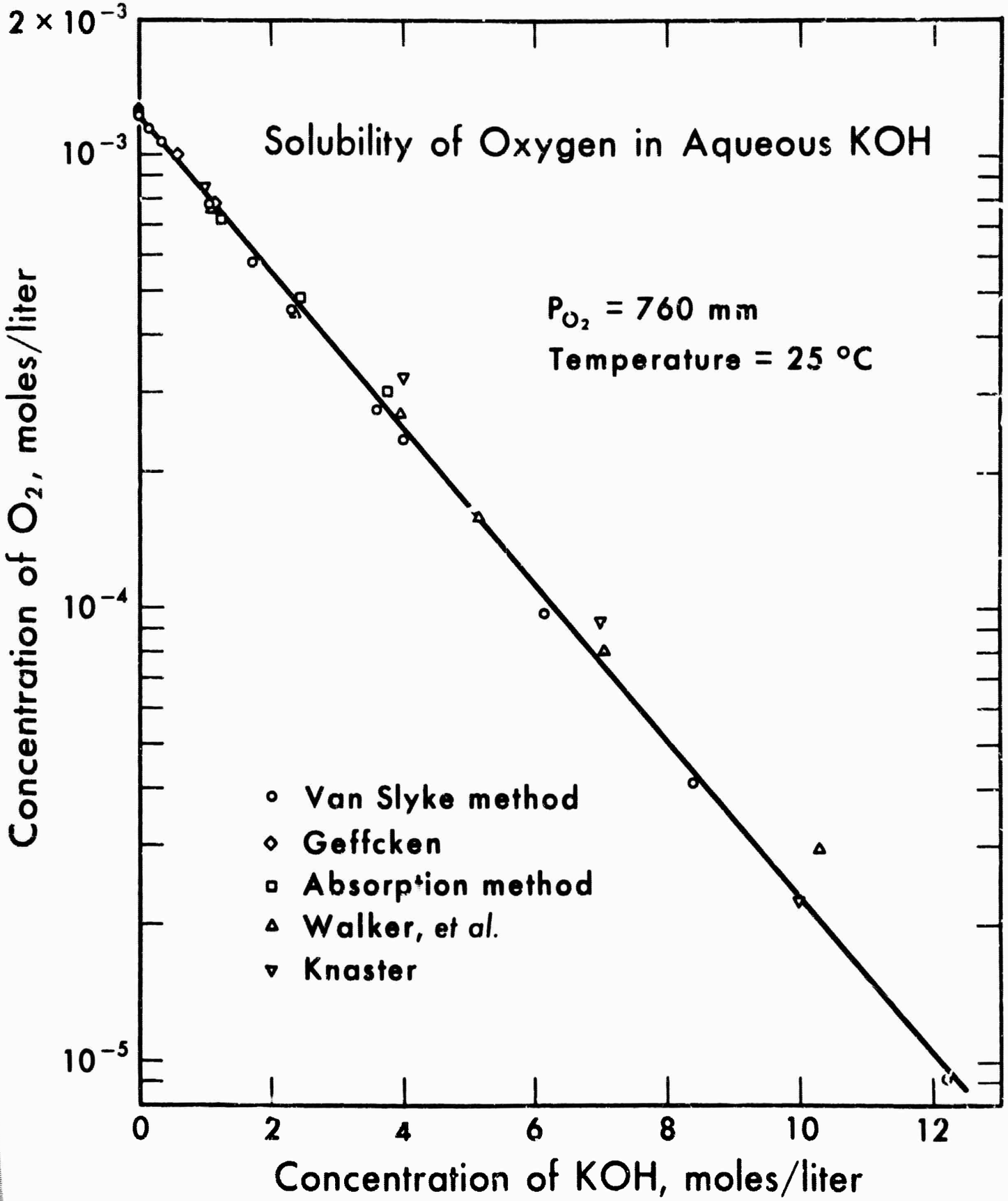
Solubility of Oxygen in Aqueous KOH
P_{O_2} = 760 mm
Temperature = 25 °C
Concentration of O_2, moles/liter
2×10^{-3}
10^{-3}
10^{-4}
10^{-5}
Van Slyke method
Geffcken
Absorption method
Walker, et al.
Knaster
0
2
4
6
8
10
12
Concentration of KOH, moles/liter

Figure 3.

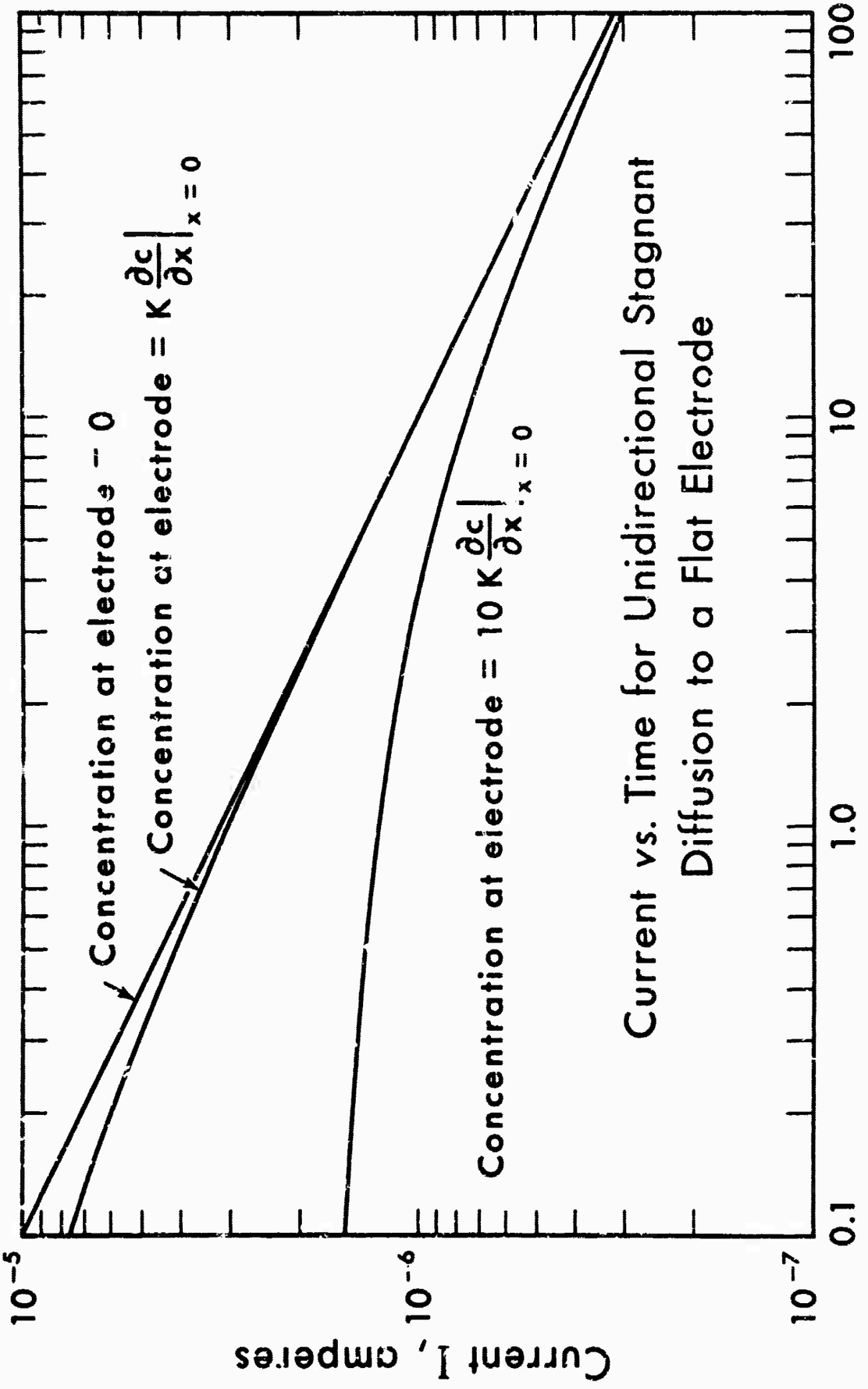
Current vs. Time for Unidirectional Stagnant Diffusion to a Flat Electrode
Concentration at electrode = 0
Concentration at electrode = $K\left|\frac{\partial c}{\partial x}\right|_{x=0}$
Concentration at electrode = $10K\left|\frac{\partial c}{\partial x}\right|_{x=0}$
Current I, amperes
10^{-5}
10^{-6}
10^{-7}
0.1
1.0
10
100
Time, minutes

Figure 4.

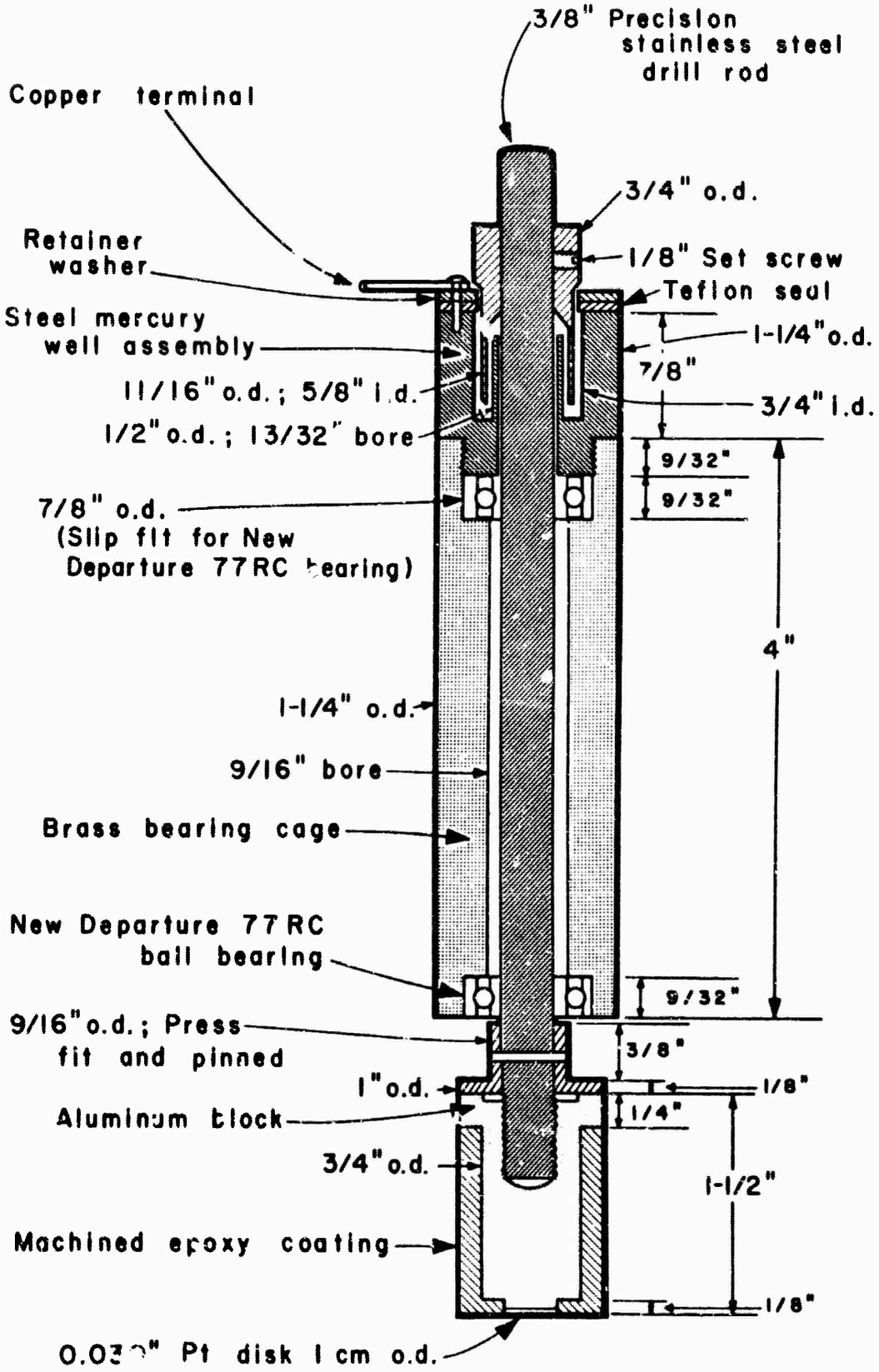

Cross Sectional View of Spindle of Rotating Disk.

Figure 5.

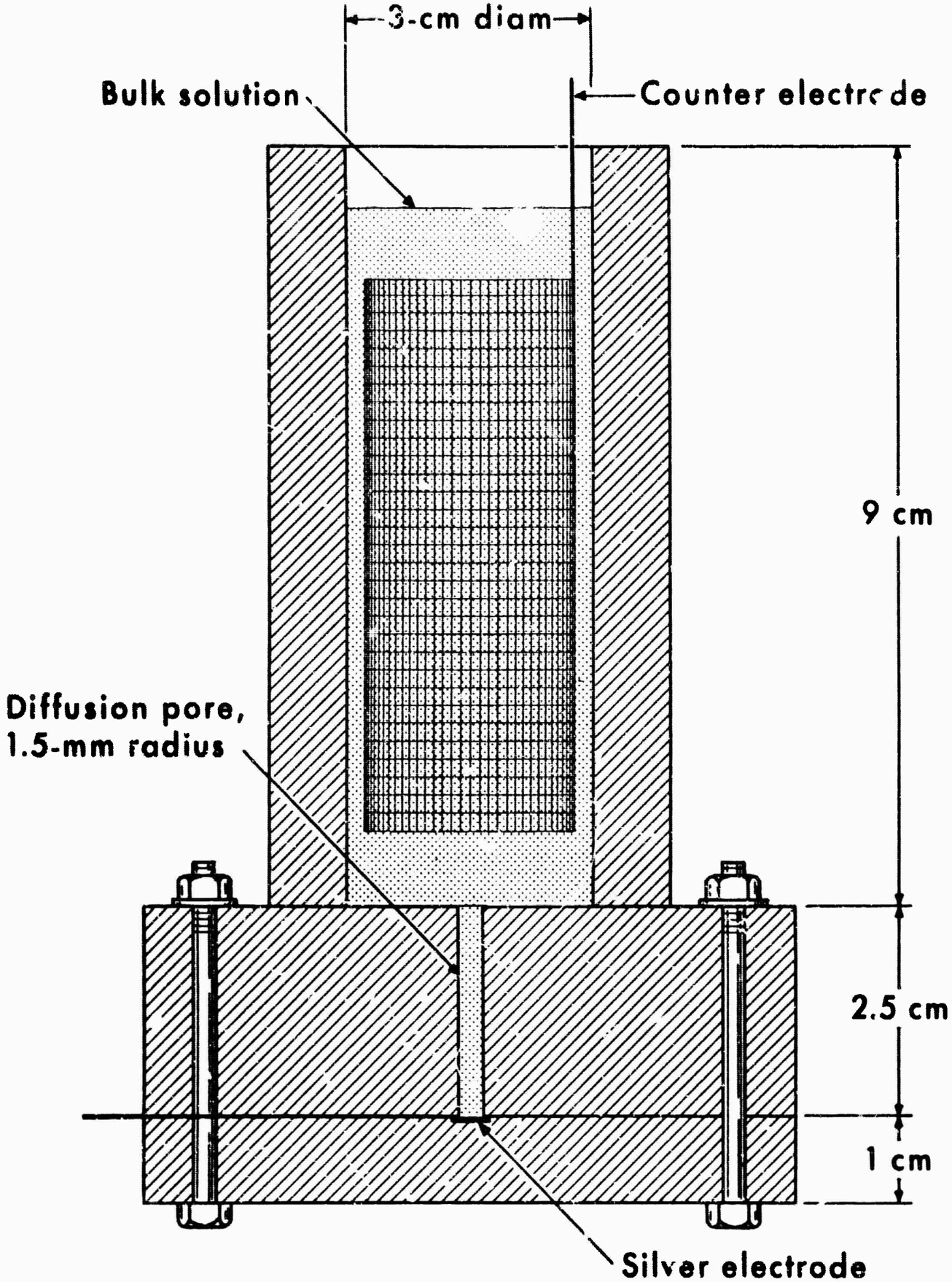

Stagnant-Diffusion Cell

Figure 6.

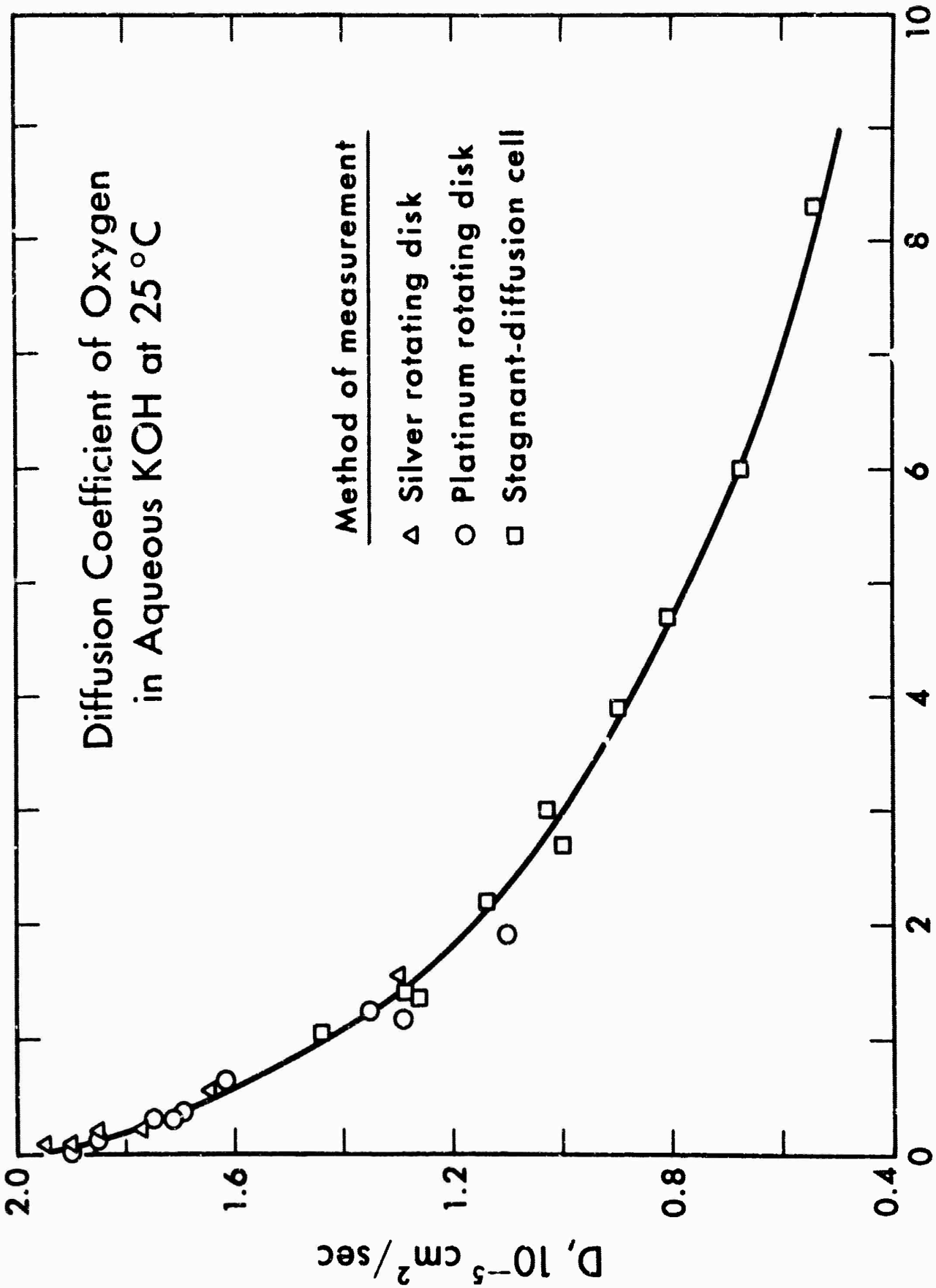
Diffusion Coefficient of Oxygen
in Aqueous KOH at 25 °C
Method of measurement
Δ Silver rotating disk
○ Platinum rotating disk
□ Stagnant-diffusion cell
D, 10⁻⁵ cm²/sec
2.0
1.6
1.2
0.8
0.4
0
2
4
6
8
10
Concentration of KOH, moles/liter

Figure 7.

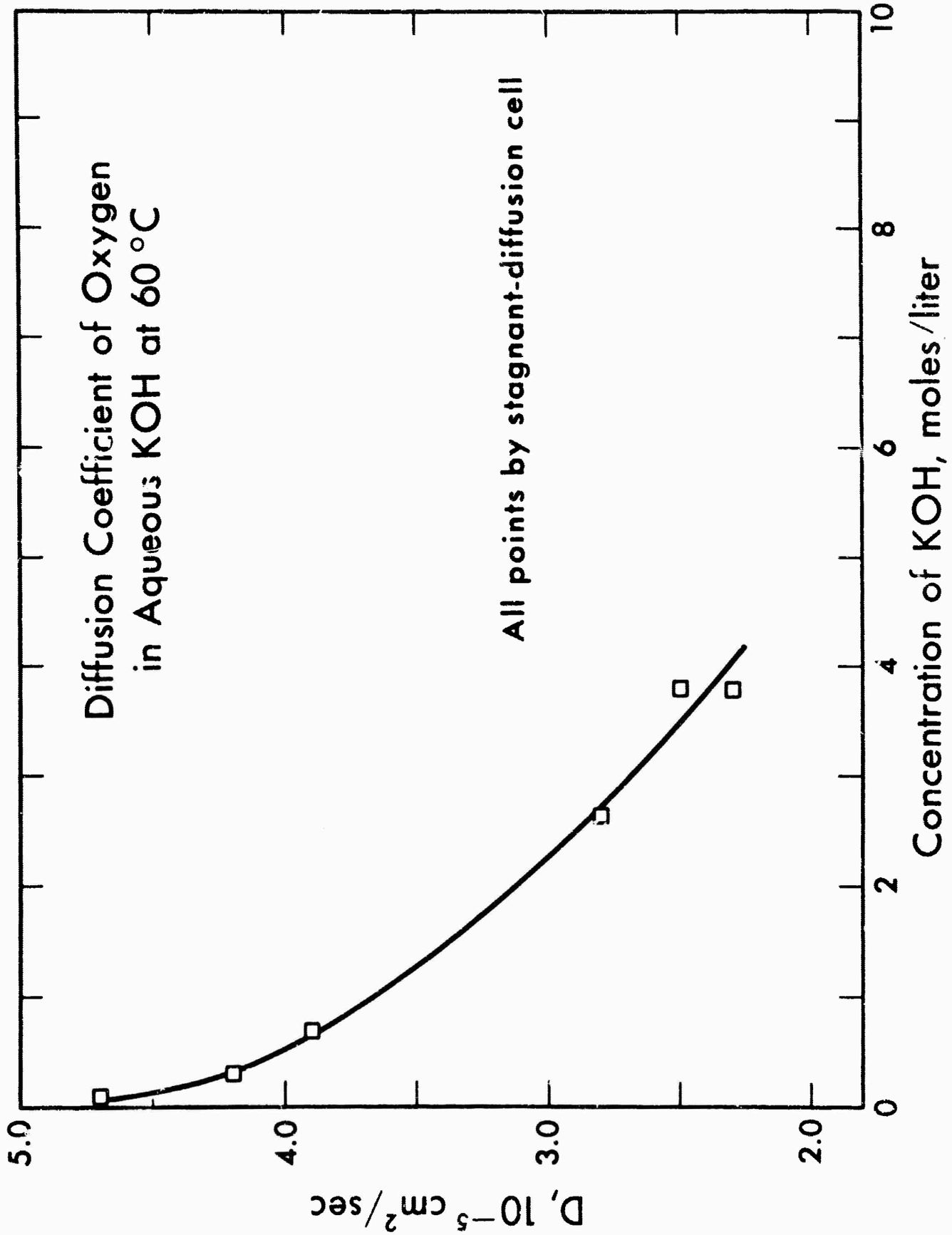
Diffusion Coefficient of Oxygen
in Aqueous KOH at 60 °C
All points by stagnant-diffusion cell
D, 10⁻⁵ cm²/sec
Concentration of KOH, moles/liter
5.0
4.0
3.0
2.0
0
2
4
6
8
10

Figure 8.

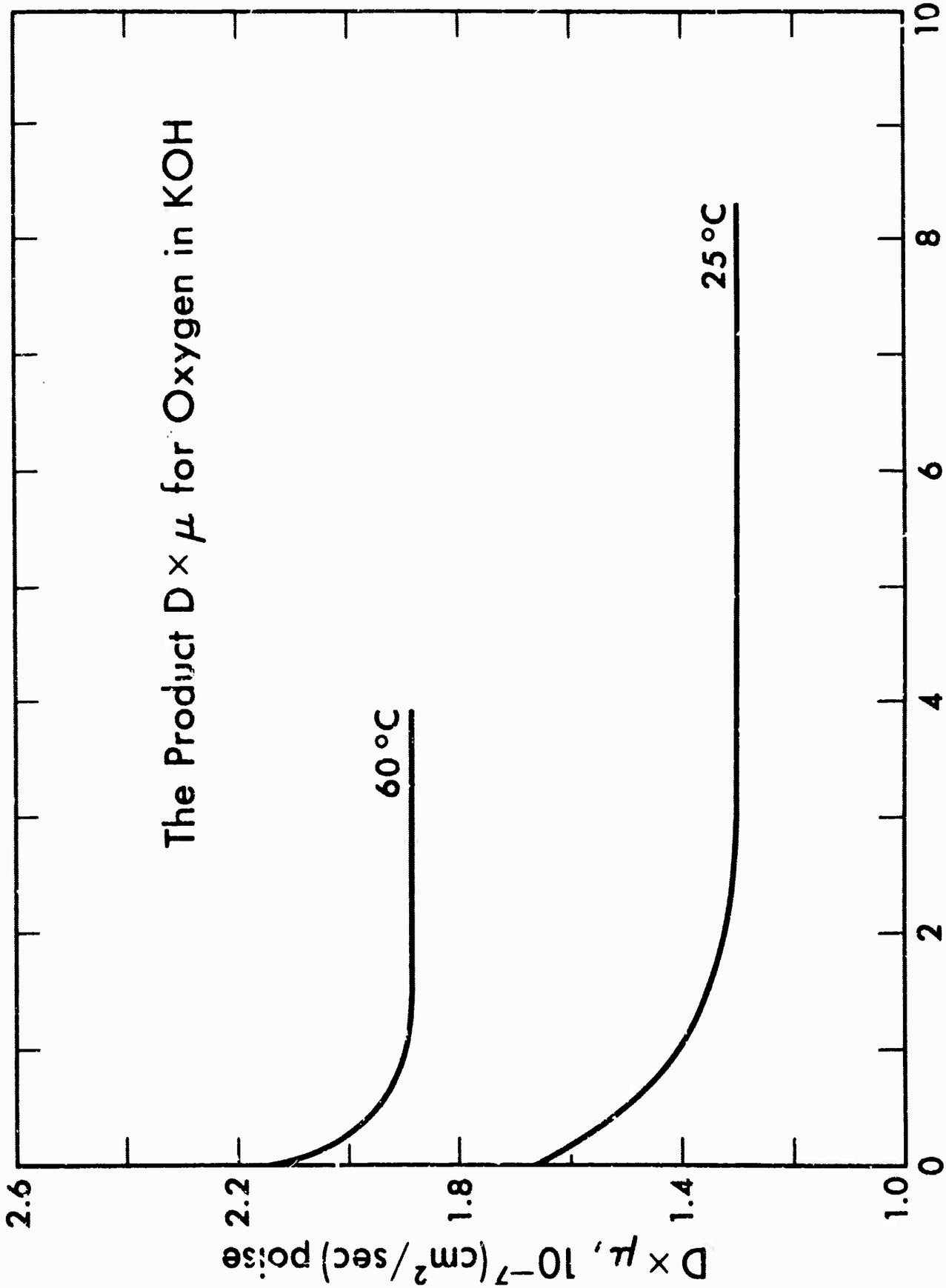
The Product D × μ for Oxygen in KOH
60 °C
25 °C
D × μ, 10⁻⁷ (cm²/sec) poise
2.6
2.2
1.8
1.4
1.0
0
2
4
6
8
10
Concentration of KOH, moles/liter

Figure 9.

PROJECT VI.

Ionic Mass Transport and Current Distribution in Channels at High Velocity Flow

Background and objectives

From a number of studies made on forced convective mass transfer[1,2,3] it has become clear that the limiting current technique, i.e., measurement of cathodic limiting current under the assumption of diffusion-controlled mass transfer, is eminently suitable for obtaining precise mass transfer coefficients and thus establishing generalized mass transfer correlations. In a number of cases the method has provided a check on such correlations as can be derived by theoretical arguments, in the case of particular geometries[3]. In turbulent mass transfer it has served to obtain a measure of the validity of certain assumptions; e.g., regarding the dependence of eddy viscosity, e.q., diffusivity, on radial coordinates, in an otherwise independent development of analogy between momentum and mass transfer[1].

Since mass transfer coefficients are of immediate practical importance in chemical and electrochemical engineering, the limiting current technique has also been applied to natural convective mass transfer, in geometries that, so far, defy analytic solutions. For example, the correlation

$$Nu_L = 0.19\ (Gr_L\ Sc)^{1/3}$$

can be mentioned, which was found to adequately represent the

empirical data for mass transfer by natural convection between two horizontal plates[4].

In the work undertaken by Hickman[5], a first attempt was made to empirically disentangle the influence of forced and free convection in superimposed forced and free convective flow. The case studied, mass transfer at horizontal electrodes, represents a situation of considerable practical interest, where analytic development has had few useful results[6]. The data obtained in the laminar region and which suggest a separation between distinct convective regimes:

$$Gr_{d^2L} > 920\ Re_d \quad \text{free convective mass transfer}$$

$$Gr_{d^2L} < 920\ Re_d \quad \text{forced convective mass transfer}$$

are very encouraging as to the continued usefulness of limiting current techniques in such complicated situations.

At the same time, the refinement introduced by using sectioned electrodes seems particularly advantageous to the empirical solution of these correlation problems, since it is necessary to distinguish current density inequalities along the electrode which are caused by not-yet-developed mass transfer profiles, from those current density increases which are caused by the onset of natural - convective instabilities.

With the limited system capacities at his disposal (5 GPM total flow rate, 14 amp total current), Hickman was not able to pursue his investigations through the forced convection transition region and into the turbulent regime. Apart from the capacity factor, there are also a few complications which

arise from the nature of the flow situation and go relatively unnoticed in the laminar range:

(1) Especially beyond the laminar regime it is necessary to depend on available semi-empirical expressions for pure forced convective mass transfer, if one wants to "sift out" any free convection influences. This in turn makes it advisable to employ simple geometries. Accordingly, the presently available wide electrode channel (cross section 15 by 1 cm) is assumed to approximate an infinite parallel-plates geometry.

(2) Furthermore, to be able to distinguish the effect of free convection on the initiation of turbulence in the channel, it is necessary to exclude external disturbances of the flow as much as possible (specifically, vibrations of the circuit induced by the circulation pump) and to control flow rates closely.

(3) As expected, and quantitatively confirmed by Hickman, any forced convection introduces a non-homogeneous boundary condition, since the leading cathode section reaches limiting current later than the trailing sections. This effect is especially noticeable at high mass transfer rates (high Re, high Gr) and is somewhat leveled off by natural convection. In the turbulent regime it is pronounced but limited to the first entrance sections of the channel.

The inequality can be overcome by using local cathodic overpotentials to indicate when local (section) current densities reach limiting values. Accordingly, a multiple measurement system developed by Hickman[5] has been added,

scanning the section current densities and corresponding section overpotentials. This refinement is most profitable when one takes an interest in the development of concentration profiles in free convective (and forced convective) mass transfer, and consequently in the mechanics of the development of natural convection flow patterns.

The apparent presence of reproducible convection patterns termed "roll cells" seems to make estimates of free convection flow pattern dimensions possible.

Disregarding, for the present, any theoretical approach to the second part of the above objectives, it can be said that continuation of experiments on combined free and forced convection poses the following requirements for the apparatus:

(1) The system should allow high enough flow rates to cover, with the existing electrode cells, the range $Re_d < 10,000$.

(2) The power source for the system should be able to supply correspondingly high currents.

(3) The flow rate measurement should have a uniform relative accuracy over the range of flow rates covered.

(4) The flow regulation should be precise over as wide as range as possible.

(5) The velocity profile in the flow cell should be well defined before mass transfer starts.

(6) Freedom from external vibrations should be assured as much as possible.

(7) Sectional current densities and reference electrode potentials should be scanned sequentially, to allow construction of local limiting current curves.

Moreover, from practical considerations, a number of additional requirements can be expressed.

(8) The temperature of the electrolyte should be kept constant to within 1°C.

(9) It should be possible to apply current to the electrodes at a pre-set rate of increase.

(10) The resistances used to measure the section currents should be adjustable within such ranges as to make the potential variation between the sections less than the assumed criterion of 2 mV.

(11) With a view to possible related studies, employing a modified arrangement, the parts of the flow circuit should be easily replaceable or interchangeable.

(12) An adequate prctection should be provided for the operator in case of a catastrophic leak or other accident involving the circulation system.

Design and construction of equipment.

Supporting structure and protection:

A. Design considerations

It was felt that an expansion of the circulation circuit made it necessary to provide an adequate support for its elements, especially the heavy electrode flow cells and the necessary valves and flowmeters. The weight of any kind of piping and the liquid hold-up could also be expected to be appreciable, since the circuit dimensions are conditioned, in part by the flow cell length (approximately 6 ft), in part by the moderate head of the available pump (14 p.s.i.). The

supporting framework would have to stand free from walls, to give maximum accessibility. It could also serve as a continuing structure, such that it would be easy to attach shielding on all sides to protect the operator of the system against accidental leaks of the corrosive electrolyte.

B. Execution

A basic supporting structure was erected consisting of 8 Unistrut Double-Reinforced Columns, mounted between floor and ceiling and forming a 4 by 2 rectangle with equal spacing. A separate support was provided for mounting the heavy circulation pump, in such a way that propagation of pump vibrations through the frame would be avoided. All heavy parts of the circulation system are supported by single or double Unistrut channels mounted onto this basic structure. Immediately above the floor, covering the entire area of the rectangular structure, a dropping tray was mounted through which spilled electrolyte is drained. On the long sides of the rectangle, at working height, stainless steel frames were mounted, in each of which four suspended plexiglass windows can slide. The windows are 39 in high by 30 in wide and fabricated from 1/4 in thick Lucite. All area under and above the windows can be covered with rectangular shields of stainless steel sheet. Fixed plexiglass windows mounted onto the short sides of the structure give a view of the inside over the whole height. All valves can be operated from outside the shielding. Connections to measuring equipment outside are protected against corrosion and stray fields.

Electrolyte circulation system:

A. Design considerations

Design calculations were based on the characteristics of the available Aurora centrifugal pump (capacity 70 GPM, total head 14 PSI). Assuming a total circuit length of approximately 10 m and employing a friction factor of 0.01, the Fanning friction relation

$$\Delta P = \frac{32\ f\ L\ e\ Q^2}{\pi^2\ D^5}$$

gives, for water, at maximum capacity D = 3.5 cm. The minimum holdup by the circulation system in that case is approximately 10 liter. The real holdup was expected to be greater, because regulation of the flow rate requires a by-pass of the electrode-cell and because the anode and the cathode compartment of the flow-cell have to be fed separately. The bi-section of anode and cathode feed line had to be designed early enough to include a flowmeter in one of them (presently the cathode feed line). This was thought preferable over measuring the total electrode flow rate, since imbalances and disturbances could easily be expected during an experiment. To avoid the cost and complications of a second flowmeter in the alternate feed line, outlets for differential pressure measurement between cathode and anode were designed at the entrance of the electrode flow channel. The design of the circuit tubing would have to be such that any of the two feed lines could be connected to any of the two electrode compartments in whatever electrode orientation with respect to the vertical would be desirable. This

could be achieved either by employing flexible tubing, or by a rigid construction employing interchangeable elements. The more costly solution of constructing a four-way combination valve of resistant material was not considered. Finally, the design would have to provide drain lines and a storage possibility for the electrolyte in such a way that handling the large volumes of corrosive solution would not present great difficulties or risks. Since in previous experiments temperature increases of several degrees centigrade due to pump energy dissipation were observed, a modest cooling facility would have to be included somewhere in the circuit, preferably in the main reservoir.

B. Execution

It was decided to use 1 1/2 in I.D. Pyrex Double-Tough Glass Tubing for the main circuit piping. In this way sagging connections were avoided and continuous support of long lines was unnecessary. Also, flanged connections could be employed. The glass tubing was available in unit elements of various length, down to 3 1/2 in. Elements are connected by Corning type flanges and sealed by Teflon O-rings. Connections to metal flanges are sealed with neoprene gaskets. The inlet and outlet of the electrode flow-cells, as well as all valves and flowmeters in the system, were provided with 1 1/2 in I.D. stainless steel flanges of 150 lbs. standard ASME specifications (a few connections were 1 in I.D.).

Regulation of flow rates through the return line, the cathode, and the anode was provided by inserting in the circuit

three Powell globe valves of 1 1/2 in I.D. stainless steel, 150 lbs ASME specifications.

Flow rate measurements are made by a magnetic flowmeter, which offers the advantage of minimal pressure loss and high accuracy over a wide range of flow rates, through adjustment of the full-scale range between 5 and 60 GPM. The transmitter signal is converted to a current and continuously recorded. For extremely low flow rates rotameter measurement can be provided by a circuit extension.

Propagation of pump vibrations through the circuit piping is prevented as much as possible by flexible connections to pump inlet and outlet.

The drain lines of the circulation system consist of two 1 in I.D. branches at the lowest points of the circuit (on the suction and on the pressure side of the circulation pump). They lead, through 1 in I.D. Edwards globe valves of stainless steel, to 1/2 in polyethylene tubing and a small Cole-Parmer polyethylene pump which can pump the electrolyte into one of two Nalgene storage bottles of 15 gallon capacity, located above the system. These storage reservoirs can empty into the main reservoir, likewise a Nalgene vessel of 15 gallon capacity. The main reservoir can be cooled by means of copper coils through which, depending on the need, tap water or refrigerated water is circulated.

Figure 1. gives a schematic representation of the electrolyte circulation system, in the form of a block diagram.

Electrode flow-cell.

A. Design considerations

The electrolyte enters the electrode channel coming out of a tube of circular cross section and 3.75 cm I.D. It has to conform itself to a rectangular channel of 15 by 1 cm cross section. The distribution device used for the wide electrode channel proved to be unsatisfactory at Re numbers beyond the laminar range. It was thought necessary to have a completely new inlet section constructed, which, like the old one[5], could be flanged onto the main flow-cell. In view of the lack of experience with entrance behavior at high flow rates, it seemed advisable to provide an excess of flow straightening devices, with the possibility to remove one or more of them if the resulting pressure drop would prove to diminish the flow range capacity of the cell too much. It was not considered necessary to revise the outlet-section of the cell, except for an enlargement of its capacity.

As mentioned already in the previous section, outlets for differential pressure measurements had to be made in the entrance of the cathode and the anode channel. The pressure drop along both channels was considered of interest for the investigation and therefore similar outlets were designed at the end of the two channels.

B. Execution

A new inlet section was constructed out of Lucite. Each circular inlet-channel branches symmetrically into 2, then 4, then 8, finally 16 circular channels, with

calming sections of proportional length inserted between the bi-section points. The total cross section of the channels stays constant throughout. The last, sixteenfold, stage empties into a short length of rectangular channel of dimensions 15 by 1 cm. Here the fluid expands slightly in the width dimension. The channel is then ended with a 15 mesh stainless steel wire screen, which can be taken out. Also, the Lucite elements in which the 8- and the 16-fold division of the flow takes place, are not glued to the first and last elements but held in place and sealed by neoprene O-rings under pressure from the inlet-section flanges. They, too, can therefore be removed, to alleviate the pressure drop.

Between the inlet section and the main electrode channel an additional calming section, of 15 cm length, can be inserted by means of flanges. It is, in turn, ended with a removable stainless steel wire screen of 15 mesh.

Pressure reading outlets were drilled in the short sides of the cathode and anode channel, at 7 cm and 5 cm, respectively, both downstream from the inlet-section and upstream from the outlet-section. The holes were 1/4 in diameter throughout the wall thickness, except for the last 1/16 in length opening into the channel which had 1/16 in diameter. The actual connection to the mercury U-tubes was a 1/8 in diameter branch, just above this point. This connection could be severed by lowering a plug into the main, 1/4 in diameter hole. The plug was machined to fit the 1/16 in diameter, flush with the channel wall.

To avoid great lengths of tubing necessary for differential pressure measurement between inlet and outlet of the same channel, it was decided to measure the absolute pressure at these points, by means of an open mercury tube. The differential pressure, however, is measured between the two channels at the inlet and outlet of the flow-cell.

Finally, the cathode holder was provided with a groove and a neoprene O-ring for seal, to avoid any degree of contamination of the electrolyte by grease.

Power supply:

A. Considerations

A new power supply had to be designed, capable of supplying currents of up to 100 amp as a current ramp. Because of the necessity of trying out several increase rates in mass transfer situations where the limiting current curve has no conspicuous plateau, the current source should be able to reach any maximum in a time that could be pre-set. A maximum voltage should not be exceeded during this process.

B. Execution

The system designed to meet these requirements is shown in the block diagram, Figure 2 . A Kintel Operational Amplifier connected as an analog integrator is used to generate the ramp function. Current maximum can be set at any value between 0 and 100 amp; time ranges are 1, 2, 5, 10 and 20 minutes. Current stability is .1% of range; linearity is .1%. A maximum voltage of 18 V is not exceeded.

The transistor bank in the power supply is cooled by water.

Electric measurement system:

A. Considerations

At higher total currents applied to the cathode, it was thought probably that the variable resistances (combined in the current shunt box) which serve to measure sectional currents, might have too little variability to allow equal IR-drops between the cathode section contactors, and the common busbar, which is connected directly to the power source. This would be caused by the fixed resistance presented by the leads and 12-pin connections in the cathode holder, as well as the slide-wire resistance and several contact resistances in the shunt box. A calibration of the total resistances involved showed that, indeed, assuming uniform current density over the cathode, deviations from equipotentiality of the central sections would amount to more than 2 mV (the assumed criterion) at total currents above approximately 30 amp. The situation would seem more serious, however, even at 10 amp, with respect to the equipotential condition of the long side-sections (carrying each 4/15 of the total current, regardless of current density distribution along the cathode). Deviations of more than 20 mV were to be expected, with respect to the central sections. It seemed advisable, as a provisional solution for low-current measurements, to drastically diminish the fixed resistance of the connections to the side-sections.

To enable a continuous measurement of (1) total current; (2) section currents; (3) local overpotentials; (4) electrolyte flow rate, an integrated electric system had to be

designed, which could be compactly housed in one or two cabinets, within the operator's reach. Such a system could be envisaged as, either leading to simultaneous recording of all data mentioned by means of single and multi-point recorders, or as a rapid sequential scanning of all signal-points by a scanner-digital voltmeter combination, the output from which could be printed and inspected, or directly punched into IBM cards to facilitate possible computer treatment of the data.

B. Execution

The current shunt box was modified by taking out the variable resistance wire corresponding to the (combined) side-sections and replacing it by two fixed copper wires of 1 mΩ resistance, eachhing leading directly to one of the side-sections. The total contactor-to-busbar resistance of the side-section connections is now 1.7 mΩ, which is expected to make the current shunt box usable up to total currents of approximately 30 amp. A decrease of total resistance has also been achieved for the other leads by eliminating the 12-point plug connection. The current shunt box has been fastened to the cathode holder.

An integrated system leading to simultaneous recording of most of the data involved has been designed and constructed (see block diagram, Figure 3.). Such a system can without effort be simplified to suit a rapid-scanning-digital voltmeter-printer combination.

The present system combines:

(1) a panel of voltage dividers which make it possible to scale each sectional current output in such a way that the recorded signal is proportional to the current density on the section;

(2) a stepping switch, actuated by the 10-point recorder, which selects the sectional current density output signals for sequential recording;

(3) a microvolt-amplifier, with ranges between 50 and 2000 μV, which serves to amplify low current section current density signals;

(4) a selector-switch which determines which 10 of 11 available current density signals will be recorded;

(5) a ten-point Leeds and Northrup x-y recorder, which registrates section current density against total current;

(6) a programming pin board which combines the leads originating in the 9 reference electrodes with branches from the 11 leads which contact the variable resistance wires at the outlet of the current shunt box;

(7) an attenuator to bring any signal from a chosen combination in (6) down to the level required by the recorder;

(8) an x-y-y recorder which registrates the chosen overpotential signals against total current;

(9) an x-y recorder to registrate the flow rate signal from the magnetic flowmeter to current converter against the total current;

(10) a shunt introduced into the power source circuit to give an output corresponding to the instantaneous current, the order of magnitude of which is kept within the mV-range by the decade-setting of the current maximum.

Literature study.

Forced convective mass transfer: The results obtained by Hickman[5] for systems considered under laminar forced convective control show a remarkable consistency with empirical correlations available for rectangular ducts:

$$Nu_d = 1.85\ Re^{1/3}\ Sc^{1/3}\ (d/L)^{1/3} \quad \text{(Norris and Streid)}$$

In particular the current density profiles for the cathode-over-anode situation, i.e., involving an indefinite hydrodynamic stability, are in perfect agreement with boundary layer theory predictions of mass transfer rates proportional to $x^{-1/3}$.

A similar agreement has not been claimed for data obtained in the range $2500<Re<6000$, which were supposed to be consistent with either the equation for fully developed mass transfer in pipes (originally developed empirically for heat transfer

$$Nu_d = 0.027\ Re^{0.8}\ Sc^{1/3}\ (\mu_o/\mu_i)^{0.14} \quad \text{(Sieder and Tate)}$$

or the equation for the entrance region:

$$Nu_d = 0.276\ Re^{0.58}\ (Sc\ d/L)^{1/3} \quad \text{(Shaw, Reiss, Hanratty[8])}$$

It is, however, doubtful whether the narrow range and the transition character of the Re numbers concerned can be considered representative for the turbulent regime. It should, in particular, be considered possible that natural convection introduces an earlier transition to turbulent flow. Exactly in that

case, the influence of natural convection occurring in the flat, rectangular geometry employed would seem to contribute to marked anisotropy of turbulent motion such as to make comparison with results obtained in pure, turbulent forced convective mass transfer deficient.

In the range of Re > 10,000, however, such a comparison would be justified and the quality of the results obtained in correlating laminar forced convective mass transfer suggests that the limiting current technique is sufficiently accurate to provide a check on the validity, for mass transfer, of the several refined analogy expressions developed for turbulent mass transfer[1,8,9] as well as the familiar Chilton-Colburn analogy

$$St = (f/2)\ Sc^{-2/3}$$

The most important aspect of this check would concern the variation of the dependence

$$(\partial\ ln\ St/\partial\ ln\ f)$$

as a function of the Sc-number. Recent experiments by Lightfoot and Hubbard[10] confirm the evidence already available that the Sc-dependence given by the Chilton-Colburn expression agrees better with the data than that implied in Deissler's analogy[7].

Though the geometry of the channel employed for such tests is of importance in the laminar range of Re numbers, it appears that in the range indicated above the results for mass transfer between parallel plates do not deviate more than 1% from those for round pipes[10]. A theoretical development of the heat transfer to friction analogy for the case of special

interest here, transfer from one wall to flow between parallel plates, is available[11].

The sectioned electrode technique enables measurements of entrance effects in turbulent transfer. Mass transfer techniques, in particular electrolytic methods, require less complications in this regard than measurements of heat transfer, where thermal insulation of short lengths of channel presents a problem. Entrance region measurements are of interest especially at very short lengths and relatively low Sc numbers, where the assumption that ϵ/ν, i.e., the rate of eddy diffusivity to kinematic viscosity, depends only on the dimensionless coordinates, y^+ and x^+, loses credibility.

Influence of free convection: instability and transition: The correlation developed by Hickman[5] to distinguish between regimes of laminar forced-convective mass transfer and free-convective mass transfer employs the modified Grashof number:

$$Gr_{d^2I} = \rho g \alpha \Delta c d_e^2 L/\nu^2 .$$

Though this dimensionless combination represents a convenient way of summarizing the basic finding, it does not contribute to its explanation since the actual value of the mass transfer boundary layer is not employed.

Also, insofar as available instability criteria can be used for comparison, it should be noted that the criterion derived by Velte[12], $Ra \geq 5300$, refers only to square cross section and utilizes exclusively the equivalent diameter.

The application of instability criteria and the analysis of transverse flow patterns with regard to the results obtained

in laminar flow through a rectangular duct, would require first a careful investigation of the transition region to turbulent flow under conditions of hydrodynamic stability, i.e., in the cathode-over-anode situation. Precise control over flow rates and absence of any gross flow disturbances are essential conditions.

Influence of free convection: transverse flow patterns: Convection patterns termed "roll cells" are apparently present in laminar flow influenced by free convection. Though their existence was not demonstrated conclusively, it has been made plausible by comparison with similar phenomena observed in heat transfer to a horizontal layer of air in shear flow[13].

For any further analysis it is necessary to have quantitative and reproducible data on the characteristic dimensions of these convection patterns and their point of initiation. The most promising approach to an explanation would be an analysis of similarity with the Taylor-Goertler vortices observed in laminar flow on highly concave walls. These "neutral" vortices are likewise the result of a three-dimensional disturbance[14].

Such an analysis, however, presents extremely complicated mathematical problems and would only be warranted, as well as considerably helped, by substantial data on the dimensions of the phenomena observed.

Since the localization of roll cells is still highly dependent on the measurement of deposition profiles, it is imperative that vibrational disturbances be avoided.

Immediate objectives.

After test runs have been completed and the regulation characteristics of the electrolyte circulation system have been established, the investigation will be conducted along the following lines:

A. Employing the wide electrode-channel and a copper deposition electrode reaction.

1. Collection and correlation of data for laminar pure forced convective mass transfer, employing the cathode-over-anode position.

2. Establishment of the laminar-to-turbulent transition Re range in pure forced convective flow.

3. Collection and provisional correlation of data for turbulent forced convective mass transfer:

a. below Re = 10,000

b. above Re = 10,000.

4. Evaluation, over the total Re range covered, of the boundary conditions existing at individual sections and their influence on generalized correlations.

5. Consideration of modified cathode segmentation (1st part).

6. Collection and correlation of sectional limiting current data for combined free and forced convective mass transfer, employing the anode-over-cathode position and a wide range of bulk concentration.

7. Collection of deposition profile data indicating onset of free convective flow patterns and correlation with

section data obtained for the initiation of free convective mass transfer regime.

8. Comparison of data with respect to the initiation of full-scale turbulence for pure forced convective and mixed convective mass transfer situations.

9. Evaluation, over the Re range covered, of the boundary conditions existing at individual sections in mixed convective mass transfer.

10. Estimation of expected current density distribution at other orientations with respect to the vertical.

11. Consideration of modified cathode segmentation (2nd part).

B. Employing the narrow electrode channel and a ferri-ferrocyanide reduction reaction on nickel cathode.

1. Collection of section current density vs overpotential data in the laminar forced convective mass transfer regime.

2. Evaluation of boundary conditions existing at individual sections, and the reliability of overpotential as an indication.

3. Collection and correlation of turbulent convective mass transfer data above Re = 10,000 with existing analogies, using extreme variations of electrolyte Sc number.

LITERATURE CITED

1. Lin, C. S., Moulton, R. W., Putnam, G. L.; Ind. Eng. Chem. 45, 636 (1953).

2. Eisenberg, M., Tobias, C. W., Wilke, C. R.; J. Electrochem. Soc. 101, 306 (1954).

3. Wilke, C. R., Eisenberg, M., Tobias, C. W.; J. Electrochem. Soc. 100, 513 (1953).

4. Fenech, E. J., Tobias, C. W.; Electrochimica Acta 2, 311 (1960).

5. Hickman, R. G.; Techn. Report No. 2, Dec. 1, 1963, Contract No. DA 36-039 SC-89153.

6. Mori, Y.; Trans. ASME/J. Heat Trf. 83, 479 (1961).

7. Deissler, R. G.; NACA Report 1210 (1955).

8. Shaw, P. Van, Reiss, L. P., Hanratty, T. J.; A.I.Ch.E. Journal 9, 362 (1963)

9. Vieth, W. R., Porter, J. H., Sherwood, T. K.; Ind. Eng. Chem. Fund. 2, 1 (1963).

10. Hubbard, D. W.; Ph.D. Thesis, University of Wisconsin, (1964).

11. Barrow, H.; J. R. Aeronaut. Soc. 60, 413 (1956).

12. Velte, W.; Z. Ang. Math. Phys. 13, 591 (1962).

13. Phillips, C. T.; J. R. Met. Soc. 58, 23 (1932).

14. Schlichting, H.; Boundary-Layer Theory (1960) p. 439.

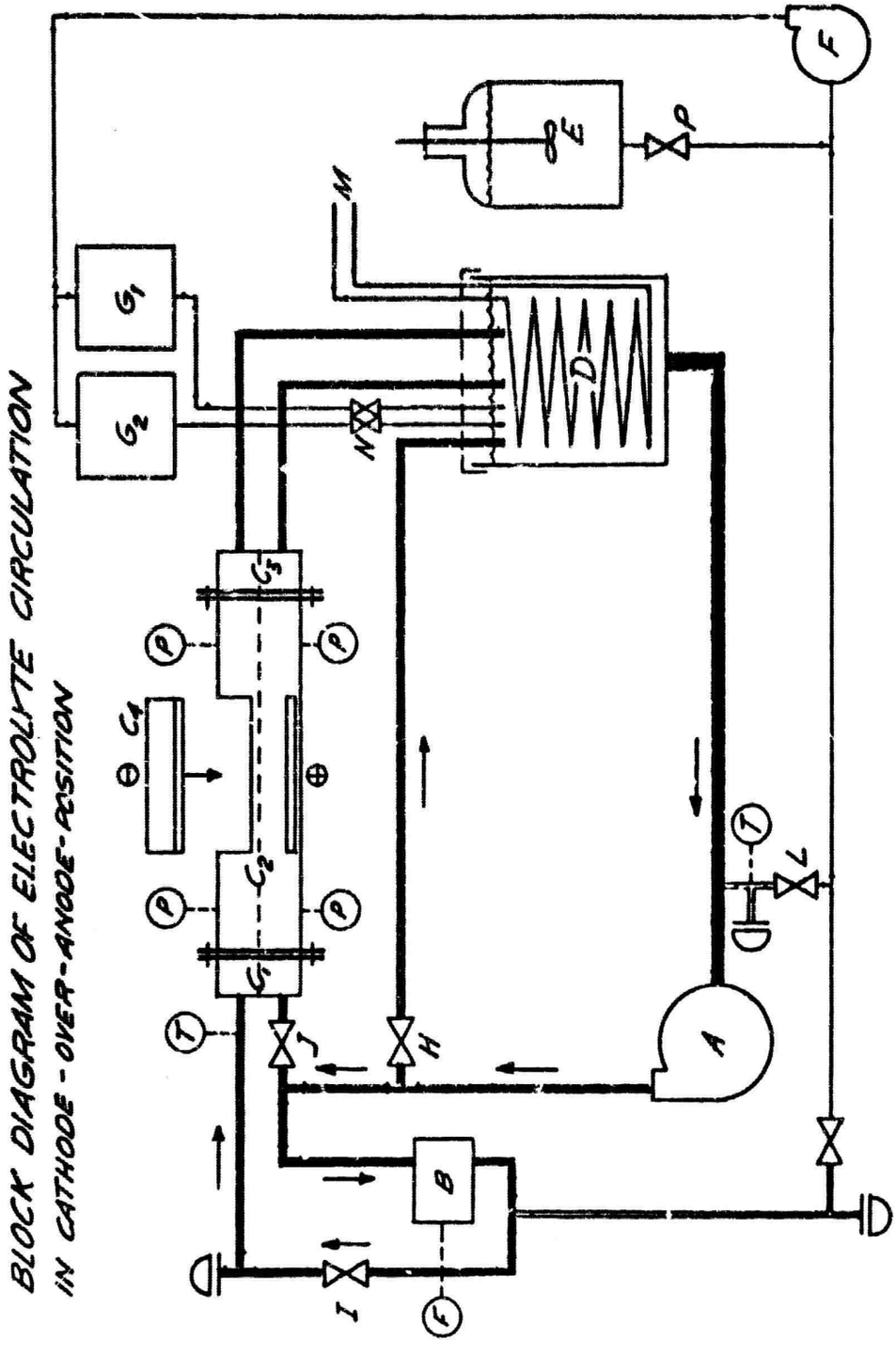
BLOCK DIAGRAM OF ELECTROLYTE CIRCULATION
IN CATHODE-OVER-ANODE-POSITION
A. CIRCULATION PUMP
B. MAGNETIC FLOWMETER
C. ELECTRODE FLOW-CELL C1 INLET C2 MAIN BODY C3 OUTLET C4 CATHODE HOLDER
E. MAKE UP RESERVOIR
F. SMALL PUMP (TO STORAGE)
G. STORAGE
H. VALVE BYPASS RETURN LINE
I VALVE CATHODE-FEED LINE
J. VALVE ANODE FEED LINE
K,L. VALVES DRAIN-LINE
M. REFRIGERATION CIRCUIT
N. EMPTYING VALVES-STORAGE
P. EMPTYING VALVES-MAKE UP RESERVOIR

Figure 1.

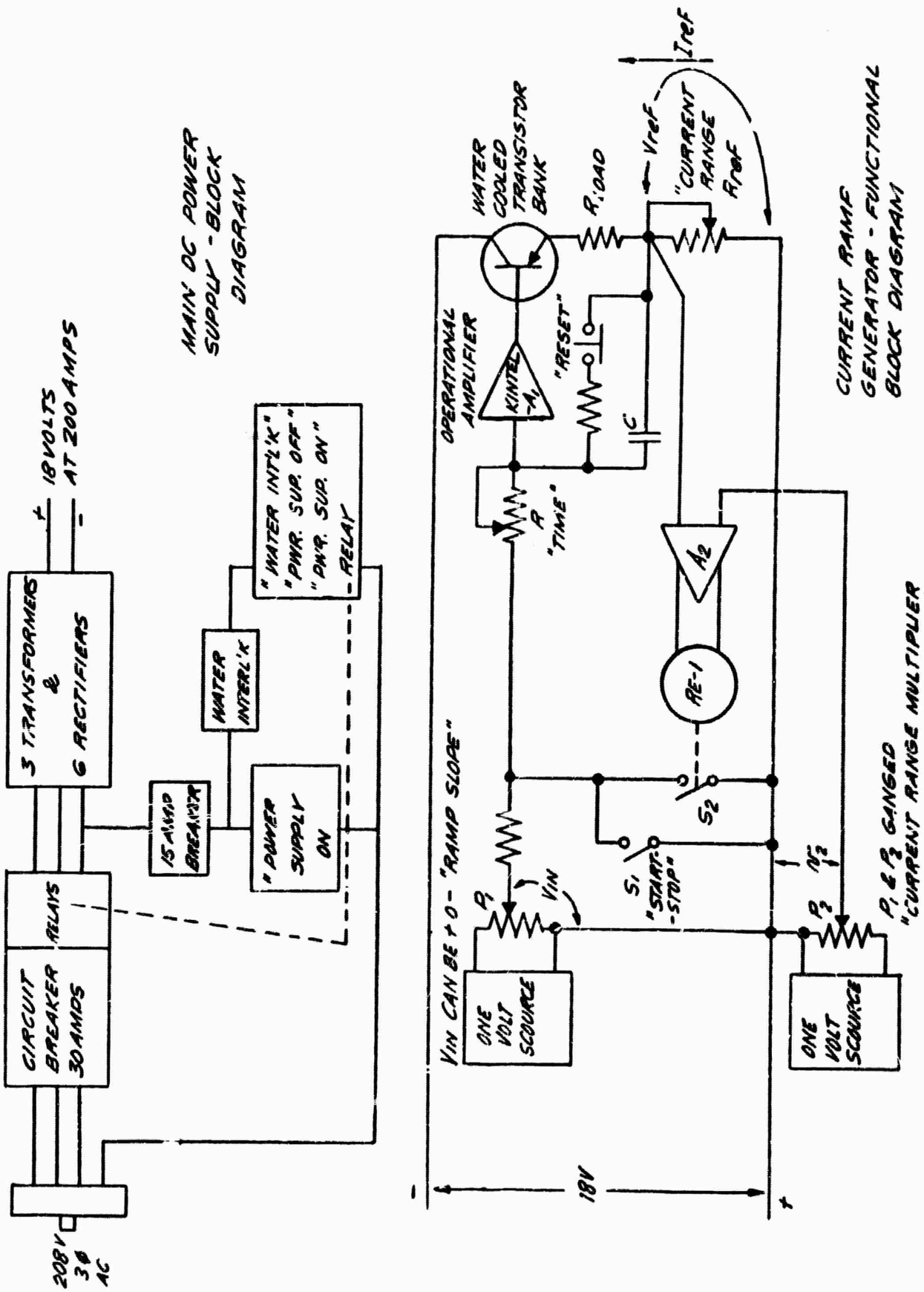
MAIN DC POWER SUPPLY - BLOCK DIAGRAM
18 VOLTS AT 200 AMPS
+
-
3 TRANSFORMERS & 6 RECTIFIERS
CIRCUIT BREAKER 30 AMPS
RELAYS
208 V 3Ø AC
15 AMP BREAKER
WATER INTERL'K
"POWER SUPPLY ON"
"WATER INT'L'K"
"PWR. SUP. OFF"
"PWR. SUP. ON"
RELAY
CURRENT RAMP GENERATOR - FUNCTIONAL BLOCK DIAGRAM
WATER COOLED TRANSISTOR BANK
OPERATIONAL AMPLIFIER
KINTEL
"RESET"
"TIME"
R LOAD
Vref
"CURRENT RANGE" Rref
Iref
A1
A2
RE-1
S1 "START-STOP"
S2
VIN CAN BE + 0 - "RAMP SLOPE"
VIN
ONE VOLT SOURCE
ONE VOLT SOURCE
P1 & P3 GANGED "CURRENT RANGE MULTIPLIER
18V

Figure 2.

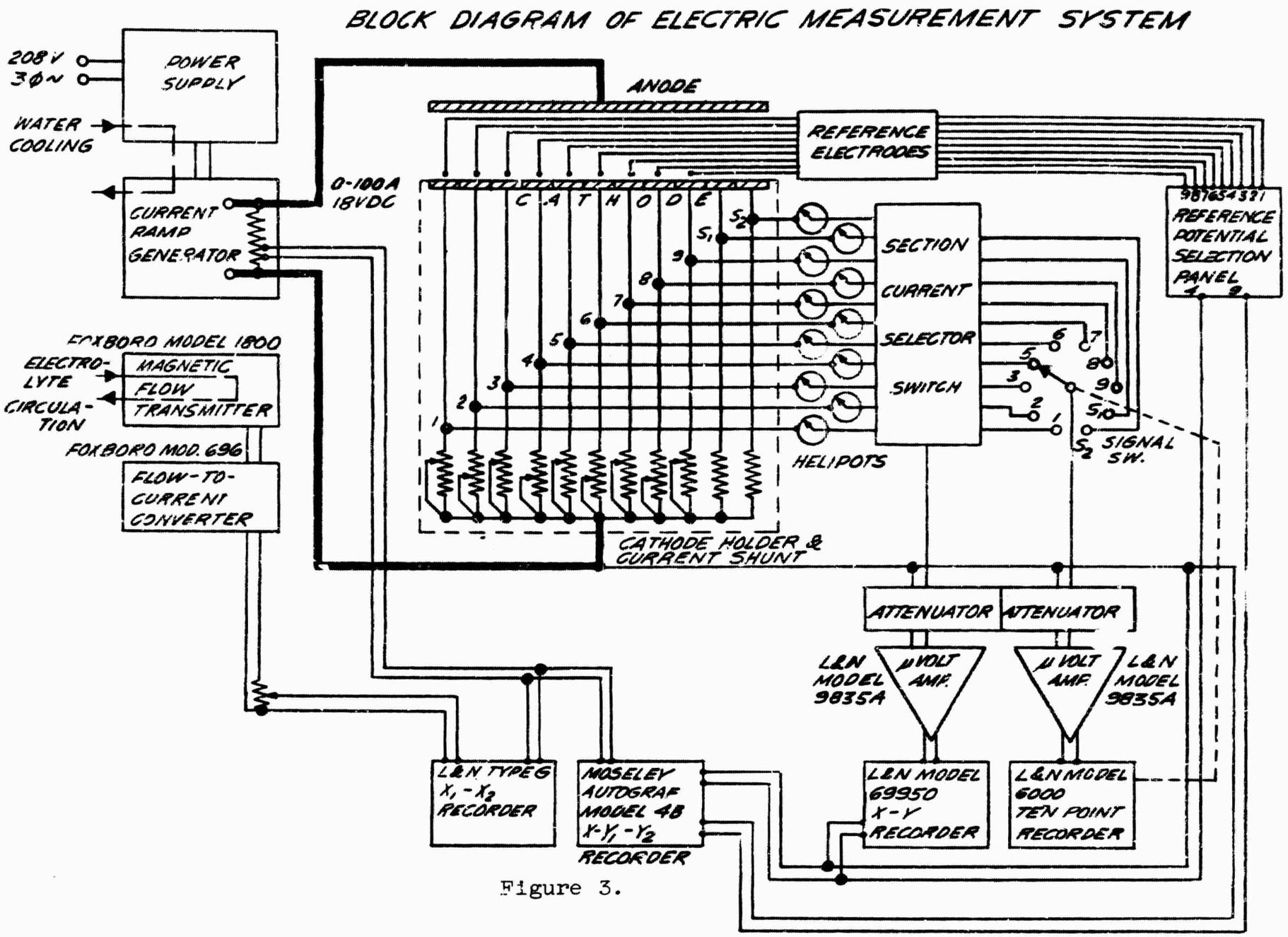
BLOCK DIAGRAM OF ELECTRIC MEASUREMENT SYSTEM
208 V
3 Ø N
POWER SUPPLY
WATER COOLING
ANODE
REFERENCE ELECTRODES
0-100A 18VDC
CURRENT RAMP GENERATOR
CATHODE
SECTION CURRENT SELECTOR SWITCH
98765432 1
REFERENCE POTENTIAL SELECTION PANEL
FOXBORO MODEL 1800
ELECTRO-LYTE CIRCULA-TION
MAGNETIC FLOW TRANSMITTER
FOXBORO MOD. 696
FLOW-TO-CURRENT CONVERTER
HELIPOTS
SIGNAL SW.
CATHODE HOLDER & CURRENT SHUNT
ATTENUATOR
ATTENUATOR
L&N MODEL 9835A
μ VOLT AMP.
μ VOLT AMP.
L&N MODEL 9835A
L&N TYPE G X1 - X2 RECORDER
MOSELEY AUTOGRAF MODEL 48 X-Y1 - Y2 RECORDER
L&N MODEL 69950 X-Y RECORDER
L&N MODEL 6000 TEN POINT RECORDER

Figure 3.

PROJECT VII.

Transport Properties of Concentrated Electrolytic Solutions

In order to make accurate mass transfer calculations in electrolytic systems, it is necessary to have correct values of the transport properties of the electrolytic solution. Cases of practical interest usually require a knowledge of the diffusion coefficients of individual species as well as conductance in a multicomponent solution over a range of temperatures and concentrations. Unfortunately, few such data are available in the literature. Most existing measurements have been made on binary electrolytes in dilute solution at 25°C. Because of these circumstances a program has been undertaken to measure and to correlate the transport properties of concentrated electrolytic solutions over a wide range of conditions.

Correlation of transport properties

The first step in systematizing the information on such solutions was to construct a rational mathematical framework of flux equations wherein all the transport properties are unambiguously defined and ascribed with a specific significance. Newman, Bennion, and Tobias[1] have pointed out the shortcomings of the classical dilute solution flux equation with regard to concentrated and multicomponent solutions. They proceeded to eliminate the inherent difficulties by using the generalized multicomponent diffusion equations:

$$c_i \nabla u_i = RT \sum_j \frac{c_i c_j}{c_T \mathcal{D}_{ij}} (\underline{v}_j - \underline{v}_i) \qquad (1)$$

where the transport properties $\mathcal{D}_{ij}$ each represent the interaction between a pair of species in the solution. It is seen that this relationship can apply to an arbitrary number of components. Also the formulation avoids a frame of reference problem usually encountered in measuring properties of concentrated solutions. It is felt that because of the straightforward significance of the $\mathcal{D}_{ij}$'s, they should lend themselves more readily to theoretical interpretation and correlate more easily than the properties defined by the classical flux equations. This is the problem which is presently under consideration.

Before dealing with the complicated problem of multicomponent systems, it is necessary to investigate first the behavior of the interaction coefficients $\mathcal{D}_{ij}$ in binary solutions of various electrolytes in order to determine their dependence on the various physical parameters of the system. All available data on densities, viscosities, activity coefficients, conductances, diffusivities, and transference numbers for binary systems have been collected from the literature. Care has been taken to critically evaluate the data where possible. It has been found that a fair amount of data are available for most of these properties, at least at 25°C. However, for diffusivity and transference number the data are very sparse for concentrated solutions. It should also be noted that diffusion data for multicomponent systems are practically nonexistent.

When all relevant data are available for a particular binary system, it is possible to calculate the three D_{ij} coefficients as was done by Newman et al. for potassium chloride. The raw data for their calculations are shown in Figure 1. It is seen that conductivity increases monatonically with concentration, the cation transference number decreases with concentration, and the measured diffusion coefficient drops rapidly to a minimum and then rises whereas the thermodynamic diffusion coefficient goes in the opposite direction. This general behavior appears to be characteristic of the alkali halides. The calculated D_{ij} functions appear in Figure 5 of the previous reference.

In Project IV. some tentative assumptions about the dependence of D_{ij} on concentration and viscosity led to a conductivity correlation based on the equation

$$- z_+ z_- eF \frac{\sqrt{\nu c c_T}}{\nu \mu} = G + \frac{AB}{\nu_+ A + \nu_- B} \frac{\sqrt{\nu c_o}}{\sqrt{c c_T}} \quad (2)$$

If A, B, and G from their equations (12) are constant, a plot of $\sqrt{\nu c c_T}/\kappa\mu$ versus $\sqrt{\nu c_o}/\sqrt{c c_T}$ should be linear. It was found that for KCl and KOH the suggested relationship was indeed linear over the entire concentration ranges at 25°C. This relationship has been investigated for a number of other systems.

In Figure 2 are plotted the conductivities of ammonium nitrate solutions of various compositions and at various temperatures. It is seen that for this salt the conductivity at any temperature goes through a maximum in the high

concentration range. This behavior is common for a number of electrolytes including KOH. It is such a maximum which often determines the choice of concentration of supporting electrolyte in a working cell. The phenomenon appears to be related to the large viscosity increase observed in concentrated solutions of many electrolytes.

In Figures 3 and 4 these data for NH_4NO_3 are plotted in the manner suggested by equation (2). A linear relationship appears to hold well over most of the concentration range but is seen in Figure 4 to fail at high concentrations. Also the data for different temperatures fall on different lines which indicates that the temperature dependence of $\mathfrak{D}_{ij}$ has not been accounted for completely.

In Figures 5, 6, and 7 three more examples are presented. The conductivity of $CuSO_4$ when plotted in Figure 6 is seen to deviate from linearity in the concentrated region as do the data for $LiNO_3$ in Figure 7. In Figure 8, however, it is seen that $LiNO_3$ in ethanol follows the linear relationship quite well.

It has been found from the analysis of the conductivity data for a large number of systems that the forms assumed in equations (12) of Newman et al. account quite well for the behavior of $\mathfrak{D}_{ij}$ in dilute binary electrolytes but that they sometimes fail in the concentrated region. The reason for success or failure in a particular case is not obvious. However, it does appear that these first approximations do take into account the proper effects and do successfully reduce

the experimental conductivity data to a well behaved form. As suggested in the original presentation a more sophisticated approach to the structure and interactions in the solutions should make improvements in the correlation possible. This problem is being given further consideration.

In Figure 9 are shown the cation transference number, measured diffusion coefficient, and thermodynamic diffusion coefficient of copper sulfate. With these data and the conductivity shown in Figure 5 it is possible to calculate the D_{ij} for copper sulfate. The results are shown in Figure 10.

Similarly, the diffusion coefficient data for ammonium nitrate are plotted in Figure 11. Unfortunately, no measurements of the transference number of this salt have been made. By assuming that $t_+ = 0.487$ it was possible to compute the D_{ij}'s for this substance. The results are shown in Figure 12.

By comparing Figures 10 and 12 with Figure 5 of Newman et al., one sees that the D_{ij} of these three systems behave qualitatively in the same way. However, a quantitative correlation is not yet obvious for these functions. In particular, the behavior of D_{+-} for the three salts differs considerably in the high concentration range, and the slopes are different even in the dilute range. Again it appears that successful correlation will require consideration of liquid structure and molecular interactions in conjunction with investigation of the behavior of many other binary electrolytic solutions.

During the collection from the literature of the data which are necessary for these calculations, it has become

obvious how scarce reliable values of diffusion coefficients for concentrated solutions are. Even where measurements have been made, one must be careful in using the reported values because in many cases they are not the intrinsic properties which are defined by a differential flux relationship. Sometimes the reported diffusion coefficient is an integral value, that is, one which represents some average over the concentration difference employed in the measurement rather than a true differential value. As indicated before, it is sometimes not clear what the frame of reference is with respect to which the diffusion coefficient was measured. And in some cases the experiment was simply not capable of very high accuracy. Discrepancies between different investigators make this fact obvious. Because of the need for much more extensive accurate data, both for practical application and as a basis for a successful theory or correlation for concentrated and multicomponent solutions, a program of diffusion coefficient measurements is being undertaken. In conjunction with this, a program of transference number measurement is also being planned.

Experimental methods for determining diffusivity

In deciding what method whould be chosen for the diffusion studies, we have considered all the techniques which are presently available. Since a number of thorough reviews on the experimental methods for measureing diffusion have appeared in the last twenty years[2,3,4,5], no detailed discussion seems

justified here.* We shall simply outline the several methods which appear to be reasonably accurate and note the advantages and disadvantages which are particularly relevant.

Optical methods: Most of the popular optical methods are based on the solution of Fick's law for free diffusion[7]. That is, diffusion takes place from an initially sharp boundary in an effectively infinite column of solution. Most methods, such as the Gouy method[8], use interferometry to observe the gradient of index of refraction. Such a measurement can be made quite accurately. Unfortunately, the complete analysis of these experiments requires the assumption of a constant diffusion coefficient. Therefore, it is necessary to work with a very small concentration difference which tends to limit precision. Furthermore, the analysis of the measurements depends rather critically on the initial condition. One must be very careful to make the initial concentration boundary as sharp as possible; it is necessary in any case to make a zero time correction.

These methods do have the advantage of affording measurements in a relatively short time, although the analysis of the fringe patterns appears to be rather tediuous. In spite of the various difficulties optical methods still offer the possibility of highly accurate measurements, and a large portion of reliable data, particularly in concentrations solutions, has been ootained by an optical technique.

---

* A particular complete discussion of the measurement of diffusivity has been given recently by Geddes[6].

Diaphragm cell: A method which is not as accurate as most of the optical methods but which is easier to use for quick, approximate measurements is the diaphragm cell[9]. This cell employs psuedo-steady state diffusion through a porous diaphragm which separates two large volumes of solution. The method is not absolute, and each diaphragm must be calibrated with some substance of known diffusivity. This cell measures an integral diffusion coefficient, but an analysis has been developed which makes it possible to calculate the differential coefficient from the measured values[10]. Because chemical analysis is possible, this type of cell offers a means for studying multicomponent diffusion.

It seems that the primary disadvantage of this method, aside from its limited accuracy, is that one may make measurements without being aware of a sizable systematic error. For example, the effective diffusion path length which is determined by calibration may change from solution to solution because of a change in the hydrodynamics at the faces of the diaphragm.

Conductimetric method: A method has been developed by Harned[11] which has made it possible to measure diffusivities of electrolytes at extremely low concentrations where the values can be compared with those calculated from the Onsager-Fucss limiting law. The excellent agreement obtained has been gratifying in verifying the theory as well as indicating high experimental accuracy. It should be noted that Harned's higher concentration measurements agree quite well with the results of the Gouy optical method.

The essential features of Harned's cell are that it is of finite length such that diffusion is of the restricted type and that the decay of a concentration gradient with time is monitored by a conductivity difference between two points in the cell. Unfortunately, this method cannot be used as accurately in its present form for studying many electrolytes in the concentrated region because of the maximum in the conductivity versus concentration curve.

After consideration of these and the other techniques for measuring diffusivity, it has been decided that two methods which offer specific advantages are a rotating disk electrode and a modified Harned type cell which incorporates an optical technique. The latter combines the mathematical advantages of the Harned cell with the precision of an optical measurement in concentrated solutions; the electrochemical method offers a means of studying diffusion in concentrated multicomponent systems by measuring the mass transfer rate of a salt to an electrode in the presence of a supporting electrolyte.

Rotating disk electrode

The rotating disk is one of very few cases of forced convection where complete solution for the velocity profile is possible. The important conclusion of the hydrodynamic analysis is that the normal component of the velocity is independent of position on the surface of the disk. Therefore, if the disk is made a cathode such that mass transfer takes place, it is possible to make limiting current measurements and with the use of the known convection term to determine the diffusion

coefficient of the species reacting at the electrode.

These results have been known for some time for the case of a constant property solution and low rates of mass transfer[12]. An analysis has been made recently in this laboratory to take into account the effect of varying solution properties as well as finite interfacial velocity due to the mass transfer. One conclusion of this analysis is that non-constant properties do not affect the uniform accessibility of the surface. The quantitative results make more exact interpretation of the experimental mass transfer measurements possible.

A rotating disk electrode and related apparati have been assembled and will be used to measure the diffusion coefficient of copper sulfate in sulfuric acid solutions at various temperatures and concentrations. A photograph of the apparatus is shown in Figure 13. In testing the apparatus several difficulties have been encountered. It was found that under certain conditions the observed polarization curves were unstable and poorly reproducible. These results indicate that turbulence occurred even though the Reynolds number was low. In these experiments the disk was actually the end of a cylinder as shown on the right in Figure 14. It was decided that the disk should be more streamlined. Therefore, the shape has been modified as shown on the left in the same figure. It is hoped that this will eliminate the problem of turbulence.

Another problem in the analysis of the copper rotating disk electrode is the electrode reaction kinetics. Because of the low exchange current density the limiting current which is

measured depends on both the concentration overvoltage and the activation overvoltage. A complete equation for determining the diffusion coefficient of copper sulfate which takes both these effects into account has been derived.

Optical restricted diffusion cell

Some of the advantages of the Harned type diffusion cell have already been mentioned. Another advantage is that the measurement is independent of the initial concentration distribution since actual determination involves an extrapolation to infinite time. Therefore, the special care which is required in setting up most optical methods is not necessary with this cell.

As indicated previously, it is difficult in many experiments to determine the true differential diffusion coefficient because of the variation of solution properties with concentration. This complication also obscures the frame of reference in many cases. In the Harned cell, however, it is possible to eliminate these difficulties.

Harned's solution of Fick's second law for the concentration profile in a column of liquid of height was made for a solution with constant properties, and he accordingly carried out his measurements using small concentrations differences. By measuring conductivity to monitor concentration at z=a/6 and z=5a/6, he was able to reduce the solution of the equation to

$$\Delta c = c\left(\frac{a}{6}\right) - c\left(\frac{5a}{6}\right) = 2A_1 \cos\left(\frac{\pi}{6}\right) e^{-Dt(\pi/a)^2} + 2A_5 \cos\left(\frac{5\pi}{6}\right) e^{-25Dt(\pi/a)^2} + \ldots . \qquad (3)$$

It is seen that a series of this form converges very rapidly with time so that at large times a plot of $\ln(\Delta c)$ versus t will be a straight line, the slope of which yields the diffusion coefficient.

Because of the several advantages of this type of measurement, we have investigated the possibility of modifying Harned's cell for application to the study of concentrated solutions. To do this it is first necessary to show that the diffusion coefficient which is obtained is a differential one.

By considering the complete flux equation for concentrated solutions derived from equation (1), which allows for flux of solvent as well as solute in the restricted cell, and by treating the concentration and all variable properties as perturbation series about their respective values at infinite time, it has been possible to derive the equation which corresponds to equation (3) but which is completely general and complete for this geometry:

$$\Delta c = A_1' e^{-D_M^\infty (\pi/a)^2 t} + A_3' e^{-3D_M^\infty (\pi/a)^2 t} + \ldots \qquad (4)$$

In this equation D_M^∞ is a well-defined differential diffusion coefficient corresponding to the uniform cell concentration at infinite time. The coefficient A_3' is a complicated combination of concentration derivatives of various solution properties; this term vanishes in the constant property case. Even though the series in equation (4) does not converge as rapidly as that in equation (4), it obviously will converge at sufficiently long times. These times will be on the order of hours

to days, depending upon the magnitude of cell height. Thus it is seen that even in the case of non-constant properties and concentrated solutions a plot of $\ln(\Delta c)$ versus t should still yield a linear region from which a differential diffusion coefficient can be obtained.

It was pointed out that in many cases conductivity cannot be used to monitor a difference in concentration in a concentration solution. It is felt that it would be well to make use here of the high accuracy of an interfermotric technique to observe the behavior of the solution. To be specific, it is planned that multiple beam interference fringes will be generated in the cell. Then as diffusion takes place, the contour of these fringes will give a direct, precise quantitative indication of the concentration profile in the cell as it decays to uniformity. In this way Δc of equation (4) can be determined as a function of time.

It is hoped that a cell such as the one just described can be perfected to give highly accurate diffusion coefficients for concentrated solutions. If this can be done, such a cell then offers the possibility for some systems of combining Harned's electrodes with the optical measurement suggested here to study multicomponent diffusion.

In summary, plans have been made to obtain more data on the transport properties of concentrated electrolytic solutions in order to investigate the general behavior of the D_{ij} coefficients of the multicomponent diffusion equation. In this way it is hoped that we shall discover how the various

physical parameters of the system affect their behavior and thereby develop some means of correlating the values of the D_{ij}'s in binary systems. From such information attempts will then be made to correlate and predict the behavior of the D_{ij}'s in multicomponent systems.

LITERATURE CITED

1. John Newman, Douglas Bennion, and Charles W. Tobias, "Mass Transfer in Concentrated Binary Electrolytes", 1965, Project 3 under this contract.

2. L. G. Longsworth, "The Diffusion of Electrolytes and Macromolecules in Solutions: A Historical Survey", Ann. N. Y. Acad. Sci. 46, 211-240 (1945).

3. Edward M. Bevilacqua, Ellen B. Bevilacque, Margaret M. Bender, and J. W. Williams, "Diffusion Constant Measurement in Theory and Practice", Ann. N. Y. Acad. Sci. 46, 309 (1945).

4. P. A. Johnson and A. L. Babb, "Liquid Diffusion of Non-Electrolytes," Chem. Rev. 56, 387 (1956).

5. R. A. Robinson and R. H. Stokes, Electrolyte Solutions, second edition (Academic Press, Inc., Publishers, New York, 1959), Chapter 10, "The Measurement of Diffusion Coefficients."

6. A. L. Geddes and R. B. Pontious, "Determination of Diffusivity" in Technique of Organic Chemistry, A. Weissberger editor, Vol. 1, Physical Methods, Part 2, 3rd edition (Interscience Publishers, Inc., New York, 1960), Chap. XVI.

7. Ibid, p. 900.

8. L. G. Longsworth, "Experimental Tests of an Interference Method for the Study of Diffusion", J. A. C. S. 69, 2510 (1947).

9. A. R. Gordon, "The Diaphragm Cell Method of Measuring Diffusion", Ann. N. Y. Acad. Sci. 46, 285 (1945).

10. R. H. Stokes, "The Diffusion Coefficients of Eight Univalent Electrolytes in Aqueous Solution at 25°C", J. A. C. S. 72, 2243 (1950).

11. H. S. Harned and D. M. French,"A Conductance Method for the Determination of the Diffusion Coefficients of Electrolytes", Ann. N. Y. Acad. Sci. 46, 267 (1945).

12. V. N. Levich, "Diffusional Flow to a Rotating Disk", Section 27 in Physicochemical Hydrodynamics (Prentice-Hall Inc., Englewood Cliffs, N. J., 1962).

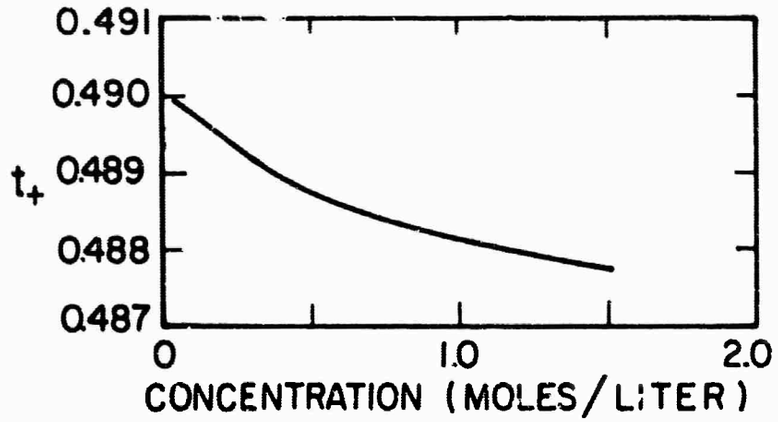

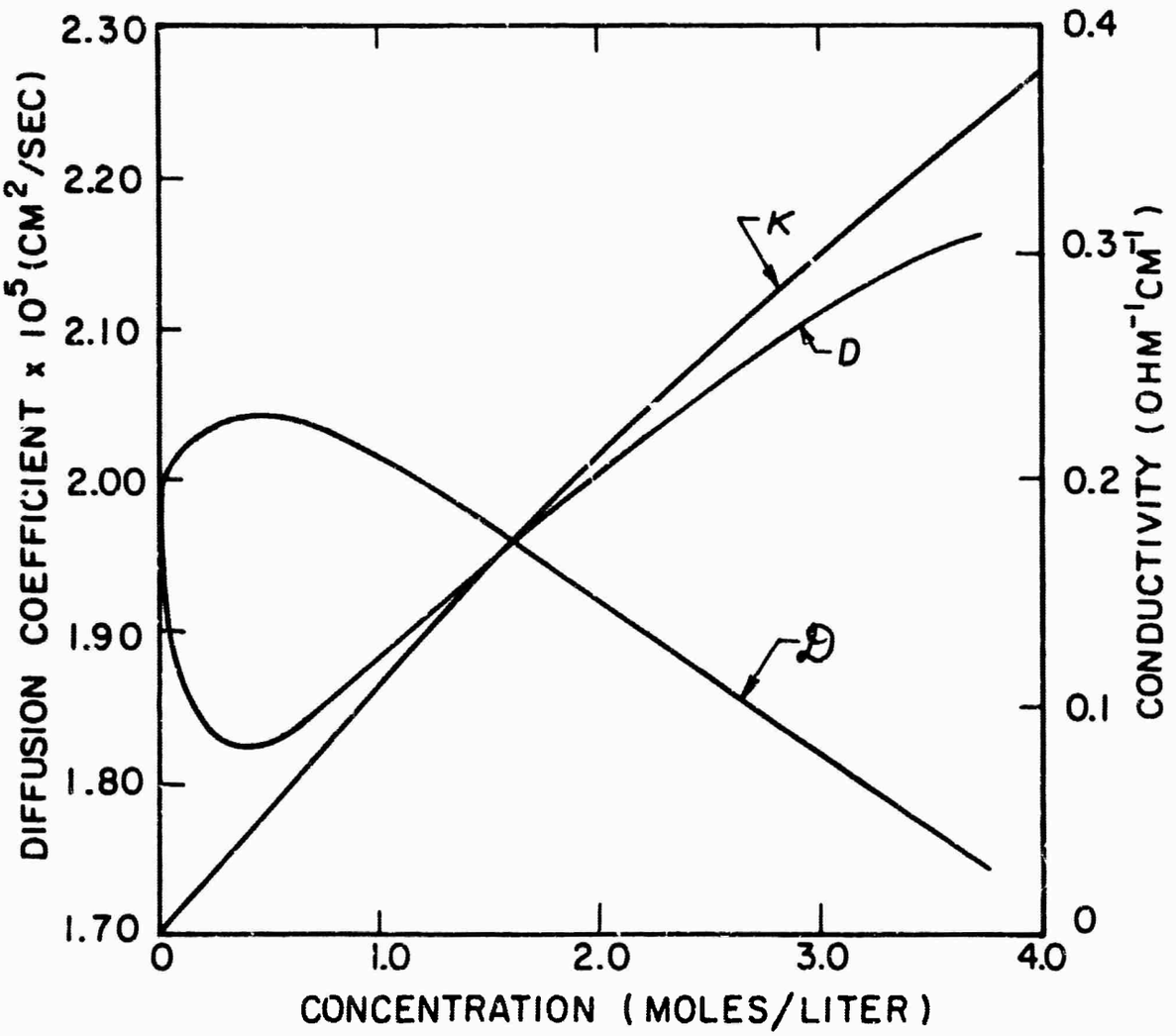

Figure 1. The conductivity, transference numbers and diffusion coefficients of potassium chloride in water at 25°C.

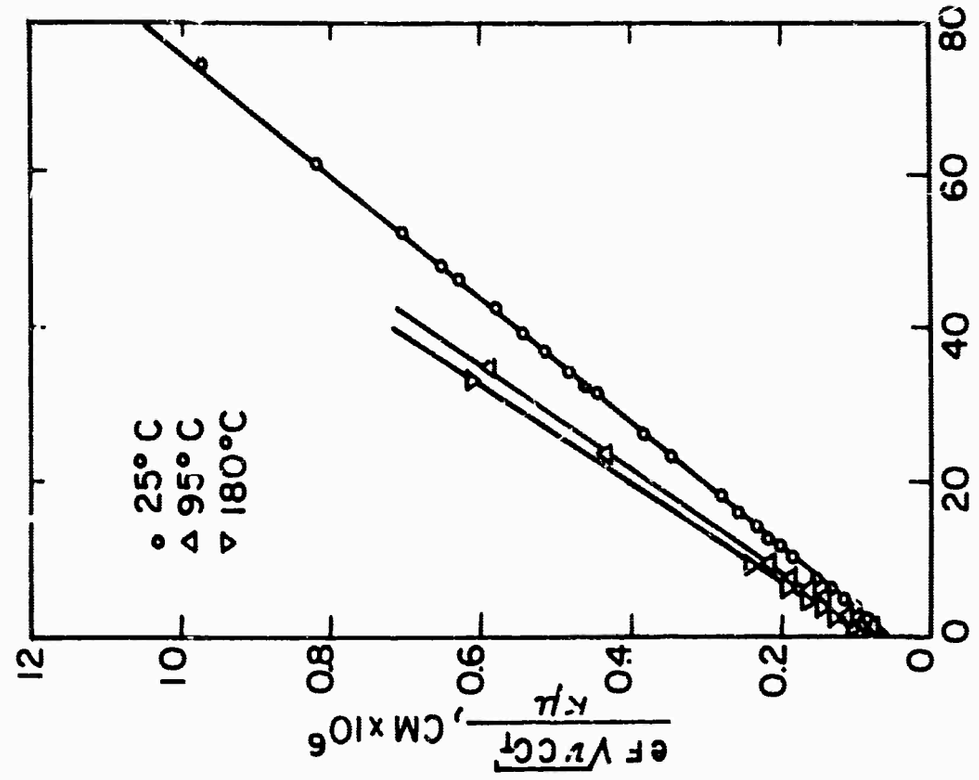

Figure 3. Correlation of conductivity of ammonium nitrate in water with concentration at various temperatures over the entire concentration range.

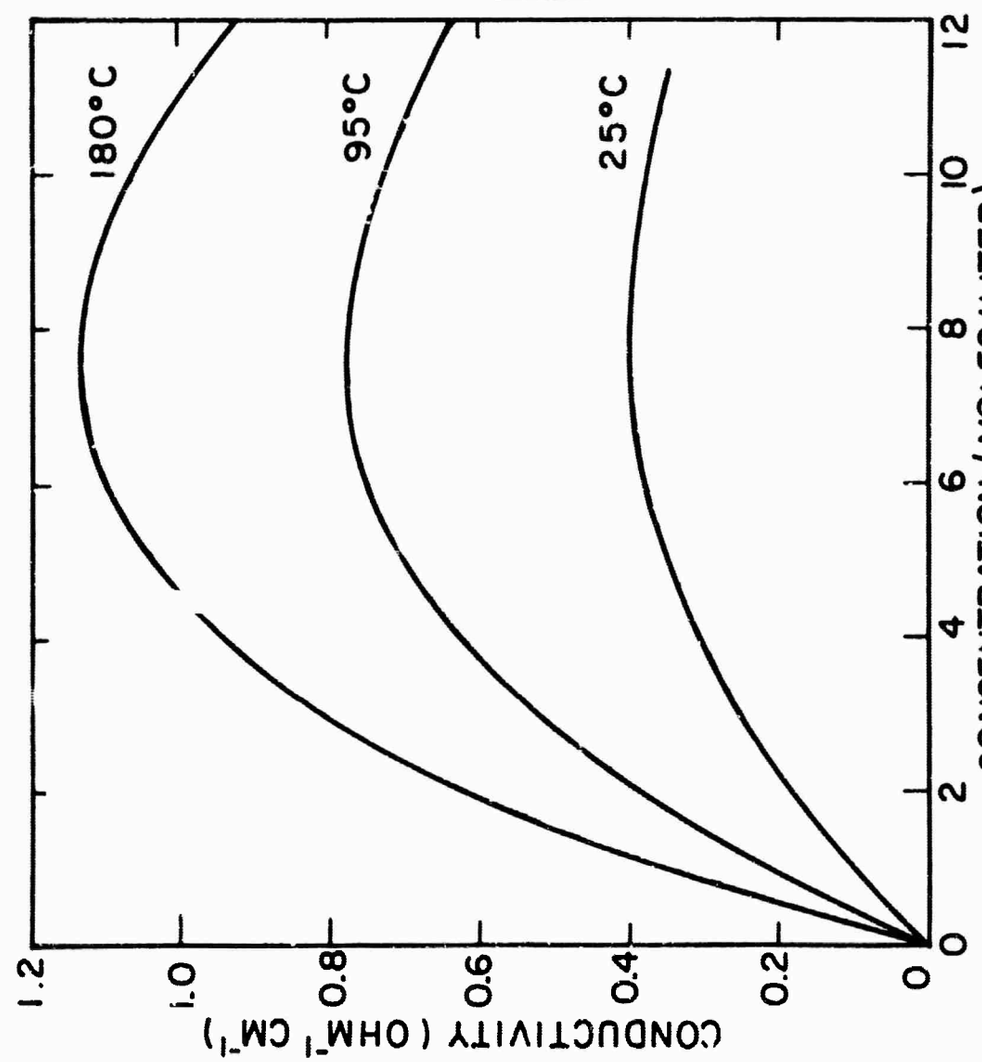

Figure 2. The conductivity of ammonium nitrate in water at various temperatures.

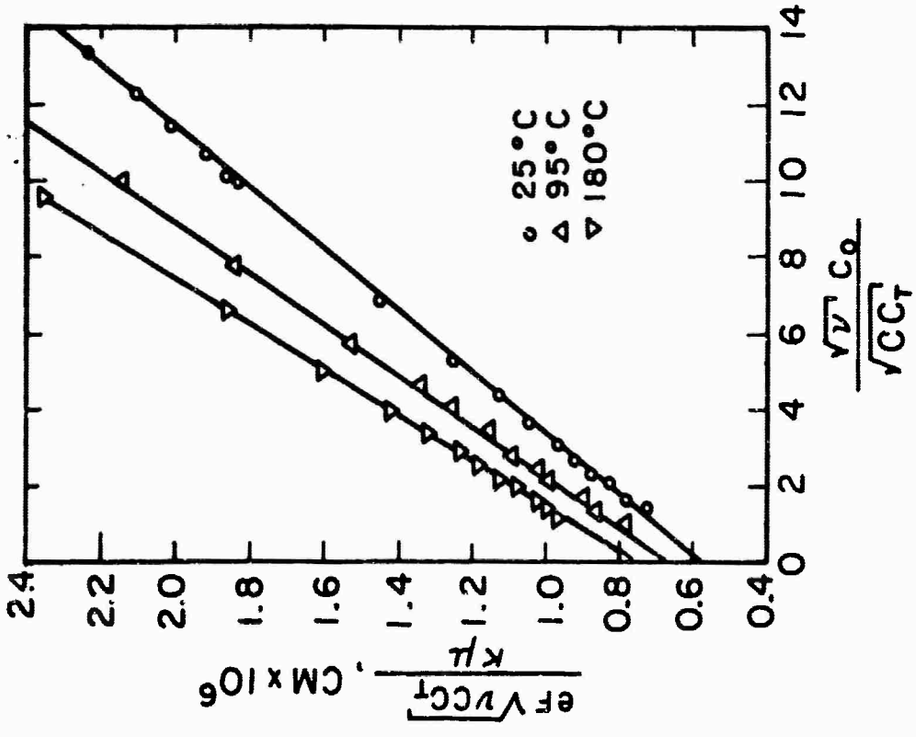

Figure 4. Correlation of conductivity of ammonium nitrate in water with concentration at various temperatures in the high concentration range.

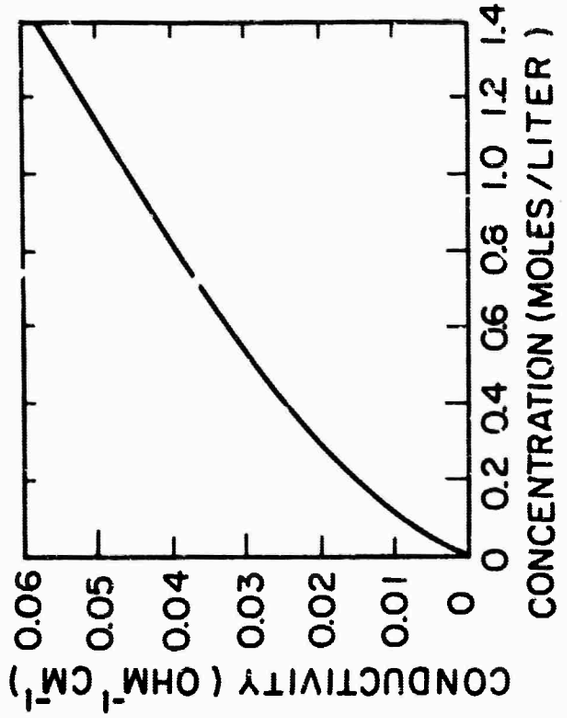

Figure 5. The conductivity of copper sulfate in water at 25°C.

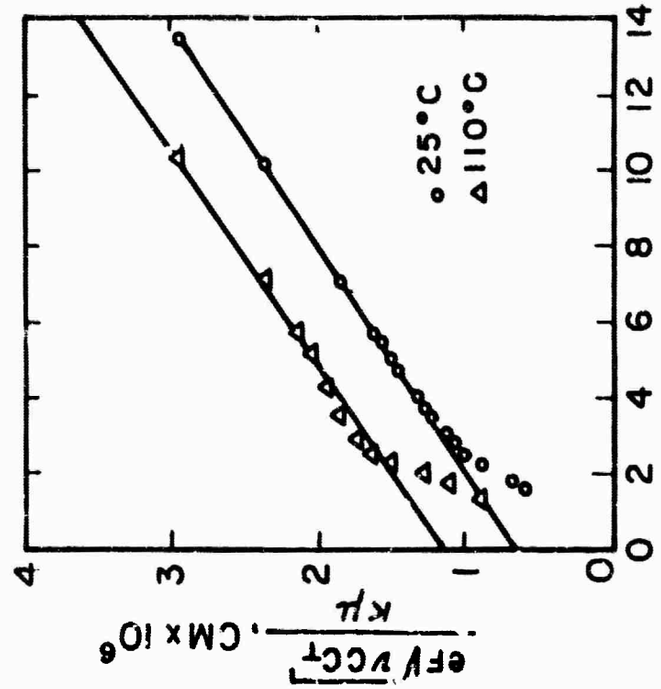

Figure 6. Correlation of conductivity of copper sulfate in water with concentration at 25°C over the entire concentration range.

Figure 7. Correlation of conductivity of lithium nitrate in water at 25°C and 110°C in the high concentration range.

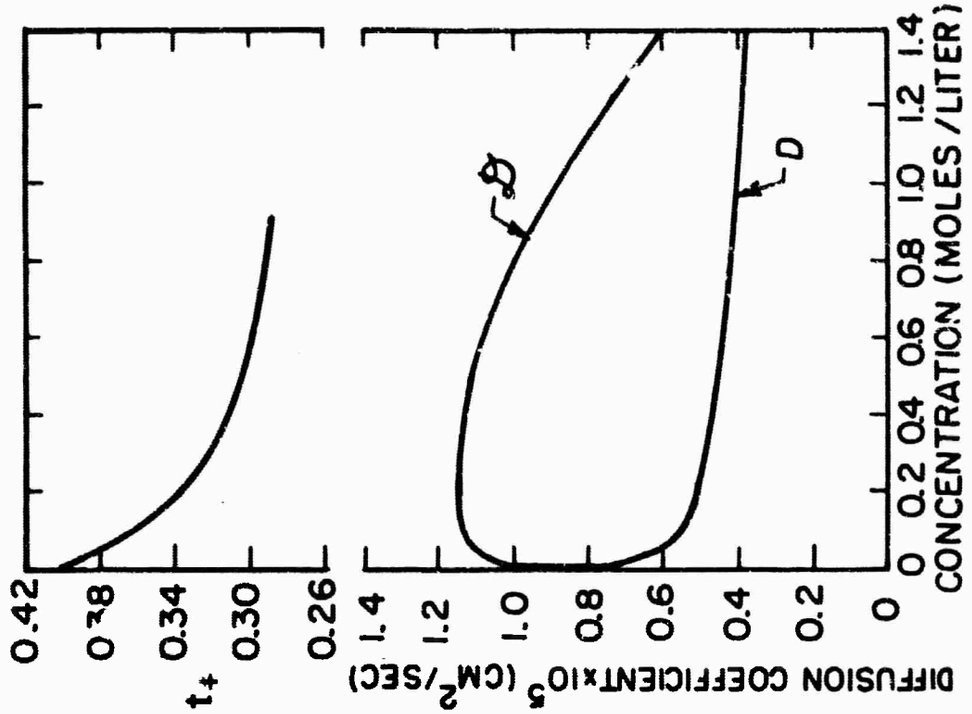

Figure 9. The diffusion coefficients and transference number of copper sulfate in water at 25°C in concentrated solutions.

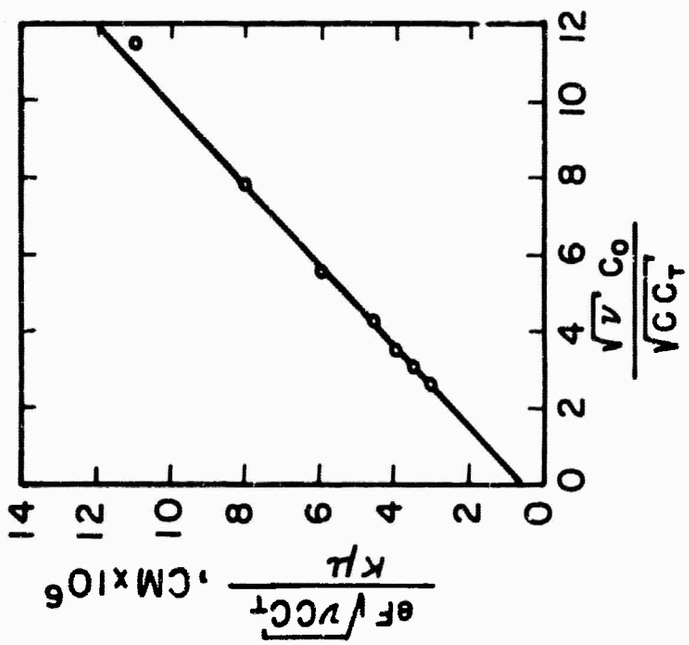

Figure 8. Correlation of conductivity of lithium nitrate in ethanol at 25°C in the high concentration range.

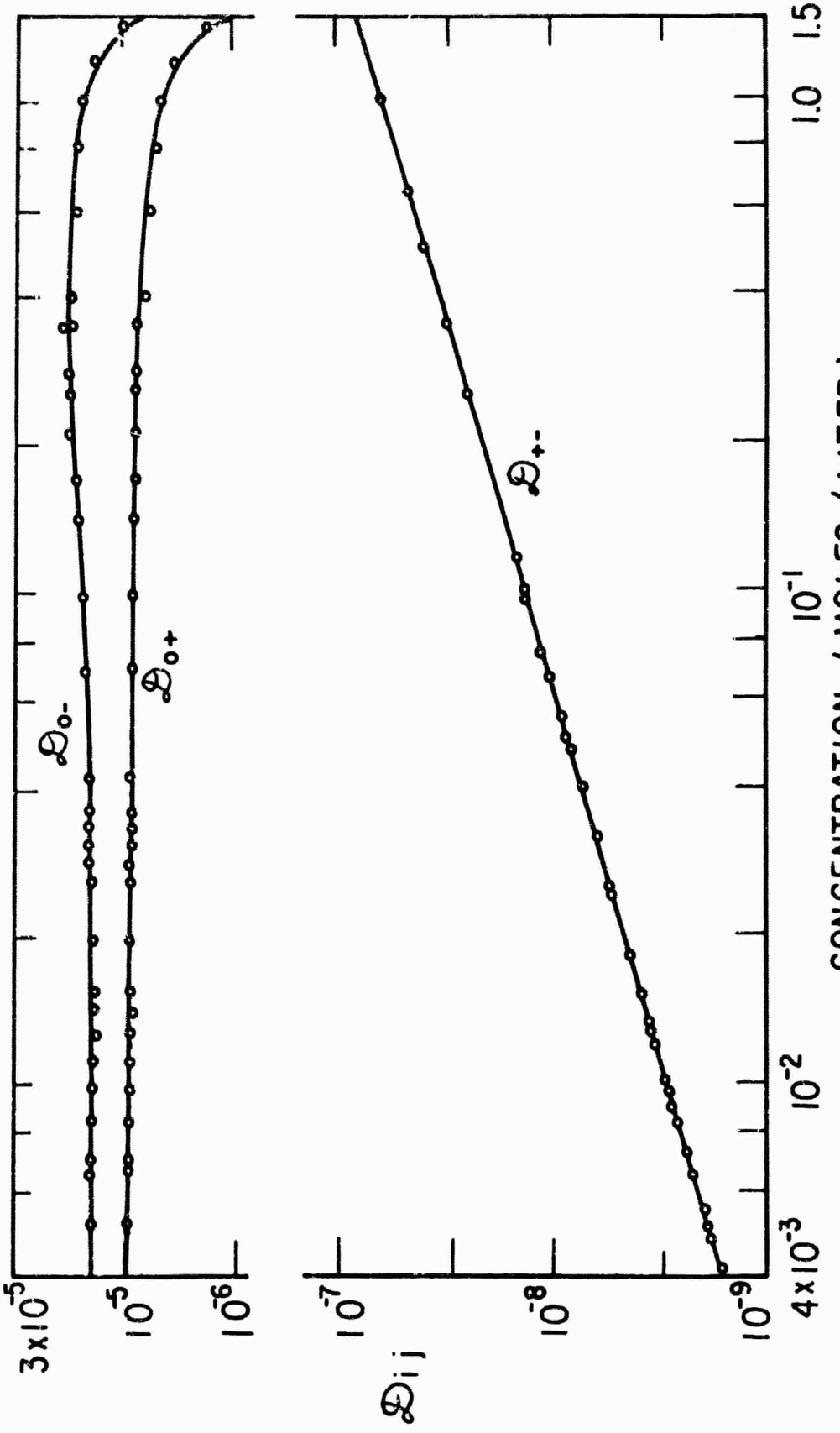

Figure 10. The multicomponent diffusion coefficients of copper sulfate in water at 25°C over the entire concentration range.

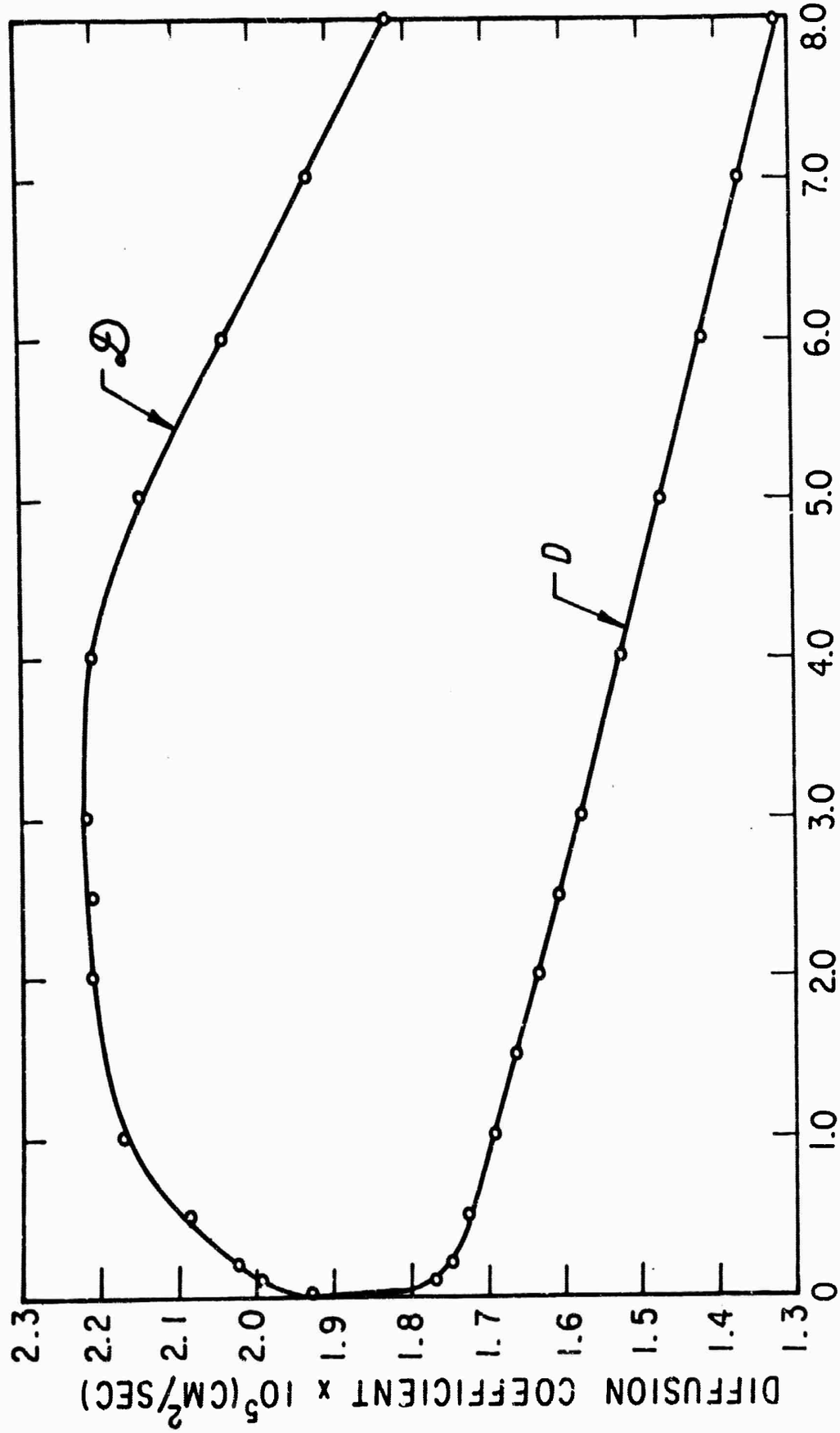

Figure 11. The diffusion coefficients of ammonium nitrate in water at 25°C in concentrated solutions.

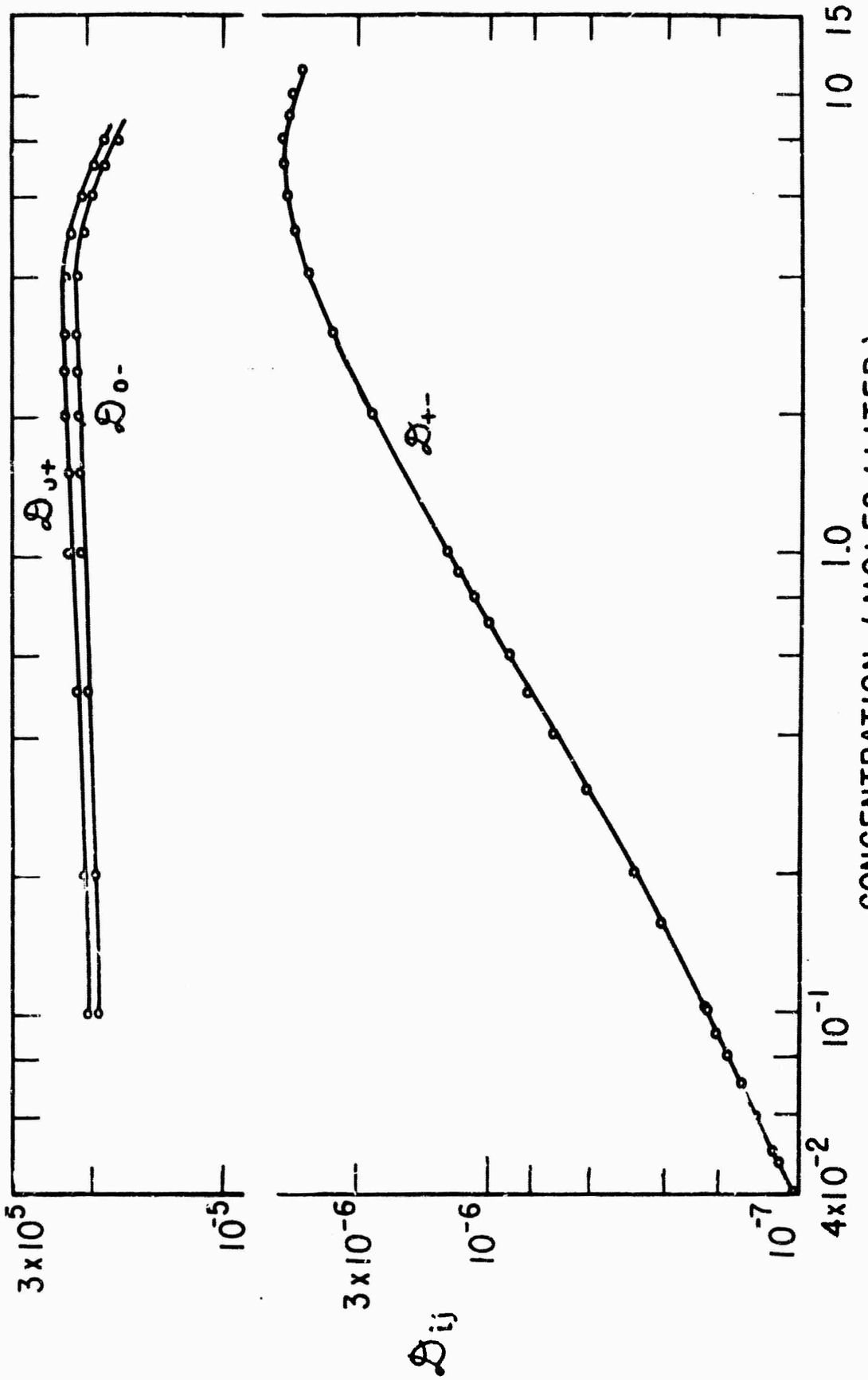

Figure 12. The multicomponent diffusion coefficients of ammonium nitrate in water at 25°C over the entire concentration range.

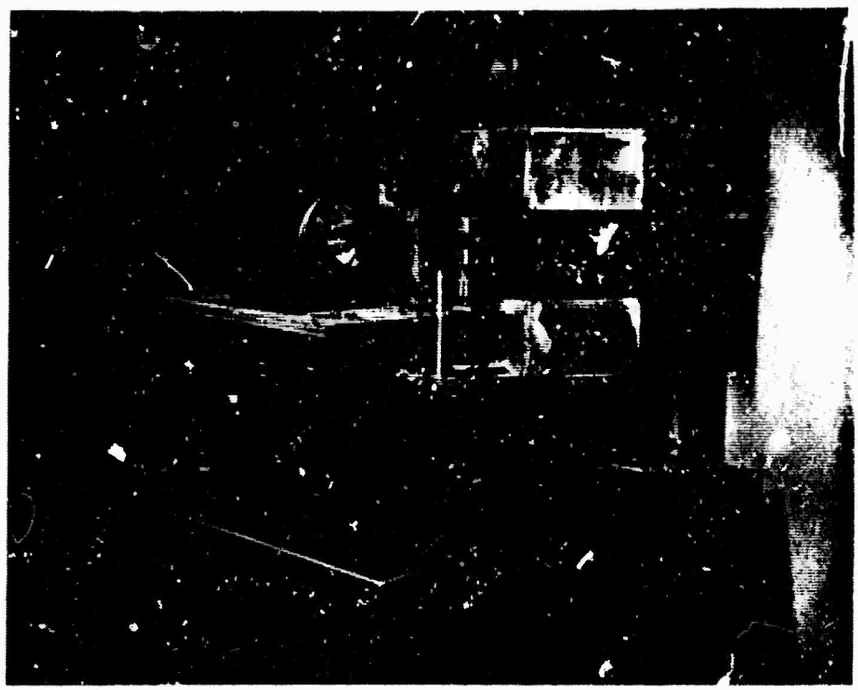

Figure 13. Photograph of the rotating disk apparatus.

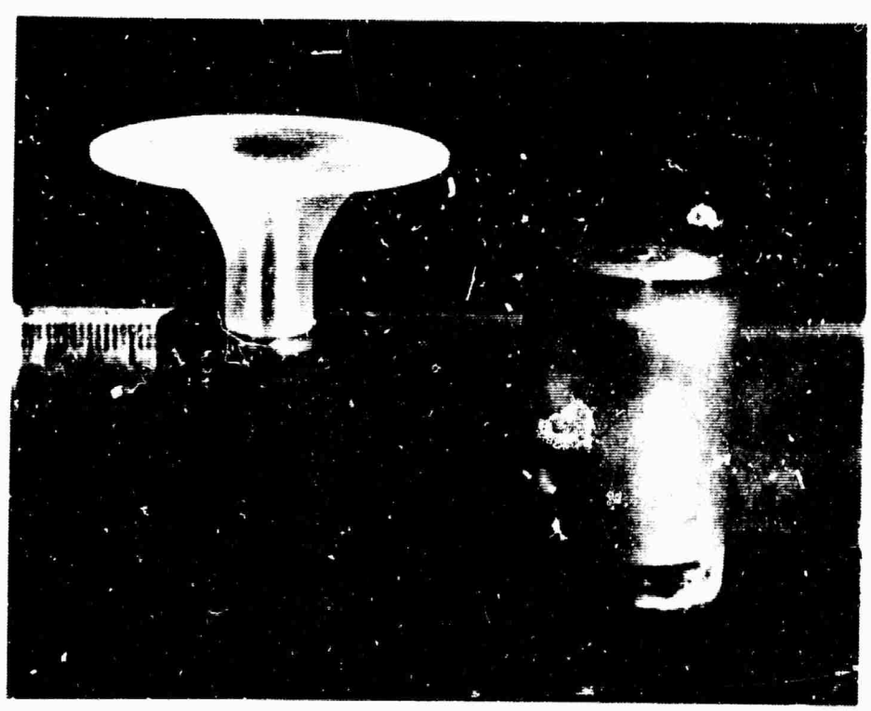

Figure 14. Photograph of the rotating disk electrode (actual size). On the right is the old disk.

E. CLOSING REMARKS AND RECOMMENDATIONS

The seven research projects supported in full or in part by this contract were aimed at gaining quantitative understanding of the role of mass transport processes in relation to charge transfer reactions at electrodes. Although the models chosen for study are illustrative of certain of the conditions prevailing in fuel cells and primary and secondary batteries, clearly the conclusions reached can only be applied to a given practical situation by intelligent examination of all characteristic system parameters.

It is evident to those who performed this research, as it will be to the reader, that further sustained research efforts related to mass transport are needed to support a rational development of future hardward devices. The following areas deserve particular attention:

1. The effect of flow past electrode surfaces and through porous electrodes on local and overall overpotential, and on current distribution, has been characterized only for a restricted range of flow and geometric variables. In particular the laminar to turbulent transition regime, pulsating flows in parallel and through flow, need to be considered. Although transport in free convection has been elucidated successfully for extended surfaces, further efforts should be directed toward the study of free convection effects where the flow is confined by closely spaced solid boundaries, such as between battery plates, or in macropores.

2. Work under this contract, together with most recent results here and abroad, on the elucidation of the mechanism of porous gas electrodes clarified the most elementary aspects of the role of ionic and gas transport. However, so far the models studied, both in respect to geometry and materials employed, and in regard to the simplifying assumptions made, can only serve as qualitative guides for further more detailed and more exact studies. The effect of interfacial tension as it is related to electrocapillarity phenomena, has not been as yet considered, neither has it been even qualitatively shown whether convection due to surface forces plays a significant role in porous gas electrodes. Although it was clearly demonstrated that when water is a reactant, its supply must occur at least to a large degree through the gas phase (and not as it was believed before, from the bulk electrolyte by diffusion into the film-reaction zone), this aspect, because of its immediate significance in fuel cell design, should be the subject of more detailed scrutiny involving both simple experimental models and actual hardware type porous electrodes.

3. The degree of usefulness of understanding of mass transport processes depends on the availability of data on equilibrium and transport properties. As long as solubilities, viscosities, conductances, transference numbers and diffusion coefficients of cell reactants and products in the concentration ranges that are typical of actual hardware applications are missing, the design and optimization of every piece of equipment will remain a costly "Edisonian" task. The

determination of the solubility and diffusion coefficient of oxygen in KOH, carried out under this contract was long overdue, and far from being enough to allow rational development of the many types of systems of practical interest involving a variety of electrolytes, reactants and products. Direct measurements of these properties over representative concentration ranges are extremely time-consuming, and therefore the development generalized methods for their prediction should receive high priority.

The research program initiated under this contract during its last year is being continued under the sponsorship of the Inorganic Materials Research Division of the Lawrence Radiation Laboratory. (Projects VI and VII.) A new project was initiated recently as a logical outgrowth of Project I, aimed at the elucidation of the mechanism of electrolytic gas evolution. As a recognition of its support during the initial phases of these projects, the U.S. Army Electronic Research Laboratory will be kept informed about the progress of this work.

BLANK PAGE

F. Identification of Personnel and Distribution of Working Hours[1]

1962

Name	Title	% Salaried Time	Started (s) Terminated (t)	Project Responsibility	Hours
Bennion, Douglas N.	Res. Assistant III	50% acad. yr. 100% summer	4/1/62 (s)	I (own thesis)	1058
Gordon, Stanley L.	Res. Assistant II	18% acad. yr. 100% summer	6/18/62 (s)	III (own thesis)	718[2]
Hickman, Robert G.	Res. Assistant III	50% acad. yr. 100% summer	4/1/62 (s)	II (own thesis)	1058
Hanson, Donald N.	Faculty Investigator	100% for one summer month	8/1/62 (s) 8/31/62 (t)	Overall consultation on numerical techniques.	176[2]
Muller, Rolf H.	Assistant Res. Chemist	33% year around	6/1/62 (s) 8/31/62 (t)	Collaborated on I,II,instrumental, optical techniques	528
Secretary	Secretary-stenographer	23% 4/1-7/1 25% thereafter	4/1/62 (s)	General secretarial support	385
Tobias, Charles W.	Principal Investigator	100% for one summer month	8/1/62 (s) 8/31/62 (t)	Overall direction of work under this contract	176[2]
Turcsanyi, Denes	Junior Engineer	33% year around	4/1/62 (s)	Equipment design and maintenance, assist I,II,III	528
					4627
				Less vacation time[3]	263
				Net total	4364

1 Basis for evaluation of work-hours - 22 days (8-hr) per month.

2 The University provided compensation for research done during the academic year (9/15-6/15).

3 This figure is obtained by subtracting 1-1/4 day vacation time/full work month (i.e., 10 hrs. out of each 176 hrs.).

F. Identification of Personnel and Distribution of Working Hours[1]

1963

Name	Title	% Salaried Time	Started (s) Terminated (t)	Project Responsibility	Hours
Bennion, Douglas N.	Res. Assistant III	50% acad. yr. 100% summer		I (own thesis)	1320
Chapman, Thomas W.	Res. Assistant II	50% acad. yr.	9/16/63 (s)	V (assist)	308
Davis, Russ	Res. Assistant	100% summer	6/10/63 (s) 9/6/63 (t)	V (assist)	528
Gordon, Stanley L.	Res. Assistant II	18% acad. yr.	6/1/63 (t)	III (own thesis)	158[2]
Hickman, Robert G.	Res. Assistant III	50% acad. yr. 100% summer	12/1/63 (t)	II (own thesis)	1320
Horvath, George L.	Laboratory Assistant	50% acad. yr. 100% summer	6/1/63 (s)	V, also general lab. assistance	880
Newman, John S.	Faculty Investigator	100% summer	6/10/63 (s) 9/9/63 (t)	IV, also direct VII, consultant for math. probl.	528[2]
Secretary	Secretary-stenographer	25% all yr.		General secretarial support	528
Tobias, Charles W.	Principal Investigator	100% for one summer month	6/1/63 (s) 6/30/63 (t)	Overall direction of work under this contract	176[2]
Turcsanyi, Denes	Junior Engineer	33% year around	9/1/63 (t)	Equipment design and maintenance, assist I,II,III	1408
					7154
				Less vacation time[3]	406
				Net total	6748

1 Basis for evaluation of work-hours - 22 days (8-hr) per month.

2 The University provided compensation for research done during the academic year (9/15-6/15).

3 This figure is obtained by subtracting 1-1/4 day vacation time/full work month (i.e., 10 hrs. out of each 176 hrs.).

F. Identification of Personnel and Distribution of Working Hours[1]

1964

Name	Title	% Salaried Time	Started (s) Terminated (t)	Project Responsibility	Hours
Bennion, Douglas N.	Res Assistant III	50% acad. yr. 100% summer	9/11/64 (t)	I (own thesis) IV (assist)	1012[2]
Boeffard, Alain J.L.	Res. Assistant I	50% year around	9/14/64 (s) 12/31/64 (t)	VI (assist)	308
Chapman, Thomas W.	Res. Assistant III	50% acad. yr. 100% summer	11/16/64 (t)	VII (own thesis)	1188
Horvath, George L.	Junior Engineer	50% thru June 100% thru 11/16	11/16/64 (t)	V, design and maint. of equipm.all projs.	1320
Hsueh, Leighton L.	Res. Assistant II	50% acad. yr.	9/14/64 (s) 12/31/64 (t)	VII (assist)	308
Newman, John S.	Faculty Investigator	100% summer	6/15/64 (s) 7/31/64 (t)	IV, direct VII, consultant for math. problems	264[2]
Secretary	Secretary-stenographer	25% year around	12/31/64 (t)	General secretarial support	528
Selman, J. Robert	Graduate Res. Chemist II	100% year around	2/1/64 (s)	VI	1963
Tobias, Charles W.	Principal Investigator	100% summer	6/15/64 (s) 9/11/64 (t)	Overall direction of work under this contract	528[2]
Youn, Kun C.	Laboratory Assistant	50% 2 mos.	7/1/64 (s) 9/1/64 (t)	I (assist)	176[2]
Stefansky Tibor	Laboratory Tech. I	100% 2 mos.	10/5/64 (s) 12/1/64 (t)	Assist G. L. Horvath	320
					7888
				Less vacation time[3]	448
				Net total	7440

[1] Basis for evaluation of work-hours - 22 days (8-hr) per month.

[2] The University provided compensation for research done during the academic year (9/15-6/15).

[3] This figure is obtained by subtracting 1-1/4 day vacation time/full work month (i.e., 10 hrs. out of each 176 hrs.).

F. Identification of Personnel and Distribution of Working Hours[1]

1965

Name	Title	% Salaried Time	Started (s) Terminated (t)	Project Responsibility	Hours
Selman, J. Robert	Graduate Res. Chemist	100% year around	2/28/65 (t)	VI, also general work in lab.	380
Neiman, John S.	Faculty Investigator		2/28/65 (t)	IV, direct VII, consultant for math. problems	
Tobias, Charles W.	Principal Investigator		2/28/65 (t)	Overall direction of work under this contract	
					380
				Less vacation time	21
				Net total	359
				Total hours worked in 3-year period of contract	18,911

ACKNOWLEDGMENT

The research work conducted under this contract resulted in the completion of one Master of Science thesis and two Ph.D. theses in Chemical Engineering. One further Master's thesis and two additional Ph.D. theses are still in preparation. Two postdoctoral trainees were also beneficiaries of the research opportunities created under this contract.

The cooperation, interest and understanding shown by the personnel of the U.S. Army Electronic Research Laboratory monitoring this contract have been greatly appreciated.

BLANK PAGE

Unclassified

Security Classification

DOCUMENT CONTROL DATA - R&D

(Security classification of title, body of abstract and indexing annotation must be entered when the overall report is classified)

1. ORIGINATING ACTIVITY (Corporate author)
The Regents of the University of California
Berkeley
California

2a. REPORT SECURITY CLASSIFICATION
Unclassified

2b. GROUP

3. REPORT TITLE

TRANSPORT PROCESSES IN ELECTRODE SYSTEMS

4. DESCRIPTIVE NOTES (Type of report and inclusive dates)
Final - 16 March 1962 through 1 March 1965

5. AUTHOR(S) (Last name, first name, initial)

Bennion, D.N., Chapman, T. W., Gordon, S.L., Hickman, R.G., Horvath, G.L., Newman, J.S., Selman, J.R., Tobias, C.W.

6. REPORT DATE	7a. TOTAL NO. OF PAGES	7b. NO. OF REFS
March 1965	233	173

8a. CONTRACT OR GRANT NO.
DA-36-039-SC-89153

b. PROJECT NO. OST 760200201

c.

d.

9a. ORIGINATOR'S REPORT NUMBER(S)

9b. OTHER REPORT NO(S) (Any other numbers that may be assigned this report)

10. AVAILABILITY/LIMITATION NOTICES
Qualified requesters may obtain copies of this report from DDC.
This report has been released to CFSTI.

11. SUPPLEMENTARY NOTES

12. SPONSORING MILITARY ACTIVITY

U.S. Army Electronics Command
Fort Monmouth, N.J. 07703

13. ABSTRACT

Results of five projects pertaining to: I. Current distribution at a gas-electrode-electrolyte interface; II. The role of ionic migration in electrolytic mass transport; diffusivities of $(Fe(CN)_6)^{3-}$ and $(Fe(CN)_6)^{4-}$ in KOH and NaOH solutions; III. Ionic mass transport by combined free and forced convection; IV. Mass transfer in concentrated binary electrolytes; V. The solubility and diffusion coefficient of oxygen in KOH, are given, and the status of two projects being continued; VI. Ionic mass transport and current distribution in channels at high velocity flow; VII. Transport properties of concentrated electrolytic solutions are described. (Author)

DD FORM 1 JAN 64 1473

Unclassified

Security Classification

14. KEY WORDS	LINK A		LINK B		LINK C	
	ROLE	WT	ROLE	WT	ROLE	WT
Ionic Mass Transport Gas-Electrode-Electrolyte Interface Transport Properties of Conc. Electrolytic Solutions Mathematical Model for O_2 Half Cell Mass Transfer in Binary Electrolytes Ionic Migration in Electrolytic Mass Transport						

INSTRUCTIONS

1. ORIGINATING ACTIVITY: Enter the name and address of the contractor, subcontractor, grantee, Department of Defense activity or other organization *(corporate author)* issuing the report.

2a. REPORT SECURITY CLASSIFICATION: Enter the overall security classification of the report. Indicate whether "Restricted Data" is included. Marking is to be in accordance with appropriate security regulations.

2b. GROUP: Automatic downgrading is specified in DoD Directive 5200.10 and Armed Forces Industrial Manual. Enter the group number. Also, when applicable, show that optional markings have been used for Group 3 and Group 4 as authorized.

3. REPORT TITLE: Enter the complete report title in all capital letters. Titles in all cases should be unclassified. If a meaningful title cannot be selected without classification, show title classification in all capitals in parenthesis immediately following the title.

4. DESCRIPTIVE NOTES: If appropriate, enter the type of report, e.g., interim, progress, summary, annual, or final. Give the inclusive dates when a specific reporting period is covered.

5. AUTHOR(S): Enter the name(s) of author(s) as shown on or in the report. Enter last name, first name, middle initial. If military, show rank and branch of service. The name of the principal author is an absolute minimum requirement.

6. REPORT DATE: Enter the date of the report as day, month, year, or month, year. If more than one date appears on the report, use date of publication.

7a. TOTAL NUMBER OF PAGES: The total page count should follow normal pagination procedures, i.e., enter the number of pages containing information.

7b. NUMBER OF REFERENCES: Enter the total number of references cited in the report.

8a. CONTRACT OR GRANT NUMBER: If appropriate, enter the applicable number of the contract or grant under which the report was written.

8b, 8c, & 8d. PROJECT NUMBER: Enter the appropriate military department identification, such as project number, subproject number, system numbers, task number, etc.

9a. ORIGINATOR'S REPORT NUMBER(S): Enter the official report number by which the document will be identified and controlled by the originating activity. This number must be unique to this report.

9b. OTHER REPORT NUMBER(S): If the report has been assigned any other report numbers *(either by the originator or by the sponsor)*, also enter this number(s).

10. AVAILABILITY/LIMITATION NOTICES: Enter any limitations on further dissemination of the report, other than those imposed by security classification, using standard statements such as:

(1) "Qualified requesters may obtain copies of this report from DDC."

(2) "Foreign announcement and dissemination of this report by DDC is not authorized."

(3) "U. S. Government agencies may obtain copies of this report directly from DDC. Other qualified DDC users shall request through _____."

(4) "U. S. military agencies may obtain copies of this report directly from DDC. Other qualified users shall request through _____."

(5) "All distribution of this report is controlled. Qualified DDC users shall request through _____."

If the report has been furnished to the Office of Technical Services, Department of Commerce, for sale to the public, indicate this fact and enter the price, if known.

11. SUPPLEMENTARY NOTES: Use for additional explanatory notes.

12. SPONSORING MILITARY ACTIVITY: Enter the name of the departmental project office or laboratory sponsoring *(paying for)* the research and development. Include address.

13. ABSTRACT: Enter an abstract giving a brief and factual summary of the document indicative of the report, even though it may also appear elsewhere in the body of the technical report. If additional space is required, a continuation sheet shall be attached.

It is highly desirable that the abstract of classified reports be unclassified. Each paragraph of the abstract shall end with an indication of the military security classification of the information in the paragraph, represented as *(TS)*, *(S)*, *(C)*, or *(U)*.

There is no limitation on the length of the abstract. However, the suggested length is from 150 to 225 words.

14. KEY WORDS: Key words are technically meaningful terms or short phrases that characterize a report and may be used as index entries for cataloging the report. Key words must be selected so that no security classification is required. Identifiers, such as equipment model designation, trade name, military project code name, geographic location, may be used as key words but will be followed by an indication of technical context. The assignment of links, rules, and weights is optional.